AB initio investigation of the ground and lower excited electronic states of indoles and their complexes with water
by David Keith Hahn

A thesis submitted in partial fulfillment Of the requirements for the degree of Doctor of Philosophy in Chemistry
Montana State University

Abstract:
The effects of basis and method on the calculated ground and lower excited state properties of indole, 3-methyl indole, and 5-methyl indole are investigated.

Ground state calculations are performed primarily at the Hartree-Fock (HF) level while the excited states are examined mainly with the Configuration Interaction-Singles method (CIS). Basis sets range in size up to triple-ζ valence with polarization functions and diffuse functions on each atom for the ground state, and up to double-ζ with polarization functions on each atom and diffuse functions on heavy atoms for the excited states. In general, little or no improvement is obtained in the calculated properties by increasing the size of the basis set.

The calculations show pronounced differences in polarity between 1La and 3La indole, thereby accounting for the comparative resolution of tryptophan's fluorescence and phosphorescence in polar environments. The difference arises in theory from large 3La off-diagonal CI dipole matrix elements that are negligible in the 1La state. It is also shown that the indoles' lower electronic manifold is qualitatively reproduced with a drastically truncated CIS wave function. Methyl indole torsion barriers calculated at this theoretical level are in qualitative agreement with observation. The calculations also reproduce the 60° change in methyl group phase accompanying 1Lb excitation of 5-methyl indole and predict pronounced vibronic coupling and the existence of two conical intersections near the 1La minimum of 3-methyl indole.

The intermolecular potential energy surface of water complexed to indole in its ground electronic state shows a global minimum resulting from the interaction with the N-H group and a local minimum arising from the interaction with the π cloud above the indole ring. The corresponding two-dimensional vibrational wave functions of the first ten bound states are localized entirely in the global minimum. Calculations at the Hartree-Fock and CIS level on the 1:1 and 1:2 complexes between indole or 3-methyl indole and water discourage an exciplex interpretation of the indoles' solvatochromism. Binding energies are typically less than I kcal/mol greater in the excited states for the 1:1 complexes, and 2 to 3 kcal/mol greater for the 1:2 complex. The results are in accord with jet-cooled spectra, where π-complex formation is observed to cause the smallest red shift in the complex origin and 1:2 complex formation causes the largest red shift.

AB INITIO INVESTIGATION OF THE GROUND AND LOWER EXCITED ELECTRONIC STATES OF INDOLES AND THEIR COMPLEXES WITH WATER

by

David Keith Hahn

A thesis submitted in partial fulfillment
Of the requirements for the degree

of

Doctor of Philosophy

in

Chemistry

MONTANA STATE UNIVERSITY
Bozeman, Montana

June, 1999

APPROVAL

of a thesis submitted by

David Keith Hahn

This thesis has been read by each member of the thesis committee and has been found to be satisfactory regarding content, English usage, format, citations, bibliographic style, and consistency, and is ready for submission to the College of Graduate Studies.

June 9, 1999
Date

Patrick R. Callis
Chairperson, Graduate Committee

Approved for the Major Department

June 10, 1999
Date

Head, Major Department

Approved for the College of Graduate Studies

6-14-99
Date

Bruce L. McLeod
Graduate Dean

STATEMENT OF PERMISSION TO USE

In presenting this thesis in partial fulfillment of the requirements for a doctoral degree at Montana State University, I agree that the Library shall make it available to borrowers under rules of the Library. I further agree that copying of this thesis is allowable only for scholarly purposes, consistent with "fair use" as prescribed in the U.S. Copyright Law. Requests for extensive copying or reproduction of this thesis should be referred to University Microfilms International, 300 North Zeeb Road, Ann Arbor, Michigan 48106, to whom I have granted "the exclusive right to reproduce and distribute my dissertation for sale in and from microform or electronic format, along with the right to reproduce and distribute my abstract in any format in whole or part."

Signature David Hahn

Date 6-21-1999

TABLE OF CONTENTS

LIST OF TABLES

LIST OF FIGURES

ABSTRACT

The effects of basis and method on the calculated ground and lower excited state properties of indole, 3-methyl indole, and 5-methyl indole are investigated. Ground state calculations are performed primarily at the Hartree-Fock (HF) level while the excited states are examined mainly with the Configuration Interaction-Singles method (CIS). Basis sets range in size up to triple-ζ valence with polarization functions and diffuse functions on each atom for the ground state, and up to double-ζ with polarization functions on each atom and diffuse functions on heavy atoms for the excited states. In general, little or no improvement is obtained in the calculated properties by increasing the size of the basis set.

The calculations show pronounced differences in polarity between ^1L_a and ^3L_a indole, thereby accounting for the comparative resolution of tryptophan's fluorescence and phosphorescence in polar environments. The difference arises in theory from large ^3L_a off-diagonal CI dipole matrix elements that are negligible in the ^1L_a state. It is also shown that the indoles' lower electronic manifold is qualitatively reproduced with a drastically truncated CIS wave function. Methyl indole torsion barriers calculated at this theoretical level are in qualitative agreement with observation. The calculations also reproduce the 60° change in methyl group phase accompanying ^1L_b excitation of 5-methyl indole and predict pronounced vibronic coupling and the existence of two conical intersections near the ^1L_a minimum of 3-methyl indole.

The intermolecular potential energy surface of water complexed to indole in its ground electronic state shows a global minimum resulting from the interaction with the N-H group and a local minimum arising from the interaction with the π cloud above the indole ring. The corresponding two-dimensional vibrational wave functions of the first ten bound states are localized entirely in the global minimum. Calculations at the Hartree-Fock and CIS level on the 1:1 and 1:2 complexes between indole or 3-methyl indole and water discourage an exciplex interpretation of the indoles' solvatochromism. Binding energies are typically less than 1 kcal/mol greater in the excited states for the 1:1 complexes, and 2 to 3 kcal/mol greater for the 1:2 complex. The results are in accord with jet-cooled spectra, where π-complex formation is observed to cause the smallest red shift in the complex origin and 1:2 complex formation causes the largest red shift.

Chapter 1

INTRODUCTION

Indole's spectroscopy is important because of the ubiquity of the indole ring in biology and chemistry. Among the more notable compounds containing this moiety are the brain metabolite serotonin, the pigments indigo and the melanins, and the plant growth hormone heteroauxin. Research on indole (Figure 1) is usually undertaken because the indole ring is also the chromophore of the amino acid tryptophan, a residue common to most proteins, and the primary participant in their near UV spectra. However, for a detailed understanding of protein spectroscopy, it is not sufficient to consider indole itself. Many of the spectroscopic properties of the indole ring depend on whether one is considering an isolated, unsubstituted molecule or a chromophore attached to a protein in its native environment.

Indole

The near degeneracy of two low-lying excited electronic states, denoted ^1L_a and ^1L_b by Platt,[1] has been the main source of puzzlement in indole's spectra. For the isolated indole molecule, the ^1L_a origin is split between several lines 1,200 to 1,460 cm^{-1} above the ^1L_b origin in the jet-cooled fluorescence excitation spectrum, as shown from a comparison with low temperature matrix-isolated spectra.[2] A 3,700 cm^{-1} vertical separation is observed in hydrocarbon solvent.[3] Thus far, only ab initio

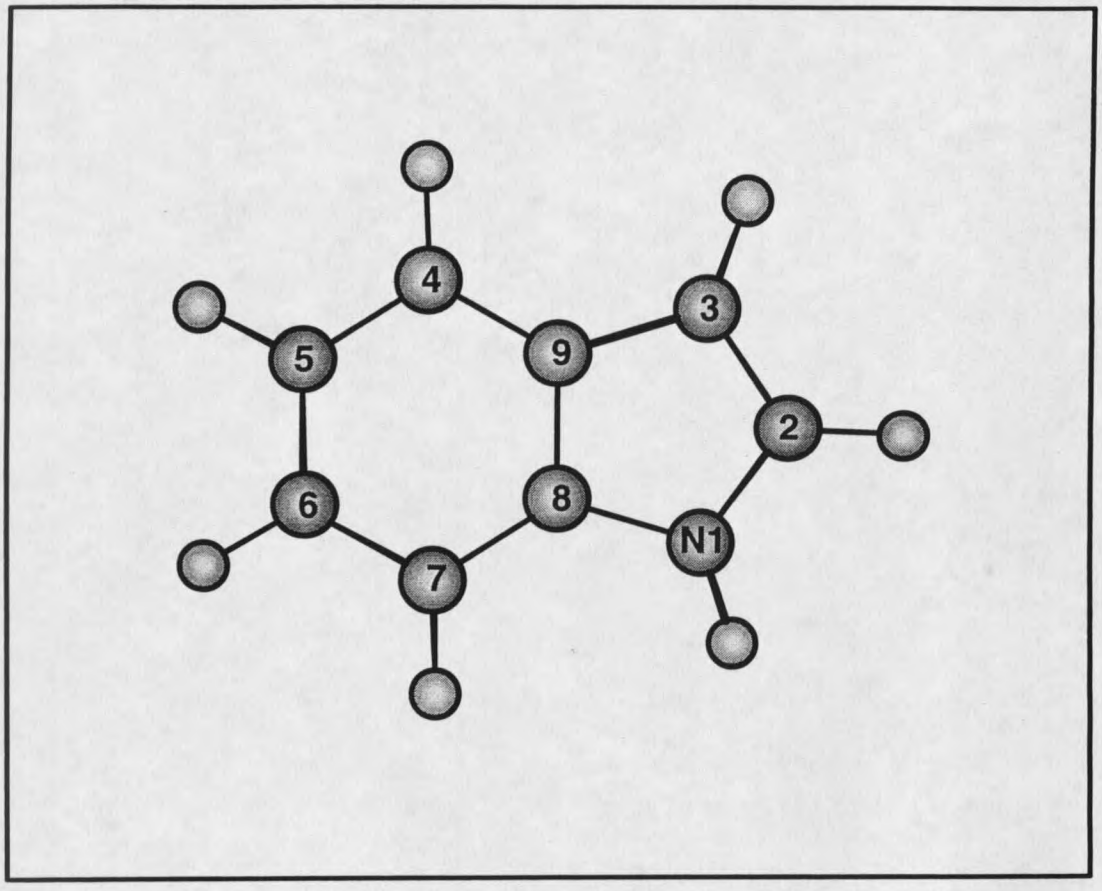

Figure 1. Numbering convention for indole.

calculations at a correlated level of theory have been able to qualitatively describe indole's lower electronic manifold.[4,5]

In contrast to its lower singlet manifold, indole's triplet manifold is not well characterized because of the weak intensity and poor resolution of its triplet-triplet absorption spectrum. Only a single transition at 23,200 cm^{-1} may be discerned.[6] Semi empirical[7] and high-level ab initio studies[5] place T_1 much lower than T_2 and T_3, which are close to ^1L_b. The T_1 state is ^3L_a in Platt notation, as semi empirical[7] and ab initio[8] calculations have shown that its wave function is dominated by the determinant formed when the highest energy occupied self-consistent field molecular orbital is replaced

with the lowest unoccupied molecular orbital (the HOMO → LUMO determinant), like ^1L_a. (Indole's ^1L_b wave function consists mainly of the HOMO-1 → LUMO and HOMO → LUMO+1 determinants.)

The geometry change following an electronic transition is important because it determines the spectrum's vibrational fine structure. The intensity of any particular vibronic line is determined primarily by the projection of the final electronic state's normal coordinates on to the geometry difference between the combining electronic states. Normal coordinates with a non-zero projection are said to be Franck-Condon allowed.

For indole, the geometry difference between the ground and ^1L_b states is characterized by radial motion in the phenyl and pyrrole rings, according to both semi empirical[9] and ab initio methods.[10] When used with ground state normal modes and frequencies calculated at a correlated level of theory, the ab initio geometry difference reproduces indole's ^1L_b dispersed fluorescence spectrum to a considerable extent. This study showed, for instance, that the mode describing radial deformation of the benzene ring carries much more intensity than any other vibration, in agreement with the observed spectrum. The semi empirical spectrum is less accurate. The geometry difference between the ground and ^1L_a states is characterized by a deformation of the C2-C3 and C6-C7 bond lengths, as both the semi empirical and ab initio analyses have revealed, and the dispersed fluorescence from this state has intensity distributed fairly evenly between three ring-stretching normal modes.

The accuracy of vibronic spectra calculated within the clamped-nuclei

approximation is sometimes worsened by geometrical distortion-induced mixing between electronic states, or vibronic coupling. That is, the nuclear displacement due to vibrational zero-point motion mixes Born-Oppenheimer states to an extent dictated to first order in perturbation theory by the quotient of the vibronic coupling matrix element and the separation in energy between the interacting electronic states.[11] Consequently, Franck-Condon forbidden transitions may acquire intensity or allowed transitions may gain intensity, such as indole's mode 28. The Franck-Condon factor for mode 28 is underestimated in the aforementioned calculated ^1L_b emission spectrum because of unaccounted vibrationally acquired ^1L_a intensity.

1:1 and 1:2 Indole:Water Complexes

The most widely celebrated spectroscopic difference between isolated and solvated indole is the differential shift of its fluorescence emission.[12] Polar solvents cause a large red shift in indole's emission band while having a modest effect on the position of the absorption band. Only to a much smaller extent do polar environments shift emission from other amino substituted aromatic molecules. The size of the red shift is important because it depends on the extent to which the indole chromophore is exposed to the surrounding medium and therefore provides information regarding the structure and environment of proteins.

The reason for the vast difference between indole and similar molecules has been thoroughly debated. It is often argued that indole's red shift results from the interaction with the dipolar reaction field.[13] This is the dipole formed in the medium

surrounding the solute by the reorientation of solvent molecule electrons and nuclei in response to the solute's presence. According to this model, the excited states are preferentially stabilized by a larger projection onto the ground state reaction field and, to an even greater degree, by inducing a larger reaction field. The stabilization is particularly pronounced in the ^1L_a state, which has a dipole 6 Debye larger than that of the ^1L_b or ground states according to both experiment[14] and high level theory.[5] In keeping with this expectation, studies of the degree to which indole's emission is shifted as a function of solvent polarity show an abrupt increase on going to solvents of intermediate polarity, signifying an abrupt change in the dipole of the fluorescing state and suggesting an inversion between ^1L_a and ^1L_b.[15]

An alternative model of indole's solvatochromism postulates that the electronically excited indole ring forms a much stronger hydrogen bond than the ground state species, i.e., forms exciplexes. The exciplex hypothesis arose from studies of the extent to which indole's emission is shifted as a function of alcohol concentration in hydrocarbon cosolvent.[16] A significant shift is obtained in extremely dilute solutions (~0.001 M), suggesting that the dielectric properties of the surrounding medium are virtually immaterial in this regard. A specific interaction, an interaction between specific molecular sites, was then proposed to exist between electronically excited indole and the polar solvent molecules.[16,17] The π cloud above C3 has been suggested as the interaction site based on the correlation between the (ground state) basicity of this atom and spectral broadening and shifting.[17] The absence of red-shifted emission in fluorescence from 5-methoxy indole,[18] a molecule of comparatively low

polarity, prompted speculation that the exciplex is mainly dipole-dipole in nature and therefore involves ^1L_a.

Evidence of exciplex formation between indole and water has been sought from jet-cooled spectroscopy, which provides the low temperatures needed to study interactions of this strength. Two cluster origins are found in the jet-cooled fluorescence excitation[19] and dispersed fluorescence[20] spectra, implying two conformations or stoichiometries. Rotationally resolved fluorescence spectra indicated,[21] and resonance enhanced multiphoton ionization spectra later proved,[22] that the less red-shifted origin, 131 cm^{-1} from the ^1L_b bare molecule origin, is a 1:1 complex. As inferred from the high resolution spectrum, the monomers are associated in a σ-complex, where the N-H group acts as a hydrogen donor to the water molecule.

The other cluster origin in the excitation spectrum, red-shifted 434 cm^{-1}, was thought to arise from a 1:1 interaction based on mass spectral data,[20] but has been conclusively assigned a 1:2 stoichiometry based on a combination of spectroscopic methods.[22] (The 1:2 cluster cation apparently dissociates before mass selection.) Based mainly on its broad and unstructured appearance, fluorescence emission from this origin was thought to be from a ^1L_a state greatly stabilized by an interaction involving C3,[20] but has since been conclusively attributed to an ^1L_b transition, like the σ-complex, based on two-photon absorptivity ratios.[23]

Thus, jet-cooled spectra provides no support for the exciplex model. However, the interaction with indole's π cloud will remain important regardless of the outcome of this debate. This is demonstrated by the fluorescence emission from N-methyl

indole, which is also red-shifted in polar solvents, only at higher concentrations.[16] Environment effects the solvatochromism of indole and N-methyl indole in the same manner, causing an abrupt increase in the red shift on going to solvents of intermediate polarity.[15] Furthermore, the jet-cooled multiphoton ionization spectrum of N-methyl indole in the presence of water shows a shifted origin.[20] The spectrum contains a very long progression of vibronic lines, indicating that the minimum is substantially displaced along an intermolecular mode upon excitation, as expected for a $\pi \rightarrow \pi^*$ transition of a π-complex. Formation of an N-methyl indole π-complex would also be anticipated based on the 1:1 benzene:water rotational spectrum, which is consistent with a structure where the water moiety is above the π cloud.[24]

Solvation has other important spectroscopic consequences. It may affect the strength of vibronic interactions by altering normal coordinates or the electronic manifold. It may also affect spectral resolution. The large ^1L_a dipole results in structureless condensed phase emission due to inhomogeneous broadening, the distribution of transition energies resulting from a distribution of chromophore environments. Surprisingly, the ^3L_a dipole is small and indole's phosphorescence is comparatively sharp in polar solution. The energy of ^3L_a indole is[25] (or is not[6]) sensitive to environment. Other information, such as the local rigidity of proteins and the solvent viscosity of protein environments, may be established from the lifetime of indole's ^3L_a state.[26]

3-Methyl Indole and 5-Methyl Indole

The separation between ^1L_a and ^1L_b is greatly decreased by 3-methyl

substitution, which increases the extent of mixing between adiabatic states. Thus, measurements of 3-methyl indole's two-photon polarization ratios in the supersonic jet show increased ^1L_a character in the ^1L_b origin, in comparison to indole, and ^1L_a character in the low frequency vibrations.[27] The ^1L_a origin is split between several peaks from 300 to 900 cm^{-1} to the blue of the ^1L_b origin. The mixing is severe near avoided crossings, the regions of an adiabatic potential energy surface where two states with the same symmetry are nearly degenerate, because of a very small energy denominator in the first-order correction to the wave function.

The methyl group also introduces additional states to the rovibronic manifold and the possibility for additional progressions in the vibronic spectra. The jet-cooled spectrum reveals slight methyl rotor activity in 3-methyl indole,[28] indicating that the torsional potential undergoes a change in amplitude, but not phase, upon excitation. The barrier to rotation is larger in the ground state than the excited states, particularly the ^1L_a state, and the ground and ^1L_b barriers are similar in size to those of methyl alkenes. In contrast, 5-methyl indole shows ample Franck-Condon activity in the methyl torsion mode upon ^1L_b excitation[28,29] and barrier sizes in each state like those of methyl benzenes. The length and pattern of 5-methyl indole's torsional progression implies a 60° change in the conformation of the methyl group upon excitation.

Statement of the Problem

Part of this thesis presents the results of an effort to determine and test a simple non-empirical model for representing the indole's lower excited electronic manifold.

the ab initio model employed therein failed in a very fundamental sense. This study used excited state geometries obtained with the full Configuration Interaction - Singles (CIS) method, which expresses the wave function as a spin-adapted linear combination of configurations formed from all possible replacements of a single molecular orbital (MO) that is occupied in the Hartree-Fock (HF) determinant with an unoccupied MO of the self-consistent field (SCF) calculation. Unfortunately, the 'singles only' approximation causes ^1L_a indole to fall below ^1L_b, with an adiabatic separation of 1,000 cm^{-1} at CIS/3-21G. The incorrect ordering makes spectra and other full CIS properties more pertinent to indole perturbed by an external electric field. Comparing these results with experimental data from isolated molecule conditions is not completely justified.

Additional calculations are aimed at appraising the validity of the exciplex interpretation of the indoles' solvatochromism. Although jet-cooled spectra have provided a great deal of data about the energetics, dynamical behavior, and structure of indole's complexes with polar solvents in the ground and excited states, there are limitations to their informativeness. For example, this technique provides no information regarding the ^1L_a complexes, aside from their being less stable than those of the ^1L_b state. No information is provided in regards to the π-complex, aside from it being less stable than the σ-complex. Jet-cooled spectra contain no information regarding absolute binding energies, nor may detailed information be gleaned in regards to the geometry of the 1:2 complex. Ab initio calculations are needed for these purposes. Calculations take on added significance in the case of the excited state

1:2 3-methyl indole:water complex. One would expect the origin of the 1:2 3-methyl indole:water complex to appear approximately 500 cm^{-1} to the red of the bare molecule origin in the fluorescence excitation[30] and dispersed fluorescence[20] spectra. For unknown reasons, the 1:2 complex origin is absent from these spectra. Thus, whether ^1L_a or ^1L_b is the lowest excited state remains undetermined.

A complete theoretical investigation of hydrogen bonding must take into account the quantum dynamical behavior of weakly associated molecules. The potential energy surface of such a system may be rather flat along one or more of the intermolecular coordinates, with zero-point motion resulting in large displacements from the energy minimum geometry. The optimized geometry is then of reduced significance because the orientation at the minimum may differ considerably from the vibrationally averaged position. Normal coordinate analyses are also of reduced significance because they only provide information in the region of the minimum. More importantly, molecular complexes may have more than one minimum, such as the σ- and π-complex, that may interconvert through quantum mechanical tunneling, resulting in anharmonicity. Thus, an emphasis must be placed on the probability densities and eigenvalues of the indole:water bound state wave functions rather than the energy minimum geometry and the normal modes of vibration.

Chapter 2

COMPUTATIONAL METHODS

All calculations were performed on an Indigo2 Silicon Graphics, Incorporated workstation with a R4400 200Mhz processor, 6 Gigabytes of disk space, and 160 Megabytes of RAM. Unless otherwise noted, all ab initio calculations were performed with the Gaussian 92 or Gaussian 94 quantum chemical program packages.[31] The internally stored basis sets of these programs were used without modification, unless otherwise noted.

Geometry Optimizations

Optimized geometries were obtained through minimization of the energy gradient by including the 'FOPT' keyword in the route card of the input file. Transition state optimizations require the 'OPT=TS' command. Molecular structure was specified in cartesian coordinates and the default Berni optimization procedure[32] was used. This algorithm calculates the gradient of the energy by interpolation and estimates or updates the second derivative matrix (the hessian). The gradient gives the direction in which the potential energy changes fastest and the hessian indicates where along the gradient a stationary point is present. For a harmonic surface, the product of the inverse of the hessian and the energy gradient yields the displacement along each dimension of parameter space needed to reach the nearest stationary point. For an

anharmonic surface, this product does not necessarily yield a stationary point and the gradient and hessian must be recalculated at the new geometry. Thus, the number of steps taken near the minimum is indicative of the anharmonicity of the potential energy surface. The geometry is considered converged when the norm of the energy gradient falls below the threshold value of 0.0001 atomic units, by default.

The frozen core approximation, which is the default, was used in all MP2 and CIS calculations, unless otherwise noted. With Gaussian 94, the CIS expansion may be further truncated by specifying the 'RW' option with the 'CIS' keyword in the route card. Ground and excited state CISD calculations were performed with the General Atomic and Molecular Electronic Structure System suite of ab initio programs,[33] or GAMESS, by specifying the appropriate variables in the '$DRT' input group. For excited state calculations, the state identities were confirmed by determining the direction of the transition dipole moment. A small Fortran program was written for this purpose, as the absence of symmetry in some systems made it too difficult to do this by inspection.

Mulliken Populations

Including the 'POP(FULL,BONDING)' command in the route card of the input file causes the density matrix and the bonding density matrix to be printed in the output file. The 'DENSITY=CI' or 'DENSITY=CURRENT' command must be used for access to the CIS generalized density matrix or MP2 density matrix. A small Fortran program was written to read these results and calculate the σ- and π-electron Mulliken populations and Mulliken overlap populations. The 'MOLPLT' utility

program of GAMESS was modified to create the population difference figures.

Projection Density Contour Maps

Density grids were constructed of the ground, ^1L_a, and ^3L_a states at the ground and ^1L_a geometries using the 6-31G(p,d) basis set. This is accomplished with the 'CUBE(DENSITY,FULL)' keyword and options. The SCF and CIS densities were used in the ground and excited states, respectively. The 'FULL' option specifies the inclusion of all electrons in the CIS calculation. The grid spacing was at 0.1 Å along the in-plane coordinate axes of the 'STANDARD ORIENTATION' of Gaussian94, which places the center of mass at the origin. The grid extended out to 5.0 Å from the origin along both in-plane coordinates. In order to create the projection density maps, this procedure was repeated from 0.0 to 4.0 Å above the molecular plane at increments of 0.1 Å. A small Fortran program was written to perform Simpson's rule integration at each in-plane grid point over the coordinate perpendicular to the molecular plane. Finally, the 'CUBMAN' utility program of GAUSSIAN was used to subtract the integrated densities, and the 'PLTORB' utility program of GAMESS was modified to produce the contour plots.

Dipole Moment Matrix Elements

Single point calculations at the CIS/3-21G level were performed on indole at its optimized ^1L_a geometry to obtain CIS coefficients for the ^1L_a and ^3L_a electronic states. All of the valence and core electrons were included in each CIS calculation. The keyword 'IOP(9/42=5)' was included in the route card of each input file so that all

CIS coefficients greater than or equal to 10^{-3} would be included in the output files. The keywords 'IOP(3/33=1)' and 'POP=FULL' were also included in the route cards in order to obtain the dipole moment matrix elements in the atomic orbital basis and the molecular orbital (MO) coefficients, respectively. As a test of the effects of basis, all calculations were repeated at CIS/6-31G(p,d). As a test of the effects of geometry, the CIS/3-21G single point calculations were repeated at the ^1L_b CIS/3-21G optimized geometry of indole, with the 'ROOT=2' option used in the ^1L_a case. The ^1L_a and ^1L_b optimized geometries were chosen so as to minimize the effects of mixing between these states, which leads to less meaningful results. At either geometry the ^3L_a state lies too far in energy below other triplet states for any significant mixing to occur.

A Fortran program was written that, using the data from these CIS single point calculations, converts the dipole moment matrix elements from the atomic orbital basis, $M^n_{\mu\nu,\lambda\sigma}$, to the CI basis, $M^n_{ij,kl}$, in terms of which the nth component of the molecular dipole moment, M^n, may be expressed as

$$M^n = \sum_{ij}\sum_{kl} M^n_{ij,kl} = \sum_{ij}\sum_{kl} a_{ij}a_{kl}\langle i \rightarrow j \,|\, m_n \,|\, k \rightarrow l\rangle \qquad (2.1)$$

Here i and k represent one of the MOs occupied in the ground state while j and l represent virtual MOs and the sums are over all possible pairs of occupied and virtual MOs. The a_{ij} and a_{kl} are coefficients for the $|i \rightarrow j\rangle$ and $|k \rightarrow l\rangle$ configurations in the CIS wave function, $\Psi_{CIS} = \sum a_{ij}|i \rightarrow j\rangle$, and m_n is the nth component of the dipole moment operator. The task of determining the CIS dipole matrix elements may be readily accomplished in the density matrix formulation of quantum theory. The diagonal elements (i = k and j = l) are given by

$$M^{n}_{ij,kl} = \left(\sum_{k} 2\rho^{kk} - \rho^{ii} + \rho^{ij}\right):M^{n}_{\mu\nu,\lambda\sigma} \qquad (2.2)$$

with $\rho^{kk} = c_k c_k^{\dagger}$ being the N × N matrix, N equalling the number of basis functions, formed by the product between the MO k coefficient column vector c_k and row vector $c_k^{\dagger}$ and the sum being taken over the p MOs occupied in the ground state. The symbol ":" is used to denote a double dot product between ρ^{kk} and $M^{n}_{\mu\nu,\lambda\sigma}$ (the sum of the products between corresponding matrix elements). The off-diagonal elements of Eqn. (2.1) ($i \neq k$ or $j \neq l$) are given by

$$M^{n}_{ij,kl} = \left(\rho^{ij}\delta_{kl} - \rho^{kl}\delta_{ij}\right):M^{n}_{\mu\nu,\lambda\sigma} \qquad (2.3)$$

The rules for evaluating matrix elements of a one-electron operator between singly substituted determinants stipulate that the $M^{n}_{ij,kl}$ vanish when $i \neq k$ and $j \neq l$. The diagonal elements may therefore be written more compactly as $M^{n}_{i,j}$ and the off - diagonal elements may be written as $M^{n}_{i,k}$ or $M^{n}_{j,l}$.

The use of Eqns. (2.2) and (2.3) in Eqn. (2.1) gives the 1 particle density matrix (1PDM) result for the dipole moment.

Normal Coordinates

All normal coordinate analyses were performed at stationary points, using the 'FREQ' command in the route card. The vibrational frequencies are determined by first calculating the second derivative matrix of the energy with respect to cartesian displacement coordinates. Frequency calculations at the Hartree-Fock level compute the first and second derivative analytically,[34] as do those at the CIS level, while MP2 frequency calculations compute the second derivatives from the finite difference

approximation using analytical first derivatives[34] ('FREQ=NUMER'). The hessian matrix elements are divided by mass-weighted coordinates and then diagonalized to produce the eigenvalues, which are finally converted to frequencies. The number of imaginary frequencies thereby obtained characterizes the nature of the stationary point - an nth order saddle point yields n imaginary frequencies. The 3 rotations and 3 translations, or 'zero frequencies', will be zero only if the calculation is performed precisely at a minimum. The size of the zero frequencies therefore characterizes the quality of calculation. Figures of the normal modes were produced with a modified version of the 'MOLPLT' graphics utility program of GAMESS.

Calculated Spectra

In order to properly calculate vibronic spectra, it is necessary for the ground and excited state geometries to differ neither by translational motion nor by rotational motion. This means that the center of mass and the moments of inertia of both structures must be identical. A Fortran program written by P. R. Callis, 'xyz6b.f', was used to satisfy both conditions. Typically, the excited state geometry was manipulated until differing from the ground state by less than 10^{-2} $Å^2$g/mol in angular momentum around any one axis. Further improvements in this regard were found to have a negligible impact on the calculated spectra. A Fortran program written by J. T. Vivian,[35] based on the Doktorov method,[36] was used to calculate the vibronic spectra. This program exploits no simplifications aside from the normal mode approximation. The intensities of all transitions up to ten vibrational quanta were calculated. Absorption spectra were weighted by the transition frequency and emission spectra was

weighted by the cube of the transition frequency, in keeping with the appropriate Einstein coefficient of each process. Finally, the spectra were broadened to simulate the jet cooled spectra, or to simulate the effects of hot bands and inhomogeneous broadening to the extent of the gas phase.

Binding Energies

The binding energies, ΔE_b, of the ground state and excited state complexes were calculated using the supermolecule method. This approach treats the complex as a single molecule, or "supermolecule", on which a geometry optimization is performed in order to obtain a minimum energy. Because the basis sets are truncated each monomer may use the functions centered on the other monomer to improve the description of its electron distribution when the energy of the dimer is calculated. This leads to the Basis Set Superposition Error (BSSE), which results in an unphysical lowering of the dimer's energy and an exaggerated binding energy. The BSSE correction to ΔE_b was computed using the full counterpoise method of Boys and Bernardi.[37] For each complex, this entails that the energy of each monomer be computed with and without the basis functions of the other monomer present. In Gaussian94, the former calculation may be accomplished by including the "MASSAGE' keyword in the route card, and entering the molecule whose energy is not being calculated as 'ghost atoms'. Thus,

$$\Delta e_b = \Delta E_{int} - \text{BSSE} - \Delta\text{ZPE}$$

where ΔE_{int} and ΔZPE are differences in electronic and vibrational energy between the complex and the monomers at 0 K. For the ground state,

$$\Delta E_{int} = E_{complex}(HF) - E_{indole}(HF) - nE_{H_2O}(HF)$$

$$\Delta ZPE = ZPE_{complex}(HF) - ZPE_{indole}(HF) - nZPE_{H_2O}(HF)$$

and for the excited states,

$$\Delta E_{int} = E_{complex}(CIS) - E_{indole}(CIS) - nE_{H_2O}(HF)$$

$$\Delta ZPE = ZPE_{complex}(CIS) - ZPE_{indole}(CIS) - nZPE_{H_2O}(HF)$$

or

$$\Delta E_{int} = E_{complex}(CIS\text{-}MP2) - E_{indole}(CIS\text{-}MP2) - nE_{H_2O}(MP2)$$

$$\Delta ZPE = ZPE_{complex}(CIS\text{-}MP2) - ZPE_{indole}(CIS\text{-}MP2) - nZPE_{H_2O}(MP2)$$

with the theoretical method used in the calculation enclosed by parentheses and n referring to the number of water molecules in the complex. Both the CIS and the CIS-MP2 methods are size consistent, i.e., they correctly predict a binding energy of zero for two infinitely separated fragments. The Hartree-Fock method is size consistent only when the isolated fragments are closed shell species, as is the case for indole and water in the ground state. Of all these methods, only the Hartree-Fock and CIS methods are variational, but the difference between two variational energies is not necessarily variational.

Morokuma Energy Decomposition

One of the drawbacks of the supermolecule method is its inability to provide information about the intermolecular forces at play in a molecular complex. The binding energy may receive contributions from five types of interactions - electrostatic, polarization, exchange, charge transfer, and dispersion.[38] The supermolecule method

only provides their sum. A Morokuma decomposition[38] of the Hartree-Fock interaction energy of the 1:1 indole:water complexes was therefore performed using GAMESS with the 6-31G basis. Because this type of calculation requires a great deal of disk space, larger basis sets could not be used. In order for the SCF calculation to converge, it was necessary to specify the 'DAMP=TRUE' parameter of the '$SCF' input group. This damps the oscillation between several successive Fock matrices in the SCF procedure. It was also necessary to increase the maximum number of SCF cycle iterations to 60 with the 'MAXIT' parameter of the '$CONTROL' input group.

Intermolecular Bound States

A coarse grid of the 1:1 indole:water complex intermolecular potential energy surface was constructed at the Hartree-Fock (HF) level of theory using the 6-31++G(p,d) basis set. With indole constrained to its uncomplexed HF/6-31++G(p,d) geometry, the water oxygen was held fixed at each grid point above or beside indole's plane while the remaining geometrical parameters were optimized, including the intermolecular distance. Freezing the geometry of the indole moiety assumes that its intramolecular modes are decoupled from the intermolecular modes, a safe assumption when the contribution to the binding energy associated with relaxation of the monomer geometry is small. The intermolecular potential was sampled in this manner at a total of 40 grid points, mostly near either minima. The spacing of the grid was 0.8 Å along lines parallel to the long and short axes of indole. The potential at all remaining points was obtained by interpolation or extrapolation. Finally, the potential energy surface was smoothed by averaging.

The bound state calculations treated the water moiety as a single particle. A Fortran program for solving the radial Schrödinger Equation, based on the method of Kimball and Shortley[39], was obtained from the Quantum Chemistry Program Exchange and modified to calculate the two-dimensional van der Waals vibrational wave functions and energy levels. The method of Kimball and Shortley treats the wave function as a numerical representation, i.e., as a discrete function of position rather than a continuous function, so that the Schrödinger Equation becomes a difference equation rather than a differential equation. Consequently, the value of the wave function at each lattice point may expressed in terms of itself and the wave function at each adjacent point. The variation theory then leads to an improvement equation for the wave function at each lattice point, an equation that lowers the calculated energy contingent on a sufficiently fine lattice. Point by point application of the improvement equation at each lattice point lowers the energy of the system if the lattice spacing is sufficiently small.

A lattice of 400 square points was used herein for the ground state and increased by increments 50 for each successive pair of higher energy excited states. The process of applying the improvement equation at each point is repeated until the energy difference between successive iterations fall below a specified threshold, taken herein as 0.2 cm^{-1}. The numerical solution becomes more exact, i.e., converges to that of the differential equation, as the lattice spacing is decreased.

As a test of the program, the ten lowest eigenstates were calculated for a two-dimensional quadratic potential. Finally, the utility program 'PLTORB' of the ab initio

program package GAMESS was modified to generate the contour plots.

Methyl Torsion Potential Energy Curves

A small Fortran program was written for rotating the methyl indoles around the exocyclic bond axis. Hartree-Fock or CIS single point calculations were taken with the methyl group rotated from 0 to 60° in increments of 5° from the equilibrium position in the ground, ^1L_a, and ^1L_b states. Because indole possesses no rotational symmetry around any of its C-H or N-H bond axes, the torsional potential of the methyl indoles contain only 3 equivalent minima corresponding to the threefold symmetry of the methyl group. Data points from 65 to 120° were therefore obtained by reflection. The methyl rotor barriers were calculated as the difference between the rotated and the energy minimum geometry.

Chapter 3

RESULTS AND DISCUSSION

Indole

Transition Energies

The transition energies between the states comprising indole's lower electronic manifold are presented in Tables 1 and 2. The vertical transition energy, ν, is calculated at the ground state Hartree-Fock geometry of each basis set while the adiabatic transition energy, $\nu_{0\text{-}0}$, is the difference between the zero point vibrational levels at the optimized geometries of the combining states. Increasing the basis size, particularly with diffuse functions, is shown to lower the excited singlet states with respect to the ground state, particularly ^1L_a, at both the vertical and adiabatic separation. Going to the triple zeta basis has a meager impact on the vertical transitions, however, suggesting a proximity to the theoretical limit in this property at CIS/6-311++G(p,d). In spite of the sizeable basis, the vertical ^1L_a and ^1L_b transitions are overestimated by about 7,000 cm^{-1} and 11,000 cm^{-1}, respectively, a result typical at this level of theory. One concludes that electron correlation lowers both excited states with respect to the ground state, assuming an equivalency in this regard between the Hartree-Fock and CIS singlet wave functions.

The incorrect ordering of the excited states in the CIS manifold is more

Table 1. Indole G → ^1L_a, ^1L_b transition energies (10^{-3} cm^{-1})

	^1L_a		^1L_b	
basis	ν	$\nu_{0\text{-}0}$	ν	$\nu_{0\text{-}0}$
3-21G	50.2	46.3	50.1	47.3
4-31G	49.7	46.1	49.8	46.9
6-31G	49.0	45.5	49.2	46.3
6-31G**	48.0	44.4	48.3	
6-31+G**	45.8	42.2[a]	46.5	
6-31++G**	45.8		46.5	
6-311++G**	45.7		46.4	
CIS(9,9)/6-31G		50.6		48.1
CIS(11,11)/6-31G	52.6	50.1	50.1	47.9
CIS(13,13)/6-31G		50.0		47.7
CIS(13,14)/6-31G	52.3	50.1	50.0	47.7
CIS(22,22)/6-31G	51.0		49.7	
CISD(11,11)/6-31G[c]	60.9		50.0	
CISD(22,22)/6-31G[c]	87.4		79.6	
EXP		~36.5[e]		35.2[b]
EXP[d]	38.9		35.2	

[a]Using HF/6-31G(p,d) & CIS/6-31G(p,d) zero point energies. [b]Reference 40.
[c]CISD/6-31G//HF/6-31G. [d]Reference 3. [e]Reference 2.

disconcerting than the absolute values of the transition energies. At CIS/6-31G the adiabatic separation is about 1,000 cm^{-1}, with ^1L_a beneath ^1L_b. However, it is possible to correct this situation by modifying the computational procedure in a very simple way. As mentioned, the full CIS wave function is formed by summing over all possible determinants obtained by replacing one of the occupied MOs in the Hartree-Fock wave function with a virtual MO of the corresponding SCF calculation. By retaining only the determinants formed from transitions between a small number of high energy occupied MOs and low energy virtual MOs for the CI calculation, it is seen from Table 1 that the correct ordering is obtained. When the 11 HOMOs and 11

LUMOs bracketing the Fermi level are retained, for example, in conjunction with the 6-31G atomic basis functions, indole's ^1L_b state is more stable than ^1L_a by 2,200 cm^{-1} in the adiabatic sense. This result is reasonably close to the observed separation of ~1,400 cm^{-1} between the ^1L_a and ^1L_b origins in the jet-cooled spectrum.[2] The ^1L_a state is above ^1L_b by over 800 cm^{-1} at the ^1L_a minimum, which is also realistic. However, the predicted vertical gap of 2,500 cm^{-1} underestimates the observed separation of 3,700 cm^{-1} between the intensity maxima of the ^1L_a and ^1L_b absorption bands,[3] indicating that the energy of one or both of these states is not sufficiently sensitive to geometry in this model. Including a few more determinants in the CI calculation causes ^1L_a to converge on the ^1L_b geometry during the energy minimization. With still more determinants, the unwanted inversion occurs.

The practice of truncating the summations is commonly used for CI methods involving multiply substituted configurations because of their enormous disk space requirements, but this option is not often exercised at the CIS level. Following the usual convention, the truncated CIS expansion is denoted herein as CIS(I,J), with I and J the number of occupied and unoccupied MOs bracketing the Fermi level between which transitions are considered in forming the excited state wave function. In addition to the modelling benefits, truncating the CIS expansion is preferable from the vantage point of computational cost. A CIS/6-31G single point calculation on indole, for instance, requires 19 minutes of CPU time using the computer referred to in Chapter 2, but less than 13 minutes of CPU time at CIS(11,11)/6-31G.

By truncating the CIS summations, determinants formed by excitation from relatively compact occupied orbitals, or by excitation to relatively diffuse virtual

orbitals, are omitted from the excited state wave function. As Table 1 shows, the ^1L_a state is raised by 3,600 cm^{-1} on going from CIS/6-31G to CIS(11,11)/6-31G, compared to a mere 900 cm^{-1} elevation of the ^1L_b state. This suggests a less compact distribution of electron density in the ^1L_a state in at least one portion of indole, a notion that is supported by the comparatively larger elements in the ^1L_a CIS/6-31G polarizability tensor. It is also fitting that the ^1L_a state shows greater sensitivity to diffuse functions in Table 1. Apparently, the preferential stabilization of ^1L_a brought about by the aforementioned determinants roughly matches the preferential stabilization of ^1L_b brought about by doubly substituted configurations,[41] resulting in a properly ordered manifold at CIS(11,11)/6-31G.

The transition energies between the ground and lower triplet states of indole are shown in Table 2. As noted,[5] an approximate value may be obtained for the vertical transition energy by reflecting indole's phosphorescence spectrum, the onset of which appears at 24,762 cm^{-1} and the maximum of which appears at 23,149 cm^{-1}. This gives ν = 26,375 cm^{-1}, in excellent agreement with the present calculations. In further contrast to the singlet states, the vertical transition energy is very insensitive to basis set size, suggesting a proximity to the theoretical limit in this quantity.

Two sets of values are given in Table 2 for the adiabatic $G \rightarrow T_1$ transition because, with the full CIS method, two energy minimum conformations are found for indole's lowest triplet state. The planar conformation is the global minimum, being 236 cm^{-1} more stable than the non-planar conformation at CIS/6-31G(p,d). The barrier between the two conformations amounts to 54 cm^{-1} relative the global minimum, according to a CIS/6-31G(p,d) transition state optimization. Regardless of the excited

Table 2. Indole G → T_n (n= 1, 2, 3) transition energies (10^{-3} cm^{-1})

	T_1		T_2	T_3
basis	ν	ν_{0-0}	ν	ν
3-21G	27.0	22.1	36.1	40.9
4-31G	26.4	21.7	35.4	40.7
6-31G	26.7	21.5	35.3	39.8
6-31G*	26.5		35.1	39.5
6-31G**	26.5	21.7	35.0	39.5
6-31+G**		21.6[d]		
6-31++G**	26.3		34.5	38.6
CIS(11,11)/6-31G	28.8	24.6	37.4	41.5
3-21G[a]		22.3		
6-31G**[a]		22.0		
UHF/3-21G		16.2		
UHF/6-31G**		15.2		
EXP[b]	~26.4	24.8		
EXP[c]		24.8		
EXP[e]		24.2		

[a]Non-planar configuration. [b]Reference 6. [c]Reference 7. [d]From HF/6-31G(p,d) & CIS/6-31G(p,d) zero point energies. [e]Reference 42.

state's conformation, the adiabatic separation is reasonably well described by, and fairly basis set insensitive within, the CIS method, as shown in the Table.

One concludes that the CIS wave function represents indole's ^3L_a state much better than ^1L_a or ^1L_b, but a more general statement is possible. Being spin-adapted, the CIS triplet wave function is the antisymmetric combination of determinants obtained from single α and ß electron excitations, while the singlet state is the symmetric combination. For a two electron system the triplet state wave function therefore vanishes when the electrons are at the same point in space, resulting in

correlated motion. For a more general system there is a measure of correlation between the unpaired electrons in the triplet state. The added correlation relative to the Hartree-Fock ground state results in a slight underestimation of the transition energy, or sometimes a smaller overestimation than that of the corresponding singlet state. The latter circumstance is apparent in the CIS study of pyridine.[43]

The accuracy of the ^3L_a CIS transition energy does not guarantee a similar level of agreement when this method is applied to T_2 and T_3. T_2 indole lies 8,200 cm^{-1} above ^3L_a at CIS/6-31+G(p,d), compared to a 4,800 cm^{-1} vertical separation in the complete active space - SCF calculation (CASPT2),[5] where all possible substitutions are considered between a limited number of configurations, serving as a reference for a second order perturbation theory calculation. This approach is usually more accurate than the CIS method (but overestimates the energy of T_1 indole by 4,000 cm^{-1}). Indole's T_3 state is 12,300 cm^{-1} above ^3L_a at CIS/6-31+G(p,d) and 10,600 cm^{-1} above ^3L_a according to the CASPT2 study. Thus, neither method predicts a dense triplet manifold near ^1L_b. Indole's triplet-triplet absorption spectrum contains a single strong band at 23,200 cm^{-1},[6] attributed to a $T_1 \rightarrow T_{13}$ transition in the CASPT2 study.

Only the non-planar geometry is a minimum energy conformation at UHF/3-21G or UHF/6-31G(p,d). The completely planar structure is a transition state, less stable than the global minimum by 2,436 cm^{-1} at UHF/6-31G(p,d). The normal coordinate of the imaginary frequency is the C2-H2 motion connecting the equivalent minima. As shown in Table 2, the UHF transition energy is much smaller than the CIS result or the observed value, probably due mainly to spin contamination. Being a single, open shell determinant, the UHF wave function is not necessarily an

eigenfunction of the S^2 operator. T_1 indole at UHF/6-31G(p,d), for instance, has an S^2 eigenvalue of 2.60, or 2.22 after annihilation of the first spin contaminant, rather than 2. This means that the UHF state is mixed with higher multiplicity, higher energy states, which artificially lowers its energy. (With the loss of C_s symmetry in the non-planar configuration, mixing between erstwhile σ and π MOs is possible and the classification scheme of Platt[1] is no longer appropriate.)

There is also an extra measure of correlation at the UHF level that further lowers the T_1 state relative to the RHF ground state; the α and ß electrons are not restricted to the same spatial orbitals in the UHF method, which correlates their motion to a certain extent.

Transition Properties

Indole's transition moments are defined in terms of a vector of magnitude μ originating from the C8-C9 bond midpoint and forming an angle θ with the long axis. Indole's long axis is the imaginary line that intersects the equilibrium C2 position and bisects the equilibrium C6-C7 bond. Negative values of θ correspond to clockwise rotation of the transition dipole vector from the long axis. The phase of θ is arbitrary because it depends on the arbitrary phases of the combining states. The tabulated direction of polarization is therefore equivalent to the resultant obtained by rotating the transition dipole vector by 180°.

The ^1L_a and ^1L_b states of indole are mixed at the HF/3-21G equilibrium geometry, resulting in transition dipoles and oscillator strengths in considerable discord with the observed values (Table 3). As the size of the basis set is increased, the interstate properties fluctuate considerably, particularly the polarization of the ^1L_b

Table 3. Indole G → ^1L_a, ^1L_b transition properties

	^1L_a				^1L_b			
basis	Θ[a]	f[b]	Φ[c]	F[d]	Θ	f	Φ	F
3-21G	-9.2	0.132	-30.9	0.352	71.6	0.088	36.7	0.100
4-31G	-37.8	0.164	-30.2	0.352	36.3	0.057	28.3	0.095
6-31G	-38.4	0.164	-29.5	0.348	34.8	0.056	29.5	0.092
6-31G**	-30.3	0.151	-28.9	0.324	48.4	0.050		
6-31+G**	-30.2	0.173	-27.2	0.350	46.5	0.058		
6-31++G**	-30.7	0.173			38.2	0.058		
6-311++G**	-29.4	0.166			38.6	0.055		
CIS(11,11)/6-31G	-39.2	0.183	-37.7	0.331	38.5	0.042	38.2	0.056
CIS(13,14)/6-31G	-38.1	0.188	-38.5	0.311	35.9	0.045	36.0	0.064
CIS(22,22)/6-31G	-39.5	0.185			30.0	0.055		
CSD(11,11)/6-31G[f]	-41.8	0.126			45.6	0.019		
CSD(22,22)/6-31G[f]	-44.0	0.169			47.0	0.031		
EXP[e]	-54	0.12			38			
EXP[g]	±45							
EXP[h]	-42				46	0.012		
EXP[i]					38			

[a]Transition dipole moment direction, in degrees, calculated at ground state geometry. [b]Oscillator strength calculated at ground state geometry. [c]Transition dipole moment direction, in degrees, at excited state geometry. [d]Oscillator strength at excited state geometry. [e]Reference 44. [f]CISD/6-31G//HF/6-31G. [g]Reference 45. [h]Reference 46. [i]Reference 47.

transition, instead of converging on a certain value. The greater sensitivity of the ^1L_b transition moment may be traced to the dominance of the HOMO→LUMO+1 and HOMO-1→LUMO configurations in the ^1L_b wave function (Tables 4 and 5). For benzene, the transition moments of these configurations are equal in magnitude and opposite in direction, resulting in cancellation and the parity forbidden nature of the ^1L_b transition. For indole, the cancellation is not total. The (1PDM) transition moment

Table 4. Indole optimum CIS coefficients

	^3L_a				^1L_a				^1L_b	
π MOs	3-21G	6-31G	6-31G**	6-31+G**	3-21G	6-31G	6-31G**	6-31+G**	3-21G	6-31G
HO→ LU	0.63	0.63	0.63	0.56	0.65	0.64	0.64	0.63	<|0.10|	<|0.10|
HO→LU+1	<|0.10|	<|0.10|	<|0.10|	0.17	<|0.10|	<|0.10|	<|0.10|	0.12	-0.33	-0.34
HO→LU+2	<|0.10|	<|0.10|	<|0.10|	-0.14	<|0.10|	<|0.10|	<|0.10|	<|0.10|	<|0.10|	<|0.10|
HO-1→LU	<|0.10|	<|0.10|	<|0.10|	<|0.10|	<|0.10|	<|0.10|	<|0.10|	<|0.10|	0.60	0.59
HO-1→LU+1	0.16	0.17	0.16	<|0.10|	0.23	0.24	0.24	-0.11	<|0.10|	<|0.10|
HO-2→LU+2	-0.20	-0.20	-0.19	<|0.10|	<|0.10|	<|0.10|	<|0.10|	<|0.10|	<|0.10|	<|0.10|

Table 5. Indole optimum CIS(I,J)/6-31G coefficients

	^1L_a			^1L_b		
π MOs	CIS(11,11)	CIS(13,14)	CIS	CIS(11,11)	CIS(13,14)	CIS
HO→ LU	0.62	0.61	0.64	<|0.10|	<|0.10|	<|0.10|
HO→LU+1	<|0.10|	0.13	<|0.10|	-0.40	-0.39	-0.34
HO-1→LU	-0.11	-0.16	<|0.10|	0.56	0.57	0.59
HO-1→LU+1	0.29	0.26	0.24	<|0.10|	<|0.10|	<|0.10|
HO-2→LU+1	<|0.10|	<|0.10|	<|0.10|	0.11	0.11	<|0.10|

between the Hartree-Fock determinant and a singly substituted configuration ($|\, i \rightarrow k >$) is the double dot product $c_i c_k^{\dagger}:M^n_{\mu\nu,\lambda\sigma}$, where c_i represents the MO coefficients of orbital i and $M^n_{\mu\nu,\lambda\sigma}$ is the dipole matrixin the AO basis. For indole's i = 30 and k = 32 at CIS/3-21G, this gives transition moment components of {-5.9,8.2} Debye parallel and perpendicular to indole's long axis, and {2.9,-4.8} D for i = 31 and k = 33. The large difference in the transition moment directions of these configurations is thus preserved in indole, and so small changes in the CI coefficients have a significant impact on the direction of the ^1L_b polarizatrion, resulting in a greater fluctuation

between basis sets. The computed oscillator strength remains fairly constant, aside from the CIS/3-21G result, as the size of the basis is increased, suggesting that the transition dipoles of these configurations are closer in magnitude when calculated with the CIS density.

The dominance of a single configuration in the ^1L_a transition (Tables 4 and 5) results in a transition moment with less computational sensitivity. For indole's i = 31 and k = 32, $c_i c_k^{\dagger} M^n_{\mu\nu,\lambda\sigma}$ = {6.2, -7.9} Debye at CIS/3-21G, giving a polarization of -38° for the HOMO → LUMO transition moment.

At CIS/6-311++G(p,d) the interstate properties are only qualitatively correct, and it is obvious that a higher level of theory must be summoned for quantitative agreement. Table 3 shows that simply increasing the active space to include doubly substituted determinants dramatically improves both the ^1L_a and ^1L_b transition properties, at least in comparison to the results of the linear dichroism study.[46] Nevertheless, the CISD(22,22)/6-31G oscillator strengths are peculiar, relative to CISD(11,11)/6-31G, given the tendency for doubles to decrease the value of this property. Going from (11,11)/6-31G to (22,22)/6-31G adds only one π MO to the CI calculation, so it is not too surprising that this modification lowers the ground state in relation to the excited states, as Table 1 shows, thereby increasing the oscillator strength if the transition moment is unchanged.

Ground State Geometry

The equilibrium bond lengths and bond angles of indole, as calculated by the Hartree-Fock method or at MP2/6-31G(p,d), are compared to the results of microwave spectroscopy in Table 6. The equilibrium structures show tiny deviations from

Table 6. Indole ground state bond lengths (Å) and bond angles (Degrees)

	HARTREE-FOCK							MP2
	3-21G	4-31G	6-31G	6-31G**	6-31+G**	6-311++G**	EXP[a]	6-31G**
N1-C2	1.3881	1.3816	1.3831	1.3725	1.3726	1.3723	1.433	1.3793
C2-C3	1.3491	1.3479	1.3526	1.3478	1.3509	1.3487	1.363	1.3752
C3-C9	1.4465	1.4421	1.4445	1.4420	1.4423	1.4421	1.443	1.4300
C4-C9	1.3936	1.3935	1.3979	1.3985	1.4002	1.3984	1.387	1.4079
C4-C5	1.3746	1.3742	1.3786	1.3746	1.3764	1.3743	1.367	1.3872
C5-C6	1.4014	1.4000	1.4043	1.4039	1.4062	1.4043	1.375	1.4121
C6-C7	1.3745	1.3745	1.3788	1.3748	1.3767	1.3746	1.369	1.3883
C7-C8	1.3903	1.3893	1.3935	1.3942	1.3956	1.3937	1.392	1.4008
C8-C9	1.4039	1.4015	1.4048	1.4007	1.4014	1.3993	1.372	1.4227
N1-C8	1.3774	1.3762	1.3787	1.3708	1.3714	1.3710	1.448	1.3765
N1-H1	0.9940	0.9879	0.9888	0.9909	0.9915	0.9907	1.00	1.0058
C2-H2	1.0656	1.0655	1.0669	1.0711	1.0709	1.0708	1.08	1.0778
C3-H3	1.0656	1.0662	1.0675	1.0708	1.0708	1.0705	1.08	1.0776
C4-H4	1.0723	1.0724	1.0736	1.0763	1.0760	1.0758	1.08	1.0836
C5-H5	1.0718	1.0718	1.0730	1.0757	1.0755	1.0753	1.08	1.0827
C6-H6	1.0721	1.0720	1.0732	1.0759	1.0757	1.0755	1.08	1.0827
C7-H7	1.0718	1.0722	1.0734	1.0762	1.0761	1.0758	1.08	1.0836
C8-C9-C3	106.80	106.81	106.83	106.68	106.70	106.72	107.7	107.05
C9-C3-H3	126.38	126.59	126.66	127.17	127.22	127.25		127.21
C9-C3-C2	107.12	107.13	107.09	106.74	106.70	106.73	105.5	107.05
C3-C2-H2	129.69	129.68	129.66	129.54	129.52	129.50		130.20
C3-C2-N1	109.67	109.66	109.63	110.06	110.02	110.00	111.5	109.30
C8-N1-H1	125.76	125.71	125.68	125.69	125.71	125.72		125.33
C8-C9-C4	119.49	119.22	119.21	119.10	119.17	119.17	121.1	118.68
C9-C4-H4	120.29	120.40	120.44	120.50	120.47	120.47		120.42
C9-C4-C5	119.02	119.07	119.04	119.08	119.04	119.04	114.6	118.94
C4-C5-H5	119.94	119.91	119.90	119.88	119.89	119.89		119.62
C4-C5-C6	120.81	120.87	120.88	120.88	120.86	120.86	124.8	121.30
C5-C6-H6	119.30	119.29	119.28	119.29	119.28	119.28		119.35
C5-C6-C7	121.22	121.21	121.22	121.27	121.28	121.28	119.7	121.28
C8-C7-H7	121.12	121.27	121.34	121.36	121.43	121.42		121.53

[a]Reference 45.

Table 7. Indole Hartree-Fock and CIS equilibrium bond length basis set effects (Å)

	G			
	3-21G→6-31G	→6-31G**	→6-31+G**	→6-311++G**
N1-C2	-0.0050	-0.0106	0.0001	-0.0003
C2-C3	0.0035	-0.0048	0.0031	-0.0022
C3-C9	-0.0020	-0.0025	0.0003	-0.0002
C4-C9	0.0043	0.0006	0.0017	-0.0018
C4-C5	0.0040	-0.0040	0.0018	-0.0021
C5-C6	0.0029	-0.0004	0.0023	-0.0019
C6-C7	0.0043	-0.0040	0.0019	-0.0021
C7-C8	0.0032	0.0007	0.0014	-0.0019
C8-C9	0.0009	-0.0041	0.0007	-0.0021
N1-C8	0.0013	-0.0079	0.0006	-0.0004

	^1L_a		
	3-21G→6-31G	→6-31G**	→6-31+G**
N1-C2	-0.0014	-0.0117	-0.0068
C2-C3	-0.0026	-0.0058	0.0052
C3-C9	0.0030	-0.0044	-0.0042
C4-C9	0.0024	0.0000	0.0024
C4-C5	0.0022	-0.0032	0.0018
C5-C6	0.0068	-0.0030	0.0009
C6-C7	-0.0031	-0.0028	-0.0004
C7-C8	0.0061	-0.0012	0.0017
C8-C9	-0.0005	-0.0030	-0.0058
N1-C8	-0.0016	0.0001	-0.0007

	^3L_a		
	3-21G→6-31G	→6-31G**	→6-31+G**
N1-C2	-0.0028	-0.0164	-0.0014
C2-C3	0.0008	-0.0164	-0.0003
C3-C9	0.0041	-0.0053	0.0013
C4-C9	-0.0009	0.0110	0.0019
C4-C5	0.0010	0.0000	0.0027
C5-C6	0.0076	-0.0069	0.0011
C6-C7	-0.0063	0.0090	0.0023
C7-C8	0.0048	0.0013	0.0031
C8-C9	0.0003	-0.0071	-0.0012
N1-C8	0.0021	-0.0106	0.0001

planarity that may be attributed to the numerical imprecisions of the calculation. All calculated dihedral angles therefore correspond to the planar geometry and are omitted from the Table.

A compilation of the changes in bond lengths with each increase of basis set size is presented in Table 7. Significant changes in length are observed in most carbon - carbon and carbon - nitrogen bonds as the basis set is modified, even between the larger basis sets, and in no way can arrival at the Hartree-Fock limit be declared with regards to most if not all of these parameters. Each modification is therefore necessary for an accurate description of the bond lengths formed by indole's heavy atoms. Conversely, the C-H and N-H bonds show little sensitivity to basis set size. Only small variations are also noted in the equilibrium bond angles (a change in bond angle of 0.01° here corresponds to a change in nuclear position of less than three ten-thousandths of an angstrom), especially those of the benzene ring, and especially between the larger basis sets, suggesting a proximity to the Hartree-Fock limit in this regard.

^1L_b Geometry

It was not possible to locate a minimum energy conformation on the ^1L_b potential energy surface when basis sets containing polarization functions were used with the full CIS wave function. Instead, the wave function would converge on the ^1L_a state during the geometry optimization. It appears that the preferential stabilization of the ^1L_a state brought about by "d" functions creates a stronger repulsion between the potential energy surfaces in the region of the avoided crossing and the ^1L_b state becomes unbound.

The ^1L_b state is less elusive than the ^1L_a state from an empirical perspective, however. Table 8 compares indole's calculated ^1L_b bond lengths with the results of

Table 8. Indole ^1L_a, ^1L_b bond lengths (Å) and bond angles (degrees)

	^1L_b				^1L_a			
	6-31G							
	3-21G	CIS	CIS(11,11)	EXP[a]	3-21G	6-31G	6-31G**	6-31+G**
N1-C2	1.4238	1.4124	1.4000	1.440	1.3645	1.3631	1.3514	1.3446
C2-C3	1.3592	1.3635	1.3633	1.370	1.4154	1.4128	1.4070	1.4122
C3-C9	1.4297	1.4279	1.4303	1.433	1.3946	1.3976	1.3932	1.3890
C4-C9	1.3990	1.4046	1.4025	1.400	1.4358	1.4382	1.4382	1.4406
C4-C5	1.4140	1.4140	1.4177	1.400	1.3979	1.4001	1.3969	1.3987
C5-C6	1.4110	1.4165	1.4181	1.400	1.3822	1.3890	1.3860	1.3869
C6-C7	1.4060	1.4089	1.4109	1.400	1.4530	1.4499	1.4471	1.4467
C7-C8	1.4069	1.4078	1.4049	1.400	1.3659	1.3720	1.3708	1.3725
C8-C9	1.4638	1.4626	1.4589	1.408	1.4355	1.4350	1.4320	1.4262
N1-C8	1.3472	1.3539	1.3637	1.438	1.3973	1.3957	1.3858	1.3851
N1-H1	0.9960	0.9902	0.9898	1.00	0.9964	0.9907	0.9927	0.9935
C2-H2	1.0635	1.0652	1.0655	1.08	1.0644	1.0658	1.0692	1.0697
C3-H3	1.0664	1.0678	1.0678	1.08	1.0662	1.0679	1.0713	1.0709
C4-H4	1.0697	1.0710	1.0713	1.08	1.0705	1.0721	1.0741	1.0740
C5-H5	1.0718	1.0729	1.0723	1.08	1.0722	1.0731	1.0757	1.0749
C6-H6	1.0703	1.0716	1.0715	1.08	1.0711	1.0724	1.0748	1.0747
C7-H7	1.0698	1.0714	1.0716	1.08	1.0700	1.0719	1.0742	1.0740
C8-C9-C3	106.17	106.20	106.24	107.7	107.36	107.25	106.98	107.23
C9-C3-H3	125.53	125.87	126.03		126.98	127.13	127.41	127.77
C9-C3-C2	108.77	108.58	108.34	105.5	108.32	108.25	108.07	107.73
C3-C2-H2	131.53	131.10	130.52		129.98	130.00	130.07	129.84
C3-C2-C1	107.85	108.16	108.62	111.5	107.62	107.72	108.03	108.09
C8-N1-H1	125.05	124.50	125.01		124.54	124.59	124.64	124.81
C8-C9-C4	118.93	118.79	119.01	121.1	118.96	118.82	118.89	119.21
C9-C4-H4	121.39	121.43	121.38		121.55	120.60	120.59	120.76
C9-C4-C5	117.87	117.86	118.08	114.6	117.99	118.06	117.92	117.68
C4-C5-H5	118.71	118.89	119.10		118.95	119.06	119.16	119.27
C4-C5-C6	122.74	122.64	122.12	124.8	122.02	121.43	121.93	121.76
C5-C6-H6	119.31	119.17	119.19		120.41	120.22	119.99	119.77
C5-C6-C7	120.97	121.12	121.15	119.7	121.15	121.21	121.44	121.72
C8-C7-H7	121.43	121.69	121.79		122.69	122.72	122.63	122.82

[a]Reference 45.

Table 9. Indole ground and ^1L_b rotational constants (MHz)

	G							
	3G	3-21G	6-31G	6-31G**	6-31++G**	6-311++G**	CISD/6-31G	MP2/6-31G**	EXP[a]
A	3920	3950	3939	3952	3943	3953	3873	3876	3878
B	1632	1648	1645	1653	1651	1653	1622	1637	1636
C	1152	1163	1160	1165	1164	1166	1143	1151	1151

	^1L_b				
	3-21G	4-31G	CIS/6-31G	CIS(11,11)/6-31G	EXP[a]
A	3808	3816	3798(-141)	3809(-130)	3743(-135)
B	1634	1641	1633(-12)	1629(-16)	1618(-18)
C	1144	1147	1142(-18)	1141(-19)	1130(-21)

[a]Reference 47.

high resolution fluorescence spectroscopy while Table 9 compares the calculated and observed ground and ^1L_b rotational constants. The CIS/6-31G and HF/6-31G geometries are of comparable accuracy. The pyrolle bond lengths generally underestimate experiment by 2.0% and the phenyl bonds are exaggerated by 0.5% at both computational levels due to correlation and basis set truncation errors. The rotational constants are overestimated, which follows from their inverse dependence on the moments of inertia.

The differences between the HF and CIS rotational constants (in parentheses) are perhaps more pertinent to calculated spectra than the absolute values, and these show good agreement with the measured results, lending a small measure of credibility to the calculated geometry change. The HF-CIS(11,11)/6-31G differences are slightly more accurate than those obtained at HF-CIS/6-31G, particularly for ΔB.

Indole's rotationally resolved fluorescence indicates that the bond angles

formed by the heavy atoms are essentially the same in the ground and ^1L_b states.[45] This is consistent only with radial displacement of the benzene and pyrrole moieties upon excitation or, of course, no displacement upon excitation (aside from zero point motion). The calculated geometry difference between the ground and ^1L_b states, Figure 2, shows that, aside from the N-H moiety, the atoms are in fact radially displaced following excitation, much like benzene's $^1B_{2u}$ transition. The amplitude of displacement on the N-H group also shows the greatest sensitivity to basis, particularly between CIS-HF/6-31G and CIS(11,11)-HF/6-31G. The remaining displacement vectors are fairly basis insensitive, at least in appearance and within this small range of sizes. Also independent of basis are the C-H and N-H bonds, nearly unchanged upon excitation, and the molecule's planarity.

^1L_a Geometry

The equilibrium bond lengths of ^1L_a indole, as calculated by the CIS method, are provided in Table 8. As shown in Table 7, the ^1L_a bond lengths are more sensitive to basis than those of the Hartree-Fock ground state, reflecting greater changes in the shape and energy of the lower virtual π MOs with increasing basis set size. This is particularly apparent from comparison of Figures 3 and 4, which show two-dimensional slices of the π MOs near the Fermi level as calculated at HF/6-31G(p,d) and HF/6-31+G(p,d). The diffuse functions contribute marginally to occupied MOs and therefore heavily to virtual MOs, which are residual functions of the SCF calculation. The virtual π MOs are also strongly mixed at HF/6-31+G(p,d), in comparison to HF/6-31G(p,d), which changes the ^1L_a wave function (Table 4).

(The diffuse nature of the virtual MOs is exaggerated by the Hartree-Fock

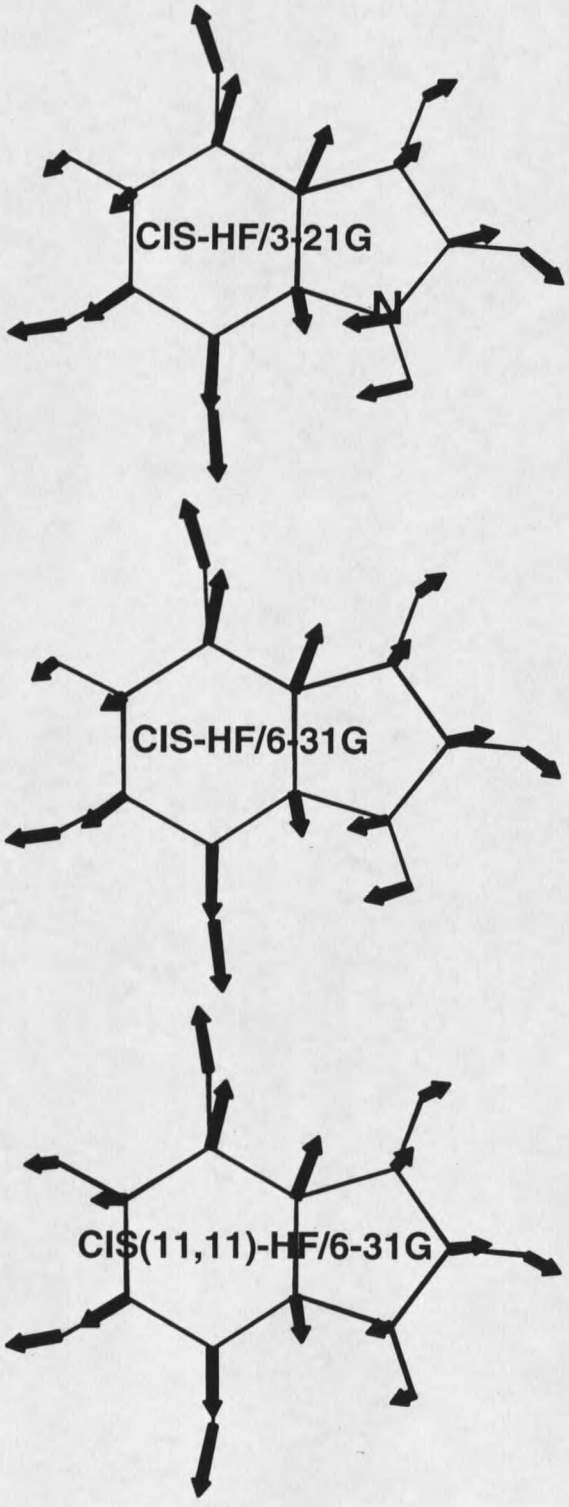

Figure 2. Indole ^1L_b - ground state geometry difference (×20).

method in another manner. The energy of an SCF virtual MO includes the repulsion terms with the charge clouds of all 2n electrons in the n MOs of the system. Consequently, they are more representative of the MOs of the corresponding anion than of the excited MOs of the neutral molecule.)

As Table 7 shows, diffuse functions effect many of the ground state and ^1L_a bond lengths in a qualitatively different manner. All bonds are lengthened by this modification in the ground state while many are shortened in the ^1L_a state, especially those of the pyrrole ring. As Figure 5 shows, however, only small changes in the calculated ^1L_a - ground state geometry difference are discernable, primarily at C3 and C9, when diffuse functions are included in the basis. The other modifications in the atomic basis functions also appear to have a small impact on the geometry difference. A larger change is present between the displacement vectors obtained with the full and truncated CIS wave functions and, as with the ^1L_b state, these appear mainly at N, C3, and C9 while the structure of the benzene ring is less sensitive to this modification. Regardless of basis, the C-H and N-H bond lengths are virtually unchanged upon excitation and the molecule remains planar.

^3L_a Geometry

As Table 7 shows, polarization functions have a much greater impact on the geometry of the triplet state (Table 10). Four ^3L_a bond lengths increase by more than one hundredths of an angstrom due to this modification, compared to one ^1L_a bond length and none in the ground state. The heightened sensitivity reflects a greater reorganization of charge on going from CIS/6-31G to CIS/6-31G(p,d), as made evident by the concommitant sign change in the non-zero off-diagonal element of the ^3L_a

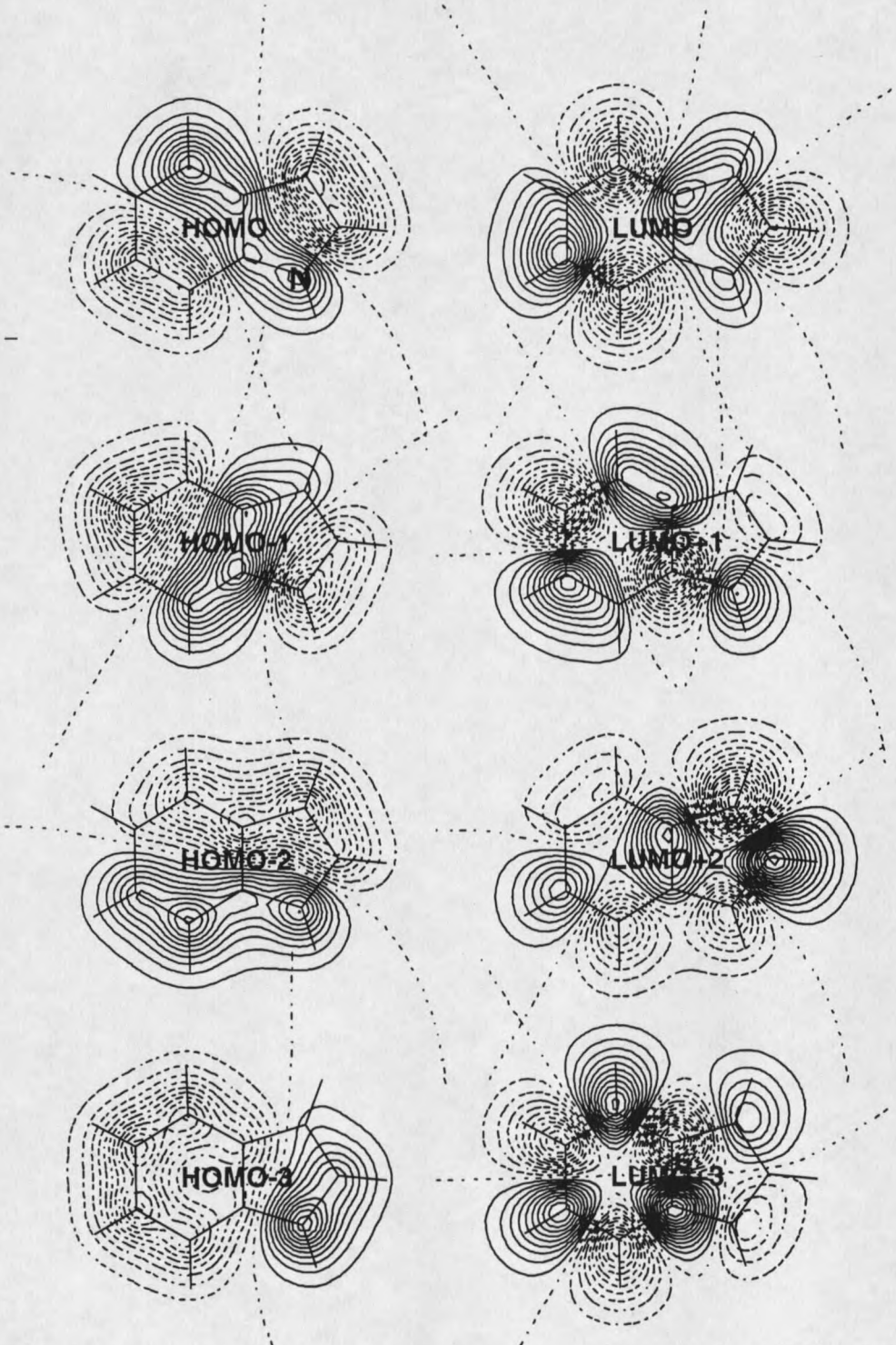

Figure 3. Indole HF/6-31G(p,d) π molecular orbitals at 1.323 Bohr (0.7 Å) above the molecular plane. Contour widths: 0.01 $Bohr^{-3/2}$. Contour range: ~-0.12, 0.10 $Bohr^{-3/2}$.

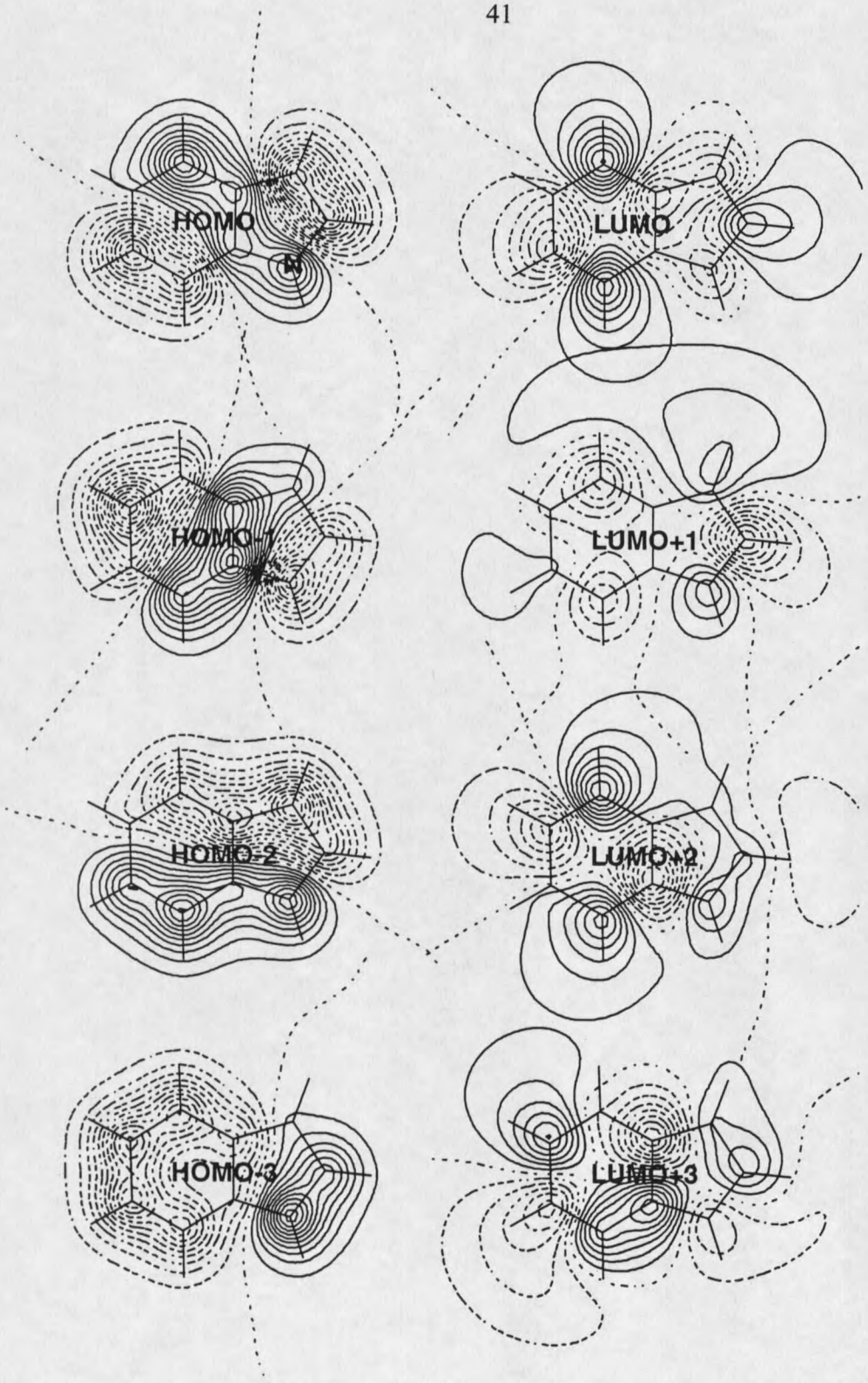

Figure 4. Indole HF/6-31+G(p,d) π molecular orbitals at 1.323 Bohr (0.7 Å) above the molecular plane. Contour widths: 0.01 $Bohr^{-3/2}$. Contour range: ~-0.12, 0.10 $Bohr^{-3/2}$ (occupied MOs), ~-0.07, 0.07 $Bohr^{-3/2}$ (virtual MOs).

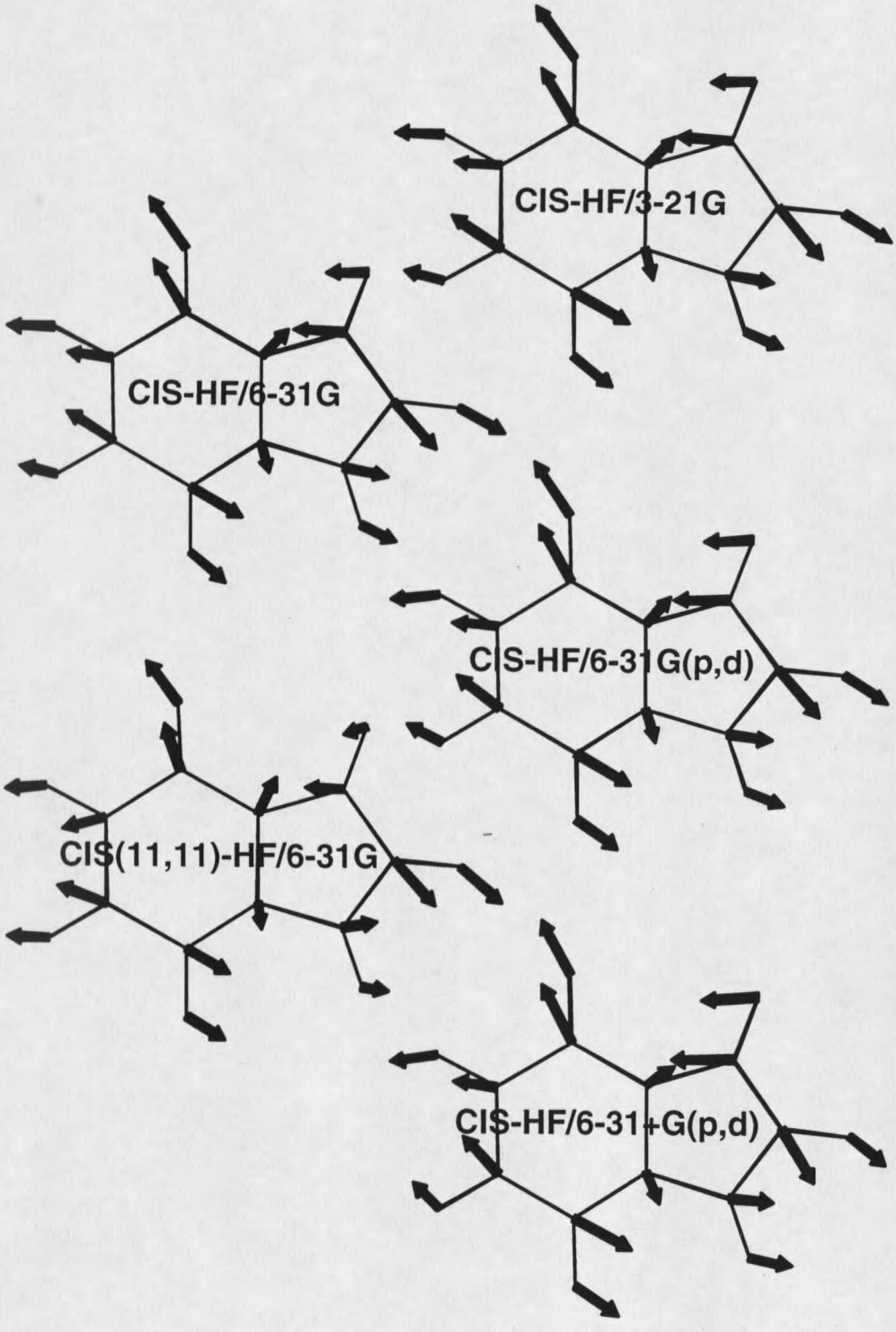

Figure 5. Indole ^1L_a - ground state geometry difference (×20).

quadrupole tensor. Less unexpected are the comparative effects of diffuse functions, which have a much smaller impact on the geometry of the ^3L_a state, in comparison to ^1L_a. This is due to its spin orthogonality with the ground state, which removes the requirement for spatial orthogonality, resulting in a more compact electron distribution. The geometry difference between ^3L_a and the ground state, Figure 6, is similar to the ^1L_a difference. Sufficiently broadened ^3L_a phosphorescence should bear a resemblance to ^1L_a fluorescence.

For the other configuration of T_1 indole, the N and C2 atoms deviate by 0.05 - 0.15 Å from the otherwise approximately planar ring. H1 and H2 deviate by ~0.30 Å at CIS/6-31G(p,d) and by 0.30 and 0.90 Å at UHF/6-31G(p,d). There is a concomitant ~0.10 Å increase in the C2-C3 bond length compared to the planar configuration. Thus, the hybridization of the N and C2 atomic orbitals is about sp^3 in non-planar T_1 while the C3 atom is still approximately sp^2 hybridized. The lowest triplet states of pyridine[49] and pyrrole[50] also have non-planar conformations, in theory, adopting boat-like structures with the nitrogen atom significantly out-of-plane.

The stability of the non-planar conformation is easily understood in terms of molecular orbital theory. Indole's LUMO and LUMO+2 (Figure 3) are distinctly antibonding in the N-C2 and C2-C3 linkages. The dominance of the HOMO→LUMO and HOMO-2→LUMO+2 configurations, amounting to 88% of the ^3L_a wave function, then leads to a pronounced weakening of these bonds. The latter configuration is virtually absent from the ^1L_a wave function, a fact that, along with the significant contribution from the HOMO-1→LUMO+1 determinant, possibly explains why only the planar conformation is stable in this state.

Table 10. Indole ^3L_a bond lengths (Å), bond angles, and dihedral angles (degrees)

	UHF		CIS					
	3-21G	6-31G**	3-21G	6-31G**	3-21G	6-31G	6-31G**	6-31+G**
N1-C2	1.4271	1.4198	1.3881	1.4138	1.3950	1.3922	1.3758	1.3744
C2-C3	1.5476	1.5220	1.3491	1.4946	1.4324	1.4332	1.4168	1.4165
C3-C9	1.3960	1.3930	1.4465	1.4006	1.3914	1.3955	1.3903	1.3916
C4-C9	1.4117	1.4179	1.3936	1.4035	1.4374	1.4365	1.4475	1.4494
C4-C5	1.3973	1.3956	1.3746	1.3945	1.4077	1.4087	1.4087	1.4114
C5-C6	1.4000	1.4045	1.4014	1.3798	1.3718	1.3794	1.3725	1.3736
C6-C7	1.4168	1.4149	1.3745	1.4203	1.4600	1.4537	1.4627	1.4650
C7-C8	1.3691	1.3753	1.3903	1.3623	1.3710	1.3758	1.3771	1.3802
C8-C9	1.4394	1.4335	1.4039	1.4242	1.4245	1.4248	1.4177	1.4165
N1-C8	1.4074	1.4147	1.3774	1.3996	1.3836	1.3857	1.3751	1.3752
N1-H1	0.9938	0.9955	0.9940	0.9946	0.9940	0.9887	0.9909	0.9917
C2-H2	1.0807	1.0844	1.0656	1.0765	1.0627	1.0641	1.0672	1.0676
C3-H3	1.0676	1.0716	1.0656	1.0711	1.0670	1.0687	1.0718	1.0718
C4-H4	1.0722	1.0755	1.0723	1.0754	1.0708	1.0723	1.0739	1.0738
C5-H5	1.0720	1.0756	1.0718	1.0753	1.0719	1.0730	1.0756	1.0754
C6-H6	1.0718	1.0753	1.0721	1.0754	1.0714	1.0726	1.0748	1.0747
C7-H7	1.0717	1.0759	1.0718	1.0754	1.0701	1.0720	1.0740	1.0740
C8-C9-C3	108.82	108.07	106.80	107.76	108.14	108.05	107.75	107.78
C9-C3-H3	127.51	127.76	126.38	127.19	126.67	126.83	127.04	127.14
C9-C3-C2	107.95	107.40	107.12	107.83	108.08	108.02	107.87	107.78
C3-C2-H2	118.99	119.00	129.69	123.21	130.94	130.91	130.78	130.77
C3-C2-N1	103.16	104.71	109.67	105.22	106.43	106.50	107.03	107.07
C8-N1-H1	123.63	116.93	125.76	119.01	124.80	124.76	124.73	124.79
C8-C9-C4	119.18	119.08	119.49	119.42	119.46	119.22	119.24	119.31
C9-C4-H4	120.15	120.33	120.29	120.26	120.32	120.45	120.48	120.53
C9-C4-C5	119.04	118.87	119.02	119.05	118.47	118.57	118.38	121.15
C4-C5-H5	119.65	119.68	119.94	119.71	119.17	119.29	119.28	121.16
C4-C5-C6	120.77	120.89	120.81	120.49	121.11	121.39	121.12	121.15
C5-C6-H6	119.83	119.60	119.30	119.71	120.32	120.07	119.91	119.97
C5-C6-C7	120.93	121.02	121.22	121.41	121.37	121.39	121.62	121.60
C8-C7-H7	121.27	121.35	121.12	120.39	122.36	122.32	122.50	122.59
C4-C9-C8-N1	181.42	-175.75	-179.75	-182.18				
C2-N1-C8-C9	-4.28	-12.24	1.29	8.49				
C3-C9-C8-C7	180.35	-178.22	-181.06	177.65				
H1-N1-C8-C9	188.65	-147.04	-182.54	150.31				
H2-C2-C3-C9	125.95	119.67	137.01	146.34				
H3-C3-C9-C8	184.94	175.89	-177.72	-178.57				

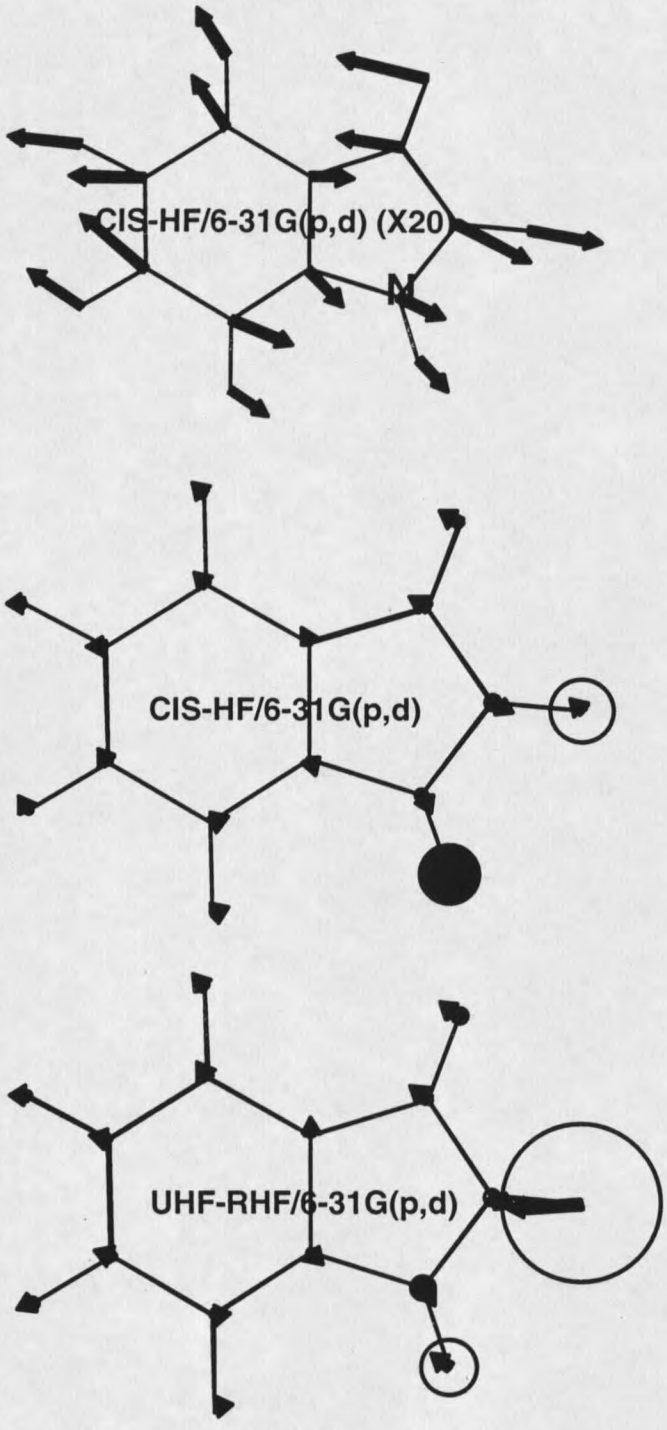

Figure 6. Indole T_1 - ground state geometry difference.

T_1 Atomic Spin Densities

The reasonably small (0.22) deviation from the true value of S^2 suggests that T_1 indole is fairly well-separated from higher spin states, and that the spin properties of this state are satisfactorily represented at UHF/6-31G(p,d). The total spin densities on each heavy atom in the triplet state, as calculated at UHF/6-31G(p,d), may therefore also be used to further rationalize the non-planar geometry. The total atomic spin density is simply the difference between the population of α- and ß-spin electrons. (Removing the restriction of α- and ß-spin electrons occupying the same spatial orbitals in Hartree-Fock theory leads to separate MOs and orbital energies for these particles in the solution to the Schrödinger equation.[51] The separate nature of the solution may carried into the population analysis, defining the population of α- and ß-spin electrons in a manner analogous to the restricted case.) On atom A, for instance, for open-shell systems there is in general a non-zero total spin density given by $P_s(A) = P_\alpha(A) - P_\beta(A)$, where $P_\alpha(A)$ is the population of electrons on A with α-spin and $P_\beta(A)$ is the population of electrons on A with ß-spin.

The results are presented in Figure 7, where unfilled circles denote an excess of α-spin density and the radii denote the extent of the surplus. For the non-planar structure, the total spin density on the benzene ring is fairly uniform from one atom to the next and its sign is alternately positive and negative. The destabilizing exchange interaction between electrons with the same spin is consequently reduced. In the pyrrole moiety, however, the alternating pattern of signs is not possible because of the odd number of atomic centers. Consequently, the total spin densities on C2 and C3 are of the same sign and in order to reduce the spin repulsion between these atoms, a

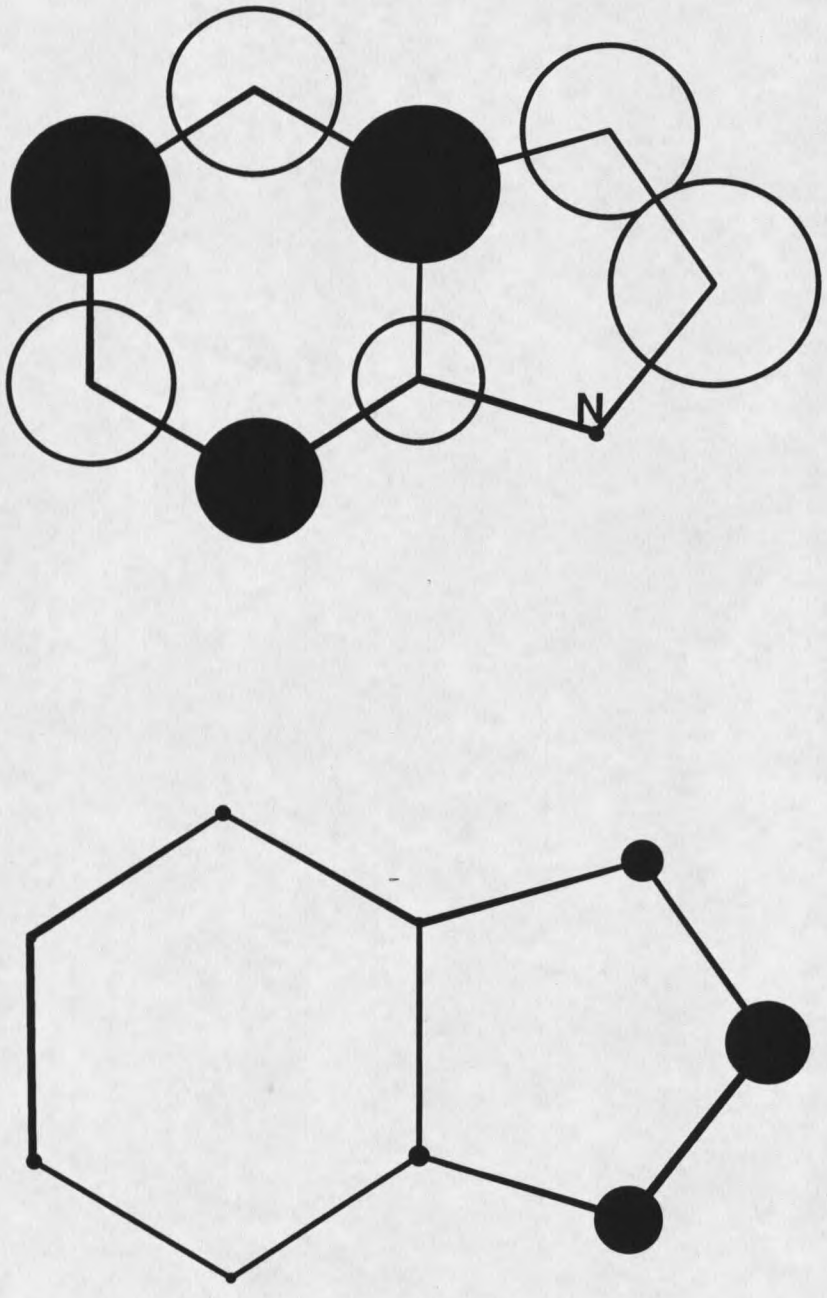

Figure 7. Indole UHF/6-31G(p,d) T_1 spin densities, non-planar (top) and planar conformations.

non-planar conformation is adopted. It is also seen that the distribution of total spin densities in the pyrrole ring is far from uniform. In particular, the lone pair character of nitrogen's p-π orbital results in a very small surplus of ß spin density on this atom, another circumstance contributing to the large deviation from planarity at C2. The loss of resonance energy is apparently compensated to some extent by a reduction in spin repulsion.

Ionization Potentials

Indole's first vertical ionization potential, as obtained from photoelectron spectroscopy, is compared with ab initio results using Koopmans' Theorem in Table 11. Koopmans' Theorem equates the nth vertical ionization potential to minus the energy of the highest occupied + 1 - n molecular orbital, $-\varepsilon_i$. For first ionization potentials this is quite often a good approximation due to a cancellation of errors - the neglect of orbital relaxation following ionization, which increases the calculated ionization potential, and the difference in electron correlation between the radical

Table 11. Indole vertical ionization potentials (eV)

FIRST VERTICAL IONIZATION POTENTIAL						
3G	3-21G	6-31G	6-31G**	6-31++G**	6-311++G**	EXP[a]
6.15	7.81	7.71	7.63	7.82	7.83	7.79

HF/6-311++G(p,d) VERTICAL IONIZATION POTENTIALS											
IP[a]	7.79	8.18	9.88	11.12	11.56	12.24	13.26	13.77	14.28	15.40	17.03	18.51
$-\varepsilon_i$	7.83	8.24	10.50	12.75	13.20	13.90	15.01	15.85/15.99	16.34/16.54	17.78/18.09	20.03	21.64/22.05

[a] Reference 52.

cation and the neutral parent molecule. For a molecule the size of indole, neither source of error would be expected to be large and, as Table 11 shows, this is indeed the case for the first ionization potential. Although the STO-3G basis significantly underestimates this quantity, the 3-21G basis set gives a very accurate result. The 3-21G result is clearly not fortuitous, as demonstrated by calculations using basis sets with longer contraction lengths, or polarization functions, or diffuse functions, or more valence basis functions, all of which have a modest impact on the outcome and illustrate the HOMO's basis insensitivity. One concludes that the orbital approximation is pertinent and that the shape and energy of indole's HOMO is well reproduced with just the 3-21G basis set.

At HF/6-31++G(p,d), Koopmans' Theorem is seen to overestimate the first ionization potential, indicating that the neglect of orbital relaxation is a greater source of error than the neglect of electron correlation. The errors associated with either approximation would be expected to increase when Koopman's Theory is applied to the higher energy lines of a photoelectron spectrum. The orbital relaxation error grows because an increasing number of MOs are shielded by the ejected electron while the correlation error grows because the smaller size of the lower energy MOs causes an increase in dynamical correlation. As Table 11 shows, the error associated with the former approximation becomes more dominant as lower energy electrons are removed from the indole molecule.

Mulliken Populations

Figure 8 demonstrates the effects of electron correlation as calculated at the MP2-HF/6-31G(p,d) and CISD-HF/6-31G levels of theory on the ground state Mulliken populations of indole. Filled circles denote a decrease in population on going to the correlated method, unfilled circles denote a gain in population, and the

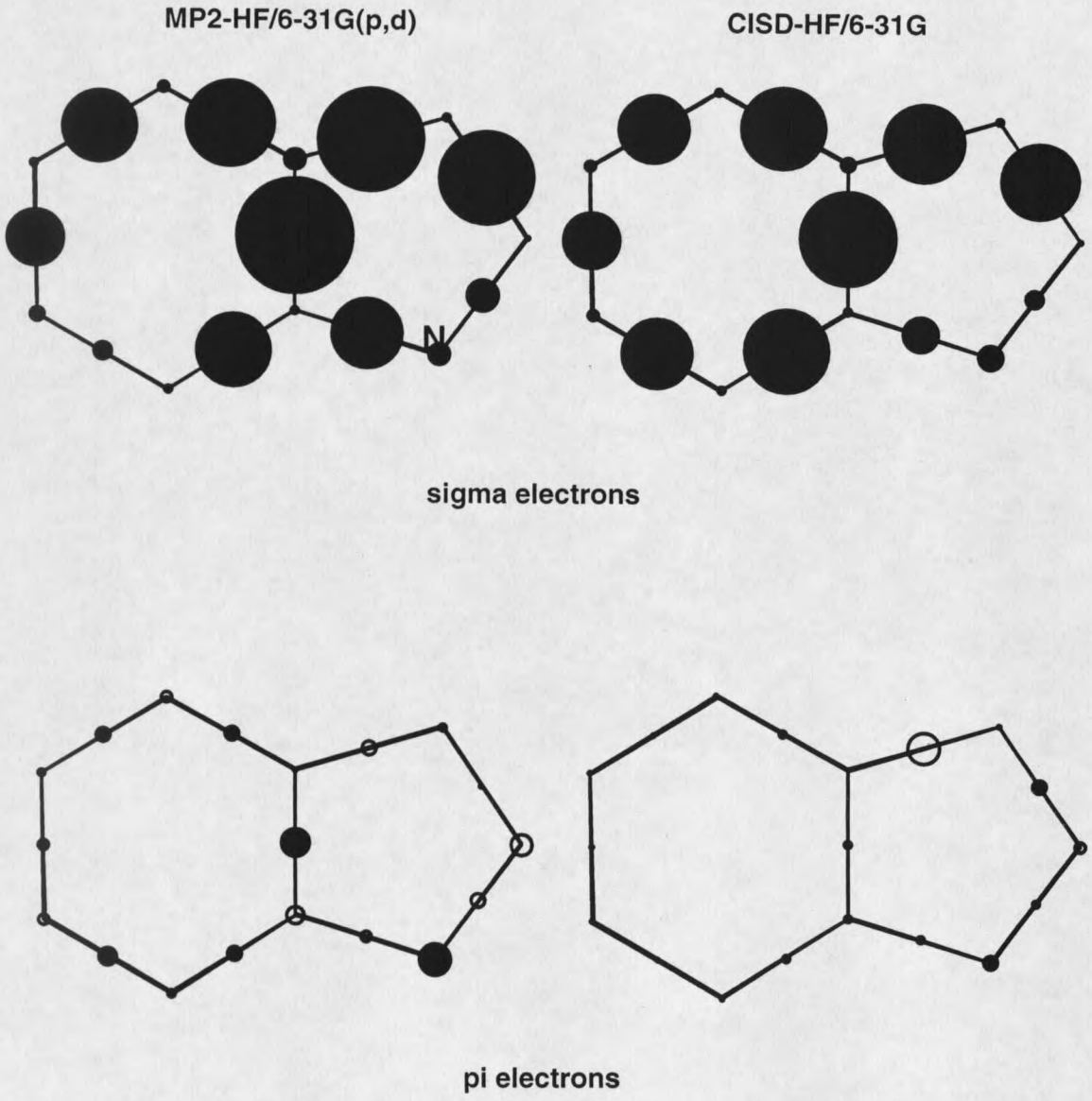

Figure 8. Indole MP2-HF and CISD-HF Mulliken population difference.

radius of each circle denotes the magnitude of the population change. The populations have been calculated at the equilibrium geometry of the correlated method.

The two methods give qualitatively the same result at each atom or bond, for both σ and π electrons, thus corroborating each other. Both methods assert that the effect of electron correlation is particularly pronounced in the C8-C9 overlap σ population, which loses 0.300 e at MP2-HF/6-31G(p,d) and 0.249 e at CISD-HF/6-31G, as well as the C2-C3 and C3-C9 overlap σ populations. At both levels of theory, the electron densities of bonds farther from indole's center of mass are generally less affected by correlation. Both methods assert that bonds between carbon atoms show greater sensitivity to correlation than the carbon-nitrogen bonds, perhaps because of their more covalent nature. Conversely, the atomic populations at the carbon atoms are less affected than those of the nitrogen atom, at both levels of theory, presumably as a consequence of less contracted orbitals.

At both computational levels, the shift of π electron density is a tiny fraction of the total effect. Although small, this shift is nonetheless interesting. Both correlated methods appear to enhance the aromatic character of the indole molecule. For instance, the increased π overlap population between C3 and C9 indicates stronger aromatic coupling between the ethylene and benzene moieties on going to the correlated density. All remaining π overlap populations between adjacent carbon atoms are decreased by correlation. The aromatic coupling between N and the benzene moiety or between N and the ethylene moiety is also strengthened, albeit minutely, as indicated by the increased overlap π population between the ring-forming bonds involving the nitrogen atom. This is also true regardless of method. Thus, lone pair density is delocalized into the indole ring, resulting in a slightly more uniformly distributed π cloud.

Further agreement between the MP2-HF and CISD-HF results are found in the

overlap populations between non-adjacent atoms. As compensation for the decrease in density in each of the above-mentioned regions, there is an increase in the MP2 and CISD overlap populations between several non-adjacent atoms. In particular, the C2-C8, C2-C9, and C3-C4 overlap σ populations increase by about 0.100 e at MP2/6-31G(p,d), while the C6-C8, C3-C8, and C7-N overlap σ populations each gain 0.050 e. Also, the hydrogen nuclei gain about 0.030 e at MP2/6-31G(p,d). The electron density is then shifted to the periphery of the molecule, as with small molecules. The CISD-HF population differences are smaller than those of MP2-HF, in further analogy to small molecules, and are more uniformly distributed between the bonds.

The effects of basis on indole's ground state Mulliken populations are presented in Table 12. Diffuse functions lead to unrealistic σ electron atomic populations and bizarre overlap populations for the σ electrons. In addition to being unrealistically large, most of the overlap σ electron populations are negative when diffuse functions are used, indicating that they are antibonding in nature. The principal assumption of the population analysis, that the atomic orbitals are well localized on the nuclei and do not contribute to the description of the adjacent atoms, apparently is no longer valid with diffuse functions in the basis set.

Figure 9 shows the CIS-HF/6-31G(p,d) Mulliken population changes brought about by vertical excitation of the indole molecule. Excitation to the ^1L_b state results in a somewhat symmetric pattern of redistribution of π electrons that is localized mostly on the benzene ring while the ^1L_a and ^3L_a excitations show a more irregular pattern involving both rings. Summing the positive or negative population changes on each atom shows that a total of 0.360, 0.213, and 0.238 electrons are transferred by ^1L_b, ^1L_a, and ^3L_a excitation, respectively, a total of 0.222, 0.142, and 0.155 being π e.

The directions of the shifts may be explained simply in terms of the HOMOs and LUMOs of Figure 3. With the ^1L_a transition, a total of 0.11 π e are transferred

Table 12. Indole Hartree-Fock Mulliken populations

	HF/3-21G			HF/6-31G			HF/6-31G(p,d)			HF/6-31++G(p,d)		
	σ	π	total	σ	π	total	σ	π	total	σ	π	total
N1	6.29	1.69	7.99	6.26	1.73	7.98	6.05	1.70	7.74	5.72	1.67	7.39
H1	0.64	0.00	0.64	0.62	0.00	0.62	0.68	0.01	0.69	0.64	0.01	0.65
C2	4.86	1.02	5.88	4.85	1.02	5.87	4.87	1.02	5.88	4.81	1.03	5.84
H2	0.74	0.00	0.74	0.77	0.00	0.77	0.83	0.00	0.84	0.82	0.00	0.82
C3	5.17	1.12	6.28	5.08	1.11	6.20	5.08	1.12	6.20	5.07	1.13	6.21
H3	0.76	0.00	0.76	0.79	0.00	0.79	0.85	0.00	0.85	0.86	0.00	0.86
C9	5.07	1.05	6.14	5.13	1.04	6.17	5.03	1.04	6.07	3.62	1.01	4.63
C4	5.23	0.99	6.22	5.15	0.99	6.14	5.14	1.00	6.13	6.10	1.00	7.10
H4	0.76	0.00	0.76	0.79	0.00	0.79	0.85	0.00	0.85	0.88	0.00	0.88
C5	5.20	1.05	6.25	5.17	1.05	6.22	5.13	1.05	6.17	4.60	1.04	5.64
H5	0.77	0.00	0.77	0.81	0.00	0.81	0.86	0.00	0.86	0.86	0.00	0.86
C6	5.23	1.01	6.23	5.21	1.03	6.22	5.15	1.01	6.16	5.52	1.01	6.53
H6	0.77	0.00	0.77	0.81	0.00	0.81	0.86	0.00	0.86	0.87	0.00	0.87
C7	5.17	1.06	6.23	5.07	1.06	6.13	5.09	1.06	6.15	4.30	1.06	5.36
H7	0.77	0.00	0.77	0.80	0.00	0.80	0.85	0.00	0.85	0.84	0.00	0.85
C8	4.56	1.00	5.57	4.68	1.00	5.68	4.71	0.99	5.70	6.49	1.02	7.52

Mulliken overlap populations

	HF/3-21G		HF/6-31G		HF/6-31G(p,d)		HF/6-31++G(p,d)	
	π	σ	π	σ	π	σ	π	σ
N1-C2	0.11	0.46	0.06	0.35	0.10	0.57	0.07	1.27
C2-C3	0.44	0.73	0.46	0.80	0.47	0.84	0.54	-4.73
C3-C9	0.14	0.67	0.13	0.74	0.14	0.83	0.13	-10.65
C8-C9	0.27	0.60	0.29	0.82	0.30	0.90	0.37	-10.25
C4-C9	0.24	0.63	0.24	0.74	0.25	0.82	0.24	-2.18
C4-C5	0.34	0.69	0.34	0.73	0.35	0.78	0.39	-7.76
C5-C6	0.25	0.69	0.25	0.76	0.25	0.81	0.28	-5.60
C6-C7	0.33	0.66	0.34	0.73	0.35	0.79	0.39	-7.05
C7-C8	0.24	0.59	0.25	0.74	0.26	0.82	0.25	-8.63
N1-C8	0.11	0.30	0.07	0.23	0.10	0.50	0.09	-0.26

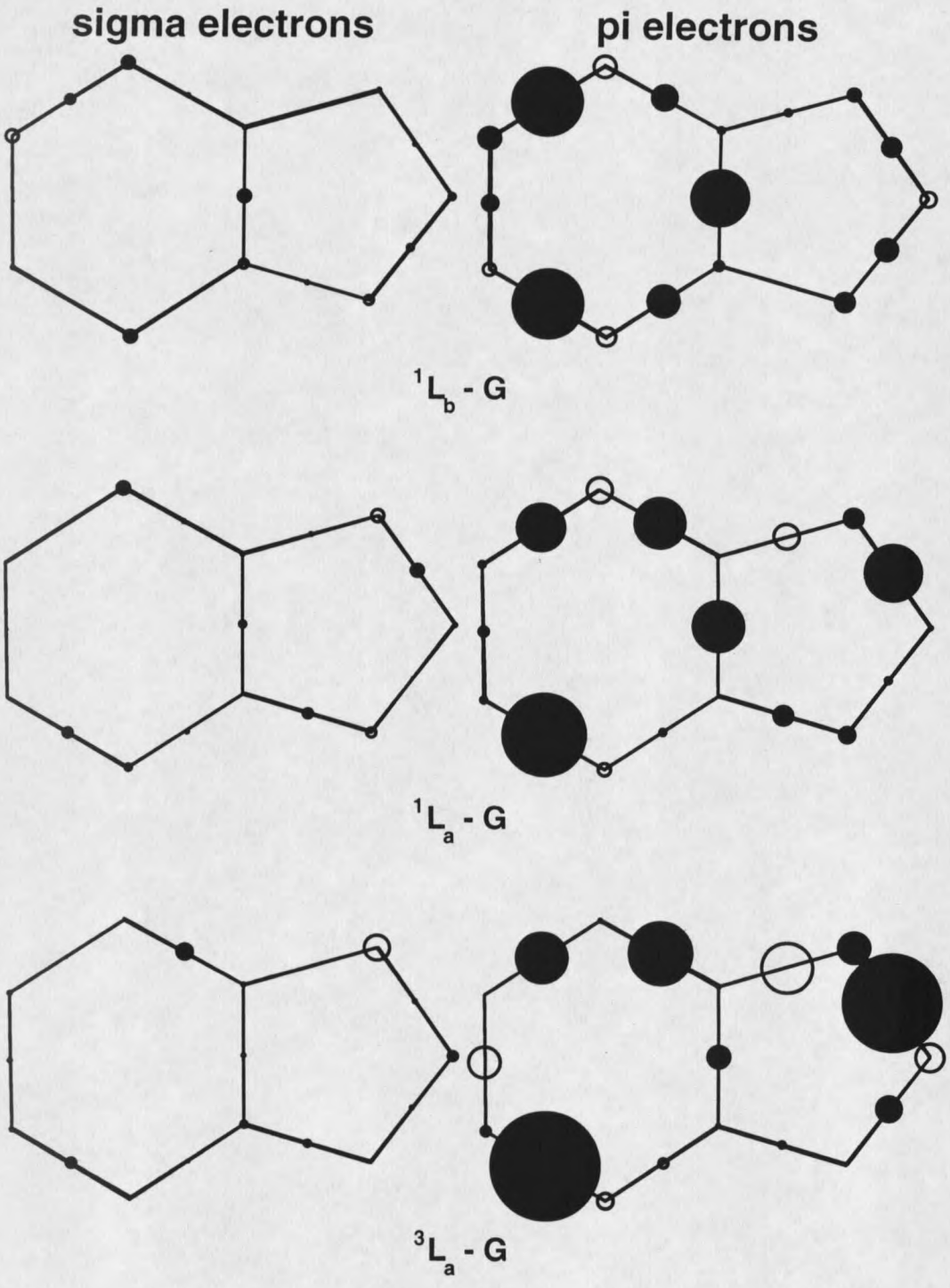

Figure 9. Indole $^1L_{a,b}$ - G and ^3L_a - G CIS-HF/6-31G(p,d) Mulliken population differences.

about evenly from N and C3, while C4 is the recipient of 0.04 π e and C7 is the recipient of 0.08 π e, and this would be anticipated by examining indole's HOMO and LUMO. The C2-C3 and C6-C7 bonds see the greatest decrease in overlap population, which is also consistent with the nodal patterns of the HOMO and the LUMO. In the ^3L_a transition, a total of 0.10 π e are transferred from C3 while C2 is the recipient of 0.09 π e and roughly 0.04 π e are transferred from C6 and to C7. Each of these changes are reflected in the amplitudes of the LUMO and LUMO+2. Thus, the ^3L_a transition involves a larger amount of charge transfer than ^1L_a, but over a much shorter distance. Also, the transfer of charge from C3 to C2 or from C6 to C7 is particularly effective at decreasing indole's polarity because these bond are approximately parallel to the dipole. With each transition, no significant changes are seen in the overlap populations between non-adjacent atoms.

Tables 13, 14, 15, and 16 show indole's excited state equilibrium geometry Mulliken populations as calculated with a variety of basis sets.

Integrated Density Difference Maps

A more detailed picture of the electronic reorganization accompanying excitation is provided by projection function difference maps, where differences in integrated molecular electron density are taken. Figure 10 shows the projection function differences between the ^1L_a or ^3L_a states and the ground state, at the ^1L_a and ground state geometries. The solid contours indicate regions in which electronic charge is increased upon excitation and the dashed contours indicate a decrease in electronic charge. Density difference maps involving the ^1L_b state are shown in Figure 11.

Table 13. Indole ^1L_b Mulliken populations

	CIS/3-21G			CIS/6-31G			CIS(11,11)/6-31G		
	σ	π	total	σ	π	total	σ	π	total
N1	6.05	1.70	7.74	6.30	1.67	7.96	6.29	1.68	7.97
H1	0.68	0.01	0.69	0.61	0.00	0.61	0.62	0.00	0.62
C2	4.87	1.02	5.88	4.83	1.09	5.92	4.84	1.06	5.90
H2	0.83	0.00	0.84	0.77	0.00	0.77	0.77	0.00	0.77
C3	5.08	1.12	6.20	5.10	1.08	6.18	5.11	1.08	6.19
H3	0.85	0.00	0.85	0.78	0.00	0.78	0.78	0.00	0.78
C9	5.03	1.04	6.07	5.13	1.02	6.15	5.13	1.02	6.15
C4	5.14	1.00	6.13	5.09	1.10	6.19	5.12	1.05	6.17
H4	0.85	0.00	0.85	0.81	0.00	0.81	0.79	0.00	0.79
C5	5.13	1.05	6.17	5.23	0.96	6.19	5.21	0.99	6.21
H5	0.86	0.00	0.86	0.81	0.00	0.81	0.81	0.00	0.81
C6	5.15	1.01	6.16	5.19	1.04	6.23	5.20	1.02	6.22
H6	0.86	0.00	0.86	0.81	0.00	0.81	0.81	0.00	0.81
C7	5.09	1.06	6.15	5.02	1.13	6.16	5.04	1.11	6.15
H7	0.85	0.00	0.85	0.80	0.00	0.80	0.80	0.00	0.80
C8	4.71	0.99	5.70	4.73	0.91	5.65	4.70	0.97	5.67

Mulliken overlap populations

	CIS/3-21G		CIS/6-31G		CIS(11,11)/6-31G	
	π	σ	π	σ	π	σ
N1-C2	0.02	0.46	-0.02	0.34	0.00	0.35
C2-C3	0.36	0.73	0.37	0.80	0.38	0.80
C3-C9	0.18	0.65	0.17	0.74	0.16	0.75
C8-C9	0.10	0.61	0.09	0.79	0.08	0.81
C4-C9	0.13	0.62	0.12	0.73	0.14	0.73
C4-C5	0.16	0.68	0.14	0.72	0.13	0.73
C5-C6	0.19	0.66	0.18	0.74	0.16	0.74
C6-C7	0.12	0.68	0.10	0.74	0.11	0.74
C7-C8	0.15	0.55	0.16	0.71	0.15	0.73
N1-C8	0.15	0.24	0.09	0.18	0.04	0.20

Table 14. Indole ^1L_a Mulliken populations

	CIS/3-21G			CIS/6-31G			CIS/6-31G(p,d)			CIS(11,11)/6-31G		
	σ	π	total	σ	π	total	σ	π	total	σ	π	total
N1	6.34	1.70	7.74	6.29	1.65	7.93	6.07	1.62	7.69	6.32	1.59	7.91
H1	0.68	0.01	0.69	0.61	0.00	0.61	0.67	0.01	0.68	0.60	0.00	0.65
C2	4.87	1.02	5.88	4.85	1.02	5.87	4.88	1.02	5.90	4.85	1.03	5.89
H2	0.83	0.00	0.84	0.76	0.00	0.76	0.82	0.00	0.82	0.76	0.00	0.80
C3	5.08	1.12	6.20	5.18	1.05	6.23	5.15	1.05	6.20	5.19	1.02	6.21
H3	0.85	0.00	0.85	0.77	0.00	0.77	0.83	0.00	0.83	0.77	0.00	0.80
C9	5.03	1.04	6.07	5.09	1.05	6.14	5.01	1.04	6.05	5.08	1.06	6.14
C4	5.14	1.00	6.13	5.08	1.07	6.15	5.09	1.08	6.17	5.10	1.07	6.17
H4	0.85	0.00	0.85	0.81	0.00	0.81	0.86	0.00	0.86	0.81	0.00	0.81
C5	5.13	1.05	6.17	5.18	1.03	6.20	5.12	1.03	6.15	5.18	1.02	6.20
H5	0.86	0.00	0.86	0.81	0.00	0.81	0.86	0.00	0.86	0.82	0.00	0.82
C6	5.15	1.01	6.16	5.19	1.02	6.22	5.15	1.02	6.17	5.17	1.07	6.24
H6	0.86	0.00	0.86	0.82	0.00	0.82	0.86	0.00	0.86	0.82	0.00	0.82
C7	5.09	1.06	6.15	5.07	1.12	6.19	5.08	1.13	6.21	5.07	1.11	6.18
H7	0.85	0.00	0.85	0.80	0.00	0.80	0.86	0.00	0.86	0.81	0.00	0.81
C8	4.71	0.99	5.70	4.68	1.00	5.68	4.70	0.99	5.69	4.67	1.02	5.69

Mulliken overlap populations

	CIS/3-21G		CIS/6-31G		CIS/6-31G(p,d)		CIS(11,11)/6-31G	
	π	σ	π	σ	π	σ	π	σ
N1-C2	0.11	0.41	0.06	0.30	0.10	0.54	0.06	0.30
C2-C3	0.20	0.70	0.21	0.75	0.23	0.79	0.24	0.76
C3-C9	0.26	0.64	0.25	0.73	0.27	0.83	0.21	0.73
C8-C9	0.16	0.61	0.16	0.81	0.17	0.87	0.13	0.81
C4-C9	0.05	0.60	0.03	0.69	0.06	0.78	0.07	0.73
C4-C5	0.21	0.70	0.21	0.75	0.22	0.78	0.18	0.76
C5-C6	0.29	0.67	0.29	0.75	0.30	0.81	0.27	0.78
C6-C7	0.03	0.66	0.02	0.70	0.04	0.74	0.03	0.76
C7-C8	0.28	0.55	0.28	0.73	0.29	0.82	0.26	0.75
N1-C8	0.07	0.28	0.02	0.21	0.06	0.47	0.03	0.19

Table 15. Indole ^3L_a Mulliken populations

	CIS/3-21G			CIS/6-31G			CIS/6-31G(p,d)		
	σ	π	total	σ	π	total	σ	π	total
N1	6.27	1.70	7.97	6.24	1.74	7.98	6.04	1.70	7.74
H1	0.64	0.00	0.64	0.63	0.00	0.63	0.68	0.01	0.69
C2	4.81	1.12	5.94	4.80	1.11	5.91	4.83	1.10	5.93
H2	0.75	0.00	0.75	0.78	0.00	0.78	0.83	0.00	0.83
C3	5.25	1.01	6.25	5.20	1.00	6.20	5.16	1.02	6.18
H3	0.76	0.00	0.76	0.78	0.00	0.78	0.84	0.00	0.84
C9	5.07	1.07	6.14	5.10	1.06	6.16	5.01	1.05	6.07
C4	5.22	0.97	6.20	5.13	0.99	6.11	5.14	0.99	6.12
H4	0.76	0.00	0.76	0.79	0.00	0.79	0.84	0.00	0.85
C5	5.21	1.04	6.25	5.17	1.04	6.22	5.12	1.04	6.16
H5	0.77	0.00	0.77	0.81	0.00	0.81	0.85	0.00	0.86
C6	5.24	0.98	6.21	5.21	0.98	6.19	5.17	0.97	6.14
H6	0.76	0.00	0.76	0.81	0.00	0.81	0.85	0.00	0.85
C7	5.15	1.12	6.26	5.08	1.11	6.18	5.09	1.12	6.20
H7	0.77	0.00	0.77	0.80	0.00	0.80	0.85	0.00	0.86
C8	4.58	0.99	5.56	4.67	0.97	5.65	4.69	0.98	5.67

Mulliken overlap populations

	CIS/3-21G		CIS/6-31G		CIS/6-31G(p,d)	
	π	σ	π	σ	π	σ
N1-C2	0.03	0.46	0.04	0.34	0.02	0.56
C2-C3	0.12	0.75	0.10	0.78	0.17	0.82
C3-C9	0.28	0.59	0.28	0.70	0.30	0.83
C8-C9	0.20	0.61	0.21	0.82	0.23	0.89
C4-C9	0.07	0.61	0.06	0.69	0.05	0.77
C4-C5	0.19	0.68	0.19	0.72	0.19	0.77
C5-C6	0.33	0.64	0.32	0.73	0.35	0.80
C6-C7	0.03	0.68	0.03	0.72	0.02	0.76
C7-C8	0.28	0.55	0.29	0.71	0.29	0.81
N1-C8	0.09	0.33	0.03	0.26	0.08	0.52

Table 16. Indole T_1 Mulliken populations, non-planar conformation

CIS/6-31G(p,d)				UHF/6-31G(p,d)					
	total		total		α	ß	total		total
N1	7.72	N1-C2	0.50	N1	3.85	3.85	7.70	N1-C2	0.51
H1	0.70	C2-C3	0.70	H1	0.36	0.36	0.71	C2-C3	0.64
C2	5.93	C3-C9	0.98	C2	3.44	2.45	5.89	C3-C9	0.97
H2	0.87	C8-C9	1.08	H2	0.44	0.46	0.89	C8-C9	1.01
C3	6.17	C4-C9	1.03	C3	3.58	2.62	6.20	C4-C9	0.95
H3	0.84	C4-C5	1.04	H3	0.39	0.46	0.85	C4-C5	1.01
C9	6.03	C5-C6	1.14	C9	2.60	3.40	6.00	C5-C6	1.01
C4	6.13	C6-C7	0.95	C4	3.49	2.63	6.13	C6-C7	0.95
H4	0.85	C7-C8	1.21	H4	0.40	0.45	0.85	C7-C8	1.11
C5	6.17	N1-C8	-0.12	C5	2.69	3.47	6.15	N1-C8	0.50
H5	0.85			H5	0.45	0.40	0.85		
C6	6.14			C6	3.50	2.65	6.15		
H6	0.85			H6	0.40	0.45	0.85		
C7	6.19			C7	2.72	3.44	6.16		
H7	0.85			H7	0.45	0.40	0.85		
C8	5.70			C8	3.25	2.51	5.76		

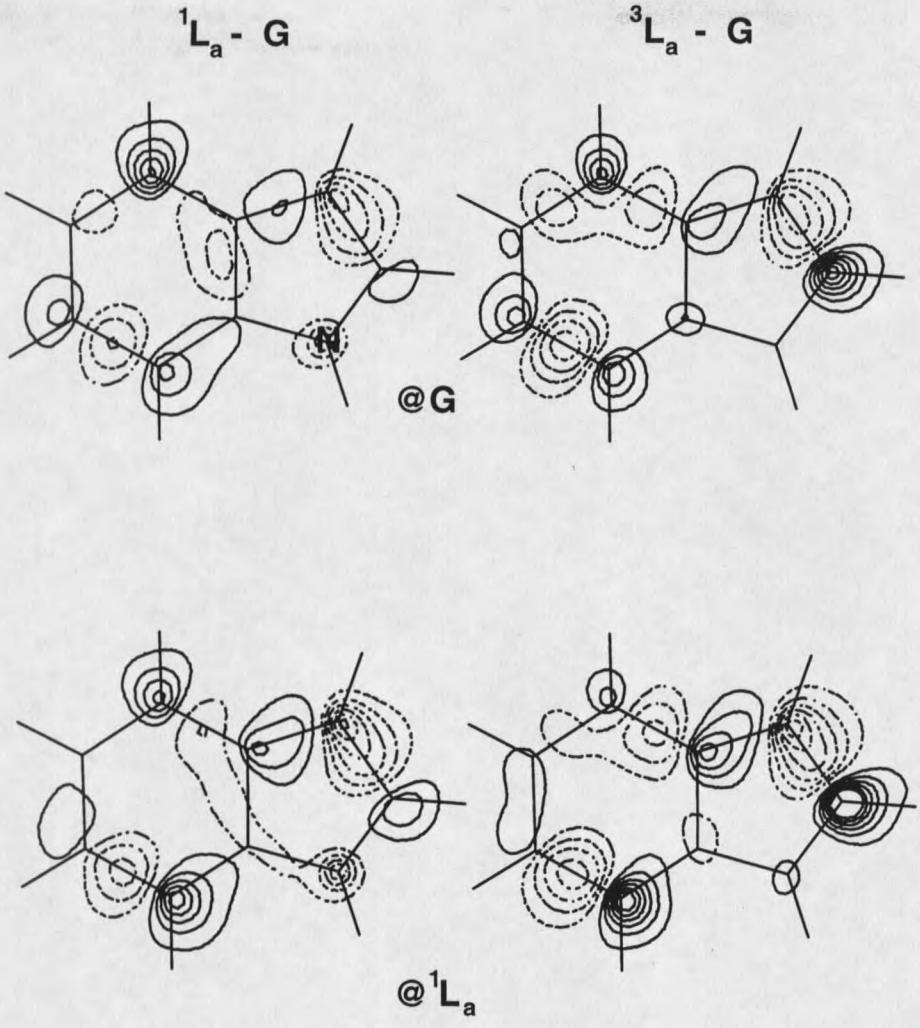

Figure 10. Indole ^1L_a - G and ^3L_a - G CIS-HF/6-31G(p,d) integrated density difference. Contour widths: 0.003 e/Bohr^3. Contour range: -0.019, 0.019 e/Bohr^3.

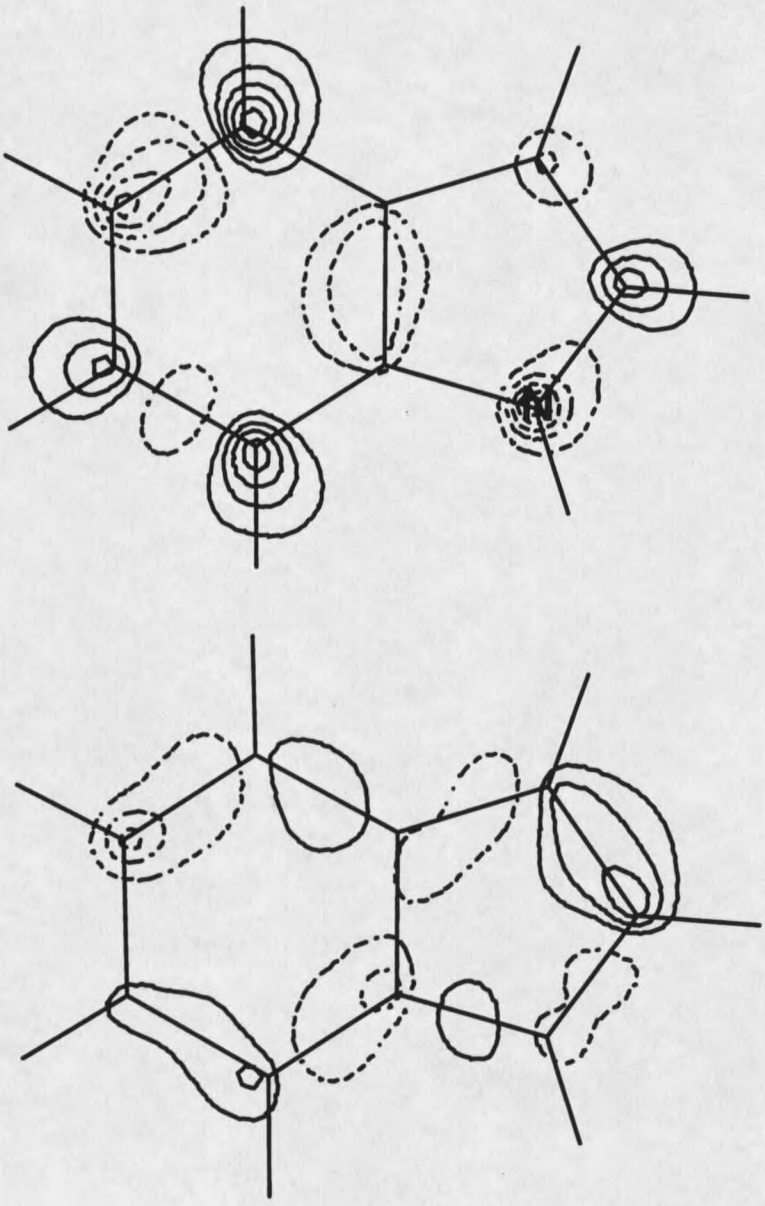

Figure 11. Indole ^1L_b - G and ^1L_b - ^1L_a CIS-HF/6-31G(p,d) integrated density difference. Contour widths: 0.003 e/Bohr^3.

At the ground state geometry, the contour minimum of the G → ^1L_a map is near C3, representing a depletion by 0.024 electrons, while N and the C6-C7 internuclear region are both depleted by 0.018 e. The contour maximum is centered on C4, which gains 0.030 e while C7 gains 0.020 e. For G → ^3L_a, the C2-C3 and C6-C7 internuclear regions both lose 0.024 e and the contour maximum is centered on C2, which gains 0.036 e. These results are consistent with the Mulliken population differences in Figure 8.

Geometry has a significant impact on the topology of both maps. At the ^1L_a geometry, the contour minimum of the G → ^1L_a map remains near C3, amounting to a 0.036 electron depletion, but N now loses 0.024 electrons, or 0.006 e more than in the ground state geometry. Also, the contour maximum has shifted from C7 to C4, which gains 0.030 e. For G → ^3L_a, the contour maximum is still centered on C2, which gains 0.060 e, but now the C2-C3 internuclear region is the sole minimum with a loss of 0.036 e, 0.012 e more than in the ground state geometry. C7 gains 0.042 e, 0.024 e more than at the ground state geometry.

The large geometry effect in the topology belies the insensitivity of indole's calculated ^1L_a and ^3L_a dipoles to small distortions in nuclear configuration.[8] For G → ^3L_a, the geometry effect may perhaps relate to the non-zero off-diagonal element of indole's quadrupole tensor, which changes sign in the triplet state on going from the ground to the ^3L_a nuclear configuration at CIS/6-31G(p,d), resulting in a significant redistribution of charge. No such changes are present between the higher order multipoles of the ground and ^1L_a states, however.

In order to quantify the total charge shift represented by each map in Figures

10 and 11, Simpson's rule numerical integration was performed over the positive amplitudes of the contour grid files and the result was then multiplied by two to account for the other side of the molecule. (Integrating over the negative amplitudes leads to virtually identical results.) According to this tabulation, at the ground state geometry, the ^1L_a transition amounts to a charge shift of 0.250 e, while the ^3L_a transition amounts to a charge shift of 0.268 e, which are comparable to the Mulliken population differences of 0.213 e and 0.240 e. A charge shift of 0.245 e accompanies the ^1L_b transition, compared to the 0.360 e sum of Mulliken population differences. A slightly greater charge redistribution occurs at the ^1L_a geometry, where 0.294 e are transferred in the ^1L_a transition and 0.330 e are transferred in the ^3L_a transition. At either geometry, the total charge shift of either ^1L_a or ^3L_a excitation is much greater than the sum of changes at a small number of atoms or bonds. Describing the ^1L_a transition as a charge transfer between N, C2, C4, and C7, as is commonly done, should be recognized as an approximation.

Dipole Moments

Table 17 shows the dipole moment of indole in each electronic state of interest, as calculated by a variety of methods and basis sets. Indole's dipole moment is defined in the same manner as its transition dipole moment, with the vector pointing towards the positive end of the molecule. This property shows little sensitivity to basis set size at the Hartree-Fock level of theory. The various modifications have small effects that largely cancel each other so that the HF/3-21G and HF/6-311++G(p,d) dipole moments are very similar in both magnitude and direction. One concludes that the gross charge distribution in the ground state of the indole molecule is adequately

Table 17. Indole ground and excited state dipole moments (Debye)

	method/basis//density	μ	θ
G	HF/STO-3G//SCF	1.80	-47.9
	HF/3-21G//SCF	2.02	-45.3
	HF/4-31G//SCF	1.90	-45.6
	HF/6-31G//SCF	1.93	-45.3
	HF/6-31G(p,d)//SCF	2.05	-45.3
	HF/6-31+G(p,d)//SCF	2.08	-45.8
	HF/6-31++G(p,d)//SCF	2.08	-46.2
	HF/6-311++G(p,d)//SCF	2.05	-45.8
	CISD/6-31G//CISD	2.13	-45.9
	MP2/6-31G(p,d)//SCF	2.11	-44.6
	MP2/6-31G(p,d)//MP2	2.19	-47.3
	EXP[a]	2.14	
^3L_a	CIS/3-21G//1PDM	1.53	-34.4
	CIS/3-21G//CIS	1.29	-37.2
	CIS/4-31G//CIS	1.12	-36.5
	CIS/6-31G//CIS	1.15	-37.4
	CIS/6-31G(p,d)//CIS	1.41	-37.3
	CIS/6-31+G(p,d)//CIS	1.41	-39.5
	CIS/3-21G//CIS[d]	0.63	
	CIS/6-31G(p,d)//CIS[d]	0.52	
	UHF/3-21G/SCF[d]	0.91	
	UHF/6-31G(p,d)/SCF[d]	1.36	
^1L_a	CIS/3-21G//1PDM	3.42	-20.7
	CIS/3-21G//CIS	3.22	-27.3
	CIS/4-31G//CIS	3.03	-27.7
	CIS(11,11)/6-31G//CIS	3.65	-22.4
	CIS/6-31G//CIS	3.07	-27.9
	CIS/6-31G(p,d)//CIS	3.19	-27.9
	CIS/6-31+G(p,d)//CIS	3.05	-31.6
	CIS/6-311++G(p,d)//CIS[e]	2.85	-27.9
	EXP[b]	~8.00	
^1L_b	CIS/3-21G//1PDM	2.42	-44.0
	CIS/3-21G//CIS	2.15	-41.3
	CIS/4-31G//CIS	2.08	-41.4
	CIS(11,11)/6-31G//CIS	2.01	-37.5
	CIS/6-31G//CIS	2.11	-41.2
	CIS/6-31G(p,d)//CIS/6-31G//CIS	2.25	-38.7
	CIS/6-311++G(p,d)//CIS[e]	2.32	-31.1
	EXP[c]	2.3	

[a]Reference 53. [b]Reference 14. [c]Reference 54. [d]Non-planar configuration. [e]CIS/6-311++G(p,d)// HF/6-311++G(p,d).

represented at just the HF/3-21G level. The dipole is less than a tenth of a Debye smaller than the measured value near the Hartree-Fock limit, and its value is increased roughly 0.15 Debyes by either of the correlated methods, reflecting the delocalization of lone pair density from N.

The comparative effects of basis on the four states in question are in keeping with results observed in other properties: polarization functions have the greatest effect on the ^3L_a dipole, diffuse functions have the greatest effect on the ^1L_a dipole, and the ^1L_a dipole shows the most sensitivity to the length of the CIS expansion. Less easily explained are the differing effects of the triple zeta basis on the excited state dipoles. In any event, Table 17 shows that a correlated density is not needed to accurately describe this property in the ^1L_b state, in contrast to the ^1L_a state.

The differences between the integrated electronic densities of the ^1L_a and ^3L_a states are presented in Figure 12 so as to appreciate their polarity disparity in the context of the projection function. The solid contours represent regions where the integrated density of the ^3L_a state exceeds that of the ^1L_a state. Fittingly, solid contour amplitudes are centered almost entirely on N and C2. The ^1L_a density exceeds that of the ^3L_a state by 0.024 e at N and 0.036 e at C2 in the ground state geometry, and by 0.036 e at N and 0.042 e at C2 in the ^1L_a geometry. That N and particularly C2 are out-of-plane in the less stable configuration of the triplet state suggests that retention of electron density at these atoms is conducive to non-planarity in the excited state.

On the benzene ring, the triplet state shows slightly greater electron density on the atoms than the singlet state and a slightly smaller density in the bonds. In this case the direction of the charge shift recalls the effect of correlation, and might simply

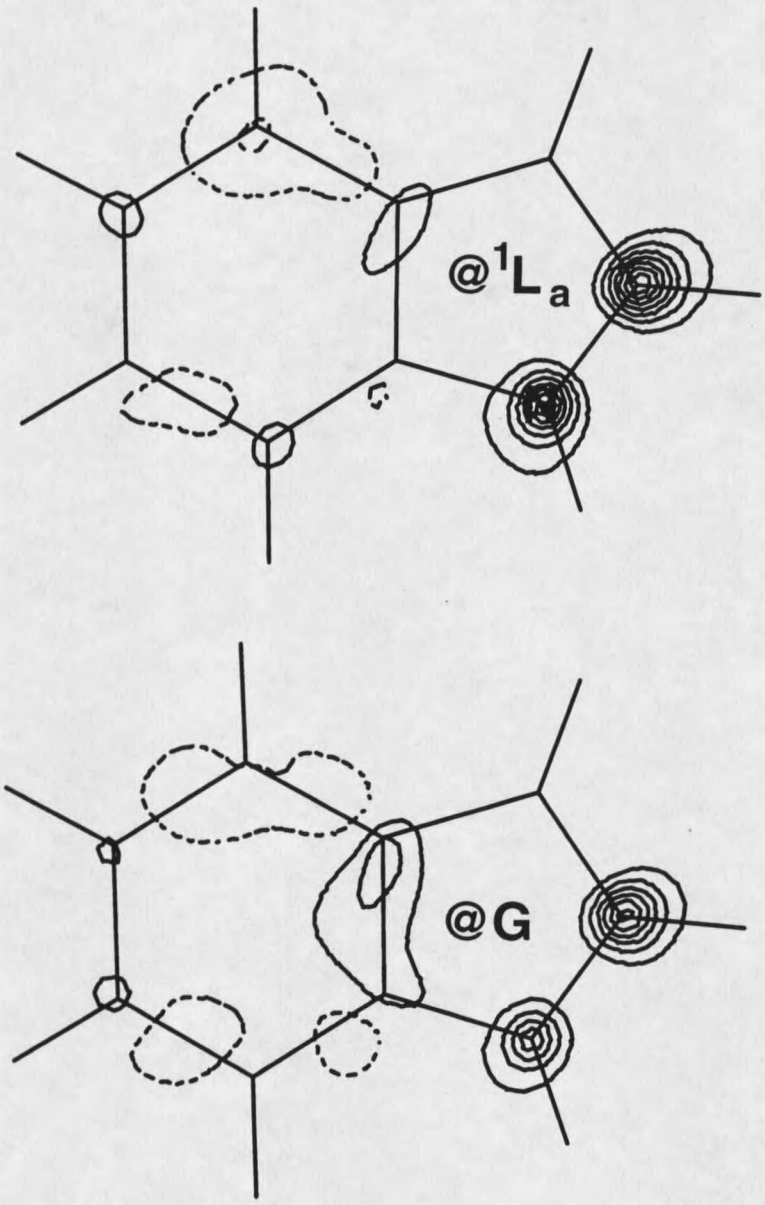

Figure 12. Indole ^1L_a - ^3L_a CIS-HF/6-31G(p,d) integrated density difference. Contour widths: 0.003 e/Bohr^3. Contour range: -0.006, 0.021 e/Bohr^3.

be an artifact of the extra correlation provided to CIS triplet states. In any event, the small density differences in this region of the molecule are seen to reinforce the dissimilarities between the ^1L_a and ^3L_a dipoles.

The lack of dashed contours in Figure 12 indicates that the charge lost at N and C2 in the ^1L_a state is somewhat uniformly redistributed around the remainder of the molecule and therefore inapparent at the present contour width. This is confirmed by integrating over the positive or negative contours in the Figure. According to either tabulation, a total of 0.180 e and 0.185 e are redistributed in the ground state and ^1L_a geometries, respectively.

Dipole Moment Matrix Elements

Using the 3-21G basis set, indole has 95 basis functions and therefore 64 virtual molecular orbitals. The dipole moment matrix then has a dimension of 1,984 resulting from the product of 31 occupied and 139 virtual MOs. Table 18 shows that only a small number of matrix elements arising from transitions between higher occupied and lower virtual MOs are needed to qualitatively reproduce the dissimilarities between ^1L_a and the other electronic states. These matrix elements are listed in bold. Also, it is shown that the dissimilarities may be explained in terms of the *x* component alone (i.e., M^x = 3.22 D for ^1L_a, 1.13 D for ^3L_a, and 2.22 D for ^1L_b), which is taken as the direction of the long molecular axis.

Table 18 and 19 show that the smaller dipoles in the ^1L_b and ^3L_a states result from a cancellation between diagonal and off-diagonal matrix elements. Each of the four largest CIS coefficients of the ^1L_a wave function involve transitions between different occupied and virtual orbitals: $|31 \rightarrow 32>$, $|30 \rightarrow 33>$, $|29 \rightarrow 34>$, and

Table 18. Indole ^3L_a and ^1L_a dipole moment matrix elements

				^3L_a			^1L_a		
i j k l	$\langle ij \mid \hat{m}_x \mid kl \rangle$	a(i,j)	a(k,l)	$M^x_{ij,kl}$[b]	a(i,j)	a(k,l)	$M^x_{ij,kl}$
31 32 31 32	3.384	0.889	0.889	**2.672**	0.919	0.919	**2.858**
30 33 30 33	3.710	0.244	0.244	**0.221**	0.329	0.329	**0.401**
29 34 29 34	-1.496	-0.275	-0.275	**-0.113**	-0.105	-0.105	**-0.016**
29 32 29 32	4.032	-0.112	-0.112	0.051	-0.007	-0.007	0.000
31 34 31 34	-2.144	-0.088	-0.088	-0.017	0.015	0.015	0.000
28 33 28 33	2.566	-0.083	-0.083	0.018	-0.005	-0.005	0.000
28 42 28 42	1.157	-0.132	-0.132	0.020	-0.071	-0.071	0.006
28 32 28 32	-1.285	0.027	0.027	-0.001	-0.013	-0.013	0.000
30 42 30 42	2.301	-0.001	-0.001	0.000	-0.033	-0.033	0.003
			OFF-DIAGONAL ELEMENTS				
31 32 29 32	12.063	0.889	-0.112	**-1.206**	0.919	-0.007	**-0.080**
31 34 31 32	12.019	-0.088	0.889	**-0.939**	0.015	0.919	**0.167**
29 34 29 32	12.019	-0.275	-0.112	0.372	-0.105	-0.007	0.009
31 34 29 34	12.063	-0.088	-0.275	0.291	0.015	-0.105	-0.019
30 33 28 33	11.189	0.244	-0.083	-0.226	0.329	-0.005	-0.017
28 42 28 33	9.183	-0.132	-0.083	0.101	-0.071	-0.005	0.003
31 32 28 32	3.975	0.899	0.027	0.094	0.919	-0.013	-0.048
30 42 30 33	9.183	-0.001	0.244	-0.002	-0.033	0.329	-0.100

				^3L_a			^1L_a		
i j k l	$\langle ij \mid \hat{m}_y \mid kl \rangle$	a(i,j)	a(k,l)	$M^y_{ij,kl}$[b]	a(i,j)	a(k,l)	$M^y_{ij,kl}$
31 32 31 32	-0.807	0.889	0.889	-0.638	0.919	0.919	-0.682
29 34 29 34	-1.838	-0.275	-0.275	-0.139	-0.105	-0.105	-0.020
30 33 30 33	-2.161	0.244	0.244	-0.128	0.329	0.329	-0.233
29 32 29 32	-0.788	-0.112	-0.112	-0.010	-0.007	-0.007	0.000
31 34 31 34	-1.857	-0.088	-0.088	-0.014	0.015	0.015	0.000
28 32 28 32	-1.822	0.027	0.027	-0.001	-0.013	-0.013	0.000
28 33 28 33	-1.971	-0.083	-0.083	-0.014	-0.005	-0.005	0.000
28 34 28 34	-2.872	-0.075	-0.075	-0.016	-0.026	-0.026	-0.002
23 34 23 34	-5.004	-0.047	-0.047	-0.011	-0.010	-0.010	0.000
			OFF-DIAGONAL ELEMENTS				
31 32 29 32	1.694	0.889	-0.112	-0.169	0.919	-0.007	-0.011
31 34 31 32	2.152	-0.088	0.889	-0.168	0.015	0.919	-0.030
31 32 28 32	6.720	0.889	0.027	0.159	0.919	-0.013	-0.082
30 33 28 33	-4.967	0.243	-0.083	0.100	0.329	-0.005	0.007
29 34 23 34	7.333	-0.275	-0.047	0.094	-0.105	-0.010	0.008
29 34 28 34	-4.075	-0.275	-0.075	-0.084	-0.105	-0.026	-0.011
31 42 31 32	6.986	0.001	0.889	0.007	-0.018	0.919	-0.121

[a]Calculated at CIS/3-21G optimized ^1L_a geometry. [b]$M^n_{ij,kl}$ = a(i,j) × a(k,l) × $\langle ij \mid \hat{\mu}_n \mid kl \rangle \times (2 - \delta_{ij,kl})$.

Table 19. Indole ^1L_b and ^1L_a dipole moment matrix elements

			^1L_b			^1L_a		
i j k l	$\langle ij \vert \hat{m}_x \vert kl \rangle$	a(i,j)	a(k,l)	$M^{x}_{ij,kl}$[b]	a(i,j)	a(k,l)	$M^{x}_{ij,kl}$
31 33 31 33	7.234	-0.595	-0.595	**2.557**	-0.002	-0.002	0.000
29 33 29 33	7.883	0.136	0.136	**0.147**	0.011	0.011	0.001
31 32 31 32	3.384	-0.008	-0.008	0.000	0.919	0.919	**2.858**
30 33 30 33	3.710	-0.010	-0.010	0.000	0.329	0.329	**0.401**
30 34 30 34	-5.669	0.075	0.075	-0.032	0.053	0.053	-0.016
30 32 30 32	-0.141	0.776	0.776	-0.085	0.013	0.013	0.000
31 42 31 42	5.826	0.047	0.047	0.013	-0.019	-0.019	0.002
31 34 31 34	-2.144	-0.048	-0.048	-0.005	0.015	0.015	-0.005
			OFF-DIAGONAL ELEMENTS				
31 33 29 33	12.063	-0.595	0.136	**-0.979**	-0.002	-0.011	0.000
30 34 30 32	12.019	0.075	0.776	**0.703**	0.053	0.013	0.008
31 42 31 33	9.183	0.047	-0.595	**-0.256**	-0.018	-0.002	0.000
31 34 31 33	3.884	-0.048	-0.595	0.110	0.015	-0.002	0.000
31 34 31 32	12.019	-0.048	-0.008	0.005	0.015	0.919	0.167
28 42 28 33	9.183	0.015	0.024	0.003	-0.071	-0.005	0.003
31 32 28 32	3.975	-0.008	0.001	0.000	0.919	-0.013	-0.048
30 42 30 33	9.183	-0.006	-0.010	0.000	-0.033	0.329	-0.100

			^1L_b			^1L_a		
i j k l	$\langle ij \vert \hat{m}_y \vert kl \rangle$	a(i,j)	a(k,l)	$M^{y}_{ij,kl}$[b]	a(i,j)	a(k,l)	$M^{y}_{ij,kl}$
30 32 30 32	-2.012	0.776	0.776	**-1.211**	0.013	0.013	0.000
31 33 31 33	-0.956	-0.595	-0.595	**-0.338**	-0.002	-0.002	0.000
31 32 31 32	-0.807	0.008	0.008	0.000	0.919	0.919	**-0.682**
30 33 30 33	-2.161	-0.010	-0.010	0.000	0.329	0.329	**-0.223**
29 33 29 33	-0.937	0.136	0.136	-0.017	0.011	0.011	0.000
30 34 30 34	-3.062	0.075	0.075	-0.017	0.053	0.053	-0.009
31 42 31 42	-1.354	0.047	0.047	-0.003	-0.019	-0.019	0.000
28 33 28 33	-1.971	0.024	0.024	-0.001	-0.005	-0.005	0.000
			OFF-DIAGONAL ELEMENTS				
31 33 29 33	1.694	-0.595	0.136	-0.137	-0.002	0.011	0.000
30 34 30 32	2.152	0.075	0.776	0.126	0.053	0.013	0.001
31 42 31 33	-3.748	0.047	-0.595	0.104	-0.019	-0.002	0.000
31 33 28 33	6.720	-0.595	0.024	-0.094	-0.002	-0.005	0.000
31 34 31 33	-2.255	-0.048	-0.595	-0.064	0.015	-0.002	0.000
31 42 31 32	6.986	0.047	-0.008	-0.003	-0.019	0.919	-0.122
31 32 28 32	6.720	-0.008	0.001	0.000	0.919	-0.013	-0.082

[a]Calculated at CIS/3-21G optimized ^1L_a geometry. [b]$M^{n}_{ij,kl}$ = a(i,j) × a(k,l) × $\langle ij \vert \hat{\mu}_n \vert kl \rangle \times (2 - \delta_{ij,kl})$.

$|28 \rightarrow 42>$. These configurations account for over 98% of the CIS ^1L_a wavefunction. Because the dipole moment operator is a one-electron operator, the off-diagonal matrix elements involving only these configurations vanish, e.g. $<31,32|\hat{m}_x|30,33> = 0$, as discussed in the Methods chapter. In contrast, the ^3L_a wave function receives a significant contributions from $|29 \rightarrow 32>$ and $|31 \rightarrow 34>$ in addition to the large contribution from $|31 \rightarrow 32>$. The latter determinant can and does form large off-diagonal matrix elements with the former determinants, as Table 18 shows. (The off-diagonal elements have been multiplied by a factor of two in order to account for the identical contribution from the transpose matrix element in the symmetric dipole moment matrix.) Similarly, the ^1L_b wave function receives a significant contribution from $|29 \rightarrow 33>$ in addition to the large contributions from $|30 \rightarrow 32>$ and $|31 \rightarrow 33>$, resulting in a large off-diagonal matrix element. Very similar results for each state are obtained at CIS/6-31G(p,d).

Ground State Normal Modes and Frequencies

Indole has 42 normal modes of vibration, of which 29 are in-plane having a′ symmetry and 13 are out-of-plane having a″ symmetry. By convention, the a′ and a″ vibrations are enumerated, in order of increasing frequency, as modes 29 through 1 and modes 42 through 30, respectively. The ground state frequencies of indole, as calculated by the Hartree-Fock method with a variety of basis sets, and at MP2/6-31G(p,d), are compared to the results of Raman spectroscopy in Table 20.

As shown in the Table, most frequencies decrease uniformly as the size of the basis set is increased. The major exception is mode 40, the a″ N-H bend, the frequency of which shows extreme sensitivity to basis set size. Using a split valence basis increases the frequency of this mode by 90% (i.e., from 330 cm^{-1} to 618 cm^{-1}), causing an inversion, while inclusion of polarization functions decreases the frequency

Table 20. Indole ground state frequencies (cm^{-1})

	HARTREE-FOCK								
	3G	3-21G	4-31G	6-31G	6-31G**	6-31++G**	6-311++G**	EXP[a]	MP2/6-31G**
42	217	246	244	242	232	230	228	207	205
41	264	282	282	279	266	264	262	240	221
40	330	494	491	486	378	383	365	420	332
39	498	618	615	604	472	471	469	516	379
38	658	665	661	654	632	631	627	570	388
37	691	690	689	682	666	661	661	601	540
36	879	852	848	842	814	810	805	715	589
35	899	883	878	872	839	835	830	738	710
34	933	920	912	903	865	860	858	791	720
33	1035	1022	1013	1005	960	957	951	850	782
32	1092	1072	1068	1061	1006	1004	1000	904	807
31	1158	1122	1116	1110	1062	1066	1059	925	860
30	1193	1168	1164	1159	1100	1107	1090	979	888
29	448	436	441	440	431	431	429	387	400
28	615	603	606	603	588	586	585	538	553
27	694	687	687	682	662	660	660	612	618
26	866	831	841	838	825	822	819	745	780
25	1002	968	976	972	946	945	942	879	896
24	1027	997	1004	1000	977	975	974	899	914
23	1183	1107	1122	1120	1109	1102	1097	1014	1050
22	1238	1151	1176	1180	1176	1173	1166	1067	1109
21	1256	1209	1219	1217	1191	1188	1181	1083	1136
20	1279	1243	1256	1253	1223	1221	1213	1122	1169
19	1321	1281	1290	1288	1243	1240	1233	1150	1199
18	1394	1320	1337	1336	1313	1311	1304	1204	1251
17	1403	1362	1397	1400	1368	1365	1358	1227	1289
16	1455	1390	1408	1410	1386	1385	1372	1244	1336
15	1499	1415	1427	1429	1398	1392	1386	1278	1410
14	1604	1506	1524	1521	1506	1501	1492	1330-47	1460
13	1692	1556	1581	1582	1575	1568	1560	1414	1503
12	1742	1616	1632	1631	1620	1613	1604	1458	1542
11	1793	1656	1675	1672	1661	1653	1645	1479	1556
10	1853	1686	1714	1711	1707	1691	1682	1520	1590
9	1921	1745	1780	1782	1779	1768	1762	1576	1651
8	1960	1783	1819	1821	1816	1805	1798		1705
7	3709	3349	3339	3349	3334	3337	3315		3246
6	3722	3358	3348	3358	3343	3346	3324		3252
5	3734	3370	3361	3371	3355	3358	3336	3051	3264
4	3742	3383	3376	3386	3368	3370	3348	3072	3276
3	3747	3432	3427	3436	3409	3410	3385		3322
2	3786	3458	3456	3465	3431	3433	3408	3118	3341
1	4147	3858	3928	3945	3939	3934	3918	3523	3746

[a]Reference 55.

by 40% (from 604 cm^{-1} to 378 cm^{-1}), once again inverting the order. Accompanying both of these shifts are large changes in the force constant and small changes in reduced mass of the normal mode. Ultimately, mode 40 underestimates the observed frequency by 13% at HF/6-311++G(p,d) while nearly all other a″ frequencies are overestimated by 10% - 15%. The a′ frequencies are overestimated by 7 - 11% at HF/6-311++G(p,d) and modes with amplitude on H1, such as 1, 9, 11, 13, and 17, comprise the upper bound. The frequencies of a′ modes that stretch the ethylene-like C2-C3 bond also tend to be less accurate at the Hartree-Fock level. The discrepancies between theory and experiment are attributable to the inflationary effects of the independent electron approximation and the harmonic oscillator approximation, which are usually reinforced by the basis set truncation error.

Electron correlation, as calculated at the MP2/6-31G(p,d) level, decreases the frequencies of most a″ modes by roughly 15%. This is attributable to the more diffuse nature of virtual π MOs, in comparison to the occupied π MOs. The contribution of the diffuse, or "outer" p function of split valence basis sets tends to be greater in the virtual π MOs than the occupied π MOs. These functions have a bearing on the MP2 energy correction and therefore the MP2 frequencies by mixing with occupied orbitals through the two electron operator. The MP2 frequencies then reflect a system with a smaller π electron density near the molecular plane, resulting in a smaller restoring force for out-of-plane motion. For indole, the MP2/6-31G(p,d) a″ frequencies are about 10% smaller than the observed values, suggesting an exaggeration of the effects of electron correlation, as is often the case with other MP2-computed properties.[56] In-plane frequencies are less sensitive to correlation, being only 5% smaller than the HF/6-31G(p,d) values. One a′ frequency, that of mode 15, is increased by the MP2

method. This mode is only 12 cm^{-1} higher in frequency than mode 16 at HF/6-31G(p,d), and 44 cm^{-1} lower than mode 14, so it is not surprising that its value gets raised.

The MP2/6-31G(p,d) normal modes, which have not been mass-weighted, are shown in Figure 13 and 14. In contrast to the frequencies, electron correlation has a greater effect on the normal coordinates of the a′ modes. In particular, modes 9 - 20, the in-plane ring skeletal modes in the 1,000 - 1,800 cm^{-1} frequency range, have normal coordinates that are very sensitive to this perturbation. The normal coordinates of the C-H bending modes also appear sensitive to electron correlation, while those of the low frequency a′ modes and the N-H and C-H stretching modes appear unaffected. Thus, each a′ mode's sensitivity appears to be dictated simply by the extent to which it is separated in energy from other a′ modes. The medium frequency a′ modes are closely spaced, helping to create a small energy denominator and therefore a large second order correction. The exceptions, modes 18, 14, and 8, are seen to be somewhat well-separated in energy from the other a′ modes, comparatively speaking, making their normal coordinates less sensitive to the effects of electron correlation, at least to second order.

Most normal coordinates of the a″ modes show little or no sensitivity to electron correlation, but the N-H out-of-plane bend is once again the exception. While this motion is limited to mode 39 at HF/6-31G(p,d), it is distributed between three a″ C-H bending modes at MP2/6-31G(p,d), as Figure 14 shows. This result defies the comparatively greater separation between mode 40 and the other a″at HF/6-31G(p,d), as shown in Table 20. It is evident that the correlation energy is particularly sensitive to displacement along this normal coordinate.

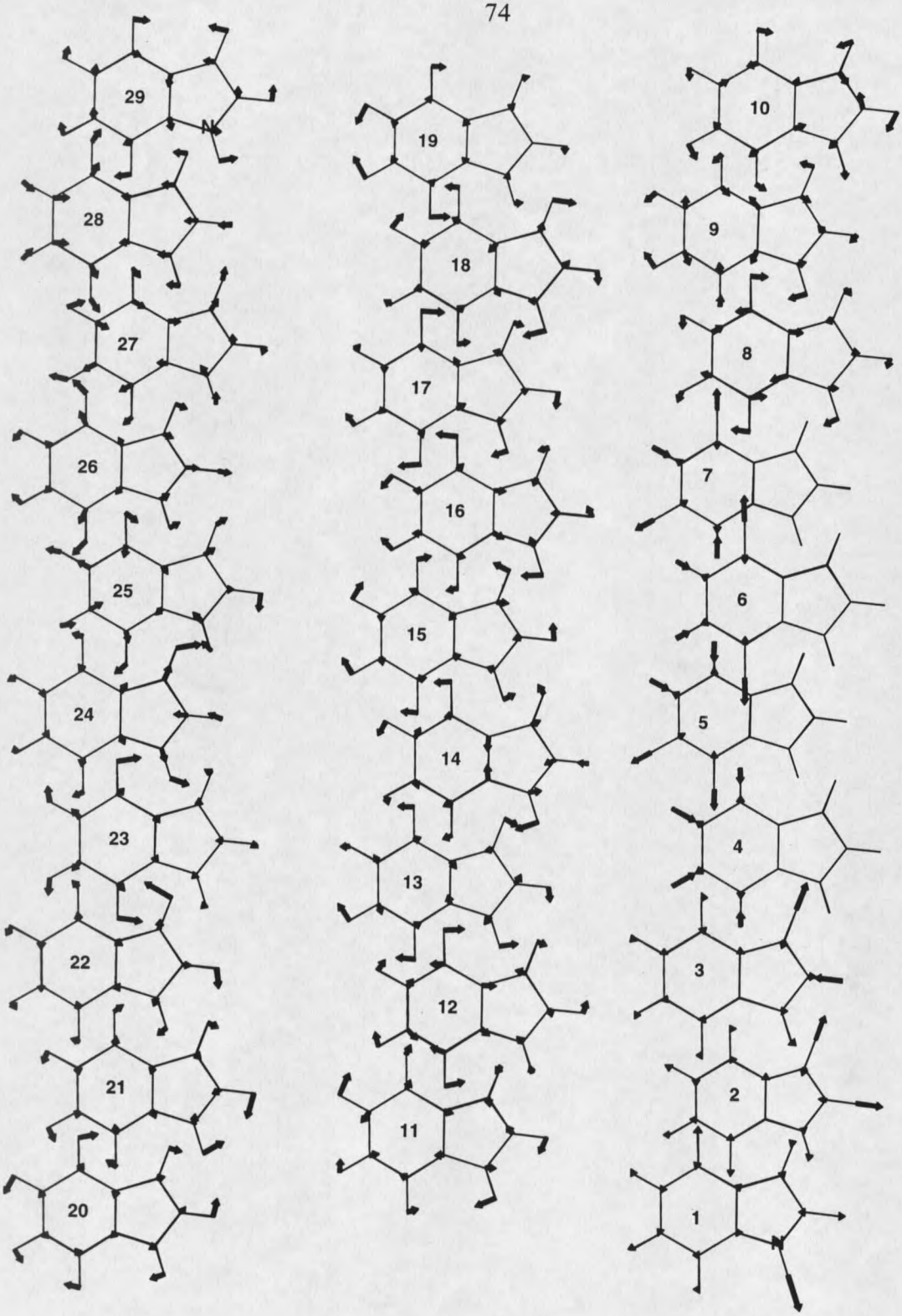

Figure 13. Indole MP2/6-31G(p,d) a′ normal modes of vibration.

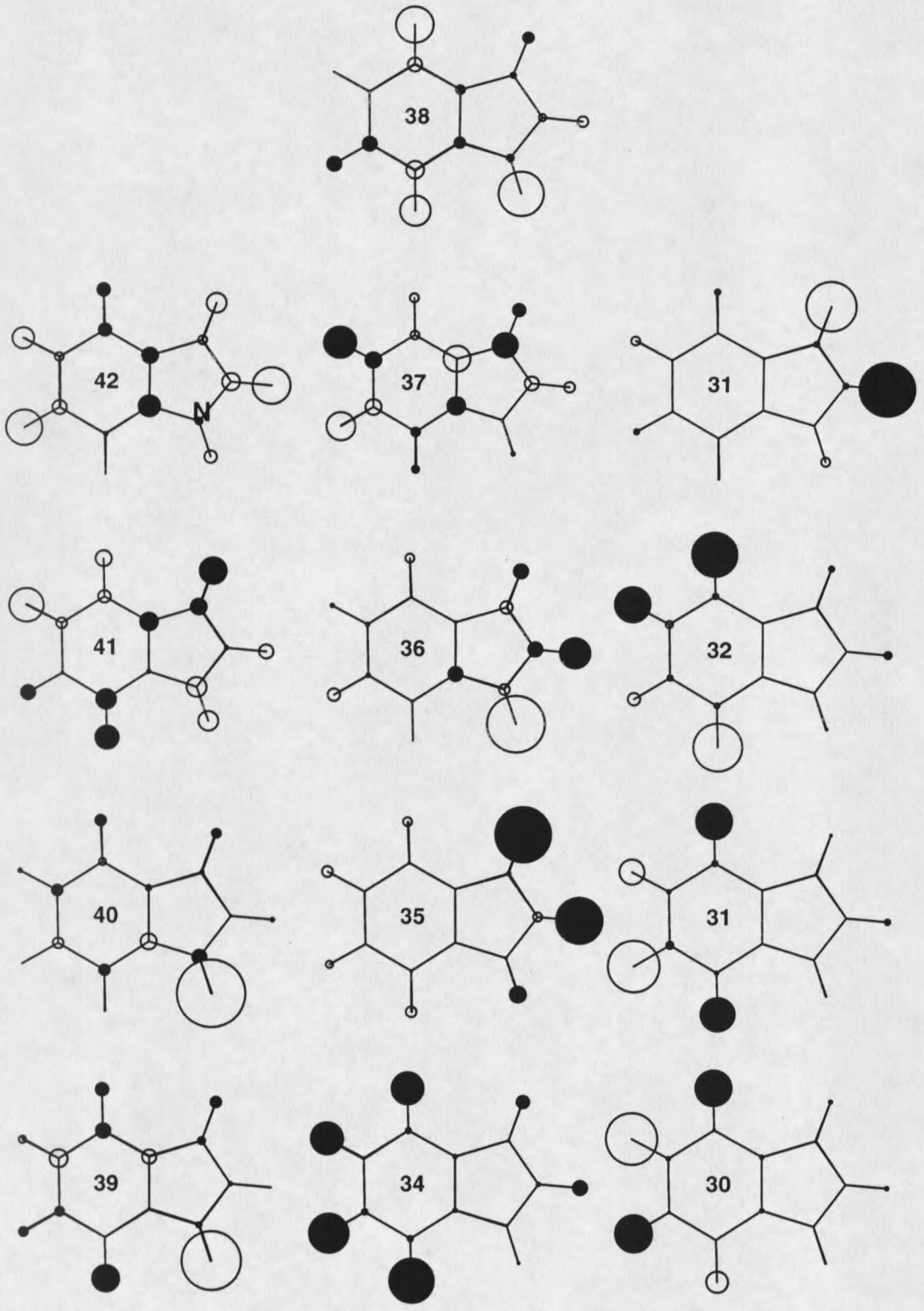

Figure 14. Indole MP2/6-31G(p,d) a″ normal modes of vibration.

Excited State Normal Modes and Frequencies

The calculated vibrational frequencies of electronically excited indole are listed in Table 21. The a′ and a″ modes are separated and listed in descending order, as with the ground state, although the Duschinsky effect and changes in the ordering may make comparisons between the two states less meaningful. The experimental results of jet-cooled spectroscopy are included alongside the calculated ^1L_b frequencies, although the paucity of experimental data make the assignments uncertain. The jet-cooled spectrum gives results very similar if not identical to those obtained in a study of indole's photoelectron spectrum. To date, very few ab initio normal coordinate analyses have been performed on the excited states of aromatic molecules, and it appears that none have been performed on indole's excited states.

As Table 21 shows, the ^1L_b low frequency a′ modes are extremely sensitivity to basis. The large fluctuation between CIS(11,11)/6-31G and CIS/6-31G is of particular interest, as it accompanies the inversion between ^1L_a and ^1L_b. Mode 28 (denoted with an asterisk), in particular, decreases in frequency by 28%, resulting in an inversion with 29. This concurs with the role mode 28 plays in vibrationally coupling ^1L_a and ^1L_b.[2] The coupling induced by this vibration is apparently strong enough to warp the ^1L_b potential energy surface from its zeroth-order topology, resulting in a softened mode.

Additional support for this assertion is found in the frequency differences between the excited and ground states, which are also important in so far as calculated vibronic spectra is concerned as they allow overtone vibrations to acquire intensity. Table 22 shows that, for the low frequency modes, the CIS(11,11)-HF/6-31G frequency differences are far superior to those of the CIS-HF/6-31G level of theory.

Table 21. Indole excited state frequencies (cm^{-1})

	^1L_b				^1L_a				^3L_a		
		6-31G				6-31G					
	3-21G	CIS	CIS(11,11)	EXP[a]	3-21G	CIS	CIS(11,11)	6-31G**	3-21G	6-31G	6-31G**
42	188	188	210	158	192	217	184	178	211	206	184
41	210	207	212	183	241	254	241	234	254	251	243
40	374	361	359	257	355	354	346	329	387	382	315
39	441	434	441	278	539	545	536	454	437	391	372
38	583	580	597	316	582	595	575	548	540	526	438
37	670	649	635	369	669	699	655	578	550	537	531
36	713	704	709	498	721	747	710	664	589	572	558
35	743	744	741		745	755	732	689	752	746	692
34	758	748	781		788	773	778	746	781	773	716
33	836	811	826		872	868	857	800	873	846	787
32	882	869	888		925	955	906	835	908	898	821
31	994	989	980		980	989	976	917	915	905	977
30	1001	999	1009		1086	1073	1078	1017	1077	1066	1011
29	401	242*	431	380	427	432	430	423	426	431	416
28	502*	467	557*	480	553	579	553	536	539	557	528
27	605	582	626	540	638	712	641	626	646	649	627
26	773	795	801	718	790	819	804	800	656	688	711
25	880	872	937	720	923	933	930	906	844	859	867
24	964	967	972		955	976	960	942	936	938	922
23	982	1027	1054	920	1005	1077	1036	1034	972	975	961
22	1057	1082	1117	990	1094	1159	1127	1122	1010	1054	995
21	1158	1151	1185	969	1128	1167	1146	1132	1087	1111	1093
20	1194	1193	1222		1194	1233	1212	1197	1181	1197	1185
19	1263	1277	1284		1211	1279	1248	1219	1231	1245	1211
18	1267	1290	1303	1122	1254	1345	1266	1248	1236	1266	1250
17	1360	1358	1385		1290	1353	1323	1304	1320	1337	1313
16	1388	1398	1408		1350	1375	1361	1345	1326	1350	1322
15	1409	1433	1483		1422	1491	1447	1420	1375	1404	1367
14	1492	1496	1531	1317	1460	1518	1492	1490	1467	1492	1462
13	1527	1530	1562		1489	1560	1514	1498	1501	1527	1505
12	1586	1589	1617		1534	1595	1557	1552	1519	1532	1550
11	1603	1620	1642		1557	1614	1566	1558	1558	1572	1554
10	1634	1663	1725		1604	1635	1623	1610	1609	1618	1604
9	1707	1736	1775		1616	1704	1635	1633	1628	1666	1664
8	1729	1775	1809		1679	1815	1709	1708	1648	1684	1669
7	3363	3367	3371		3354	3357	3357	3343	3355	3356	3343
6	3379	3379	3380		3372	3370	3372	3358	3371	3370	3358
5	3393	3395	3394		3384	3379	3384	3371	3382	3381	3370
4	3401	3404	3405		3393	3393	3394	3378	3390	3391	3377
3	3434	3438	3437		3438	3445	3441	3414	3428	3430	3406
2	3475	3480	3477		3464	3483	3474	3443	3475	3483	3453
1	3833	3925	3933		3829	3914	3921	3916	3855	3944	3935

[a]Modes 42, 41, 39, 37, 36 : reference 57, 58. Modes 40, 38: reference 57.

Table 22. Indole ^1L_b - ground state frequency differences (cm^{-1})

mode	CIS/3-21G	CIS/6-31G	CIS(11,11)/6-31G	EXP[a]
29	36	198	9	7
28	101	136	46	58
27	82	100	56	72
26	57	43	35	27
25	89	100	37	159
42	55	54	32	49
41	72	72	67	57

[a] References 55, 57.

For modes 29 through 26, even the relative sizes of the differences are reproduced by the truncated wave function. At CIS/6-31G, vibronic coupling lowers the ^1L_b frequencies, and exaggerated differences are obtained. At CIS/3-21G, the effect of vibronic coupling is much less apparent because of the mere 80 cm^{-1} change in the 0-0 separation between the excited states.

The smaller frequencies of the CIS/6-31G method means that the simple picture attached to second order Jahn-Teller type interactions, where the upper state has the sharper well and the lower surface has the flatter well due to the mutual repulsion of surfaces, is not pertinent in the present situation. This is because the potential energy curves are displaced along the normal coordinate in question, so that ^1L_b is the lower state at or near its own minimum. Other ab initio calculations have shown that indole's avoided crossing is near the ^1L_b minimum,[59] which agrees with the larger frequency shift in this state. Near the ^1L_a minimum the surfaces are well-separated in energy and the shift in mode 28 is less pronounced.

Although the effect of vibronic coupling is particularly apparent in the lower vibrational manifold, and at first glance confined to these states, its consequences are actually rather pervasive according to the present calculations. Aside from the C-H

Table 23. Indole Hartree-Fock & CIS(11,11)/6-31G vibrational properties

	μ^1			κ^2		
	G	^1L_a	^1L_b	G	^1L_a	^1L_b
42	4.11	3.39	3.53	0.14	0.09	0.09
41	3.59	4.03	4.03	0.16	0.15	0.11
40	2.80	2.66	2.95	0.39	0.20	0.22
39	1.14	2.06	2.42	0.24	0.36	0.28
38	3.24	2.45	1.52	0.82	0.51	0.32
37	2.95	1.28	1.72	0.81	0.37	0.41
36	1.47	1.36	1.85	0.62	0.45	0.55
35	1.40	1.64	1.49	0.63	0.55	0.48
34	1.96	1.45	1.35	0.94	0.51	0.48
33	1.57	1.61	1.79	0.93	0.71	0.72
32	1.40	1.94	1.42	0.93	1.04	0.66
31	1.40	1.46	1.55	1.02	0.84	0.88
30	1.40	1.55	1.40	1.10	1.05	0.84
29	3.73	3.78	3.86	0.42	0.42	0.42
28	6.60	6.81	6.81	1.41	1.35	1.25
27	6.56	6.29	6.39	1.80	1.88	1.48
26	5.17	5.04	4.84	2.14	1.99	1.83
25	4.83	5.05	5.19	2.69	2.59	2.69
24	4.36	4.65	4.64	2.57	2.61	2.58
23	2.31	2.48	2.69	1.70	1.69	1.76
22	2.23	1.73	3.01	1.83	1.37	2.21
21	1.38	1.87	1.80	1.21	1.50	1.49
20	1.55	1.71	1.26	1.44	1.53	1.11
19	1.28	1.24	1.85	1.25	1.20	1.80
18	2.24	2.09	1.45	2.36	2.23	1.45
17	2.00	2.26	1.49	2.30	2.44	1.68
16	2.64	2.41	3.02	3.09	2.69	3.53
15	2.81	1.99	2.17	3.38	2.61	2.81
14	1.75	3.01	1.60	2.39	4.09	2.22
13	1.91	2.26	1.96	2.82	3.24	2.81
12	2.36	1.93	2.19	3.70	2.89	3.38
11	2.43	3.10	2.46	4.01	4.75	3.91
10	3.86	2.17	3.98	6.67	3.42	6.97
9	4.97	3.03	5.79	9.30	5.19	10.74
8	5.84	7.24	8.36	11.40	14.05	16.11
7	1.09	1.09	1.09	7.18	7.22	7.28
6	1.09	1.09	1.09	7.25	7.31	7.33
5	1.10	1.09	1.09	7.34	7.35	7.42
4	1.10	1.10	1.10	7.43	7.44	7.50
3	1.09	1.09	1.09	7.54	7.66	7.61
2	1.11	1.10	1.10	7.83	7.86	7.85
1	1.08	1.08	1.08	9.91	9.76	9.85

[1]Reduced mass. [2]Force constant in amu.

Table 24. Indole ^1L_b isotope shift ($\nu_{Indole(D1)} - \nu_{Indole(H1)}$) ($cm^{-1}$)

mode/basis	CIS/3-21G	CIS/6-31G	CIS(11,11)/6-31G	EXP[a]
42	0	0	-6	-1
41	-6	-6	-1	-3
40	0	0	0	---
39	-6	-7	-11	-6
38	---	---	---	---
37	---	---	---	-1
29	-7	-2	-8	-4
28	-4	-7	-2	-2
27	-3	-2	-2	-2
26	-9	-9	-7	-4

[a] Reference 57.

and N-H stretches, every ^1L_b a′ mode decreases in frequency on going from CIS/6-31G to CIS(11,11)/6-31G while the same modification causes the frequency of every ^1L_a a′ mode increase. Also, the higher frequency ^1L_a a′ modes tend to be shifted further than those of the ^1L_b state. (The absence of significant vibronic activity in mode 24 rebukes the 24_0^1 assignment[60] for the 737 cm^{-1} transition in the ^1L_b excitation spectrum and supports the 37_0^2 assignment.[57]) Thus, the changes in zero-point motion caused by the inversion are predicted to have a small effect on the relative stability of these states.

The decrease in vibrational frequency, relative to the ground state, following ^1L_a and ^1L_b excitation results primarily from smaller force constants, especially those of the a″modes, as Table 23 shows. The reduced masses of both the a′ and a″ normal modes are generally larger in the excited states than in the ground state, indicating that the modes are more localized and involve larger amplitude motion on fewer atoms. The effect of vibronic coupling decreases the force constant of mode 28 from 1.25 to 0.24 mDyne/Å between CIS(11,11)/6-31G and CIS/6-31G while the reduced mass goes from 7.01 to 6.81.

The ^1L_b CIS(11,11)/6-31G normal coordinates are shown in Figures 15 and 16.

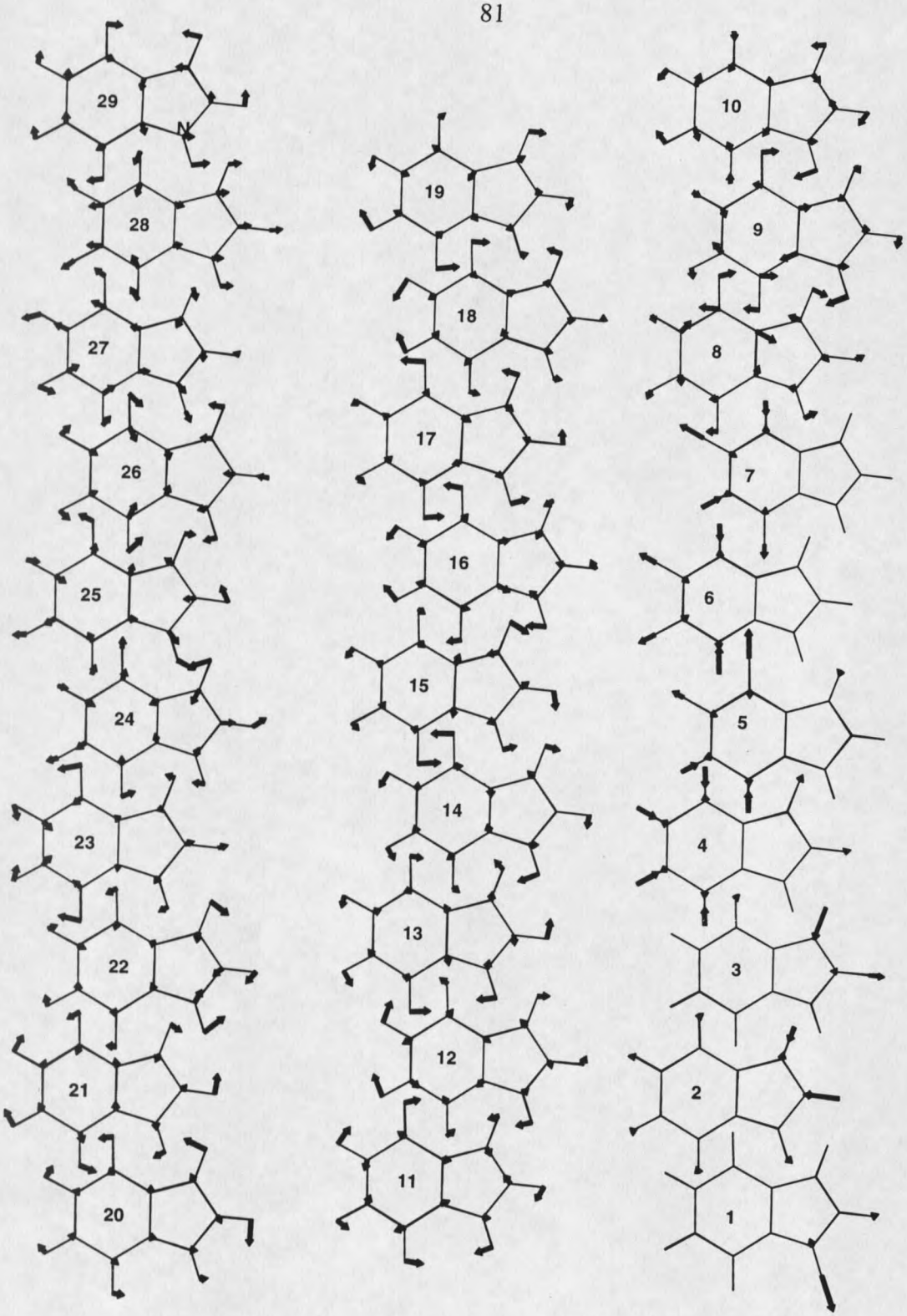

Figure 15. Indole ^1L_b CIS(11,11)/6-31G a′ normal modes of vibration.

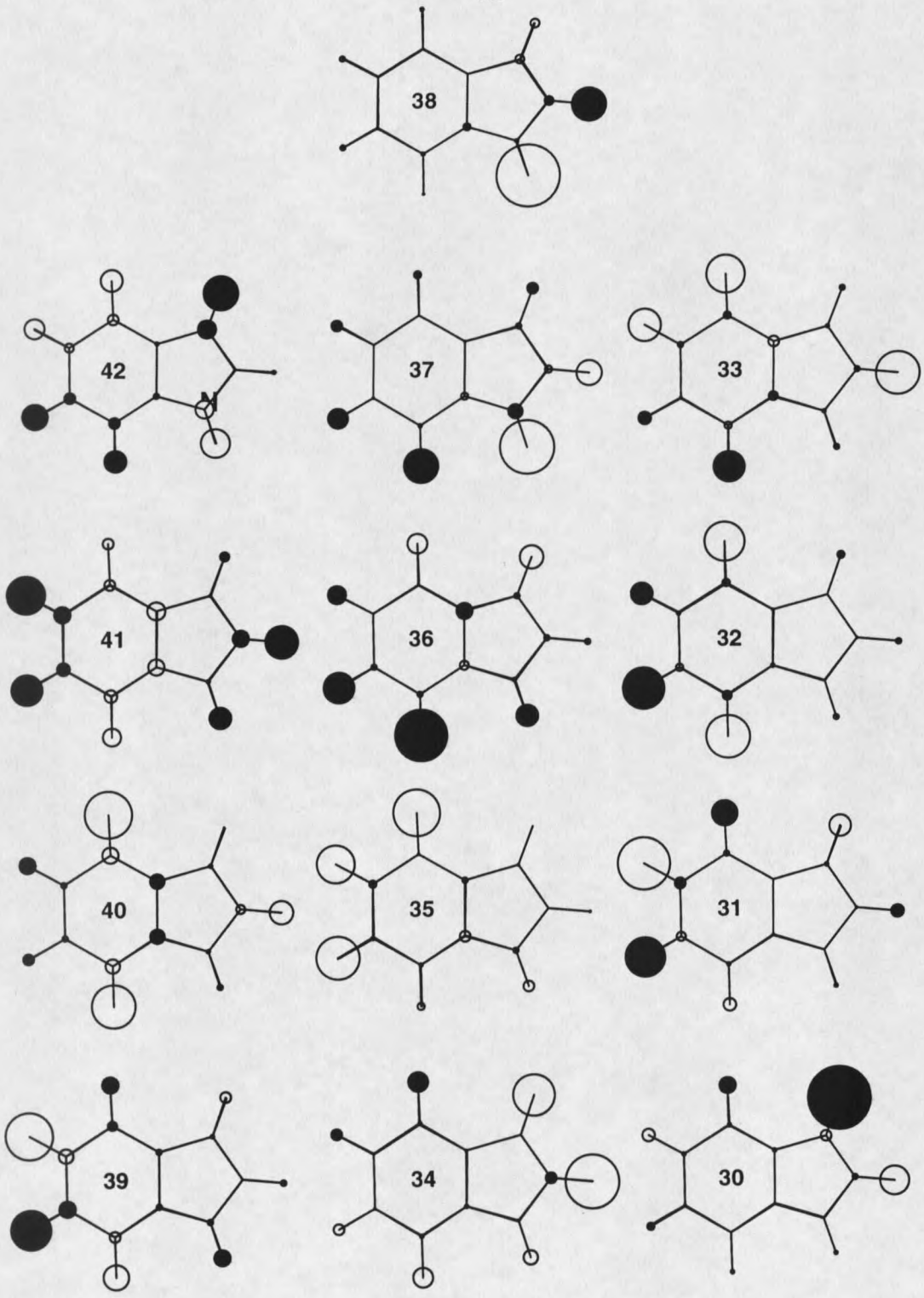

Figure 16. Indole ^1L_b CIS(11,11)/6-31G a″ normal modes of vibration.

The effect of deuterium substitution at H1 on the frequencies of the low energy ^1L_b normal modes are presented in Table 24. In general there is a one-to-one correlation between the calculated a″ modes of indole-H1 and indole-D1 up until mode 38, at which point the modes become mixed.. Virtually no mixing is predicted in the four lowest a′ modes upon deuteration, regardless of basis. As the Table shows, there is an inversion between modes 29 and 28 on going from the truncated to full CIS wave function, thereby demonstrating another effect of vibronic coupling, and the CIS(11,11)/6-31G a′ shifts are more consistent with the observed results. However, the a″ shifts are better described at CIS/6-31G. In either case, the shifts are generally exaggerated by theory, meaning that the calculated amplitudes of vibration are too localized on H1 in certain modes. The observed shifts indicate that H1 vibrational motion is distributed more evenly between the various modes, particularly those of a″ symmetry, then is predicted by the calculations.

Additional computational evidence of vibronic coupling is provided by a large variation in the infrared absorption intensity. Mode 28 has an IR intensity of 2.63 KM/Mole at CIS(11,11)/6-31G and 89.4 KM/Mole at CIS/6-31G. The latter result is consistent with significant redistribution of electronic charge when the nuclei are displaced from the equilibrium position.[61]

The situation regarding vibronic coupling is complicated by substantial mixing of normal modes at CIS/6-31G. Mode mixing results from changes in the off-diagonal elements of the force constant matrix that may accompany electronic excitation. When the energy separation between two modes having the same symmetry is small, changes in the coupling constants lead to mixing between ground state normal coordinates. Table 25 shows the ^1L_b Dushinsky matrix elements of indole as calculated at CIS(11,11)/6-31G, in relation to HF/6-31G normal modes. Indole's a′ C-H and N-H bending modes constitute a fairly dense manifold of vibrational states and, as a

Table 25. Indole ^1L_b CIS(11,11)/6-31G mode mixing

42″ = -0.19*42′ + 0.98*41′
41″ = -0.97*42′ - 0.18*41′ + 0.14*40′
40″ = 0.15*42′ + 0.98*40′
39″ = 0.26*39′ + 0.92*38′ + 0.16*37′ - 0.17*36 - 0.13*34
38″ = -0.66*39′ + 0.72*37′ - 0.15*35′ + 0.11*33
37″ = -0.64*39′ + 0.35*38′ - 0.62*37′ + 0.15*36 + 0.18*34 + 0.10*33
36″ = 0.25*39′ + 0.13*38′ + 0.22*37′ + 0.64*36 - 0.23*35 + 0.61*34
35″ = -0.10*39′ + 0.91*35′ + 0.35*34′
34″ = -0.10*39′ + 0.66*36′ + 0.22*35′ - 0.56*34 - 0.30*33 + 0.30*32
33″ = 0.11*35′ - 0.32*34′ + 0.91*33′ + 0.19*32
32″ = 0.26*32′ + 0.96*31′
31″ = 0.12*36′ + 0.13*33′ - 0.35*32′ + 0.91*30
30″ = -0.26*36′ + 0.23*34′ + 0.83*32′ - 0.26*31 + 0.36*30

29″ = 1.00*29′
28″ = -0.98*28′ - 0.13*27′ + 0.14*26′
27″ = -0.14*28′ + 0.98*27′
26″ = 0.13*28′ + 0.98*26′ + 0.15*24′
25″ = -0.86*25′ - 0.48*24′
24″ = -0.12*26′ - 0.51*25′ + 0.84*24′
23″ = 0.96*23′ - 0.24*22′
22″ = 0.11*24′ + 0.24*23′ + 0.94*22′ + 0.16*20′
21″ = -0.82*21′ + 0.53*20′ + 0.11*19′
20″ = -0.16*22′ + 0.55*21′ + 0.77*20′ + 0.21*19′ - 0.13*15′
19″ = -0.11*24′ - 0.17*20′ + 0.72*19′ + 0.57*18′ + 0.31*15′
18″ = 0.53*19′ - 0.77*18′ - 0.25*16′ + 0.17*15′
17″ = 0.13*20′ - 0.11*18′ + 0.67*17′ + 0.61*16′ + 0.38*15′
16″ = -0.13*18′ - 0.73*17′ + 0.57*16′ + 0.29*15′
15″ = 0.14*19′ + 0.17*16′ - 0.20*15′ + 0.83*14′ - 0.33*13′ + 0.30*12′
14″ = -0.10*19′ + 0.21*15′ + 0.53*14′ + 0.70*13′ - 0.37*12′ - 0.11*9′
13″ = 0.10*15′ - 0.12*14′ + 0.51*13′ + 0.79*12′ + 0.21*10′ + 0.14*9′
12″ = 0.84*11′ + 0.47*10′ + 0.15*9′ - 0.18*8′
11″ = 0.28*12′ + 0.47*11′ - 0.80*10′ - 0.17*9′ - 0.13*8′
10″ = -0.17*16′ + 0.25*15′ - 0.11*12′ - 0.23*10′ + 0.86*9′ + 0.28*8′
9″ = 0.14*19′ + 0.20*16′ - 0.34*15′ + 0.18*13′ + 0.24*11′ - 0.12*9′
8″ = 0.10*20′ - 0.27*19′ - 0.33*16′ + 0.59*15′ + 0.12*14′ - 0.27*13′
7″ = 0.96*7′ + 0.13*6′ + 0.19*5′ - 0.12′
6″ = -0.17*7′ + 0.96*6′ + 0.21*5′ - 0.12*4′
5″ = -0.16*7′ - 0.24*6′ + 0.96*5′
4″ = 0.10*7′ + 0.12*6′ + 0.98*4′
3″ = 0.98*3′ + 0.22*2′
2″ = -0.22*3′ + 0.97*2′
1″ = 1.00*1′

Table 26. Indole ^1L_b CIS/6-31G mode mixing

42″ = -0.97*42 + 0.23*40
41″ = 0.99*41
40″ = 0.25*42 + 0.96*40
39″ = 0.24*39 + 0.91*38 + 0.17*37 - 0.20*36 - 0.14*34
38″ = -0.52*39 + 0.83*37 - 0.11*35
37″ = -0.66*39 + 0.35*38 - 0.45*37 + 0.21*36 - 0.24*35 + 0.25*34 + 0.20*33
36″ = 0.39*39 + 0.24*37 + 0.69*36 + 0.49*34 + 0.20*33 + 0.15*32
35″ = 0.25*39 - 0.17*36 - 0.93*35 - 0.17*32
34″ = -0.12*39 + 0.55*36 - 0.14*35 - 0.70*34 - 0.20*33 + 0.33*32 + 0.13*30
33″ = -0.13*38 - 0.30*34 + 0.89*33 + 0.20*32 + 0.19*31 - 0.16*30
32″ = 0.11*35 + 0.18*33 - 0.16*32 - 0.95*31 - 0.14*30
31″ = -0.28*36 - 0.12*35 + 0.16*34 - 0.20*33 + 0.75*32 - 0.12*31 - 0.51*30
30″ = -0.18*36 + 0.22*34 + 0.12*33 + 0.45*32 - 0.20*31 + 0.81*30

29″ = 0.50*29 + 0.35*28 + 0.65*27 - 0.11*26 - 0.12*25 - 0.22*24 + 0.17*20
28″ = -0.85*29 + 0.34*28 + 0.33*27 - 0.10*24
27″ = 0.13*29 + 0.84*28 - 0.51*27
26″ = -0.17*28 - 0.18*27 - 0.94*26 - 0.21*24
25″ = -0.37*27 + 0.28*26 - 0.51*25 - 0.61*24 + 0.21*20 + 0.13*12 + 0.16*8
24″ = 0.11*26 + 0.82*25 - 0.54*24
23″ = -0.15*24 - 0.62*23 + 0.70*22 - 0.15*18 - 0.11*14 + 0.16*13
22″ = -0.77*23 - 0.61*22 - 0.10*21
21″ = -0.13*27 + 0.11*25 + 0.36*24 - 0.13*23 + 0.12*22 - 0.15*21 + 0.80*20
20″ = -0.13*24 - 0.96*21 - 0.10*10
19″ = -0.13*24 + 0.11*21 + 0.15*20 + 0.87*19 + 0.12*18 - 0.15*17 - 0.19*16
18″ = -0.21*22 + 0.22*20 - 0.89*18 - 0.14*17 - 0.18*16 - 0.11*15 + 0.12*13
17″ = -0.24*20 + 0.26*19 - 0.31*18 + 0.68*17 + 0.16*16 + 0.35*15 + 0.17*12
16″ = 0.27*20 - 0.10*19 + 0.77*16 + 0.35*15 - 0.21*14 - 0.23*12 - 0.19*10
15″ = -0.16*22 + 0.17*20 - 0.16*19 + 0.16*18 + 0.61*17 - 0.32*16 - 0.36*14
14″ = 0.13*20 + 0.26*17 - 0.25*15 + 0.76*14 - 0.19*13 - 0.18*12 - 0.22*10
13″ = -0.11*17 + 0.28*15 + 0.45*14 + 0.80*13 + 0.20*10
12″ = 0.14*16 - 0.12*15 + 0.22*13 + 0.85*12 - 0.30*10 - 0.30*8
11″ = 0.11*13 - 0.87*11 - 0.35*10 + 0.27*8
10″ = 0.13*19 + 0.19*16 - 0.22*15 - 0.42*11 + 0.73*10 - 0.42*8
9″ = -0.15*10 + 0.94*9 - 0.21*8
8″ = -0.12*20 + 0.29*19 + 0.37*16 - 0.65*15 + 0.32*13 - 0.13*12 + 0.18*11
7″ = 0.92*7 + 0.20*6 + 0.28*5 - 0.20*4
6″ = 0.28*7 - 0.93*6 - 0.13*5 + 0.19*4
5″ = 0.24*7 + 0.20*6 - 0.95*5
4″ = -0.15*7 - 0.23*6 - 0.96*4
3″ = -0.97*3 - 0.26*2
2″ = -0.24*3 + 0.97*2
1″ = -1.00*1

consequence, are considerably mixed in the ^1L_b state while the low frequency modes and very high frequency a′ modes correlate to a small number of ground state modes.

As Table 26 shows, the modes are mixed to a considerably greater extent at CIS/6-31G. While the CIS(11,11)/6-31G normal coordinates of the low frequency a′ modes correlate to a single ground state mode at around 98%, the CIS/6-31G normal coordinates correlate in a range from 94% to 50%. This also suggests that the CIS(11,11)/6-31G normal coordinates are more accurate. Indole's single vibrational level fluorescence shows a 1:1 correlation between the low energy ground and ^1L_b state frequencies for modes up to ~800 cm^{-1}.[57] In particular, a 1:1 correlation was found to exist between mode 28, in the ground and ^1L_b states, which is much more in keeping with the CIS(11,11)/6-31G Duschinsky matrix elements. At CIS/6-31G, the vibronically active mode is a strong mixture of modes 27, 28, and 29 of the Hartree-Fock ground state.

The Duschinsky effect is more pronounced in the ^1L_a state (Table 27), particularly between 1,000 and 2,000 cm^{-1}, and this is anticipated from its larger and less radial geometry difference with the ground state.

The sparsity of the transition density between ^1L_a and ^1L_b[62] suggests that the HT activity in mode 28 is due mainly to a large projection onto the geometry difference between these states (Figure 17 at CIS/6-31G). This is supported by the present calculations. Modes 27 and 28, Figure 16 at CIS/6-31G, have the largest projections, at 0.191, and 0.157, respectively. For mode 28, the projection is mainly onto N-H1 and C3-H3, suggesting that these distortions are effective at decreasing the energy gap between ^1L_a and ^1L_b. For mode 27, the projection is mainly onto C4-H4 and C7-H7.

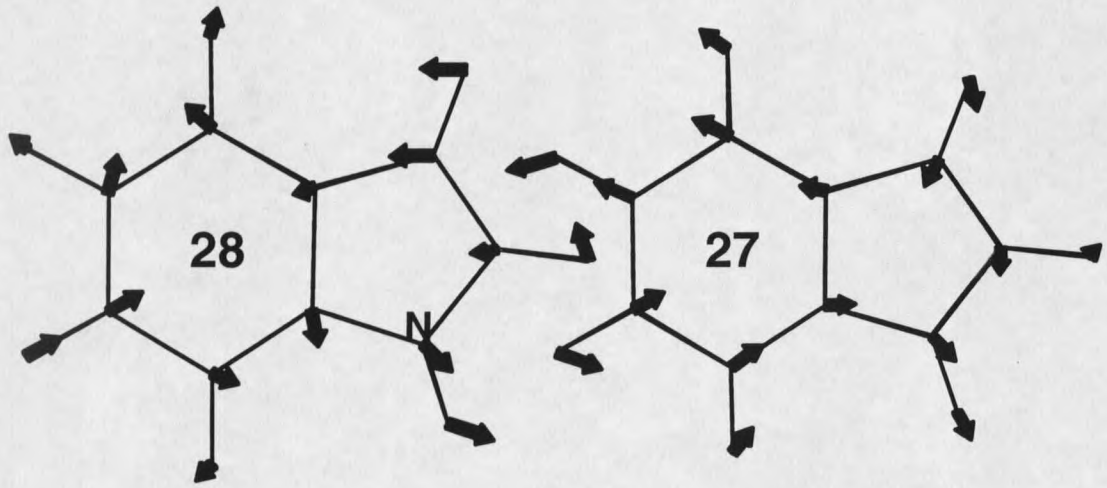

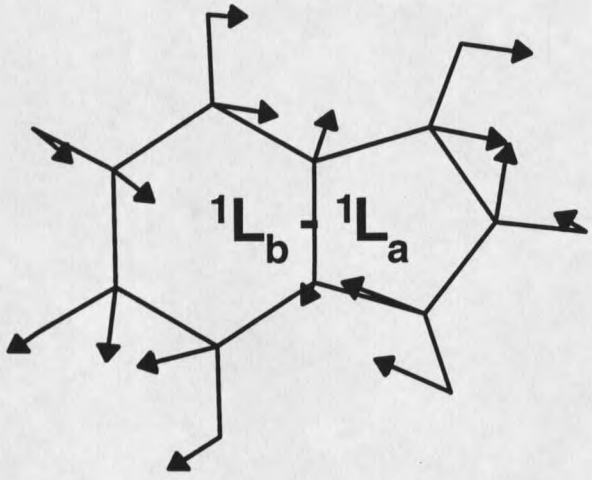

Figure 17. Indole ^1L_b mode 28 , 27, and ^1L_a - ^1L_b geometry difference at CIS/6-31G.

Table 27. Indole CIS(11,11)/6-31G ^1L_a mode mixing

42″ = -0.57*42′ + 0.82*41′
41″ = 0.81*42′ + 0.56*41′
40″ = 0.97*40′ + 0.16*38′ - 0.14*35′
39″ = -0.12*41′ + 0.19*40′ - 0.39*39′ - 0.75*38′ - 0.36*37′ + 0.13*36′
38″ = -0.11*39′ - 0.41*38′ + 0.88*37′ - 0.12*35′ - 0.14*32′
37″ = -0.67*39′ + 0.24*38′ + 0.28*36′ - 0.23*35′ - 0.50*34′ + 0.12*33′
36″ = -0.50*39′ + 0.31*38′ - 0.24*36′ - 0.22*35′ + 0.66*34′ - 0.30*32′
35″ = 0.29*38′ + 0.26*37′ + 0.28*36′ + 0.70*35′ + 0.20*34′ + 0.32*33′
34″ = -0.28*39′ - 0.76*36′ + 0.45*35′ - 0.36*34′ - 0.11*33′
33″ = 0.13*39′ - 0.30*36′ - 0.16*35′ + 0.57*33′ + 0.33*32′ + 0.65*31′
32″ = -0.16*39′ + 0.17*36′ + 0.22*35′ + 0.16*34′ - 0.63*33′ + 0.14*32′
31″ = -0.28*36′ - 0.16*35′ + 0.28*34′ - 0.27*33′ + 0.78*32′ - 0.35*31′
30″ = 0.15*35′ + 0.15*34′ + 0.19*33′ - 0.14*31′ + 0.95*30′

29″ = 1.00*29′
28″ = 0.98*28′ - 0.15*27′
27″ = 0.14*28′ + 0.98*27′
26″ = 0.99*26′
25″ = -0.47*25′ - 0.84*24′ - 0.10*22′ - 0.13*19′
24″ = -0.87*25′ + 0.48*24′
23″ = -0.90*23′ + 0.12*22′ - 0.20*21′ + 0.11*20′ + 0.23*19′ + 0.11*16′
22″ = 0.28*23′ + 0.60*22′ - 0.69*21′ + 0.14*20′ + 0.12*18′ - 0.13*10′
21″ = 0.15*23′ - 0.40*22′ - 0.11*21′ + 0.78*20′ + 0.26*19′ + 0.23*18′
20″ = 0.56*22′ + 0.66*21′ + 0.20*20′ + 0.29*19′ + 0.29*18′ - 0.12*17′
19″ = -0.13*24′ + 0.19*23′ - 0.13*22′ - 0.11*21′ - 0.27*20′ + 0.82*19′
18″ = 0.10*21′ + 0.54*17′ + 0.45*16′ + 0.63*15′ - 0.18*10′ + 0.15*8′
17″ = -0.10*23′ + 0.11*22′ + 0.22*19′ + 0.73*17′ - 0.50*16′ - 0.21*15′
16″ = -0.15*22′ - 0.34*20′ + 0.79*18′ - 0.11*17′ - 0.24*16′ + 0.32*15′
15″ = 0.13*20′ - 0.11*18′ - 0.17*17′ - 0.51*16′ + 0.25*15′ - 0.45*14′
14″ = 0.24*17′ - 0.16*15′ - 0.71*14′ + 0.34*13′ - 0.34*12′ - 0.39*9′
13″ = -0.15*20′ + 0.23*16′ - 0.13*15′ - 0.39*14′ - 0.17*13′ + 0.74*12′
12″ = 0.13*20′ + 0.11*18′ + 0.12*16′ - 0.18*14′ - 0.21*13′ + 0.66*11′
11″ = 0.13*22′ + 0.16*20′ - 0.11*18′ - 0.18*16′ + 0.37*15′ - 0.15*14′
10″ = -0.21*15′ + 0.21*13′ + 0.43*12′ + 0.27*11′ - 0.77*10′ - 0.15*8′
9″ = -0.11*18′ + 0.33*13′ + 0.55*11′ + 0.14*10′ + 0.32*9′ + 0.65*8′
8″ = -0.15*22′ - 0.20*20′ + 0.18*19′ + 0.28*18′ + 0.29*16′ - 0.28*15′
7″ = 0.90*7′ + 0.42*6′
6″ = 0.33*7′ - 0.79*6′ + 0.50*5′
5″ = -0.27*7′ + 0.43*6′ + 0.84*5′ - 0.21*4′
4″ = 0.20*5′ + 0.97*4′
3″ = 0.96*3′ + 0.29*2′
2″ = -0.29*3′ + 0.96*2′
1″ = 1.00*1′

Calculated Spectra

Benzene. As a test of the computational procedures, the excitation spectrum of the vibrationally induced $^1A_{1g} \rightarrow {}^1B_{2u}$ transition of benzene was calculated. Table 28 compares the observed and calculated relative Franck-Condon factors for the benzene ring 'breathing' vibration. The Franck-Condon factor of the origin, 0.36 at CIS-HF/3-21G, is undoubtedly an overestimation as the calculated geometry change is much too small. Experimentally, benzene's C-C bond lengths increase by 0.0340 Å with $^1B_{2u}$ excitation,[63] while the calculated change is only 0.0155 Å at CIS-HF/3-21G. The computation correctly predicts the fundamental of the ring breathing mode to be the most intense transition of the progression. Appropriately, this is the only transition with more computed or intensity than the origin. However, the level of agreement between theory and experiment becomes progressively worse with increasing quanta, due probably to a breakdown of the harmonic approximation. (For a harmonic oscillator, the relative intensity of the nth member of a progression is given by the

Table 28. Benzene $^1A_{1g} \rightarrow {}^1B_{2u}$ relative Franck-Condon factors ($f_{0\rightarrow n}/f_{0\rightarrow 0}$) for the ring 'breathing' vibration.

n	3-21G	3-21G[a]	6-31G	6-31G(p,d)	EXP[b]	EXP[c]
0	1.000	1.000	1.000	1.000	1.00	1.00
1	1.154	1.162	1.151	0.957	1.36	1.19
2	0.664	0.675	0.665	0.457	0.98	0.88
3	0.255	0.261	0.250	0.145	0.62	0.37
4	0.073	0.075	0.072	0.035	0.42	
5	0.017	0.018	0.017	0.007	0.35	
6	0.002	0.004	0.002	0.001		

[a]'Fopt=VeryTight'. [b]Reference 64. [c]Reference 65.

Poisson distribution function, $(\lambda^n e^{-\lambda})/n!$, with λ the intensity ratio of the origin and fundamental.) Using a tighter convergence criteria for the energy gradient during the geometry optimization leads to a minuscule improvement, while polarization functions worsen the level of agreement. The inferiority of the 6-31G(p,d) results stems from the greater impact polarization functions have on the excited state geometry. Inclusion of d functions decreases the C-C bond lengths by 0.0030 Å in the $^1B_{2u}$ state and by 0.0021 Å in the ground state, resulting in an even greater underestimation of the geometry change.

Indole ^1L_b Emission and Excitation. Table 29 compares the observed and calculated Franck-Condon factors of indole's ^1L_b dispersed fluorescence spectrum. The calculated spectra use ground state MP2/6-31G(p,d) modes and frequencies in both the ground and excited states. The intensities of overtone and combination transitions are thereby neglected and only the quality of the geometries may be assessed by the differences in the calculated spectra. The total number of lines with intensity greater than one ten-thousandths of the origin ranges from 904 at CIS-HF/3-21G to 433 at CIS(11,11)-HF/6-31G. The sum of these lines ranges from 0.97 at CIS-HF/3-21G to 0.98 at CIS(11,11)-HF/6-31G. Regardless of basis, no progression is predicted to contain more than two members, which agrees with the observed spectrum and justifies the use of MP2 modes in the ground and excited states.

Table 29 shows that while the CIS-HF/3-21G and CIS-HF/6-31G ^1L_b emission spectra are very similar, significant differences exist between CIS-HF/6-31G and CIS(11,11)-HF/6-31G. As with benzene's $^1B_{2u}$ transition, the intensity of the origin transition is overestimated at the CIS-HF level, for instance, and this flaw is amplified

Table 29. Indole ^1L_b fluorescence emission Franck-Condon factors

	CIS-HF/3-21G[a]	CIS-HF/6-31G[b]	CIS(11,11)-HF/ 6-31G[c]	EXP[d]
29	0.0076	0.0063	0.0024	0.004
28	0.0036	0.0059	0.0015	0.012
27	0.0139	0.0098	0.0069	0.030
26	0.0935	0.1074	0.1216	0.138
25	0.0011	0.0017	0.0022	0.000
24	0.0074	0.0111	0.0148	0.005
23	0.0297	0.0360	0.0534	0.052
22	0.0145	0.0147	0.0093	0.041
21	0.0079	0.0077	0.0034	0.012
20	0.0018	0.0008	0.0002	0.004
19	0.0015	0.0019	0.0017	0.000
18	0.0004	0.0001	0.0003	0.000
17	0.0025	0.0029	0.0037	0.005
16	0.0322	0.0339	0.0357	0.010
15	0.0046	0.0050	0.0050	0.058
14	0.0838	0.0808	0.0699	0.027,22
13	0.0000	0.0000	0.0002	0.016
12	0.0011	0.0007	0.0028	0.008
11	0.0000	0.0003	0.0000	0.003
10	0.0005	0.0001	0.0011	0.000
9	0.0003	0.0004	0.0001	0.000
8	0.0000	0.0008	0.0005	0.000
7	0.0000	0.0000	0.0000	
6	0.0000	0.0000	0.0000	
5	0.0000	0.0000	0.0000	
4	0.0003	0.0000	0.0000	
3	0.0000	0.0000	0.0000	
2	0.0000	0.0001	0.0000	
1	0.0000	0.0000	0.0000	

FC origin = [a]0.2287, [b]0.2781, [c]0.3325 [d]0.20. [d]Reference 57.

at CIS(11,11)-HF/6-31G. The intensities of modes 28 and 27 are also more accurately reproduced at CIS-HF/6-31G.

In other respects, however, the CIS(11,11)-HF/6-31G spectrum is more accurate. In particular, the intensities of modes 26, 22, 21, 19, and 15 are significantly closer to their experimental values at CIS(11,11)-HF/6-31G. Also, mode 13 is predicted to be Franck-Condon active at CIS(11,11)-HF/6-31G, in accordance with experiment and in contrast to the CIS-HF/6-31G spectrum. It is clear that the low energy region of the spectrum is more accurately described by the full CIS wave

function while the high energy region is more accurately described by the truncated wave function.

The CIS-HF/6-31G and CIS(11,11)-HF/6-31G geometry changes differ mainly at the N-H moiety, as shown in Figure 2, which is less displaced at CIS(11,11)-HF/6-31G. The greater and more accurate intensity of mode 26 at CIS(11,11)-HF/6-31G apparently results from a smaller negative projection on to the displacement of the N-H group. This, in turn, results in a smaller cancellation with the positive projection this mode has onto the displacements on the benzene ring. A similar explanation might pertain to modes 13, 15, and 21, which also have significant amplitude on H1 and have intensities that are more accurately provided at CIS(11,11)-HF/6-31G.

The calculated and observed ^1L_b emission stick spectra are compared in Figure 18 and the broadened spectra are compared to the observed band shape[66] in Figure 19.

Table 30 compares the observed and calculated Franck-Condon factors for ^1L_b fluorescence excitation. The first column of Franck-Condon factors are calculated entirely at the CIS-HF/6-31G level of theory, the second column is entirely at the CIS(11,11)-HF/6-31G level, and the third column is the CIS(11,11)-HF/6-31G geometry difference with MP2 modes and frequencies in the ground and excited states (i.e., identical to the dispersed fluorescence but weighted by the frequency rather than the cube of the frequency.) The CIS-HF/6-31G spectrum contains 1,653 lines with intensity at least 10^{-4} that of the origin, summing to 0.94, while the CIS(11,11)-HF/6-31G spectrum contains 911 lines summing to 0.98. The spectrum is shown in Figure 20.

Mode 26, the benzene ring contraction, is the most intense fundamental transition in the excitation spectrum according to both theory and experiment. As Figure 14 shows, the atomic displacements of mode 26 are approximately equal in magnitude but opposite in direction to those of mode 26 of the ground state, the most

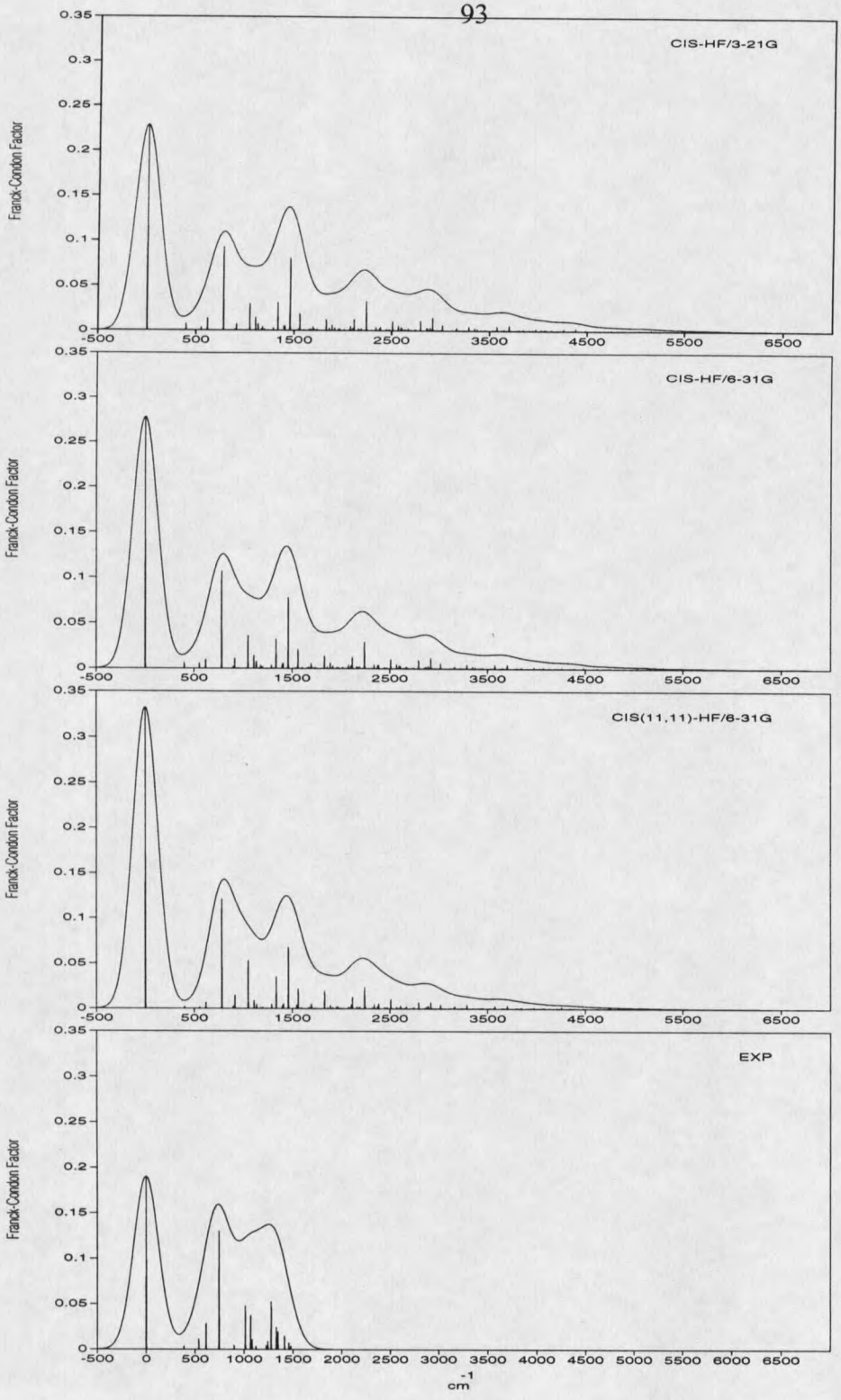

Figure 18. Indole ^1L_b fluorescence emission as calculated with CIS and HF geometries and MP2/6-31G(p,d) normal modes in the ground and ^1L_b states. Broadening factors: 3 and 300 fwhm.

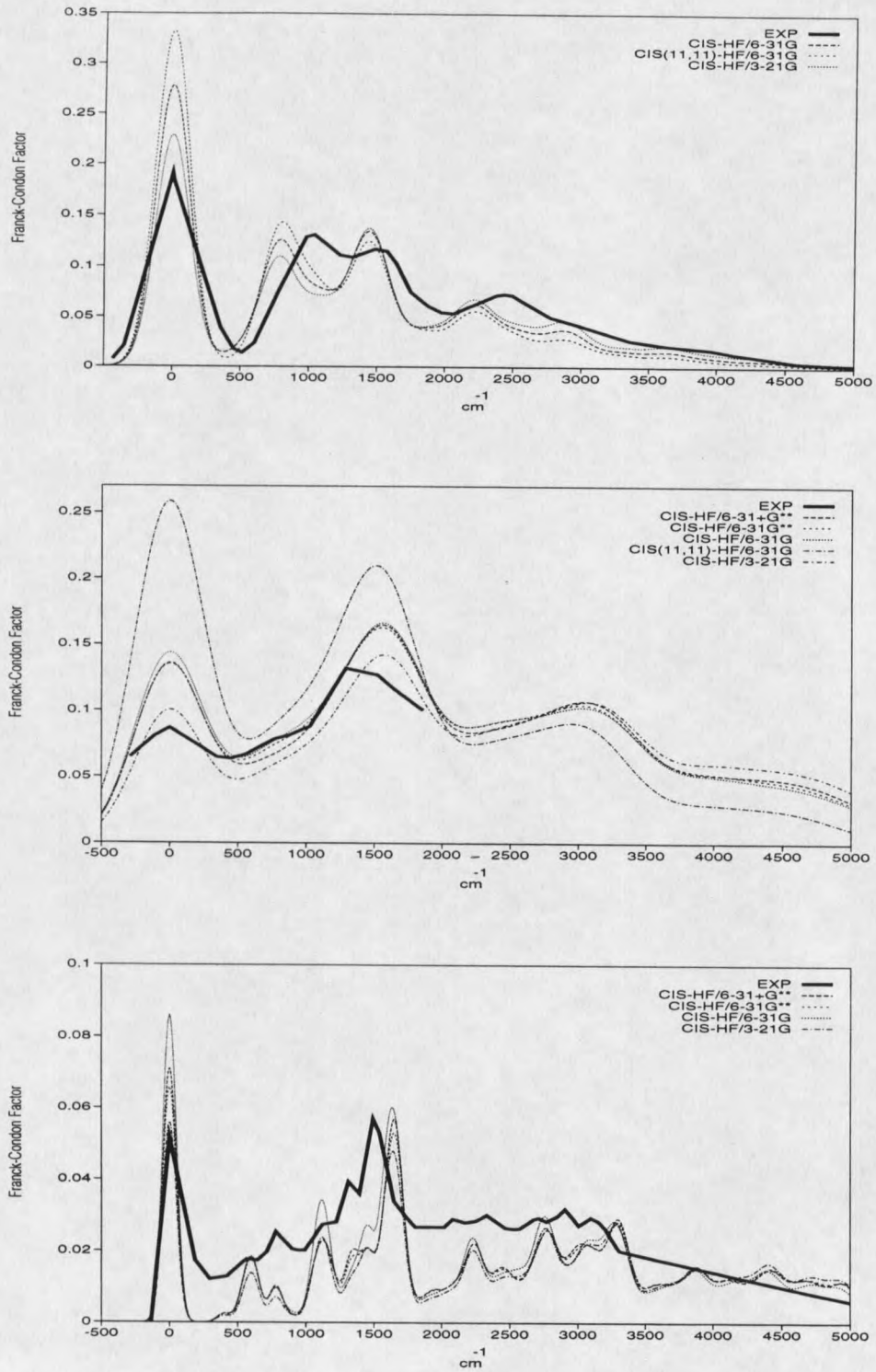

Figure 19. Indole ^1L_b, ^1L_a, and ^3L_a calculated and observed emission band shapes. Broadening factors: ^1L_b, ^1L_a 300 fwhm, ^3L_a 120 fwhm.

Table 30. Indole ^1L_b fluorescence excitation Franck-Condon factors

mode	CIS-HF/6-31G	CIS(11,11)-HF/6-31G	CIS(11,11)-HF/6-31G[a]	EXP[b]
29	0.0012	0.0033	0.0066	0.004
28	0.0054	0.0015	0.0062	0.021
27	0.0092	0.0063	0.0105	0.021
26	0.1108	0.1462	0.1161	0.160
25	0.0037	0.0065	0.0018	0.100
24	0.0052	0.0001	0.0122	0.009
23	0.0003	0.0413	0.0400	0.060
22	0.0610	0.0344	0.0164	
21	0.0000	0.0004	0.0086	
20	0.0026	0.0066	0.0011	
19	0.0115	0.0076	0.0021	
18	0.0037	0.0004	0.0002	
17	0.0101	0.0016	0.0033	
16	0.0081	0.0512	0.0388	
15	0.0480	0.0259	0.0058	
14	0.0045	0.0039	0.0936	
13	0.0016	0.0012	0.0002	
12	0.0297	0.0006	0.0009	
11	0.0014	0.0011	0.0000	
10	0.0116	0.0081	0.0002	
9	0.0034	0.0044	0.0002	
8	0.0047	0.0060	0.0005	
7	0.0000	0.0000	0.0000	
6	0.0000	0.0000	0.0000	
5	0.0000	0.0000	0.0000	
4	0.0000	0.0000	0.0000	
3	0.0000	0.0000	0.0000	
2	0.0000	0.0000	0.0000	
1	0.0000	0.0000	0.0000	

[a]MP2/6-31G(p,d) modes and frequencies. [b]Reference 67.

intense vibration of the emission spectra. The countervailing effects of mode mixing and frequency weighting increase the measured intensity of this vibration by 16% in relation to the dispersed fluorescence spectrum, while a 20% and 3% increase are predicted at CIS(11,11)-HF/6-31G and CIS-HF/6-31G, respectively.

The overtone of ν_{37}, an intense transition observed at 737 cm^{-1} in the ^1L_b excitation spectrum, is completely absent from the calculated spectra. Instead, mode 22 of Figure 14 is the second most intense vibration, although this seems reasonable since its atomic displacements are equal and opposite to mode 23 of the ground state,

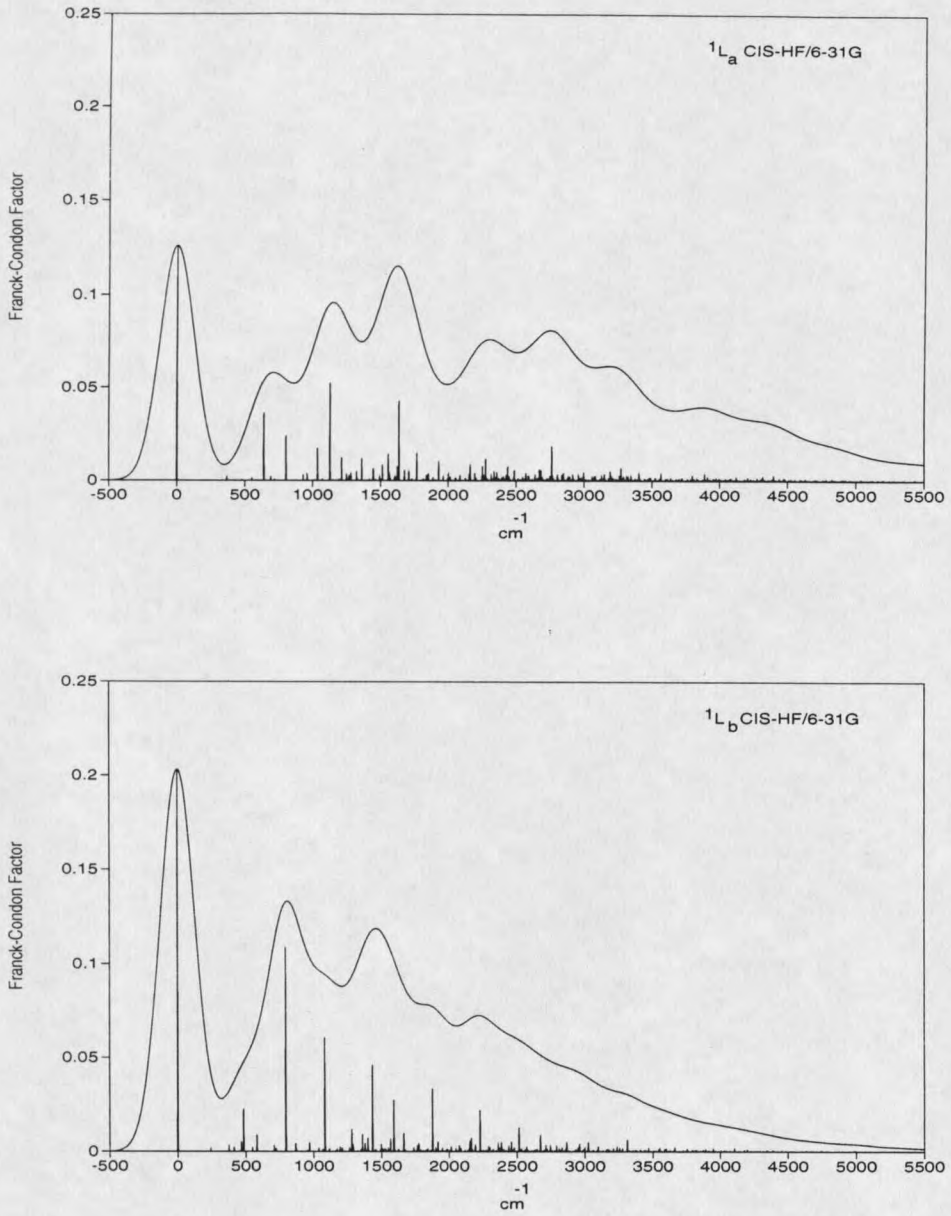

Figure 20. Indole ^1L_a and ^1L_b fluorescence excitation as calculated at CIS-HF/6-31G. Broadening factors: 3 and 300 fwhm.

which is active in the emission spectrum. Other vibrations with calculated intensity include modes 16 and 23 of Figure 14. The $39_0^1 41_0^1$ transition also carries a small amount of intensity, in agreement with matrix-isolated and jet-cooled spectra,[2] as do $40_0^1 41_0^1$ and 39_0^2.

Indole ^1L_a Emission. Calculated ^1L_a fluorescence emission stick spectra are compared in Figure 21. The geometry differences are at the CIS-HF level while the ground state MP2/6-31G(p,d) modes and frequencies are used in both the ground and excited states. The total number of lines with intensity greater than one ten-thousandths of the origin ranges from 4,368 at CIS-HF/3-21G to 1,199 at CIS(11,11)-HF/6-31G, summing from 0.93 at CIS-HF/3-21G to 0.96 at CIS(11,11)-HF/6-31G.

At CIS-HF/6-31G, the origin accounts for less than 15% of the total intensity. Intensity is distributed evenly between modes 27 and 26 near 700 cm^{-1}, and modes 10, 9, and 8 near 1,650 cm^{-1}, and the remaining strength (~81%) appears in much weaker lines. Polarization functions slightly decrease the origin's intensity, in contrast to benzene's $^1B_{2u}$ transition, and alter the relative intensities of some of the aforementioned modes. Diffuse functions bring about virtually no change in the spectrum. The CIS expansion length has considerable effect on the intensity of the origin, which accounts for over 25% of the total intensity at CIS(11,11)-HF/6-31G. The origin's intensity increases upon truncation because the high energy virtual π MOs omitted from the CI calculation (Figure 3) are more likely to have a node in any particular C-C bond. Mode's 26, 14 at 1,450 cm^{-1}, and 10 are similarly affected.

The broadened ^1L_a emission spectrum is compared to the experimental band shape[66] in Figure 19.

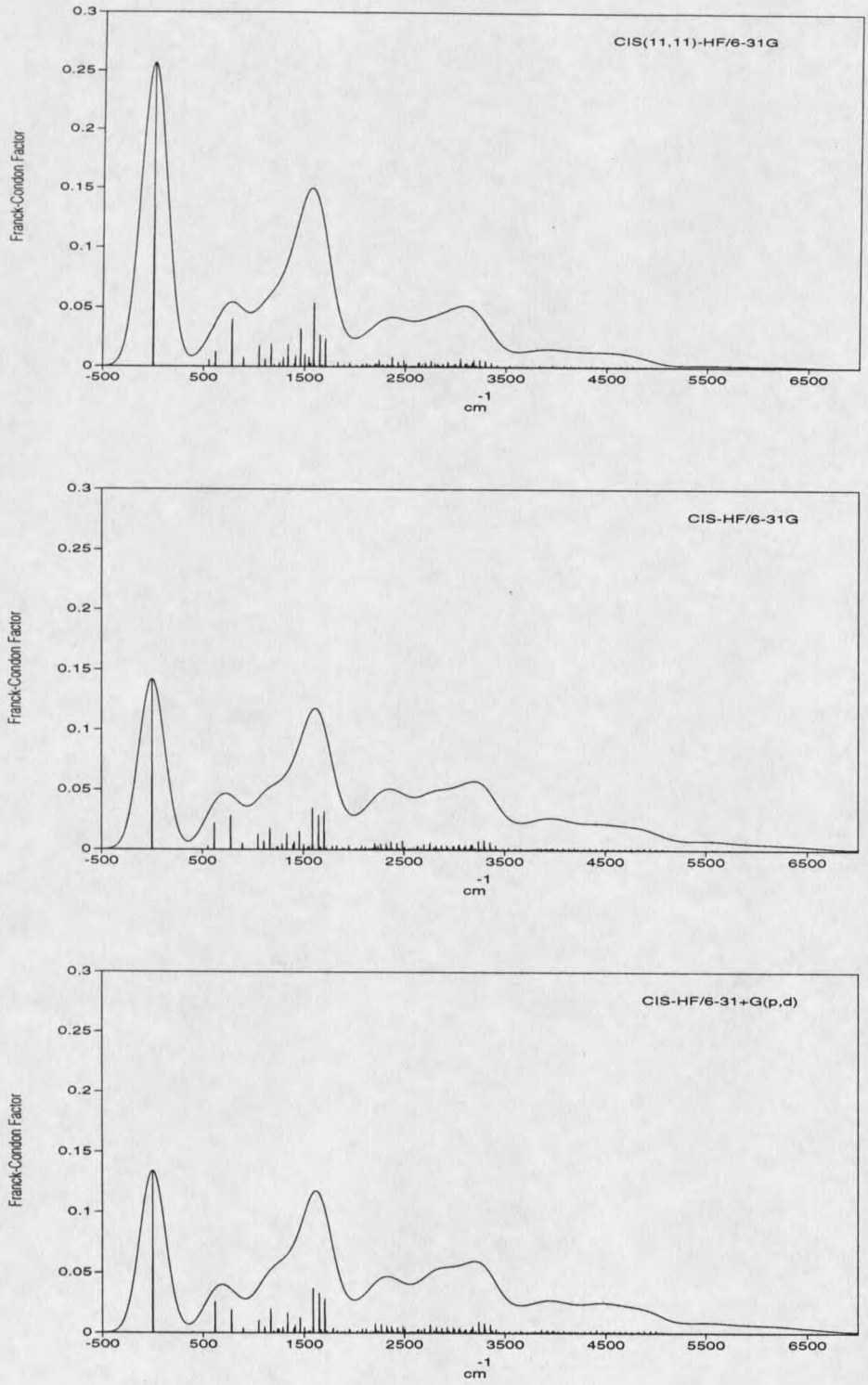

Figure 21. Indole ^1L_a fluorescence emission as calculated with CIS and HF geometries and MP2/6-31G(p,d) normal modes in the ground and excited states. Broadening factors: 3 and 300 fwhm.

Indole ^3L_a Emission Table 31 compares the observed and calculated Franck-Condon factors of indole's phosphorescence spectrum. The Franck-Condon factors are reported relative to the intensity of the origin transition. MP2/6-31G(p,d) modes and frequencies are used in the ground and excited state. The planar conformation is used for the triplet state. The total number of lines with intensity greater than one ten-thousandths of the origin ranges from 8,323 at CIS-HF/3-21G to 5,410 at CIS-HF/6-31G, summing from 0.89 at CIS-HF/3-21G to 0.92 at CIS-HF/6-31G.

At CIS-HF/3-21G and /6-31G, the origin is the most intense transition and mode 9 is the most intense vibration, in concurrence with experiment. Mode 10 is second in intensity, both at CIS-HF/3-21G or /6-31G and experimentally. Polarization functions diminish the quality of the spectra in these regards. The moderate intensities of modes 27, 26, and 14 are reflected in the computed spectra, regardless of basis, as are the weak intensities of modes 29, 25, 24, 21, 20, 19, and 15. The greatest discrepancies with experiment are in modes 22 and 16, which are too intense. The intensities of most if not all modes are exaggerated due to intersystem crossing.

The calculated stick spectra are shown in Figures 22 and 23. Interestingly, the intensities of the four vibrations clustered around the 1,100 cm^{-1} region of the spectrum, modes 23 to 20, are sensitive to basis but the relative intensities of these transitions are unchanged with each modification. The same observation pertains to modes 10, 9, and 8 in the 1,650 cm^{-1} region and the peaks spanning the 400 - 700 cm^{-1} region, modes 29, 28, and 27. Consequently, the broadened ^3L_a phosphorescence spectra (Figure 19), is very insensitive to basis. It also compares well to the observed band shape.[68] The presence of intensity in clusters of closely spaced vibrations is believed to give tryptophan's phosphorescence its simple appearance.[69]

Table 31. Indole ^3L_a emission relative Franck-Condon factors ($f_{0\rightarrow n}/f_{0\rightarrow 0}$)

mode	CIS-HF/3-21G[a,b]	CIS-HF/6-31G[a,c]	CIS-HF/6-31+G**[a,d]	EXP[e]
29	0.0346	0.0293	0.0356	0.05
28	0.1084	0.0980	0.1238	0.06
27	0.1985	0.1723	0.1990	0.11
26	0.1302	0.1180	0.1510	0.10
25	0.0283	0.0252	0.0177	0.03
24	0.0019	0.0021	0.0038	0.01
23	0.1176	0.0971	0.1189	0.01
22	0.2622	0.2622	0.1665	0.05
21	0.0721	0.0710	0.0400	0.03
20	0.0970	0.0743	0.0973	0.07
19	0.0322	0.0262	0.0522	0.05
18	0.0017	0.0008	0.0036	
17	0.0443	0.0387	0.0268	
16	0.1523	0.1000	0.2270	0.03
15	0.0957	0.0894	0.0529	0.05
14	0.2825	0.2425	0.2221	0.10
13	0.0119	0.0081	0.0139	
12	0.0300	0.0189	0.0427	
11	0.0112	0.0128	0.0015	
10	0.4110	0.3811	0.2668	0.12
9	0.5348	0.4123	0.2073	0.21
8	0.2172	0.1680	0.0001	0.06
7	0.0000	0.0000	0.0015	
6	0.0012	0.0007	0.0001	
5	0.0000	0.0000	0.0020	
4	0.0017	0.0013	0.0010	
3	0.0009	0.0009	0.0020	
2	0.0031	0.0030	0.0010	
1	0.0001	0.0001	0.0000	

[a]MP2/6-31G(p,d) modes. FC origin = [b]0.0560, [c]0.0859, [d]0.0709. [e]Reference 30.

The program for calculating spectra could not run to completion when the non-planar T_1 conformation was used. Perhaps the geometry difference with the ground state is unrealistically large when calculated at this level of theory. Or perhaps the geometries are accurate and theFranck-Condon overlap between non-planar T_1 and the ground state is too small for this conformation to be observed in the electronic spectra. Its phosphorescence would exhibit a very long progression along at least one erstwhile out-of-plane mode.

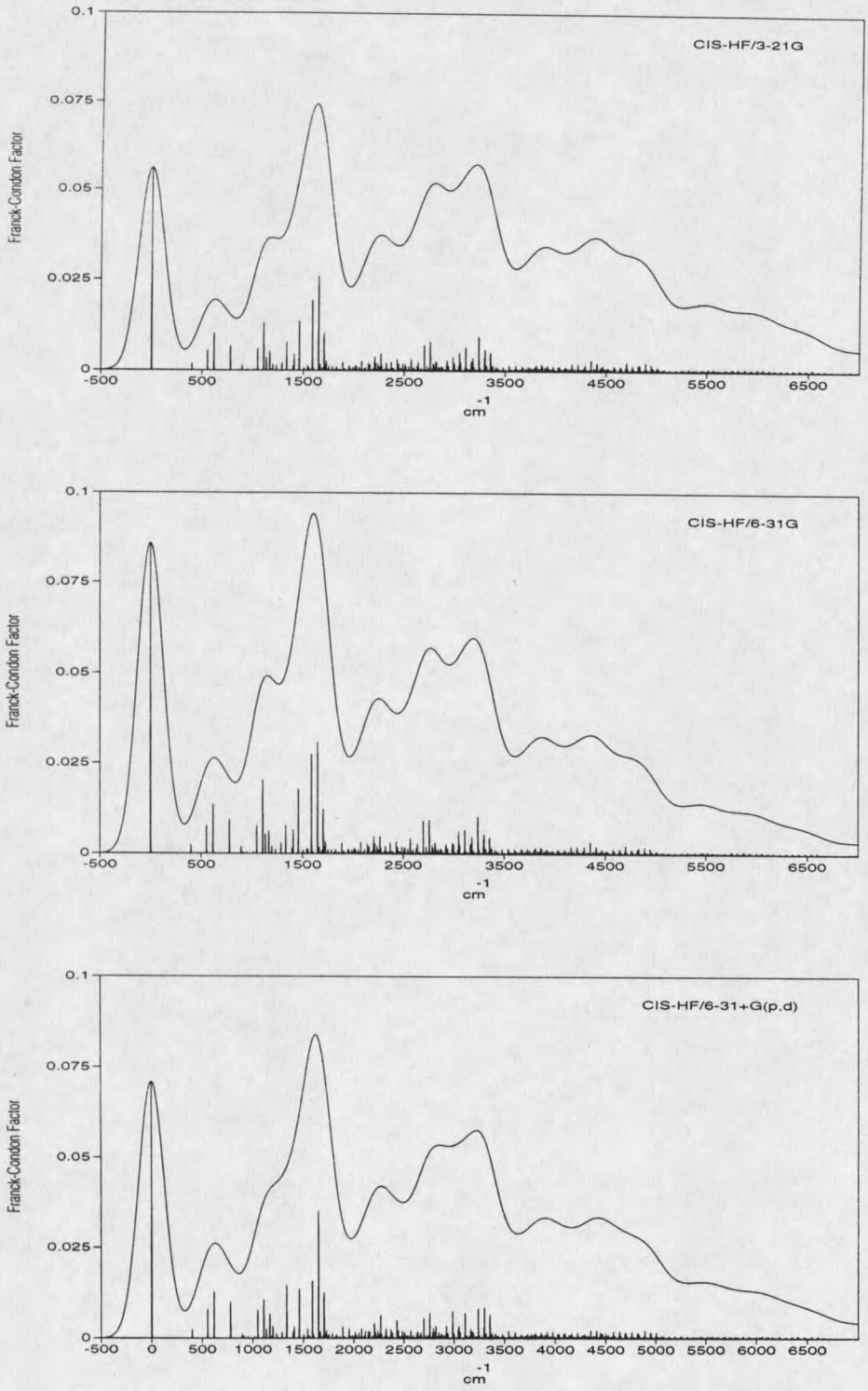

Figure 22. Indole ^3L_a phosphorescence as calculated with CIS and HF geometries and MP2/6-31G(p,d) normal modes in the ground and excited states. Broadening factors: 3 and 120 fwhm.

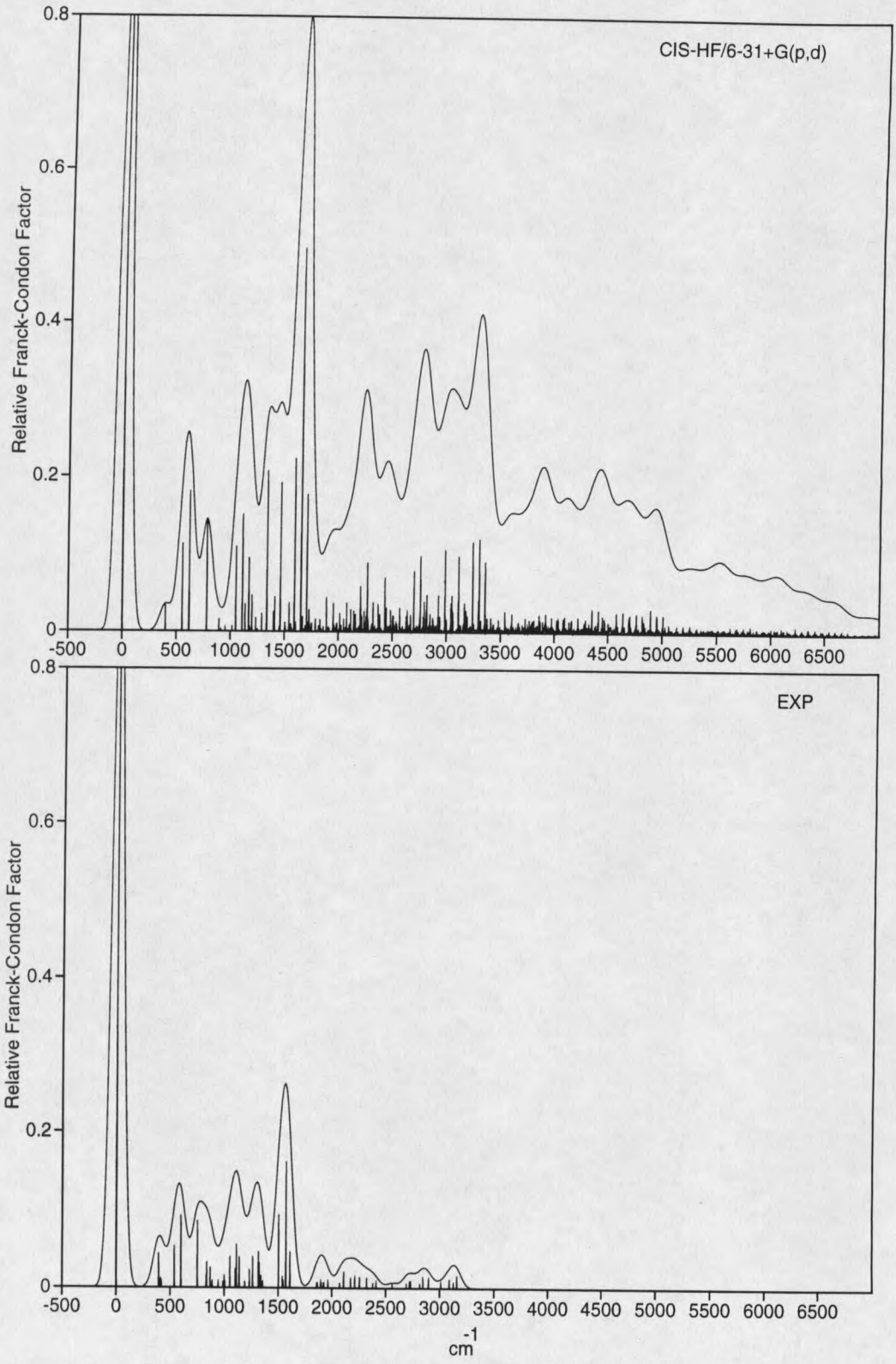

Figure 23. Indole ^3L_a emission observed and calculated relative Franck-Condon factors. Broadening factors: 3 and 120 fwhm.

1:1 and 1:2 Indole:Water Complexes

Intermolecular Geometries

σ-complex. Figure 24 shows the energy minimum ground and excited state 1:1 indole:water complexes. Each water in Figure 24 indicates the equilibrium position of this monomer in a 1:1 complex with indole.

In each state the σ-complex has C_s symmetry with the molecular planes perpendicular to each other. The intermolecular geometries are summarized in Table 32. Rotationally resolved fluorescence indicates a linear hydrogen bond is formed in the ground state and ^1L_b σ-complexes.[21] As indicated by the bond angle $\angle_{N\text{-}H1\text{-}O}$, the present calculations predict that this orientation corresponds to the energy minimum geometry only when basis sets containing diffuse functions are used. The angle formed by the plane of the water moiety and the axis of the hydrogen bond, $\angle_{H1\text{-}O\text{-}H}$, has been estimated as ~125° in the ground state according to the high resolution spectrum,[21] which is very close to the calculated value in the equilibrium geometry. In the ^1L_b state, this angle increases to 180° according to the spectrum, but the equilibrium value decreases by nearly 3° according to Table 32. In general, the effects of polarization functions and diffuse functions roughly cancel so that the 6-31G intermolecular angles are close to those of the 6-31++G(p,d) basis set.

(The truncated CIS wave function is not size consistent and therefore a less practical tool for examining the excited state complexes than full CIS. The CIS(14,13) wave function, rather than CIS(11,11), is used herein to account for the high energy occupied and low energy virtual MOs localized on the water moiety that take part in the configuration interaction.)

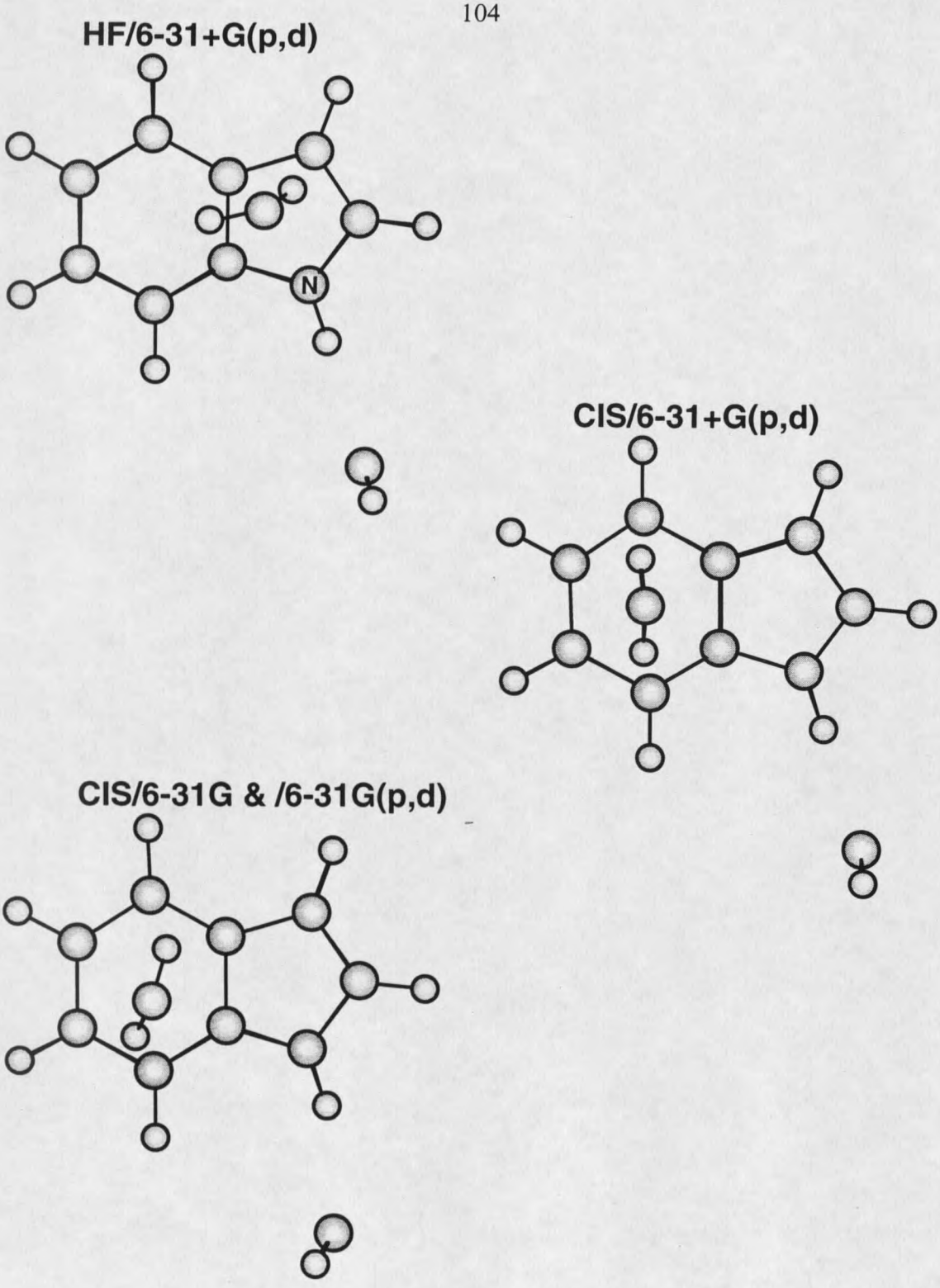

Figure 24. Indole:water 1:1 complexes in the ground, ^1L_a, and ^1L_b (bottom) states.

Table 32. Indole:water 1:1 complex intermolecular geometries

	π-complex							
	$z^{cm}_{Ind\text{-}H2O}$(Å)				$\angle_{Ind\text{-}H2O}$			
	G				G			
basis	πa	πb	^1L_a	^1L_b	πa	πb	^1L_a	^1L_b
6-31G	3.35	3.38	3.28	3.33	60.1	79.9	80.9	75.2
6-31G(d)	3.32	3.40	3.24		56.1	77.4	81.0	
6-31G(p,d)	3.38	3.40	3.31		56.4	78.0	79.7	
6-31+G(p,d)	3.48		3.56		64.1		85.0	
6-31++G(p,d)	3.52				65.4			

	σ-complex								
	$R_{N\text{-}O}$			$\angle_{N\text{-}H1\text{-}O}$			$\angle_{H1\text{-}O\text{-}H}$		
basis	G	^1L_a	^1L_b	G	^1L_a	^1L_b	G	^1L_a	^1L_b
6-31G[b]		2.86	2.91		174.2	174.0		122.9	123.4
6-31G	2.93	2.89	2.90	173.0	173.7	174.0	123.6	123.0	123.5
4-31G(p,d)	3.04	3.00	3.01	166.3	165.3	165.1	119.8	116.7	117.9
6-31G(p,d)	3.06	3.01	3.02	166.7	167.5	167.1	122.5	118.6	119.9
6-31+G(p,d)	3.09	3.02		179.9	180.0		126.2	125.0	
6-31++G(p,d)	3.09			179.9			126.2		
EXP[a]	2.935		2.934						

[a]Reference 70. [b]CIS(14,13)/6-31G.

The hydrogen bond length of the σ-complex, $R_{N\text{-}O}$, is exaggerated by the Hartree-Fock method when an extended basis is used, assuming a small effect from vibrational averaging on an accurately determined observed distance. Regardless of basis, a decrease in separation is predicted to accompany ^1L_b excitation, which is consistent with the H1 Mulliken populations (Tables 12,13) and the more acidic nature of this state.[71] A much larger (0.1 Å) decrease has been predicted based on center of

Table 33. Indole:(water)$_n$ (n=1,2) H_2O center of mass displacement (Å).

	^1L_a					^1L_b				
basis	πa	πb	σ	IW2a	IW2b	πa	πb	σ	IW2a	IW2b
6-31G			0.061[b]	0.250[c]	0.439[c]			0.022[b]	0.224[c]	0.418[c]
6-31G	2.048	0.499	0.031	0.238	0.399	2.011	0.531	0.025	0.270	0.424
4-31G**	2.119	0.479	0.048					0.076		
6-31G**	2.040	0.397	0.040					0.052		
6-31+G**	1.780		0.053							
EXP[a]								0.16	0.33	0.33

[a]Reference 19. [b]CIS(14,13)-HF/6-31G. [c]CIS(17,15)-HF/6-31G.

mass displacements,[21] and amuch smaller (0.001 Å) decrease is observed in the rotational spectrum. Exitation to the ^1L_a state results in a slightly larger decrease in $R_{N\text{-}O}$ according to the Table, regardless of basis.

Table 33 shows that, for the σ-complex, the displacement of the water moiety following ^1L_b excitation is underestimated in the present computations, particularly when polarization functions are omitted from the basis set. This suggests that the difference between the hydrogen bond strengths of the ground and excited state complexes is underestimated. However, the intermolecular geometry change also depends crucially on the intramolecular charge redistribution in the indole monomer, due either to excitation or the interaction itself, and this also may be slightly mischaracterized. In any event, the amplitude of the displacement vectors strongly suggests Franck-Condon activity in at least one intermolecular mode.

In addition to improving the amplitude, polarization functions also have a great effect on the direction in which the water moiety is displaced by the transition, as shown in Figure 25, giving it axial character. Part of the axial character results from the radially directed displacement amplitudes on the N-H group that accompany the ^1L_b

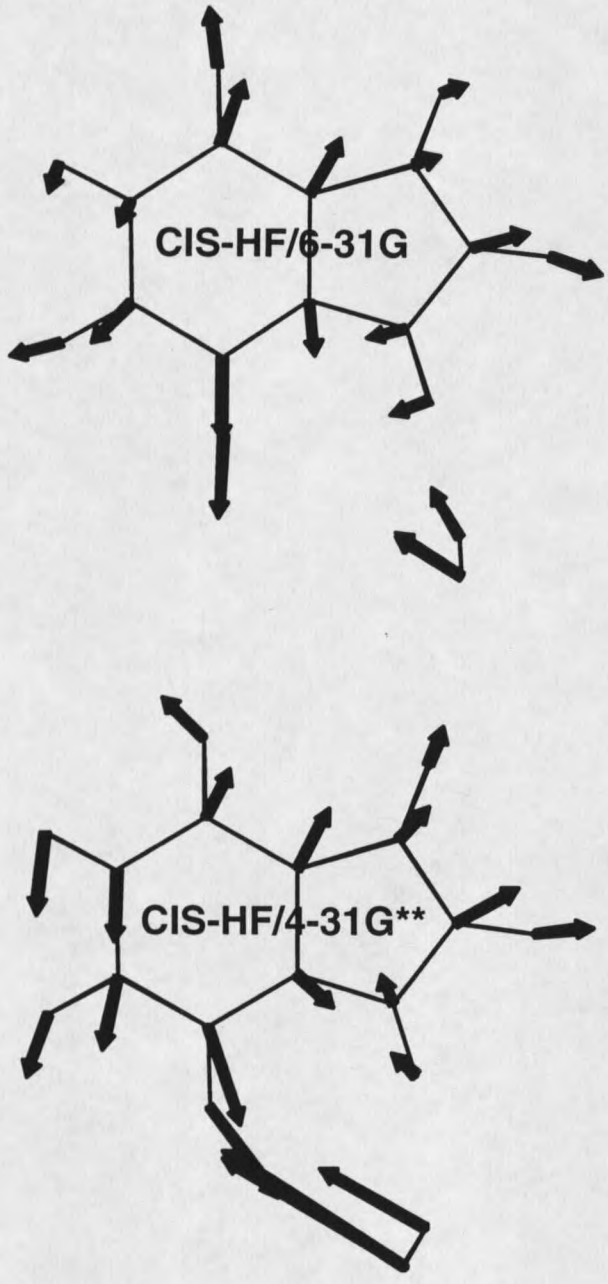

Figure 25. Indole:water σ-complex ^1L_b - G geometry difference.

Table 34. Indole:water σ-complex rotational constants (Mhz)

	G					^1L_b			
	6-31G	4-31G**	6-31++G**	EXP[a]	MP2/6-31G**	6-31G[b]	6-31G	4-31G**	EXP[a]
A	2079	1990	2138	2063	1902	2051	2041	1928	1988
B	970	996	904	945	1065	966	971	1019	964
C	663	666	637	649	685	659	660	669	650

[a]Reference 21. [b]CIS(14,13)/6-31G.

stransition, as shown in Figure 2. It is also possible that d functions bring about a tronger interaction between the water moiety and the phenyl ring in the excited state.

Table 34 compares the observed and calculated rotational constants of the ground and ^1L_b σ-complex. Surprisingly, the HF/6-31G rotational constants are in better agreement with experiment than those obtained with larger basis sets or both a larger basis set and a correlated density. Similarly, the CIS/6-31G rotational constants are closer to experiment than the CIS/4-31G(p,d) results, exaggerating the measured values by 10 - 20%. However, the differences between the ground and ^1L_b σ-complex rotational constants suggest that the geometry change is more accurately depicted at CIS-HF/4-31G(p,d). Experimentally, ΔA = -75, ΔB = 19, and ΔC = 1 Mhz, compared to -62, 23, and 3 Mhz at CIS-HF/4-31G(p,d) or -38, 1, and -3 Mhz at CIS-HF/6-31G.

In each electronic state, σ-complex formation has a negligible effect on the intramolecular geometry of the indole moiety (less than a 0.004 Å change in the C-C or C-N bond lengths) according to the present calculations. Also, the ^1L_a or ^1L_b character of the wave function, as defined by the square of the HOMO→LUMO CIS coefficient or by the sum of the squares of the HO-1→LU+1 and HO→LU+2 coefficients, remains virtually unchanged in these respective states (Table 35). These

Table 35. Indole:(water)$_n$ (n=0,1,2) ^1L_b CIS/6-31G coefficients

π MOs	indole	σ-complex	IW2a
HO→LU+2	-0.399	-0.390	-0.357
HO-1→LU+1	0.562	0.570	0.588
HO-2→LU+1	0.112	0.114	0.116

results suggest that indole's electronic structure is only weakly perturbed by complex formation with polar molecules, in contrast to a molecule involved in exciplex formation.

No other σ-complex energy minimum geometry could be found involving the N-H group in any of the herein investigated electronic states. In particular, rotating the H_2O moiety by 180° around the N-H bond axis and using the result as a starting geometry in a new optimization did not lead to a different result. This may simply be due to the more favorable electrostatic interaction between the water hydrogens and C7 which, according to the Mulliken populations (Table 12), is more π electron rich than C2. Geometry optimizations performed with the indole and water moieties restricted to co-planarity produce structures that are saddle points rather than minima on the intermolecular potential energy surface, regardless of the electronic state. This is consistent with the isotope effect exhibited by the progressions of the indole:water σ-complex origin. The intermolecular separation increases by about 0.1 Å when the moieties are co-planar, indicating that internal torsional by the water moiety is coupled with the intermolecular stretch, as has been suggested elsewhere.[21]

π-complexes. Included in Figure 24 are the energy minimum geometries of the hypothetical ground and excited state indole:water π-complex. The

minimum above the benzene ring (denoted πb) is found only with the Hartree-Fock method, and only when basis sets without diffuse p functions on the heavy atoms are used. The excited state π-complexes, however, possess a single energy minimum at the CIS level, regardless of basis. The position of the water moiety in the ^1L_a π-complex, over the benzene rather than the pyrrole ring, reflects the transfer of π electron density from atoms 1, 3, and 4 to 7 and 9 associated with the ^1L_a transition. Consequently, the water moiety center of mass is displaced by 1.764 Å from its HF/6-31+G(p,d) equilibrium position, indicating a very flat intermolecular potential energy surface. The ^1L_b state π-complex shows an equally large intermolecular geometry change, which is expected from the N-methyl indole:water excitation spectrum.[20]

At MP2/6-31G(p,d), the center of mass separation between the indole and water moieties of the π-complex is 3.01 Å,[24] compared to 3.18 Å for the benzene:water π-complex at the same level of theory. A significant change in the intermolecular distance, Δz_{cm}, is predicted upon excitation. For the ^1L_a transition, Δz_{cm} = -0.0674 at CIS-HF/6-31G, but Δz_{cm} = +0.0469 at CIS-HF/6-31+G(p,d). A stronger interaction in the excited state would, of course, result in a large negative value for Δz_{cm}. For the ^1L_b transition, Δz_{cm} = -0.0368 at CIS-HF/6-31G. In each state, π-complex formation has a negligible impact on the geometry of the indole ring. The ring does not adopt a non-planar structure, as suggested in a semi empirical study.[72]

1:2 complexes. The HF/6-31G 1:2 complex energy minima, IW2a and IW2b, are shown in Figure 26. The intermolecular geometry has both water moieties on one side of indole's molecular plane, in somewhat distorted conformations of the water dimer that allows for both σ- and π-complex type interactions with indole. The two

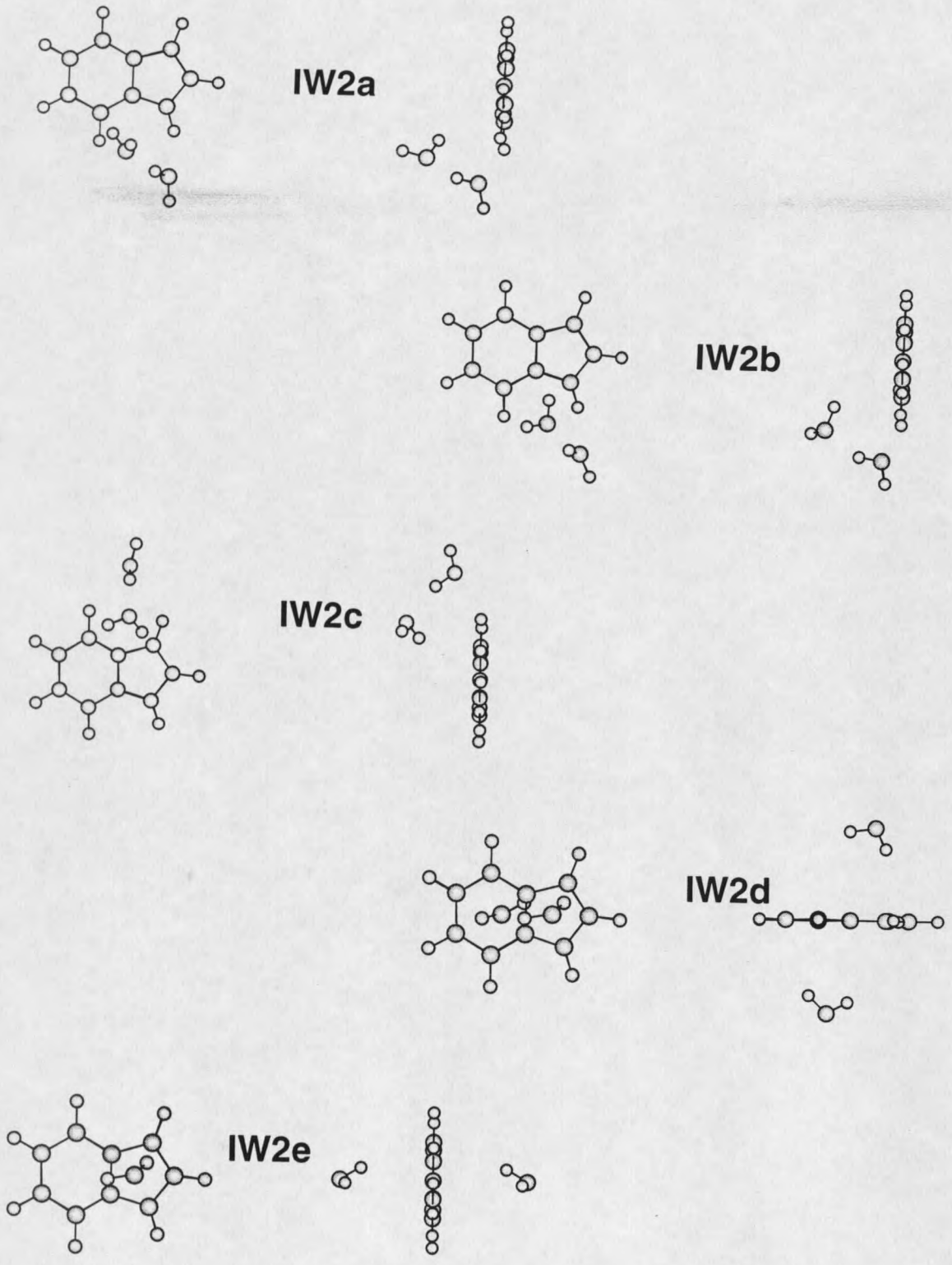

Figure 26. Indole:water ground state HF/6-31G 1:2 complexes.

minima differ mainly in regards to which lone pair of the π-bound water accepts a hydrogen from the σ-bound water. These geometries differ from the results of the density functional study.[25] The two DFT minima differ in regards to which lone pair of the σ bound water accepts a hydrogen from the N-H group. This suggests that at least three minima may be found in this region of the ground state potential energy surface. Only the IW2a conformation is reported in both the DFT study and the present study. For IW2b, the convergence criteria had to be relaxed slightly in order to consider the structure at an energy minimum at HF/6-31G, perhaps accounting for its absence from the DFT study.

Only an IW2a-type conformation could be located in either the ^1L_a or ^1L_b states, as Figure 26 shows. The decrease in π density above the pyrrole ring apparently renders the IW2b conformation unbound in these states. This supports the argument that tunneling between the multiple ground state conformations causes the 1:2 complex dispersed fluorescence to be more complex than its excitation spectrum.

Included in Figure 26 are some of the other 0 K minimum energy conformations that exist, at HF/6-31G, for the indole:water 1:2 complex. These complexes are predicted to be far less stable than IW2a and IW2b, or even unstable with respect to the isolated monomers (IW2e). The structure of IW2d, with waters forming π hydrogen bonds on opposite sides of the indole plane, is nonetheless interesting in light of the inability of benzene to form this type of complex with water, at least in theory. Indole is considered soluble in water at room temperature, whereas benzene is only slightly soluble.[73] Thus, the differences in condensed phase room temperature miscibility between indole and benzene are already suggested by the

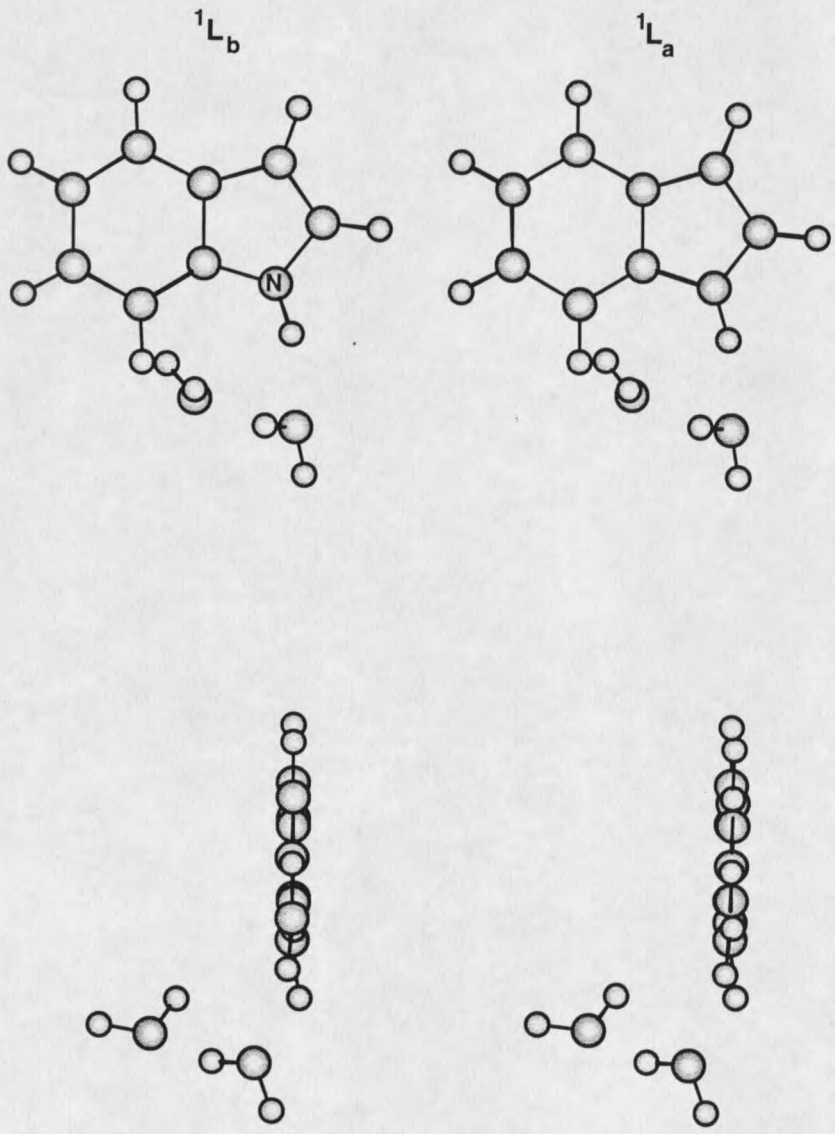

Figure 27. Indole:water excited state CIS/6-31G 1:2 complexes.

theoretical 0 K 1:2 complexes.

Transition States

A transition state is necessarily located between the σ- and π-complexes. At this point the water moiety is in a minimum energy conformation along every geometrical coordinate except for center-of-mass displacement approximately parallel to the short axis of indole, at which it is a maximum. A HF/6-31G transition state optimization indicates that this conformation is 150 cm^{-1} above the π-complex energy minimum. This would be a barrier that exceeds the zero point energy of either π-complex intermolecular bending vibration (Table 47) by a considerable margin, so at least one vibrational level should be held in the π-complex well bottom. The absence of the π-complex from the jet-cooled spectra may be explained in terms of the conditions present during the expansion of the sample molecules through the nozzle of the supersonic jet. In the early part of this process, the vibrational temperature of the gas exceeds 50 K, or 35 cm^{-1}, resulting in a Boltzmann factor of $\exp(-150/35) \propto 10^{-2}$. Thus, the transition state is populated by 1% of the π-complexed water molecules at any given instant under these conditions. In relation to the σ-complex, the Boltzmann factor is $\exp(-1{,}550/35) \propto 10^{-20}$, making the probability of thermal activation from this minimum negligible.

Single Point Calculations

Single point calculations and constrained optimizations were performed in an effort to assess the dynamical behavior of the 1:1 complexes. Rotating the σ-complexed water moiety by 90° around its C_2 axis increases the calculated interaction

energy by 338 cm^{-1} at HF/6-31++G(p,d), a barrier an order of magnitude above the zero point energy. However, this neglects the strong coupling that often exists between intermolecular normal modes. The aforementioned geometry optimizations performed with the indole and water moieties co-planar indicate a much smaller C_2 rotation barrier of 132 cm^{-1} at HF/6-31++G(p,d). A torsional barrier height of 198 cm^{-1} in relation to an internal axis has been reported in the ground state σ-complex.[21]

In addition to the rotational motion of the water moiety in the σ-complex, the translational motion of H_2O parallel and perpendicular to the plane of the indole moiety is also of large amplitude and therefore cannot be neglected. According to classical mechanics, the most probable electronic transition is at the turning point of the final state's potential energy curve, which is where the potential and total energy of the system are equivalent. At the classical turning point, the normal mode displacements $\varepsilon_{i,\,jc\varphi}$ are related to the cartesian displacements $\varepsilon_{i,\,j}$:

$$\varepsilon_{i,\,jc\phi} = \sqrt{\frac{\hbar}{\mu_j\,\omega_j}} \times \varepsilon_{i,\,j}$$

or

$$\varepsilon_{i,\,jc\phi}(\text{Å}) = \frac{5.806}{\sqrt{\mu(AMU)\,\bar{\nu}(cm^{-1})}} \times \varepsilon_{i,\,j}$$

where μ and ν are the reduced mass and frequency of mode *i* and the subscript *j* refers to a coordinate axes. This formula gives, for the HF/6-31++G(p,d) σ-complexed water moiety, an in-plane center-of-mass displacement of 0.21 Å from the equilibrium

position. Most of the displacement is due to the zero point motion of the a′ bend, for which $\varepsilon_{i\,,\,jc\varphi}$ = 0.18 Å, and the rest is due to the intermolecular stretch. The out-of-plane displacement, due entirely to the a″ bend, amounts to 0.12 Å, which is considerably smaller than the value of 0.35 Å obtained from the rotationally resolved fluorescence.[21] The harmonic approximation obviously is not valid in this regard. However, the computed results do agree with the rotationally resolved spectrum in that the in-plane amplitude is greater than the out-of-plane amplitude, and in that the out-of-plane displacement remains unchanged upon ^1L_b excitation.

For the π-complex, rotating the water moiety by 90° around its C_2 axis increases the calculated interaction energy by 450 cm^{-1} relative to the energy minimum at HF/6-31++G(p,d). Rotation by 90° followed by an optimization of the water moiety's distance above indole lowered the calculated barrier to 380 cm^{-1}, and accounting for differences in BSSE between the rotated and non-rotated geometries lowered the barrier to 320 cm^{-1}.

Ground and Excited State Binding Energies

Table 36 provides a comparison of the binding energies of the 1:1 ground state indole:water complexes. The π-complex is slightly more stable than the benzene:water π-complex, for which $-\Delta E_b$ = 1.80 kcal/mol at MP2/6-31G(p,d) after correction for the BSSE,[24] and for which $1.78 < -\Delta E_b < 2.78$ kcal/mol by way of microwave spectroscopy.[24] This can be rationalized in terms of the greater and more localized π electron density above the indole ring due to the heteroatom. The odd-membered ring also contributes to the lessened uniformity of the π cloud. The πa- and πb-complexes are nearly isoenergetic, in contrast to indole's 1:1 clusters with metal cations, which

Table 36. Indole:water 1:1-complex ground and excited state binding energies (kcal/mol)

		method/basis	$-\Delta E_{int}$	BSSE	ΔZPE	$-\Delta E_b$
σ	G	HF/6-31G	7.59	0.87	1.68	5.04
		HF/6-31G*	5.76	0.92	1.37	3.47
		HF/6-31G**	5.75	0.97	1.35	3.43
		HF/6-31+G**	5.24	0.68	1.38	3.18
		HF/6-31++G**	5.25	0.70	1.38	3.17
		MP2/6-31G**	8.12	2.90		
		EXP[c]				4.67
	^1L_a	CIS/6-31G[d]	3.96		3.41	
		CIS/6-31G	8.91	0.97	1.83	6.11
		CIS/6-31G**	6.75	0.91	1.68[b]	4.16
		CIS/6-31+G**	6.61	0.68	1.67[b]	4.26
		CIS-MP2/6-31G[a]	8.21			
	^1L_b	CIS/6-31G[d]	8.16		1.57	
		CIS/6-31G	8.25	0.93	1.86	5.46
		CIS-MP2/6-31G[a]	3.84			
πa	G	HF/6-31G	3.59	1.04	1.25	1.30
		HF/6-31G*	3.42	1.22	1.28	0.92
		HF/6-31G**	3.30	1.03	1.26	1.01
		HF/6-31+G**	3.01	0.71	1.03	1.27
		HF/6-31++G**	2.92	0.63	0.97	1.32
		MP2/6-31G**	5.92	3.14		
	^1L_a	CIS/6-31G	4.30	1.18	1.41	1.71
		CIS/6-31G**	3.90	1.28	1.30[b]	1.32
		CIS/6-31+G**	3.01	0.72	1.05[b]	1.24
		CIS-MP2/6-31G[a]	3.03	1.88		
	^1L_b	CIS/6-31G	3.61	1.30	1.09	1.22
		CIS-MP2/6-31G[a]	-0.52	1.94		
πb						
	G	HF/6-31G	3.48	1.01	1.12	1.35
		HF/6-31G*	3.32	1.00	1.00	1.32
		HF/6-31G**	3.19	0.97	1.08	1.14

[a]CIS/6-31G//CIS-MP2/6-31G. [b]Estimated value. [c]Reference 75. [d]CIS(14,13)/6-31G.

are 4 kcal/mol more stable over the phenyl ring at HF/6-31G(d).[74] Multipole-multipole interactions are of obvious important in the present system.

The calculated ground state binding energies of the σ-complex bracket the result of threshold ionization experiments after the BSSE and ΔZPE corrections are applied. The σ-complex has a significantly greater binding energy than the π-complex, in contrast to molecular mechanics results,[76] which possibly accounts for the latter cluster's absence from the jet spectra, "In supersonic jet expansions the effective temperature of the gas is very low and only the (more stable complex) will be observed even when the energy difference is very small."[77] Part of the σ-complex's stability apparently arises from the interaction between the water moiety and the phenyl ring; the pyrrole:water σ-complex has a slightly weaker interaction in theory, $-\Delta E_{int}$ = 5.36 kcal/mol at HF/6-31G(d) and 7.56 kcal/mol at MP2/6-31G(d).[78]

As shown in Table 37, the two ground state 1:2 complexes are nearly isoenergetic and have a much greater binding energy than the π- or σ-complexes. Other possible conformations with 1:2 stoichiometry are shown to have much smaller binding energies and therefore may also be dismissed on thermodynamic grounds when considering the participants of the jet-cooled spectra.

The disparity between the π-complex, σ-complex, and IW2 binding energies persists in the excited states according to Tables 36 and 37. The concentration dependence 3-methyl indole's fluorescence intensity in polar/non-polar cosolvent systems is consistent with an activation energy of 8.79 kcal/mol for the 3-methyl indole:butanol '1:1 exciplex'.[17] However, interpreting this result in terms of a specific interaction in the excited state is not justified by the computed interaction energies of Table 36 an 37, particularly in light of the stronger acidicity of H_2O. The excited state

Table 37. Indole:water 1:2-complex ground and excited state binding energies (kcal/mol)

			$-\Delta E_{int}$	BSSE	ΔZPE	$-\Delta E_b$
IW2a	G	HF/6-31G	19.76	3.06	4.63	12.07
	^1L_a	CIS(17,15)/6-31G	20.66		3.54	
		CIS/6-31G	23.31	3.20	5.21	14.90
	^1L_b	CIS(17,15)/6-31G	21.93		4.77	
		CIS/6-31G	21.89	2.80	5.12	13.97
IW2b	G	HF/6-31G	19.25	2.69	4.25	12.31
IW2c	G	HF/6-31G	12.78			
IW2d	G	HF/6-31G	6.51			
IW2e	G	HF/6-31G	-1.29			

interaction energies are only about 1 kcal/mol greater than those of the ground state for the 1:1 complexes, but 2 - 3 kcal/mol greater for the 1:2 complexes. The latter result suggests a greater cooperative effect in the excited state. This is the non-additivity in the binding energies of a system having more than one hydrogen bond. A comparison of the sum of the σ-complex, π-complex, and water dimer binding energies with the 1:2 complex binding energies suggests a 1.5 kcal/mol stabilization due to cooperativity in the ground state at HF/6-31G, a 2.8 kcal/mol ^1L_a cooperative effect at CIS/6-31G, and a 3.0 kcal/mol ^1L_b cooperative effect.

The effect of basis on the interaction energies of ground state molecular complexes has been the subject of numerous papers.[79] The present calculations show basis set size to have a very similar effect on the CIS and Hartree-Fock interaction energies. For all complexes, the CIS method yields only a slightly larger BSSE than the Hartree-Fock method, and this is at least partly due to the slightly smaller intermolecular separations. The sameness of the BSSE's suggests a sort of

equivalency between the Hartree-Fock and CIS methods regarding supermolecular calculations, as the size of this error increases on going to a correlated method. This is obvious from a comparison of the HF and MP2/6-31G(p,d) ΔE_{int}'s in Table 36. Comparing the 1:1 complex BSSE's shows that this amounts to a larger percent error in the π-complex, due probably to the fact that two hydrogens are directly involved in the interaction, rather than one.

In Table 38, the ground state interaction between indole and water is resolved into each of the components described elsewhere[38] with the Morokuma scheme.[38]

Table 38. Indole:water Morokuma HF/6-31G energy decomposition (kcal/mol)

	πa	πb	σ
electrostatic	3.69	3.43	10.71
exchange	-1.62	-1.24	-5.95
charge transfer	1.26	1.08	1.67
polarization	0.33	0.29	1.06
mix	-0.02	-0.04	0.25
total	3.64	3.53	7.72

Because the Hartree-Fock method treats electronic repulsion in a time-averaged sense, it does not account for dispersion forces. This interaction results from the attraction between the instantaneous multipole moments of one subunit and the induced instantaneous multipole moments of the other subunits. The difference between the HF/6-31G(p,d) and MP2/6-31G(p,d) interaction energies, after correction for the BSSE, is often used to estimate the contribution made by dispersion forces to the binding energy of the complex. The third and fourth order contributions are much smaller and usually cancel.[80] By this criterion, then, dispersion forces account for about 20% of the stabilization of the σ-complex, and 30% of the π-complex interaction energy.

These results should be considered approximate. Electron correlation also affects the binding energy by modifying the monomer multipole moments, and this effect is not negligible for indole or for water. In particular, the Hartree-Fock method underestimates the electron density at the periphery of the molecule, i.e., in the intermolecular region, so the one-electron approximation leads to an underestimation of the binding energy in this manner as well.

As Table 36 shows, the CIS-MP2//CIS/6-31G binding energies are qualitatively incorrect, so the effect of dispersion forces on the stability of the excited state complexes will have to remain a mystery.

Transition Energy Shifts

Table 39 compares the shifts in indole's vertical and adiabatic CIS transition energies brought about by complex formation with water. The calculated red shifts of the adiabatic transition to the ^1L_b state are reasonably close to the measured value, especially for the σ-complex, and larger red shifts are appropriately obtained for the ^1L_a transition. The smaller shifts shown upon π-complex formation are in keeping with the observed results for N - methyl indole in polar solvents. The interaction solely between the π cloud and the water moiety also red shifts the adiabatic transition of the ^1L_a state to a greater extent than ^1L_b, which is also expected based on the inversion between these states in polar environments.

Although reasonably accurate, the calculated ^1L_b shifts can not be considered conclusive because of their sensitivity to basis. Polarization functions stabilize the ground state σ-complex in relation to the excited states, regardless of conformation, while diffuse functions have the opposite effect. The countervailing influences of

Table 39. Indole:(water)$_n$ (n=1,2) CIS transition energy shifts (cm^{-1})

		$\Delta\nu_{vert}$		$\Delta\nu_{0\text{-}0}$	
	basis	^1L_a	^1L_b	^1L_a	^1L_b
σ	6-31G	-444.4	-266.2	-374.2	-146.9
	6-31G(d)	-311.3	-222.0		
	6-31G(p,d)	-308.1	-229.1	-255.3[b]	
	6-31+G(p,d)	-456.9	-311.3	-381.2[b]	
	EXP[a]				-131.7
πa	6-31G	61.3	90.3	-143.4	27.9
	6-31G(d)	69.4	81.1		
	6-31G(p,d)	66.1	70.2	-108.4[b]	
	6-31+G(p,d)	257.3	183.1	30.0[b]	
πb	6-31G	-96.0	16.1	-125.9	45.4
	6-31G(d)	-76.0	6.4		
	6-31G(p,d)[a]	-70.2	3.2	-63.0[b]	
IW2a	6-31G	-1032.4	-684.8	-989.8	-664.5
	EXP[a]				-449.4
IW2b	6-31G	-596.1	-292.8		

[a]Reference 19. [b]Using estimated ΔZPEs of Table 36.

these modifications, along with the cancellation of the BSSE's in the ground and excited states, results in a strong similarity between the 6-31G and 6-31+G(p,d) shifts. However, the ^1L_b state does show much less sensitivity than ^1L_a in regards to the effect these modifications have on $\Delta\nu_{vert}$.

The calculated transition energy shifts depend strongly on what part of the indole moiety is involved in the interaction. The interaction between the pyrrole ring and the water moiety, for instance, results in a blue shift of the vertical ^1L_a transition due to the absence of a minimum over this region in the excited state. Conversely, the interaction between the benzene ring and the water moiety results in a red shift. It is only to a lesser extent that the sizes of the shifts depend on which excited state is

involved in the transition. Stoichiometry is also seen to have a large impact on the relative sizes of the ^1L_a and ^1L_b shifts. The adiabatic ^1L_a red shift is about 200 cm^{-1} greater than that of the ^1L_b state for the σ-complex but 300 cm^{-1} greater for the 1:2 complex. Both results are consistent with the jet-cooled spectra, which found ^1L_b optical character in the emission from both complexes.[23]

Transition Properties

The transition dipole remains entirely in indole's molecular plane upon π-complex formation (another departure from exciplex behavior) and may still be defined in terms indole's long and short axes alone. Table 40 shows that relative sensitivity of the ^1L_a and ^1L_b polarizations depends on which part of the indole molecule is interacting with the water moiety. Formation of the σ-complex rotates the polarizations of the vertical ^1L_a and ^1L_b transitions in a clockwise sense by 1.7° and 4.1° at CIS/6-31++G(p,d), respectively, while formation of the π-complex rotates these vectors clockwise by 2.4° and 1.5°. These results are somewhat basis dependent but the relative sensitivity shown by each state remains the same; at CIS/6-31G, the polarization of the ^1L_a (^1L_b) transition is rotated clockwise by 6.8° (11.1°) upon σ-complex formation and by 14.7° (7.1°) upon π-complex formation. The same trends appear in the fluorescence emission transition moments. Thus, the polarization of the ^1L_a transition is more sensitive to interaction with indole's π cloud while the ^1L_b polarization is more sensitive to interaction with the N-H group.

The oscillator strength of the ^1L_a transition is decreased by complex formation regardless the basis, the intramolecular or intermolecular geometry, or the stoichiometry. The effect of complexation on the ^1L_b oscillator strength is smaller and

either increasing or decreasing depending upon the basis, the intramolecular or intermolecular geometry, and the stoichiometry. The net oscillator strength decreases, in keeping with the condensed phase spectrum.[81]

Table 40. Indole:(water)$_n$ (n=1,2) CIS transition energies and transition properties

	π-complex											
	^1L_a						^1L_b					
basis	ν^a	Θ^b	f^c	$\nu_{0\text{-}0}{}^d$	Φ^e	F^f	ν	Θ	f	$\nu_{0\text{-}0}$	Φ	F
6-31G	49.1	-45.5	0.149	46.5	-30.8	0.331	49.3	20.1	0.067	47.8	31.4	0.087
6-31G*	48.1	-34.8	0.140				48.4	38.6	0.053			
6-31G**	48.0	-33.9	0.143	45.5	-29.7	0.310	48.0	41.4	0.052			
6-31++G**	46.0	-33.1	0.149	43.4	-28.2	0.275	46.7	36.7	0.057			
	σ-complex											
6-31G	49.2	-46.8	0.146	36.2	-36.2	0.329	49.5	21.2	0.072	48.1	38.6	0.093
4-31G**	48.2	-34.5	0.142	45.8	-31.4	0.312	48.5	39.1	0.058	47.0	42.1	0.098
6-31G*	47.7	-36.3	0.138				48.1	35.3	0.059			
6-31G**	47.7	-35.5	0.141	46.3	-31.7	0.308	48.0	37.3	0.058	46.5	46.8	0.095
6-31++G**	45.3	-32.4	0.163	43.0	-27.8	0.335	46.2	34.1	0.063			
	IW2a											
6-31G	48.0	-51.8	0.142	46.5	-37.6	0.331	49.3	20.1	0.067	47.8	31.4	0.087
	IW2b											
6-31G	49.8	-48.8	0.142	47.1	-31.1	0.355	49.9	14.8	0.075	48.3	40.8	0.089

[a]Transition energy in thousands of cm^{-1}, at the ground state geometry. [b]Transition dipole moment direction in degrees, at the ground state geometry. [c]Oscillator strength at the ground state geometry. [d]Transition energy in thousands of cm^{-1}, between zero-point vibrational levels. [e]Transition dipole moment direction in degrees, at the excited state geometry. [f] Oscillator strength at the excited state geometry.

Ionization Potentials

The adiabatic ionization potentials of the 1:1 and 1:2 indole:water complexes are compared to vertical Koopman's Theory results in Table 41. The corresponding shifts from the ionization potential of uncomplexed indole are listed in Table 42. Formation of the σ-complex raises indole's HOMO by over 2,600 cm^{-1} at HF/6-31G(p,d) due to the unfavorable electrostatic interaction with the water oxygen. Formation of the π-complex lowers indole's HOMO by nearly the same amount due to the favorable electrostatics. There is also a small delocalization of the HOMO onto the water moiety, decreasing the charge in the ring and further lowering the eigenvalue. Their is a concomitant destabilization of the water HOMO. The 1:2 complex

Table 41. Indole:$(water)_n$ (n=1,2) first ionization potentials (eV)

basis	σ-complex[a]	IW2a[a]	IW2b[a]	πa	πb
6-31G	7.235	7.449	7.454	8.056	8.052
6-31G*	7.269			7.935	7.940
6-31G**	7.282			7.929	7.935
6-31++G**	7.459				
EXP[a]	7.384	7.647	7.647		

[a] Reference 82.

Table 42. Indole:$(water)_n$ (n=1,2) first ionization potential shift (eV)

basis	σ-complex[a]	IW2a[a]	IW2b[a]	πa	πb
6-31G	-0.447	-0.234	-0.228	0.374	0.370
6-31G*	-0.336			0.330	0.334
6-31G**	-0.323			0.324	0.329
6-31++G**	-0.333				
EXP[a]	-0.375	-0.121	-0.121		

[a] Reference 82.

ionization potential lies between the two 1:1 complexes, reflecting a combination of the favorable and unfavorable electrostatics.

A strong charge transfer interaction requires a donor molecule with a low ionization potential. In this regard, the σ- and 1:2 complexed indole should participate in stronger charge transfer than the uncomplexed molecule while this interaction is weakened in the π-complex. The first observation is slightly surprising in light of the inability of indole to form σ- and π-complexes simultaneously, and the second observation is consistent with the instability of the sandwich-like 1:2 complexes in Figure 26.

The ionization potentials also reflect the stability of the neutral complex in relation to that of the cationic complex. In this regard, Table 42 indicates that even if indole does form a π-complex with water, it could not be detected by mass spectroscopy as the cation is less stable than the neutral cluster by 0.3 eV or 7 kcal/mol at HF/6-31G(p,d). It is therefore unstable in relation to the uncomplexed indole cation, resulting in dissociation. Similarly, the size of the HOMO's red shift upon 1:2 complex formation provides an explanation for why the associated origin was misidentified as a 1:1 complex by mass spectroscopy. A much more stable σ-complex cation is formed when one of the waters is lost upon photo ionization, according to the Table, and so this is the only mass selected ion cluster. The σ-complex cation is predicted to be 7.7 kcal/mol more stable than the neutral cluster, compared to an observed value of 9.0 kcal/mol.[75]

Dipole Moments

The σ-complex dipole moments and the components of the π-complex dipole moments perpendicular ($\mu\perp$) and parallel ($\mu_{\parallel}$) to indole's plane are given in Table 43. The effects of polarization functions and diffuse functions again roughly cancel, so that the smallest and largest basis sets give very similar results. Differences between states, basis sets, or methods may be explained in terms of the geometries and vector addition. A slightly less obvious influence arises from the distortion of the monomer electron clouds by the electrostatic interaction, mutual polarization, which leads to a non-additivity of the dipoles. Thus, the σ-complex dipole is 0.3 Debyes greater than the sum of the monomer dipoles at HF/6-31+G(p,d). In the ^1L_a state, the σ-complex CIS/6-31+G(p,d) dipole moment is 0.5 Debyes greater than the sum of the monomer dipoles calculated at CIS/6-31+G(p,d) and HF/6-31+G(p,d). For the π-complex, mutual polarization and electron transfer results in $\mu\perp > \mu(H_2O)$. This inequality is also more pronounced in the ^1L_a state, due in part to nearly perpendicular molecular planes in the equilibrium intermolecular geometry (as shown in Table 32).

Mulliken Populations

The Mulliken population differences between σ-complexed and isolated indole, at the complexed geometry, are shown in Figure 27. In each state the largest decrease in π density is at N (e.g., 0.065 e in the ^1L_b state). For ^1L_b, a total of 0.186 e are redistributed, compared to 0.117 e in ^1L_a and 0.087 e in the ground state. In each state there is an increase in the total population of indole with complex formation, and so the larger net shifts in ^1L_a and ^1L_b are due to intermolecular charge transfer as well as the greater polarizability of these states. Namely, 0.091 e are transferred to the σ-

Table 43. Indole:water 1:1 complex ground and excited state dipole moments (Debye)

		σ-complex	
	method/basis//density	μ	θ
G	HF/6-31G//SCF	5.31	-66.9
	HF/4-31G(p,d)//SCF	4.19	-78.5
	HF/6-31G(p,d)//SCF	4.42	-75.5
	HF/6-31+G(p,d)//SCF	4.98	-60.9
	HF/6-31++G(p,d)//SCF	4.97	-61.2
	MP2/6-31G(p,d)//MP2	3.70	-86.2
^1L_a	CIS(13,14)/6-31G//CIS	6.45	-48.7
	CIS/6-31G//CIS	6.04	-54.4
	CIS/4-31G(p,d)//CIS	4.52	-61.0
	CIS/6-31G(p,d)//CIS	4.80	-59.5
	CIS/6-31+G(p,d)//CIS	6.18	-52.8
^1L_b	CIS(13,14)/6-31G//CIS	5.32	-62.9
	CIS/6-31G//CIS	5.38	-63.7
	CIS/4-31G(p,d)//CIS	4.04	-75.6
	CIS/6-31G(p,d)//CIS	4.27	-71.9

		π-complex		
	method/basis//density	$\mu_\perp$	μ	$\theta_\parallel$
G	HF/6-31G//SCF	-2.14	0.98	-64.0
	HF/6-31G(p,d)//SCF	-2.08	0.95	-64.5
	HF/6-31++G(p,d)//SCF	-2.33	1.38	-67.0
	MP2/6-31G(p,d)//MP2	-1.96	1.00	-56.5
^1L_a	CIS/6-31G//CIS	-3.07	3.39	-27.6
	CIS/6-31G(p,d)//CIS	-2.71	3.39	-27.4
	CIS/6-31+G(p,d)//CIS	-2.77	3.38	-27.4
^1L_b	CIS/6-31G//CIS	-2.88	2.03	-25.8

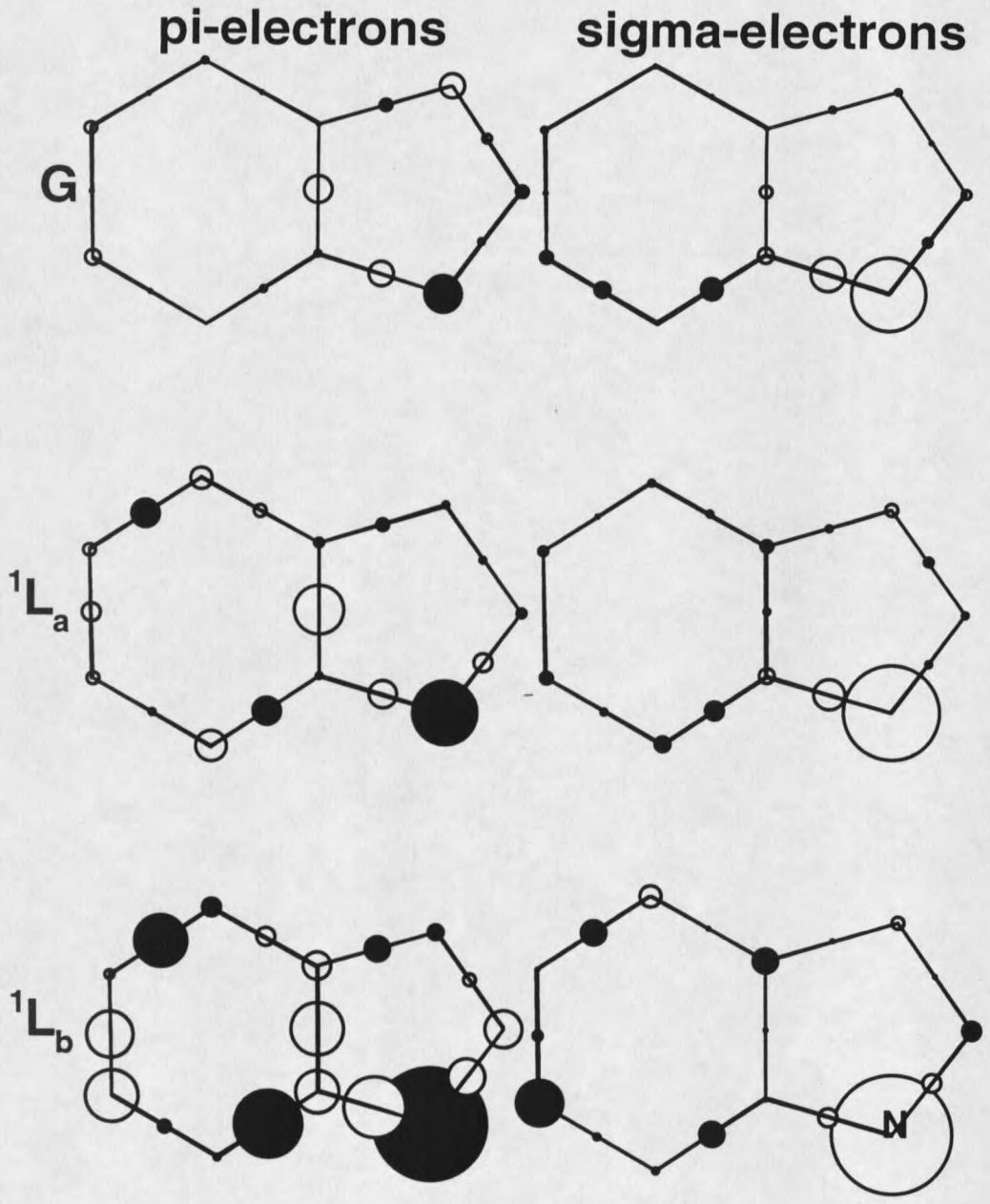

Figure 28. Indole:water CIS/ and HF/6-31G(p,d) σ-complex population difference with bare indole in the ground, ^1L_a, and ^1L_b states.

Table 44. Indole:water 1:1 complex MP2/6-31G(p,d) Mulliken populations

	indole			π-complex			σ-complex		
	σ	π	total	σ	π	total	σ	π	total
N1	5.99	1.62	7.61	6.06	1.53	7.59	6.04	1.59	7.63
H1	0.70	0.01	0.71	0.69	0.01	0.70	0.66	0.01	0.67
C2	4.86	1.07	5.93	4.93	1.01	5.94	4.86	1.07	5.93
H2	0.86	0.00	0.86	0.85	0.00	0.85	0.87	0.00	0.87
C3	5.07	1.10	6.17	5.13	1.07	6.20	5.07	1.11	6.18
H3	0.87	0.00	0.87	0.86	0.01	0.87	0.88	0.00	0.88
C9	4.97	1.03	6.00	5.01	1.01	6.02	4.97	1.03	6.00
C4	5.11	1.02	6.13	5.11	1.02	6.13	5.11	1.02	6.13
H4	0.88	0.00	0.88	0.87	0.01	0.88	0.88	0.00	0.88
C5	5.10	1.03	6.13	5.12	1.01	6.13	5.10	1.03	6.13
H5	0.89	0.00	0.89	0.88	0.00	0.88	0.89	0.00	0.89
C6	5.12	1.03	6.15	5.15	1.00	6.15	5.11	1.04	6.15
H6	0.88	0.00	0.88	0.88	0.00	0.88	0.89	0.00	0.89
C7	5.07	1.05	6.12	5.08	1.04	6.12	5.06	1.06	6.12
H7	0.88	0.00	0.88	0.87	0.01	0.88	0.91	0.00	0.91
C8	4.72	1.04	5.76	4.79	1.00	5.79	4.73	1.04	5.77
	water								
O	7.04	1.60	8.64	6.76	1.91	8.67	7.33	1.30	8.63
H	0.67	0.01	0.68	0.67	0.01	0.68	0.64	0.02	0.66
H	0.67	0.01	0.68	0.66	0.01	0.67	0.64	0.02	0.66

MP2/6-31G(p,d) Mulliken overlap populations

	indole		π-complex		σ-complex	
	π	σ	π	σ	π	σ
N1-C2	0.10	0.57	0.15	0.45	0.15	0.47
C2-C3	0.47	0.84	0.36	0.58	0.37	0.59
C3-C9	0.14	0.83	0.14	0.57	0.19	0.55
C8-C9	0.30	0.90	0.26	0.54	0.22	0.59
C4-C9	0.25	0.82	0.21	0.59	0.21	0.59
C4-C5	0.35	0.78	0.24	0.66	0.31	0.59
C5-C6	0.25	0.81	0.27	0.61	0.23	0.66
C6-C7	0.35	0.79	0.28	0.60	0.31	0.58
C7-C8	0.26	0.82	0.17	0.63	0.22	0.55
N1-C8	0.10	0.50	0.13	0.26	0.15	0.33

Table 45. Indole:water π-complex HF & CIS/6-31G(p,d) Mulliken populations

	G			^1L_a		
	σ	π	total	σ	π	total
N1	6.44	1.29	7.73	6.40	1.30	7.70
H1	0.67	0.02	0.68	0.66	0.02	0.68
C2	5.01	0.88	5.89	5.01	0.88	5.89
H2	0.83	0.00	0.83	0.81	0.00	0.81
C3	5.18	1.05	6.23	5.15	1.05	6.20
H3	0.83	0.01	0.84	0.82	0.01	0.83
C9	5.13	0.94	6.07	5.10	0.94	6.04
C4	5.05	1.08	6.13	5.14	1.07	6.21
H4	0.84	0.01	0.85	0.84	0.01	0.85
C5	5.21	0.97	6.18	5.18	0.97	6.15
H5	0.85	0.00	0.85	0.85	0.00	0.85
C6	5.20	0.97	6.17	5.20	0.97	6.17
H6	0.85	0.00	0.85	0.85	0.00	0.85
C7	5.09	1.07	6.16	5.17	1.06	6.13
H7	0.84	0.01	0.85	0.84	0.01	0.85
C8	4.78	0.93	5.71	4.75	0.94	5.69
	water					
O	6.77	1.92	8.69	7.36	1.34	8.70
H	0.65	0.01	0.66	0.64	0.02	0.66
H	0.64	0.01	0.65	0.65	0.01	0.66

Mulliken overlap populations

	G		^1L_a	
	π	σ	π	σ
N1-C2	0.24	0.42	0.23	0.44
C2-C3	0.40	0.90	0.35	0.68
C3-C9	0.04	0.93	0.05	1.06
C8-C9	0.53	0.67	0.51	0.56
C4-C9	0.14	0.93	0.12	0.70
C4-C5	0.11	1.03	0.11	0.87
C5-C6	0.49	0.57	0.49	0.64
C6-C7	0.14	1.00	0.12	0.65
C7-C8	0.09	0.98	0.11	0.98
N1-C8	0.04	0.54	0.04	0.50

Table 46. Indole:water σ-complex HF & CIS/6-31G(p,d) Mulliken populations

	G			^1L_a			^1L_b		
	σ	π	total	σ	π	total	σ	π	total
N1	6.09	1.68	7.77	6.13	1.59	7.72	6.14	1.59	7.73
H1	0.63	0.01	0.64	0.62	0.01	0.63	0.62	0.01	0.63
C2	4.87	1.01	5.88	4.88	1.01	5.89	4.84	1.10	5.94
H2	0.84	0.00	0.84	0.82	0.00	0.82	0.83	0.00	0.83
C3	5.08	1.13	6.21	5.16	1.05	6.21	5.10	1.08	6.18
H3	0.85	0.00	0.85	0.84	0.00	0.84	0.84	0.00	0.84
C9	5.03	1.04	6.07	5.00	1.05	6.05	5.03	1.03	6.06
C4	5.13	1.00	6.13	5.09	1.09	6.18	5.09	1.10	6.19
H4	0.85	0.00	0.85	0.86	0.00	0.86	0.85	0.00	0.85
C5	5.12	1.05	6.17	5.12	1.03	6.15	5.18	0.96	6.14
H5	0.86	0.00	0.86	0.87	0.00	0.87	0.85	0.00	0.85
C6	5.15	1.01	6.16	5.14	1.03	6.17	5.12	1.06	6.18
H6	0.86	0.00	0.86	0.87	0.00	0.87	0.86	0.00	0.86
C7	5.09	1.06	6.15	5.07	1.14	6.21	5.04	1.14	6.18
H7	0.86	0.00	0.86	0.87	0.00	0.87	0.87	0.00	0.87
C8	4.72	0.99	5.71	4.71	0.99	5.70	4.76	0.93	5.69
	water								
O	7.38	1.30	8.68	7.37	1.31	8.68	7.37	1.30	8.67
H	0.63	0.02	0.65	0.63	0.02	0.65	0.63	0.02	0.65
H	0.63	0.02	0.65	0.63	0.02	0.65	0.63	0.02	0.65

Mulliken overlap populations

	G		^1L_a		^1L_b	
	π	σ	π	σ	π	σ
N1-C2	0.11	0.57	0.13	0.55	0.04	0.55
C2-C3	0.47	0.84	0.23	0.78	0.40	0.83
C3-C9	0.15	0.83	0.27	0.83	0.18	0.83
C8-C9	0.30	0.89	0.18	0.87	0.14	0.85
C4-C9	0.24	0.83	0.07	0.79	0.15	0.83
C4-C5	0.36	0.78	0.21	0.78	0.14	0.75
C5-C6	0.25	0.80	0.31	0.81	0.22	0.79
C6-C7	0.35	0.78	0.04	0.74	0.12	0.79
C7-C8	0.26	0.81	0.28	0.81	0.15	0.79
N1-C8	0.11	0.52	0.08	0.49	0.16	0.49

complexed indole moiety in the ^1L_b state, or 0.060 e in the ^1L_a state and 0.047 e in the ground state. In each state the σ and π density changes cancel at the atoms and reinforce at the bonds, resulting in a net transfer of electron density between internuclear regions. It is mostly π density that is redistributed in the ^1L_b state, unlike the ground state and ^1L_a.

Tables 44, 45, and 46 show the equilibrium populations of the ground and excite state 1:1 complexes.

Intramolecular Frequency Shifts

Regardless of the conformation, stoichiometry, or electronic state, the frequency of mode 40, the N-H out-of-plane bend, is shifted further than any other intramolecular mode, thereby accounting for the absence of the overtone of this vibration from the dispersed fluorescence[23] and fluorescence excitation[83] of the indole:water complex. At HF/6-31G, mode 40 is blue shifted 346 cm^{-1} in the σ-complex, 371 cm^{-1} in IW2a, and 403 cm^{-1} in IW2b. At HF/6-31++G(p,d), this mode is blue shifted 351 cm^{-1} by σ-complex formation. For the ^1L_a state, mode 40 is blue shifted 383 cm^{-1} and 464 cm^{-1} in the σ-complex and 1:2 complex, respectively, at CIS/6-31G. In general, the other ^1L_a shifts are also somewhat larger than those of the ground state, possibly another consequence of the greater polarizability.

Intermolecular Frequencies

The 1:1 clusters have six intermolecular normal modes that arise from the loss of three translations and three rotations with complex formation. For the σ-complex, the a′ and a″ bends and the intermolecular stretch arise from the lost translational

motion, while the a′ and a″ wags and the H_2O C_2 torsion mode arise from the lost rotational motion. Although the practice of evaluating intermolecular modes within the harmonic approximation is often frowned upon,[84] modes originating from the lost translational motion generally amount to smaller displacements from the equilibrium geometry and are often satisfactorily described by a quadratic potential.[85]

In each electronic state, regardless of basis, the lowest frequency intermolecular mode of the σ-complex is the a′ intermolecular bend (Figures 29, 30), where the water moiety moves in a clockwise sense while the indole moiety moves in a counterclockwise sense, preserving the total linear and angular momentum of the system so that no net translational or rotational motion is present. Having translational parentage, the reduced mass of this vibration is comparatively large for an intermolecular mode, resulting in a relatively small amplitude of vibration. Nevertheless, the computed value of the ^1L_b a′ bend overshoots the observed value by 50%, as Table 47 shows. This is due at least partly to the BSSE; at HF/6-31++G(p,d), the a′ bend has a frequency of 27.7 cm^{-1}, 18% smaller than its HF/6-31G value.

The a″ intermolecular bend is slightly higher in frequency than the a′ bend, in each electronic state, followed by the intermolecular stretch, the C_2 torsion mode and the in-plane wag. The a″ wag is the highest frequency intermolecular mode, and it is mixed with indole's intramolecular mode 41 in each state. (The other intermolecular modes are not coupled with intramolecular modes, which is consistent with the absence of combination bands involving both types of vibrations from the low temperature spectra.) These results are also independent of basis. Most rotational modes are then higher in frequency than the translational modes, having large

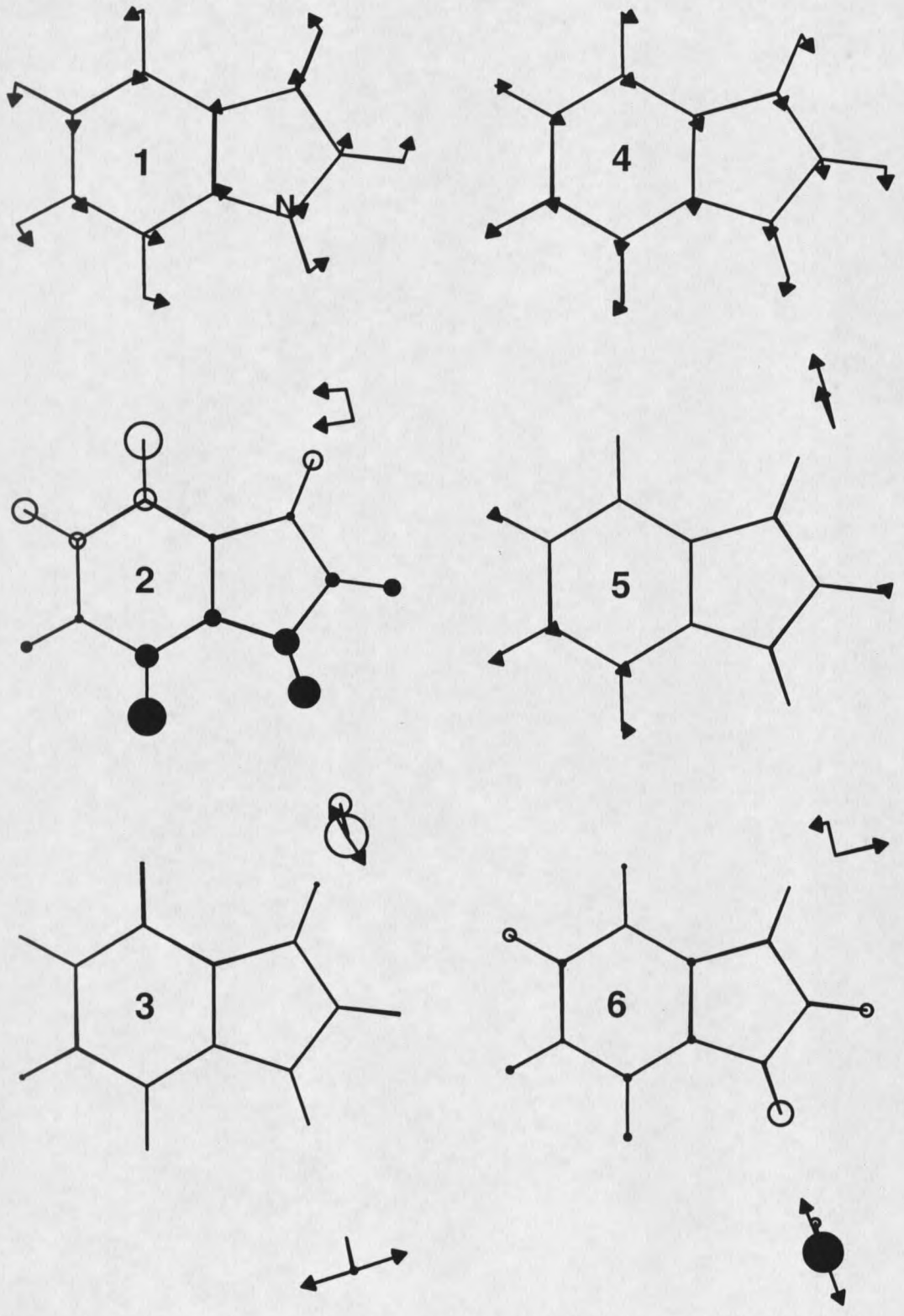

Figure 29. Indole:water σ-complex HF/6-31++G(p,d) intermolecular normal modes.

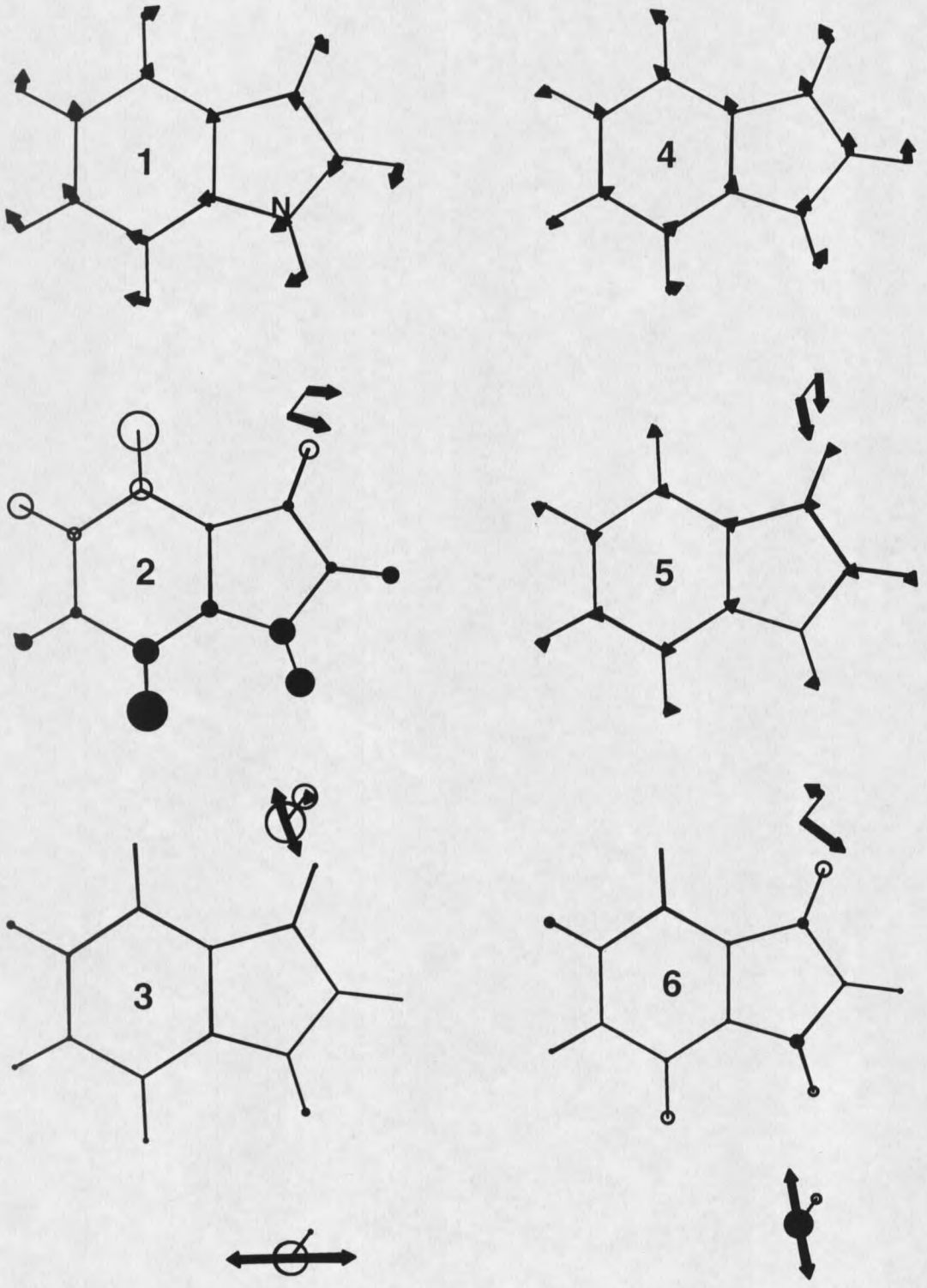

Figure 30. Indole:water σ-complex CIS/4-31G(p,d) ^1L_b intermolecular normal modes.

Table 47. Indole:(water)$_n$ (n=1,2) HF & CIS/6-31G intermolecular frequencies (cm^{-1})

	π-complex			σ-complex				
						^1L_b		
mode	G	^1L_a	^1L_b	G	^1L_a	CIS/6-31G	CIS/4-31G**	EXP
1	26.7	34.9	20.9	33.6	38.1	36.0	36.3	24.4[a]
2	30.4	43.3	35.6	44.8	48.0	49.4	40.4	
3	90.9	98.5	95.0	124.2	115.5	117.7	112.1	
4	145.2	135.7	75.4	153.6	166.7	153.8	137.5	128.2[c]
5	161.6	163.4	165.1	250.8	282.6	264.6	199.0	
6	331.5	378.6	283.0-317.0	232.6-296.6	232.9-305.2	208.0-284.6	203.5-259.6	

	IW2b		IW2a			
	G				^1L_b	
mode	HF/6-31G	EXP[b]	HF/6-31G	^1L_a	CIS/6-31G	EXP[a]
1	19.7	17.7	35.5	45.4	44.5	39.5
2	40.3		51.0	66.0	67.3	
3	50.4		63.5	69.1	68.7	48.5
4	56.2		104.7	122.9	120.3	
5	93.4		130.7	180.4	174.5	
6	156.9		171.7	237.1	181.0	
7	175.1		221.3	250.5	227.2	188.8
8	236.7		238.3	342.4	256.9	
9	268.7		297.9	383.3	337.7	
10	293.4		378.4	463.9	448.2	
11	364.7		525.6	584.5	574.1	
12	572.2		839.9	895.1	883.9	

[a]Reference 19. [b]Reference 86. [c]Reference 75.

vibrational amplitudes localized on the water hydrogens. The σ-complex intermolecular frequencies vary little from one electronic state to the next and no mixing takes place between the first 4 intermolecular modes with ^1L_a or ^1L_b excitation, regardless of basis. These features indicate that only small changes arise in the shape of the potential energy surface near the minimum upon ^1L_a or ^1L_b excitation.

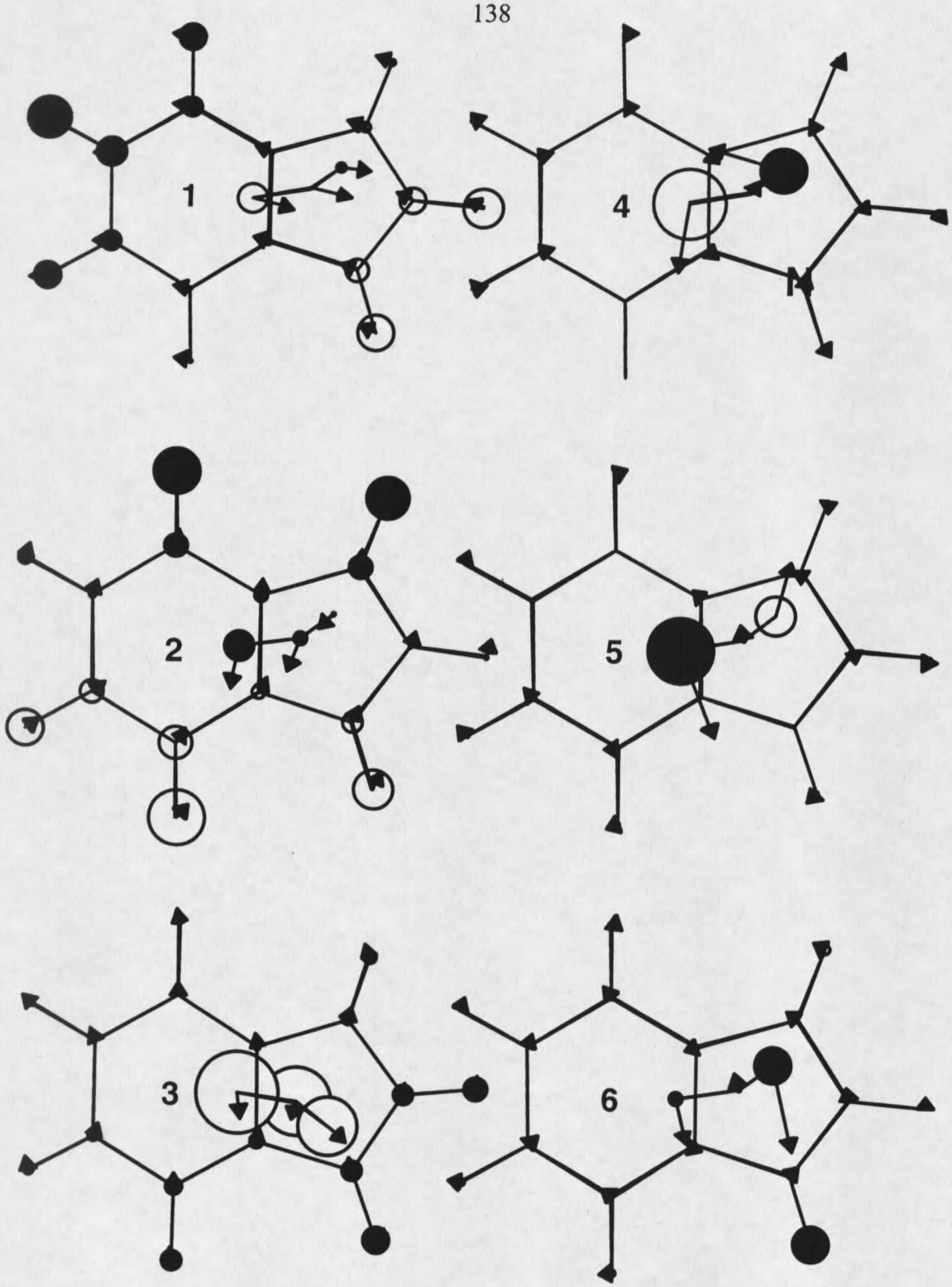

Figure 31. Indole:water π-complex HF/6-31++G(p,d) intermolecular normal modes

In spite of the lack of symmetry, the intermolecular normal modes of the hypothetical indole:water π-complex (Figure 31) can also be loosely classified as bends, stretches, torsions, and wags. As with the σ-complex, in each state the bending modes are lowest in frequency and one of the wags is highest in frequency. Unlike the σ-complex, mixing with the intramolecular modes is not apparent in the highest frequency vibration, and this is due to the weakness of the interaction. In further contrast to the σ-complex, mode crossing occurs with ^1L_b excitation. The frequency of the H_2O C_2 torsion mode is considerably lower in the ^1L_b state, indicating a much flatter potential energy surface along this normal coordinate near the minimum, and resulting in an inversion with the intermolecular stretch. Perhaps this frequency decreases because the water moiety interacts with the C4-C9 and C6-C7 bonds in the ^1L_b equilibrium geometry while the interaction is with atoms in the other states, as Figure 24 shows. The N-methyl indole:water π-complex emission spectrum shows a low frequency vibration of 26 cm^{-1},[23] which is compatible with Table 47.

Formation of the 1:2 complex causes the loss of six rotational degrees of freedom and six translational degrees of freedom, resulting in 12 intermolecular modes. Unlike the 1:1 clusters, the intermolecular modes can not be classified as bends, stretches, or wags, due to their complexity. Furthermore, tunneling between the isoenergetic conformations makes the harmonic approximation inappropriate, at least in the ground state. Thus, any resemblance between the measured and calculated intermolecular frequencies of the ground state 1:2 complex is largely coincidental. The high frequency intermolecular modes of the 1:2 complex are mixed with intramolecular modes, or only involve the water dimer.

In the ^1L_b state, the inflationary effect of the BSSE has probably been canceled to some extent by maintaining a partly frozen geometry for the indole moiety, resulting in a reasonably accurate lowest 1:2 complex frequency. Relaxing the intramolecular geometry invariably increases the binding energy, resulting in higher intermolecular frequencies. The added stabilization ensuing the removal of these constraints is small for weakly bound complexes, but could have a large impact on very low frequencies.

Deuteration Shifts

In each electronic state, deuteration of the σ-complexed water molecule (and indole at H1) results in virtually no rotation of the intermolecular modes according to the present calculations. Because the mass difference between the isotopomers does not cause mixing, the frequency shifts may be attributed entirely to changes in the reduced mass of each mode. Table 48 shows that the rotational modes of the ^1L_b σ-complex exhibit larger isotope shifts than translational modes, given that they have amplitude localized mainly on the water hydrogens. Both the CIS/6-31G and CIS/4-31G(p,d) ^1L_b shifts adequately reproduce the experimental results. This suggests that the intermolecular normal coordinates are fairly accurate, and that the 24 cm^{-1} progression in the indole:water ^1L_b excitation spectrum should be assigned to the in-plane intermolecular bend. Assuming that the usual electric dipole selection rules pertain to the σ-complex, for one quantum transitions the a′ bend is symmetry allowed while the a″ bend is symmetry forbidden and of very weak intensity if at all present.

Franck-Condon Factors

The calculated and observed Franck-Condon factors of the ^1L_b σ-complex intermolecular modes are compare in Table 48. The intermolecular bend and stretch

Table 48. Indole:(water)$_n$ (n=1,2) ^1L_b intermolecular vibrational properties and Franck-Condon factors.

IW2a

	$(\nu_{D2O}/\nu_{H2O})^2$		$f_{0\rightarrow1}/f_{0\rightarrow0}$		$\varepsilon_{i,jc\varphi}$(Å)[a]	
mode	6-31G	EXP[c]	6-31G[d]	EXP[c]	6-31G	EXP[c]
1	0.871	0.915	0.92	1.41	0.11	0.19
2	0.885	0.972	0.09	0.26	0.09	0.16
3	0.938		0.13	0.00	0.07	
4	0.930		0.16	0.00	0.06	
5	0.562		0.00	0.00	0.04	
6	0.957		0.05	0.00	0.05	
7	0.544		0.00	0.00	0.03	
8	0.882		0.00	0.00	0.04	
9	0.557		0.21	0.24?	0.05	
10	0.694		0.00	0.00	0.02	
11	0.547		0.00	0.00	0.02	
12	0.507		0.00	0.00	0.01	

σ-complex

	$(\nu_{D2O}/\nu_{H2O})^2$			$f_{0\rightarrow1}/f_{0\rightarrow0}$			$\varepsilon_{i,jc\varphi}$ (Å)		
	6-31G	4-31G**	EXP[c]	6-31G	4-31G**	EXP[c]	6-31G	4-31G**	EXP[c]
1	0.886	0.882		0.00	0.07	0.15	0.20	0.18	0.17
2	0.867	0.915	0.904	0.00	0.00	0.00	0.14	0.11	
3	0.712	0.512		0.00	0.04	0.02	0.04	0.02	
4	0.917	0.856		0.03	0.00	0.00	0.10	0.11	
5	0.461	0.761		0.00	0.00	0.00	0.06	0.01	
6	0.519	0.771		0.00	0.00	0.00	0.04	0.00	

[a]Classical turning point. [c] Reference 19. [d] IW2a ground state geometry.

show slight Franck-Condon activity at the CIS-HF/4-31G(p,d) level of theory, in agreement with experiment. The total intensity of the fundamental transitions of the intermolecular modes is also reasonably well represented at CIS-HF/4-31G(p,d). In

contrast, at CIS-HF/6-31G, activity appears only in the in-plane wag and the total intensity is considerably smaller than what is observed.

Accurate computation of the Franck-Condon factors of the 1:2 complex is a more stringent test of the theoretical model because of the low symmetry of this system, as every vibration is potentially Franck-Condon active. With the IW2a ground state geometry, Franck-Condon activity is predicted in 6 of the fundamental vibrations of the ^1L_b 1:2 complex intermolecular modes, but activity is observed in only 3. Theory correctly predict the greatest intensity to be in the lowest energy vibronic transition, and the predicted sum of the Franck-Condon factors (1.56) is close to experiment (1.91). Thus, the quality of the calculation is surprisingly good in light of the poor FC factors obtained at the same computational level for the σ-complex. Calculated spectra using the π-complexes or IW2b could not be obtained because the unrealistically large geometry changes prevent the program from running to completion.

Indole:Water Potential Energy Surface

As shown in Figure 32, at least two minima are found on the indole:water HF/6-31++G(p,d) intermolecular potential energy surface. The σ-complex is the global minimum, being 700 cm^{-1} deeper than the π-complex. A more extensive investigation would probably uncover additional minima, particularly one with the C3-H3 group acting as the proton donor. However, the minima of such complexes are extremely shallow, as indicated by previous ab initio studies,[87] and as suggested by the binding energy of the 1:2 complex IW2c in Figure 26 (about 10 kcal/mol smaller than IW2a

IW2b at HF/6-31G).

The anharmonic character of the surface was assessed with least squares fits using data from the potential energy curves intersecting the global minimum, out to 0.5 Å, in the directions parallel and perpendicular to indole's long axis, taken herein as the *x* and *y* directions, respectively. The coefficients of the resulting polynomials are shown in Table 49. In the *x* direction, the quadratic term is dominant regardless of the

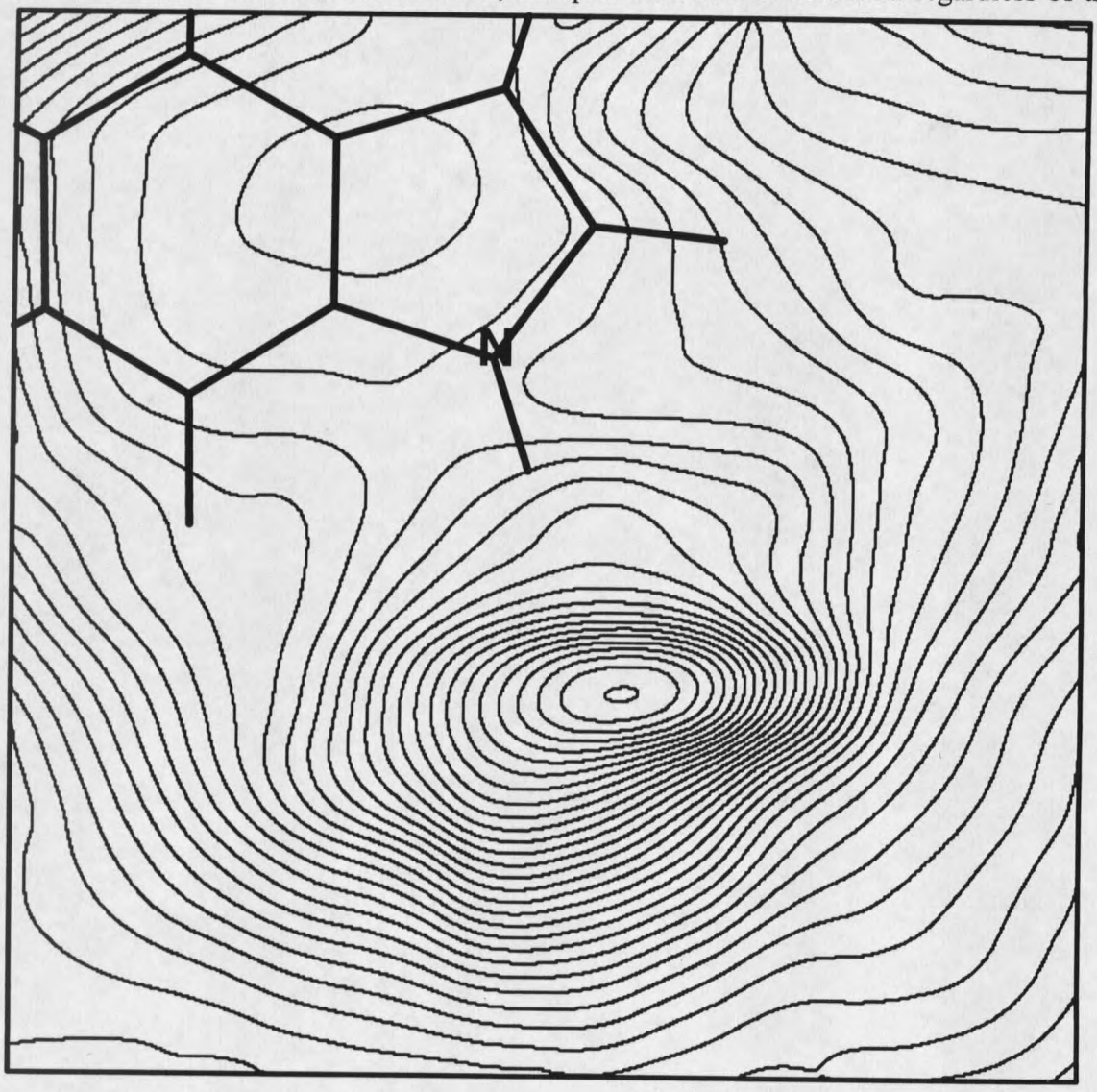

Figure 32. Indole:water HF/6-31++G(p,d) intermolecular potential energy surface.

Table 49. Potential energy surface least-squares-fit polynomial coefficients (au×10^6)

n[a]	x^2	x^3	x^4	x^5	x^6	corr.
1	303.26					0.999295
2	303.26	37.94				0.999827
3	284.02	37.94	83.19			0.999999
4	284.02	36.16	83.19	5.96		0.999999
5	281.47	36.16	111.88	5.96	-78.75	
	y^2	y^3	y^4	y^5	y^6	corr.
1	1550.89					0.999669
2	1550.90	111.80				0.999847
3	1463.39	111.79	378.41			0.999984
4	1463.38	232.28	378.44	-403.61		0.999994
5	1426.16	232.30	797.30	-403.66	-1149.50	

[a]Number of non-linear terms in polynomial.

order of the polynomial and, according to the correlation coefficient, including the quartic or higher order terms of the polynomial does little to improve the accuracy of the fit. In the *y* direction, the sextuple term is nearly as large as the quadratic term and the higher order terms have a greater effect on the correlation coefficient. The harmonic model should then be a better approximation to center-of-mass motion along *x* than along *y*.

In addition to being less anharmonic, the potential is much flatter along *x*. A comparison of the quadratic coefficients in Table 50 indicates that the force constant for H_2O center-of-mass displacement in the *y* direction is 5 times greater than that for the *x* direction, i.e., $k_x = 6.1 \times 10^{-4}$ Hartree/Bohr^2 and $k_y = 3.1 \times 10^{-3}$ Hartree/Bohr^2 according to the second degree polynomials. Thus, water moiety translational motion

Table 50. π-complex potential energy surface least-squares-fit polynomial coefficients (au×10^6)

n[a]	x^2	x^3	x^4	x^5	x^6	corr.
1	39.93					0.999402
2	39.93	-3.71				0.999696
3	42.72	-3.71	-12.07			0.999906
4	42.72	-11.06	-12.07	-24.63		0.999964
5	41.95	-11.06	-3.31	-24.63	-24.04	

[a]Number of non-linear terms in polynomial.

will be much more floppy in the *x* direction than the *y* direction.

The surface is flatter still near the π-complex minimum. The contours in this region roughly reflect the shape of the molecular skeleton; the π electron network extends farther along *x*, resulting in a slightly flatter surface in this direction. Also, the presence of the heteroatom results in a significant perturbation of the well's symmetry. Thus, the polynomial coefficients obtained from least-squares-fits, Table 50, show that cubic and higher order terms are needed to accurately model the surface in this region. It is also worth noting that the region around the π-complex minimum does not amount to a much larger "target" for the water moiety than does the σ-complex minimum, if it all. Kinetic factors would not necessarily favor formation of the π-complex over the σ-complex in jet-cooled spectra. The region in between the two minima is also extremely flat, amounting to a 100 cm^{-1} barrier with respect to the π-complex minimum.

The surface in Figure 32 was not corrected for the BSSE, nor were corrections made for the zero point energy and electron correlation. Whether this surface is

parallel to the true surface therefore hinges on whether the sum of these errors remain about constant with variations in intermolecular separation and orientation. A constancy of this sort appears to be approximately present in the BSSE; Table 36 shows that the σ-complex BSSE is only 0.07 kcal/mol greater than the π-complex BSSE at HF/6-31++G(p,d). The weak nature of the interaction and the fact that both monomers are closed shell systems would also seem to largely preclude any variation in the correlation energy as the H_2O molecule moves across the surface. Indeed, Table 36 shows that the correlation correction of the π-complex exceeds that of the σ-complex by only 0.25 kcal/mol at MP2-HF/6-31G(p,d). The ΔZPE correction is determined mainly by the intermolecular frequencies, which in turn depend on the strength of the interaction. Consequently, it is somewhat more variable between the σ- and π-complexes than either the BSSE or the correlation correction, being 0.41 kcal/mol larger for the σ-complex at HF/6-31++G(p,d). However, most of this error is canceled by the correlation correction, at least between the two minima, so the net difference in error between the σ- and π-complexes amounts to 0.23 kcal/mol, or 80 cm^{-1}, out of a change in binding energy of 800 cm^{-1}. The vibrational properties of the water dimer are reproduced with a Hartree-Fock potential energy surface[88], indicating parallelism with the true surface.

σ-Complex Eigenstates and Eigenvalues

The presence of more than one minimum in Figure 31 suggests more than one conformation for the indole:water complex. In order to determine whether the region above indole is energetically accessible to the water molecule at 0 K, the vibrational

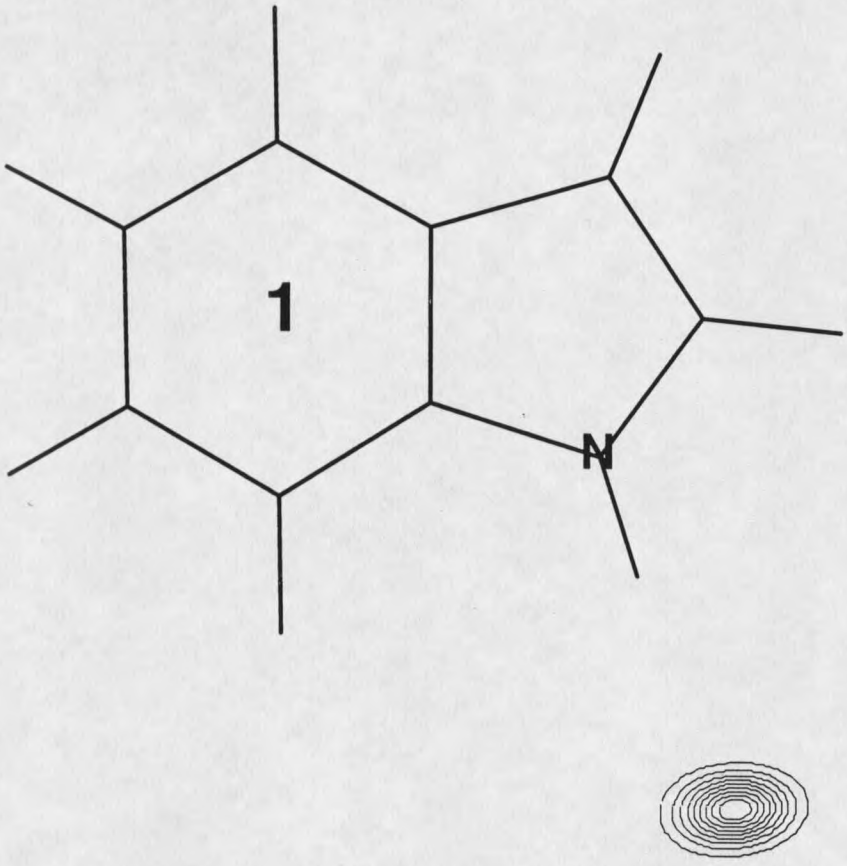

Figure 33. Indole:water vibrational ground state wave function. Contour spacing equals ten percent of maximum amplitude.

wave functions of the low energy bound states of the 1:1 indole:water complex were calculated. A contour plot of the lowest van der Waals state is presented in Figure 33. The ground state strongly resembles that of a two-dimensional anisotropic harmonic oscillator. That is, it takes the form $\Psi = N_n(H_\upsilon(\xi_x)e^{-kxx^2} \times H_\mu(\xi_y)e^{-kyy^2})$, where N_n is a normalization factor, the reduced variable $\xi_x = x/(\hbar/\mu_x\omega_x)$, the gaussians guarantee a well-behaved solution in the limit of infinite separation along x or y, and $H_\upsilon(q)$ is a hermite polynomial of degree υ. For $\upsilon = 0, 1, 2, 3, 4, \ldots\ldots, H_\upsilon(q) = 1, 2q, 4q^2-2, 8q^3-12q, 16q^4-48q^2+12\ldots\ldots$ The spatial distribution of Ψ in any given state is then a gaussian of the restoring force modified by υ through the number of roots of polynomial $H_\upsilon(q)$. For the anisotropic case, $k_x \neq k_y$, and so the ground state wave function is shaped like an ellipse.

Thus, the water moiety's center-of-mass motion along x and y is separable in the ground state, and the corresponding wave function may be expressed as a product of functions of these independent variables. This remains true for the lower excited indole:water vibrational states, Figure 34. The wave function for state number 2 may be associated with one vibrational quantum of excitation of the bending motion in the x direction. In this state, motion in the x direction is not coupled with motion in the y direction, as indicated in Figure 34 by the well-defined node along the y axis. Similarly, the third state is associated with one vibrational y quantum, although the node of this wave function is slightly distorted. This is the first sign of a Fermi resonance, and it appearance in this state is consistent with the less harmonic potential in this direction. The fourth state is associated with two quanta of excitation of the

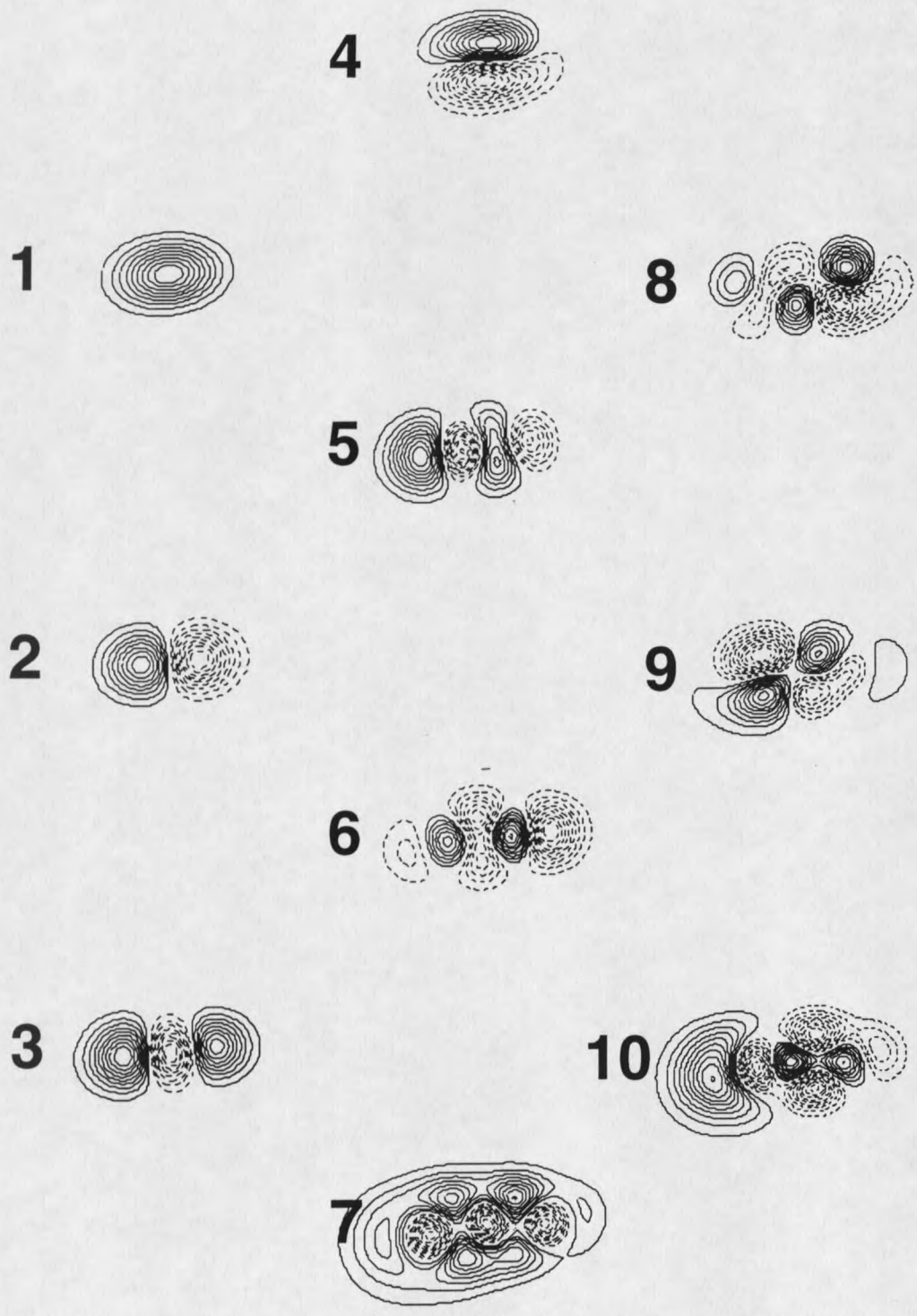

Figure 34. Indole:water vibrational wave functions. Contour spacing equals ten percent of maximum amplitude.

Table 51. Indole:water σ-complex vibrational properties

State	ΔE (cm^{-1})	$\langle x \rangle$(Å)[a]	Δx[b]	$\langle y \rangle$	Δy
1	0.0	-0.053	0.367	-0.005	0.249
2	24.0	0.045	0.582	-0.011	0.263
3	56.4	-0.060	0.362	-0.009	0.408
4	57.0	-0.188	0.749	0.016	0.235
5	96.2	-0.499	0.578	-0.022	0.416
6	98.4	-0.623	0.717	0.078	0.268
7	104.3	0.448	0.731	-0.071	0.300
8	116.6	0.376	0.626	0.055	0.365
9	147.5	-0.810	0.912	0.112	0.390
10	162.5	-0.346	0.874	-0.006	0.503

[a]Expectation value relative to the location of the energy minimum. [b]$\Delta x = (\langle x \rangle^2 - \langle x^2 \rangle)^{1/2}$.

bending mode in the *x* direction, as demonstrated by the nodal pattern of the wave function. The fifth and sixth states also show small signs of mixing between the *x* and *y* modes, but may be loosely assigned to 3 and 4 *x* quanta transitions. After the sixth or seventh state, the nodal patterns of these wave functions become rather complicated and it is no longer possible to make an assignment.

As Table 51 shows, characterizing the low energy van der Waals states in terms of the number of *x* or *y* quanta is justified by the vibrational amplitudes, Δx and Δy. The value of Δx increases on going from state 1 to state 2, with no concomitant increase in Δy, which is consistent with a one *x* quantum transition. Similarly, state 3 has an increased Δy in relation to state 1 with no concomitant increase in Δx, and this is to be expected for a one *y* quantum transition. Up to state 4, the changes in Δx and Δy with each increase in quantum number are fairly uniform. In the higher states, the

mixing between the *x* and *y* quanta transitions is manifested through irregular differences in Δx and Δy between successive levels.

The effect of anharmonicity on the vibrational amplitudes may be quantified. Approximating the complex as a harmonically oscillating diatomic molecule, the amplitude of vibration in state n is given by $((n + 1)h/(k\mu)^{1/2})^{1/2}$. Using $k_x = 6.1 \times 10^{-4}$ Hartree/Bohr^2, $k_y = 3.1 \times 10^{-3}$ Hartree/Bohr^2, and $\mu = 2.8 \times 10^4$ au, this gives Δx = 0.49 Å and Δy = 0.32 Å for the ground state. These amplitudes exceed those of the Table, indicating that the HF/6-31++G(p,d) surface is steeper than a parabola in both directions. The increase in vibrational amplitude would be expected to scale as $(n + 1)^{1/2}$ for a transition from the ground state to state n. This rule is somewhat closely obeyed only by the second state $(([\Delta x_2^2 + \Delta y_2^2]^{1/2})/([\Delta x_1^2 + \Delta y_1^2]^{1/2}) = 1.44$, compared to 1.41 for the harmonic oscillator) and the fourth state ($([\Delta x_4^2 + \Delta y_4^2]^{1/2})/([\Delta x_1^2 + \Delta y_1^2]^{1/2})$ = 1.77, compared to 1.73). For the first *y* quanta transition, this ratio is 1.23, another reflection of the greater anharmonicity in this direction of the surface.

The vibrational amplitudes are also indicative of floppy intermolecular behavior. Table 51 thus confirms the anticipated greater floppiness in the *x* direction, and shows that it generally increases in both directions with each increase in quantum number. The total in-plane amplitude $([\Delta x^2 + \Delta y^2]^{1/2})$ of 0.44 Å in the ground vibrational state is consistent with the rotationally resolved spectrum, which indicates an out-of-plane displacement of 0.35 Å for the σ-complex that is smaller than the in-

plane displacement.[21]

The position operator expectation values (relative to the location of the potential energy minimum) of the ten lowest van der Waals states are included in Table 51. These quantities give the vibrationally averaged position of the water moiety. For a harmonic oscillator, <x> = 0 and <y> = 0 in each state; hermite polynomials are symmetric or antisymmetric functions of position, and therefore the expectation values of the antisymmetric position operators vanish in each state. For a general system, the average positions tend to deviate farther from the minimum with increasing quantum number in order for the orthogonality requirement to be met. For the σ-complex, the average position remains rather close to the minimum along *y* even in the excited states (a negative <y> corresponds to a location between the minimum and indole) due to the larger force constant, while becoming rather distant from the minimum along *x* (increasingly large negatives value for <x> in Table 51 correspond to average water positions increasingly closer to H7). Most of the states are skewed towards H7, in some cases very drastically, possibly because of the weak, stabilizing interaction between the water moiety and the phenyl ring.

The energy levels of the first ten eigenstates of the indole:water complex are included in Table 51. The zero point energy is 72.2 cm^{-1}, compared to a value of 75.7 cm^{-1} as calculated from the HF/6-31++G(p,d) frequencies of the σ-complex intermolecular stretch and a′ bend (normal modes of a″ symmetry or arising from

internal rotation by the water (i.e., the a′ wag) are excluded from the tabulation because of the single particle approximation.) The spacings between the lower states are seen to only approximately follow the harmonic model. For instance, the increase in energy between the first x and y quanta transitions would be expected to scale as $\sqrt{k_y/k_x} = 2.26$ for a harmonic oscillator, and this is roughly obeyed ($\Delta E_3/\Delta E_2 = 2.35$). The separation between the energy levels increases with increasing quantum number, indicating that the HF/6-31++G(p,d) surface is steeper than a quadratic surface near the global minimum.

The lowest energy transition, 24.0 cm^{-1}, is comparable to the 27.7 cm^{-1} frequency of the σ-complex a′ intermolecular bend at HF/6-31++G(p,d), suggesting the single particle approximation is valid for motion in this direction. However, the one y quanta transition energy of 56.4 cm^{-1} is inconsistent with the frequency of the σ-complex intermolecular stretch, 123.6 cm^{-1} at HF/6-31++G(p,d). Having translational parentage, intermolecular stretching frequencies are usually adequately reproduced by the harmonic oscillator model, as shown in Table 47 for the ^1L_b state. Perhaps modeling the water monomer as a single particle has come back to haunt this investigation, and the coupling between the stretching mode and the internal motion of the water moiety must be taken into consideration for motion in the y direction, as suggested by the rotational spectra.[21]

To summarize, in each of the 10 lowest states the water moiety has no

amplitude in the π-complex minimum. The probability densities are then vanishing in this region as well, of course. Unfortunately, the size of the potential energy surface makes it difficult to calculate the two-dimensional wave functions of higher energy states with the present computational power. The corresponding one-dimensional problem was therefore solved for the potential energy on the line connecting the bottoms of the two minima in Figure 32. Figure 35 shows the potential and the bound state wave functions of this system. It is seen that state 4 is the lowest energy eigenfunction with amplitude in the π-complex well, lying 604 cm^{-1} above the ground state. Wave functions with amplitude in this region apparently correspond to very high energy states of the σ-complex and are extensively delocalized over the entire surface.

π-complex

In order to investigate the vibrational states of the π-complexed water moiety, the potential surface was approximated by extrapolating out from the potential points taken neara the π-complex energy minimum, i.e., by ignoring the σ-complex minimum. These results are thus more pertinent to the N-methyl indole:water complex. Contour plots of the first ten states are given in Figure 36, with the corresponding energy levels, expectation values, and vibrational amplitudes provided in Table 52.

The delocalized nature of the π-complexed water moiety is made clear by the Figure. In particular, the notion of a specific interaction between a water molecule and

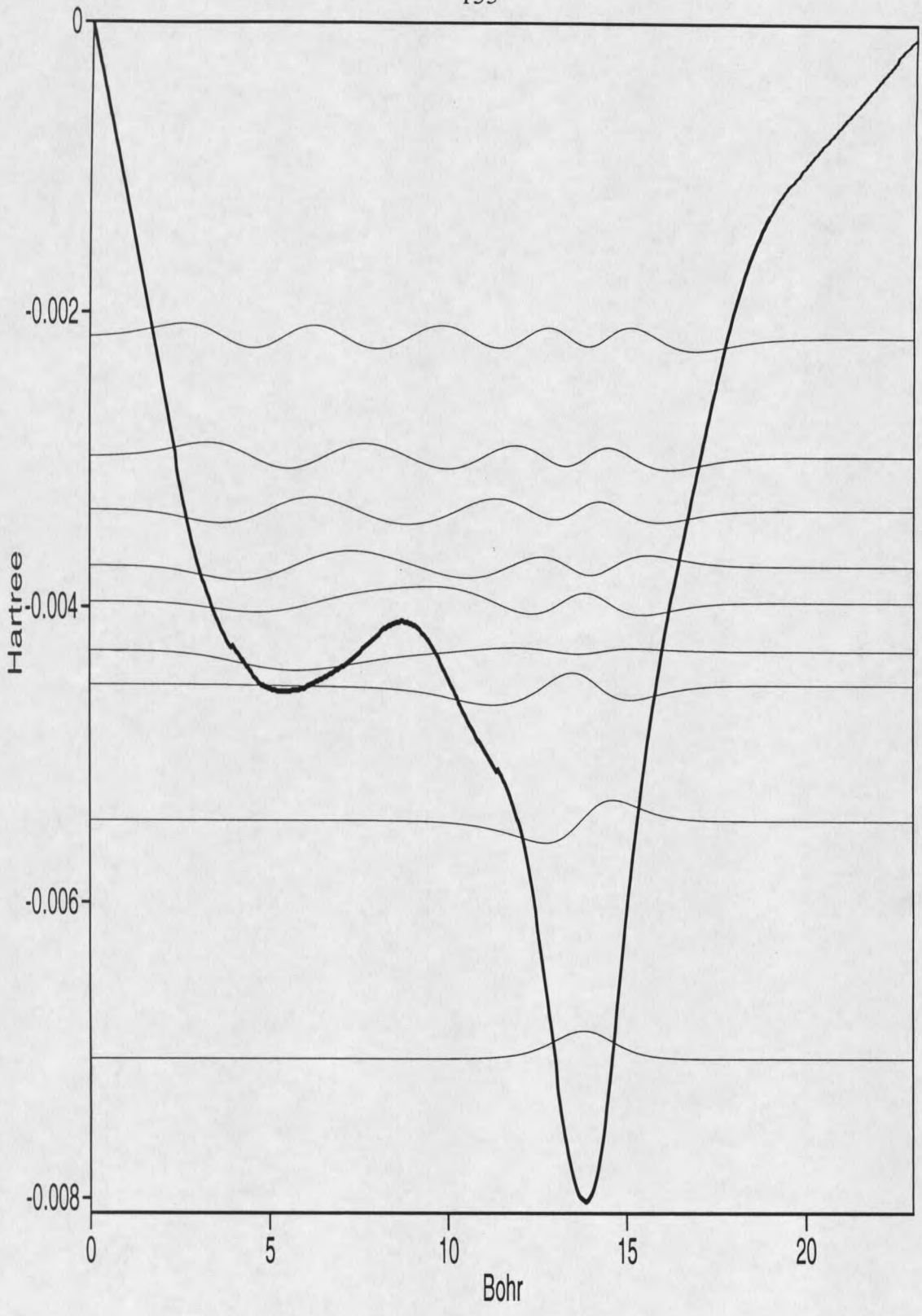

Figure 35. Indole:water one-dimensional potential and bound state wave functions.

Table 52. Indole:water π-complex vibrational properties.

State	ΔE (cm^{-1})	⟨ x⟩(Å)[a]	Δx[b]	⟨ y⟩	Δy
1	0.0	0.0821	0.3554	0.0013	0.2953
2	11.5	0.0279	0.5116	0.0034	0.3387
3	12.4	0.3424	0.4662	0.0661	0.4261
4	18.3	0.3115	0.6724	0.1050	0.3194
5	26.0	0.0736	0.3635	-0.0608	0.6077
6	27.2	0.1823	0.7509	0.0668	0.3729
7	35.3	0.1719	0.5214	0.2559	0.5768
8	51.6	0.2189	0.6864	0.0358	0.4600
9	57.4	0.1159	0.6607	0.0708	0.6123
10	97.3	0.3502	0.5661	0.1586	0.6106

[a]Expectation value relative to the energy minimum. [b]$\Delta x = (\langle x \rangle^2 - \langle x^2 \rangle)^{1/2}$.

the indole ring's π cloud above C3 in aqueous solutions, as has been postulated,[17] is not supported by these results. The 90% contour of the ground state wave function, for example, covers almost the entire pyrrole ring, resulting in a total vibrational amplitude ($[\Delta x^2 + \Delta y^2]^{1/2}$) of 0.46 Å. Furthermore, vibrational averaging moves the water moiety away from C3 in each state. This is due to the heteroatom in the aromatic ring, which skews the wave functions of nearly every state onto its side of the long axis. Another consequence of the heteroatom is the rotation of the state 2 and 3 wave functions into ~45° and ~135° angles with the short axis. Both the skewing and the rotating of the wave functions have the effect of increasing the vibrational amplitude near the transition state. The manner in which the wave functions are distorted is thus consistent with very few bound states, if any, being held by the actual indole:water π-complex well.

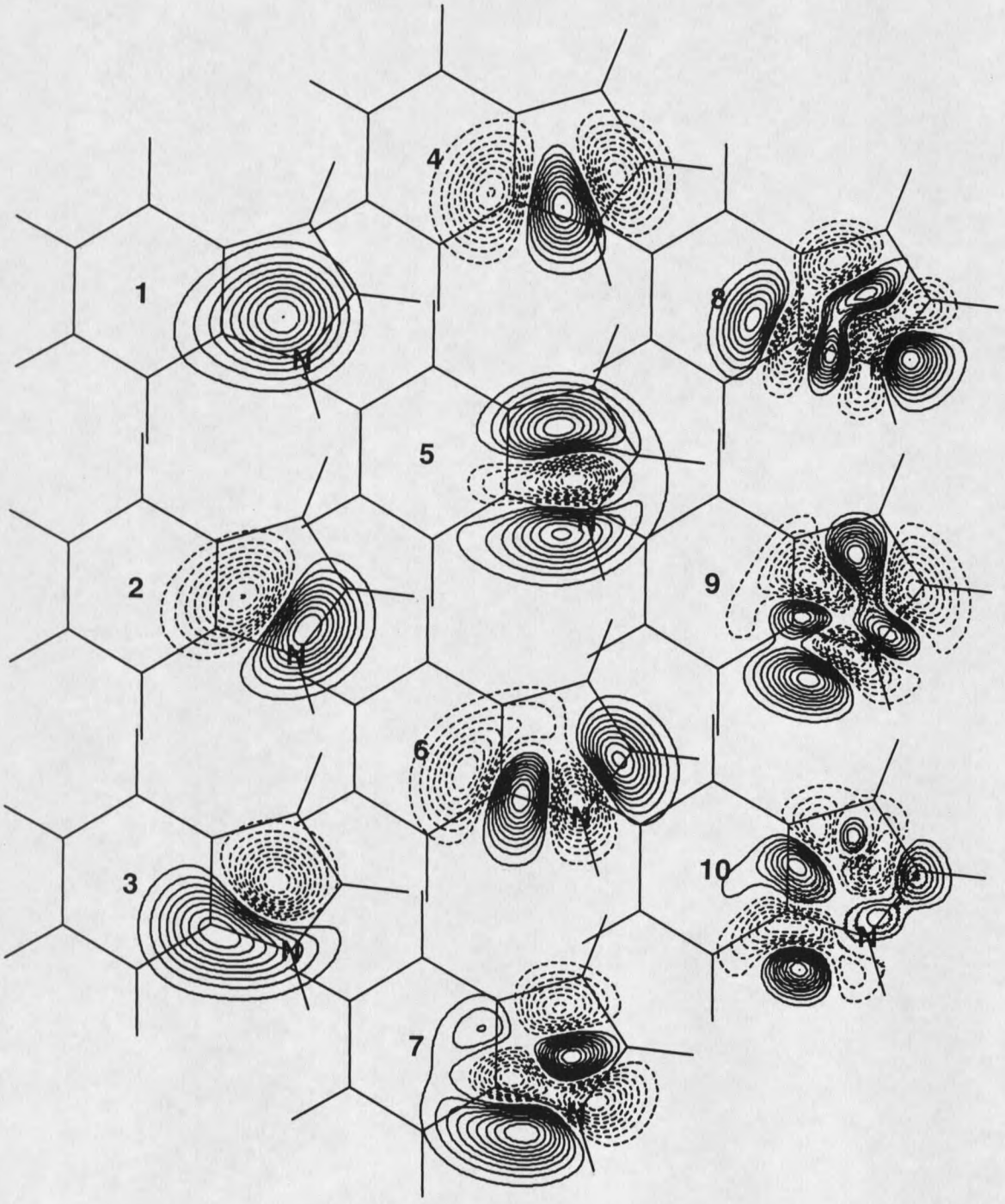

Figure 36. Indole:water π-complex bound state wave functions. Contour widths equal ten percent of the maximum amplitude.

3-Methyl and 5-Methyl Indole

Transition Energies

The positions of the absorption band maxima indicate a 1,300 cm^{-1} decrease in the vertical separation between ^1L_a and ^1L_b when H3 is replaced with a methyl group.[3] A comparison of Tables 53 and 1 shows that this modification lowers ^1L_a by only 400 cm^{-1} and ^1L_b by 200 cm^{-1} at the ground state geometry, at both CIS/6-31G and CIS/6-31++G(p,d). Furthermore, there is a 100 cm^{-1} increase in the Franck-Condon separation between these states at CIS(11,11)/6-31G, perhaps partly because the truncated CIS wave function is not size consistent. The methyl group adds 4 occupied MOs and, with a split valence basis, 9 virtual MOs, resulting in 571 additional configurations in the full CIS wave function, so the 121 determinants arising from transitions between 22 MOs span a smaller region of the complete configuration space. Fittingly, a slight increase in the number of configurations comprising the excited state wave function lowers ^1L_a by 400 cm^{-1} in relation to ^1L_b at the ground state geometry, as Table 53 shows.

The 0-0 separation between ^1L_a and ^1L_b decreases by roughly 1,000 cm^{-1} upon 3-methyl substitution.[27] Unfortunately, no minimum could be found on 3-methyl indole's CIS/6-31G ^1L_b potential energy surface - the wave function collapses to ^1L_a. The 0-0 separation between ^1L_a and ^1L_b amounts to 1,900 cm^{-1} at CIS(11,11)/6-31G,

Table 53. 3-Methyl Indole and 5-methyl indole CIS transition energies (10^{-3} cm^{-1})

	3-methyl indole							
	^1L_a		^1L_b		T_1		T_2	T_3
basis	ν	ν_{0-0}	ν	ν_{0-0}	ν	ν_{0-0}	ν	ν
CIS(11,11)/6-31G	52.7	50.2	50.1	48.3	26.2		34.2	38.1
CIS(13,14)/6-31G	52.1	51.4	49.9	47.6				
6-31G	48.6	45.0	49.0		26.0		34.8	39.8
6-31G(d)		44.2[b]				23.4[b]/22.5[b,c]		
6-31++G(p,d)	45.3		46.2					
EXP	35.5[e]	~35.5[a]	34.9[e]	34.9[a]		23.9[d]		
	5-methyl indole							
CIS(11,11)/6-31G	53.0	50.1	49.7	47.2				
CIS(13,14)/6-31G	52.4	49.6	49.6	47.0				
CIS/6-31G	48.9	45.2	48.6	45.5				
EXP[a]		36.8[a]		35.4[a]				

[a]Reference 27. [b]Using CIS-HF/6-31G(p,d) zero-point energies of indole. [c]Non-planar configuration. [d]Reference 6. [e]Reference 3.

400 cm^{-1} smaller than that of indole at this computational level. Oddly, a small increase in the number of configurations destabilizes ^1L_a by 1,900 cm^{-1} in relation to ^1L_b at the 0-0 separation.

In regards to the triplet manifold, a methyl group at the 3 position is predicted to decrease the ^3L_a vertical transition energy by 200 cm^{-1} at CIS/6-31G(d) (compared to indole at CIS/6-31G(p,d)). Conversely, the adiabatic separation is increased by 1,700 cm^{-1} for the planar configuration and by 500 cm^{-1} for the non-planar configuration. Thus, the non-planar configuration is the global minimum, by 900 cm^{-1} at CIS/6-31G(d). Perhaps this is because the symmetry requirements governing the interaction

between the methyl group and the indole orbitals vanish in the non-planar conformation. With the indole ring bent, the hyperconjugation interaction is no longer limited to the methyl group orbital with π symmetry, permitting a greater delocalization of charge. The vertical T_2 transition is stabilized by 500 cm^{-1} relative to indole at CIS/6-31G(p,d) while T_3 is unaffected.

The ^1L_a state of 5-methyl indole is inappropriately below ^1L_b by 238 cm^{-1} at CIS/6-31G. The 5-methyl modification lowers the 0-0 ^1L_b separation with the ground state by 950 cm^{-1} in cyclohexane[90] and by 600 cm^{-1} at CIS(13,14)/6-31G. The 0-0 ^1L_a state is unshifted in cyclohexane and lowered by less than 200 cm^{-1} at CIS(13,14)/6-31G. The ^1L_a and ^1L_b origins are separated by at least 1,424 cm^{-1} in the jet[28] and by 2,700 cm^{-1} at CIS(13,14)/6-31G. The observed[3] vertical separation of 3,900 cm^{-1} is compatible with the present calculated value of 3,200 cm^{-1}.

Transition Properties

Study of UV and IR linear dichroism indicates a 10° counterclockwise rotation of indole's ^1L_b transition dipole moment at the ground state geometry (Θ) in response to 3 position methyl substitution.[89] Comparison of Tables 54 and 3 shows that it is only with the truncated CIS wave function that a qualitatively correct result is obtained in this regard. Specifically, a 4° counterclockwise rotation of the ^1L_b vector is obtained at CIS(11,11)/6-31G, while a 27.7° clockwise rotation is predicted at CIS/6-31G and an 11° clockwise rotation is predicted at CIS/6-31++G(p,d). However, the polarization of 3-methyl indole's ^1L_b transition is very sensitive to basis, so this may perhaps be due merely to fortune. Like indole, the ^1L_b wave function is an approximate equimixture of the HOMO→LUMO+2 and HOMO-2→LUMO

Table 54. 3-Methyl Indole and 5-methyl indole CIS transition properties

	3-methyl indole							
	^1L_a				^1L_b			
basis	Θ	F	Φ	f	Θ	F	Φ	f
CIS(11,11)/6-31G	-40.0	0.181	-40.0	0.325	42.0	0.042	41.9	0.056
CIS(13,14)/6-31G	-41.8	0.170	-40.5	0.318	47.9	0.039	45.3	0.053
6-31G	-55.7	0.129	-34.4	0.323	7.1	0.078		
6-31++G(p,d)	-40.4	0.152			27.3	0.070		
EXP[a]	-47	0.127			55	0.027		
	5-methyl indole							
CIS(11,11)/6-31G	-35.4	0.154	-41.0	0.292	44.2	0.056	35.0	0.096
CIS(13,14)/6-31G	-36.1	0.152	-40.0	0.298	45.7	0.051	35.9	0.090
CIS/6-31G	-40.9	0.128	-34.0	0.314	31.9	0.077	50.6	0.119
EXP[a]	-39	0.129			50	0.027		

[a]Reference 90.

configurations (Table 55), reflecting the similarities between the indole and 3-methyl indole π MOs (Figure 37). The effect of going from indole to 3-methyl indole on the ^1L_a transition moment is also less inaccurately depicted at the truncated CIS level. A 7° counterclockwise rotation has been observed in the dichroism study, while a 1° clockwise rotation is obtained at CIS(11,11)/6-31G. In contrast, a 17° (11°) clockwise rotation is obtained at CIS/6-31G (CIS/6-31++G(p,d)). The experimental fact that the direction of the ^1L_a polarization is less sensitive to 3-methyl substitution is therefore captured at CIS(11,11)/6-31G and CIS/6-31G, but not at CIS/6-31++G(p,d).

For 5-methyl indole, the experimental ^1L_b and ^1L_a transition dipole vectors are rotated 5° and 15°, in the counterclockwise sense, with respect to their indole brethren. At CIS(11,11)/6-31G, 3.0° and 4.5° counterclockwise rotations are obtained and at

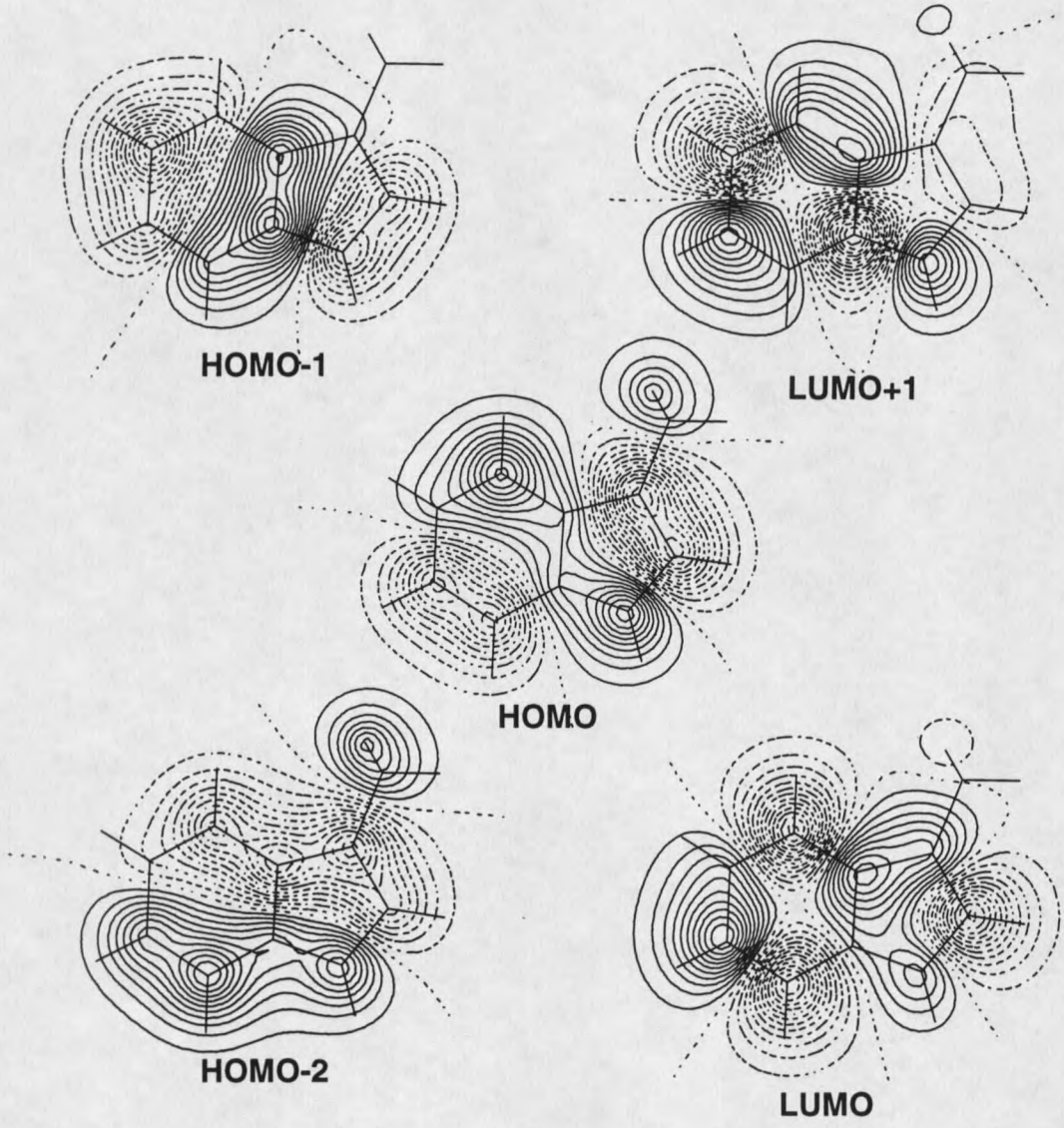

Figure 37. 3-Methyl indole HF/6-31G π molecular orbitals at 1.323 Bohr (0.7 Å) above the molecular plane. Contour width: 0.01 $Bohr^{-3/2}$. Contour range: -0.10 to 0.10 $Bohr^{-3/2}$.

CIS/6-31G, 2.9° and 2.5° clockwise rotations are obtained. The 5-methyl indole π MOs are very much like indole's in the ground state geometry (Figure 38) and extensively mixed in the ^1L_b geometry (Figure 39), resulting in a changed wave function (Table 55).

In cyclohexane, indole and 3- and 5-methyl indole have very similar ^1L_a oscillator strengths.[90] The CIS/6-31G 3- and 5-methyl indole ^1L_a oscillator strengths are very similar but much smaller than indole's. The CIS(11,11)/6-31G indole and 3-methyl indole ^1L_a oscillator strengths are very similar but much larger than 5-methyl indole's. The increase in ^1L_b intensity with 5-methyl substitution is reflected in the CIS/6-31G and CIS(11,11)/6-31G oscillator strengths. The increase in ^1L_b intensity with 3-methyl substitution is reflected only in the CIS/6-31G oscillator strengths.

Table 55. 3-Methyl Indole and 5-methyl indole optimum CIS/6-31G coefficients

	3-methyl indole					
	^1L_b			^1L_a		
π MOs	CIS	CIS(13,14)	CIS(11,11)	CIS	CIS(13,14)	CIS(11,11)
HO→LU	-0.343	-0.391	-0.390	0.648	0.636	0.637
HO→LU+1	0.591	0.561	0.564	<|0.10|	<|0.10|	<|0.10|
HO-1→LU	<|0.10|	<|0.10|	<|0.10|	<|0.10|	<|0.10|	<|0.10|
HO-1→LU+1	<|0.10|	<|0.10|	<|0.10|	0.236	0.271	0.271
HO-2→LU+1	<|0.10|	0.135	0.141	<|0.10|	<|0.10|	<|0.10|
	5-methyl indole					
HO→LU	0.572	0.376	0.356	0.645	0.634	0.635
HO→LU+1	0.112	0.281	0.289	<|0.10|	<|0.10|	<|0.10|
HO-1→LU	0.255	0.454	0.468	<|0.10|	<|0.10|	<|0.10|
HO-1→LU+1	-0.264	-0.220	-0.213	0.241	0.279	0.286
HO-2→LU+1	<|0.10|	0.107	0.110	<|0.10|	<|0.10|	<|0.10|

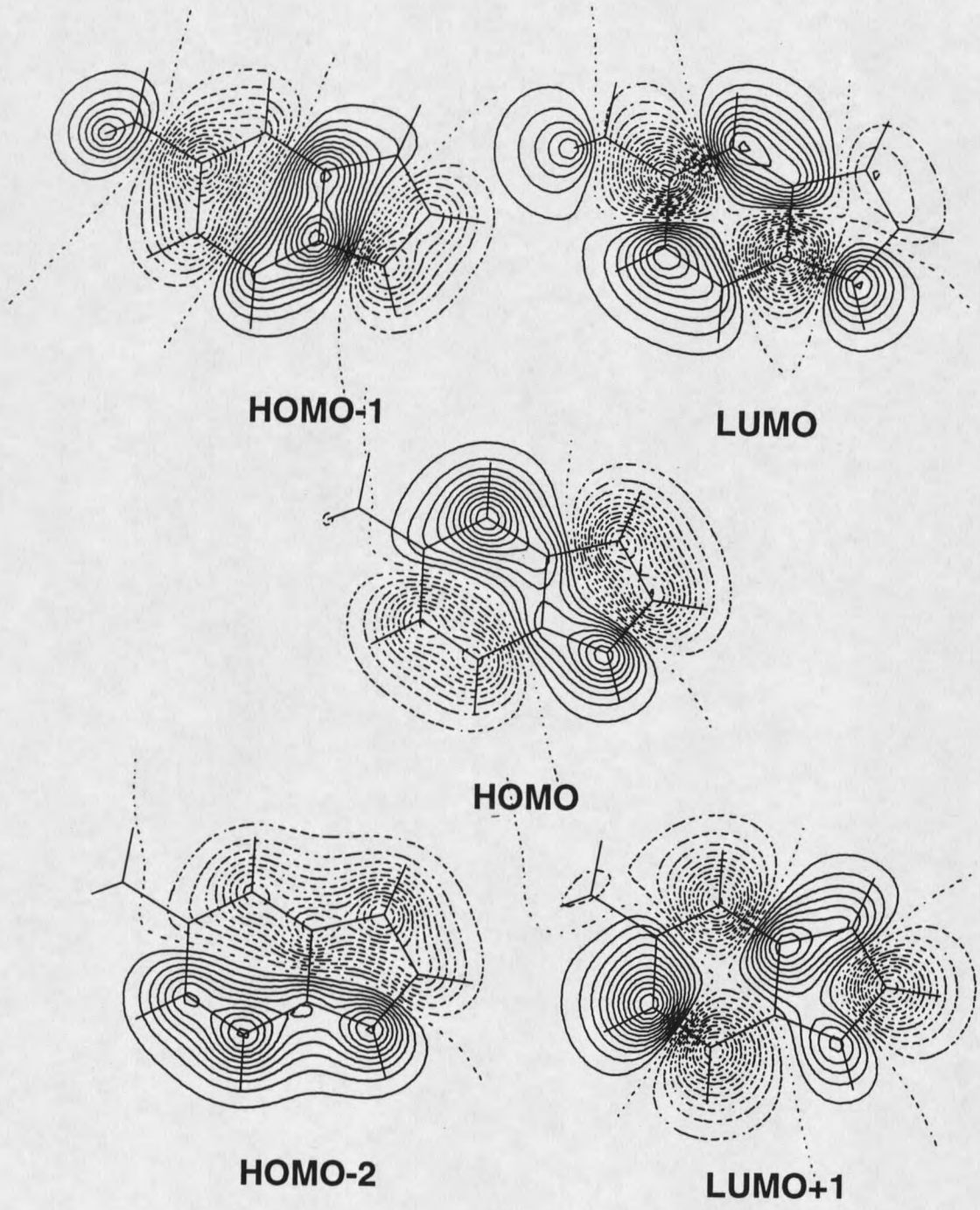

Figure 38. 5-Methyl indole HF/6-31G π molecular orbitals at 1.323 Bohr (0.7 Å) above the molecular plane, ground state geometry. Contour width: 0.01 $Bohr^{-3/2}$. Contour range: -0.10 to 0.10 $Bohr^{-3/2}$.

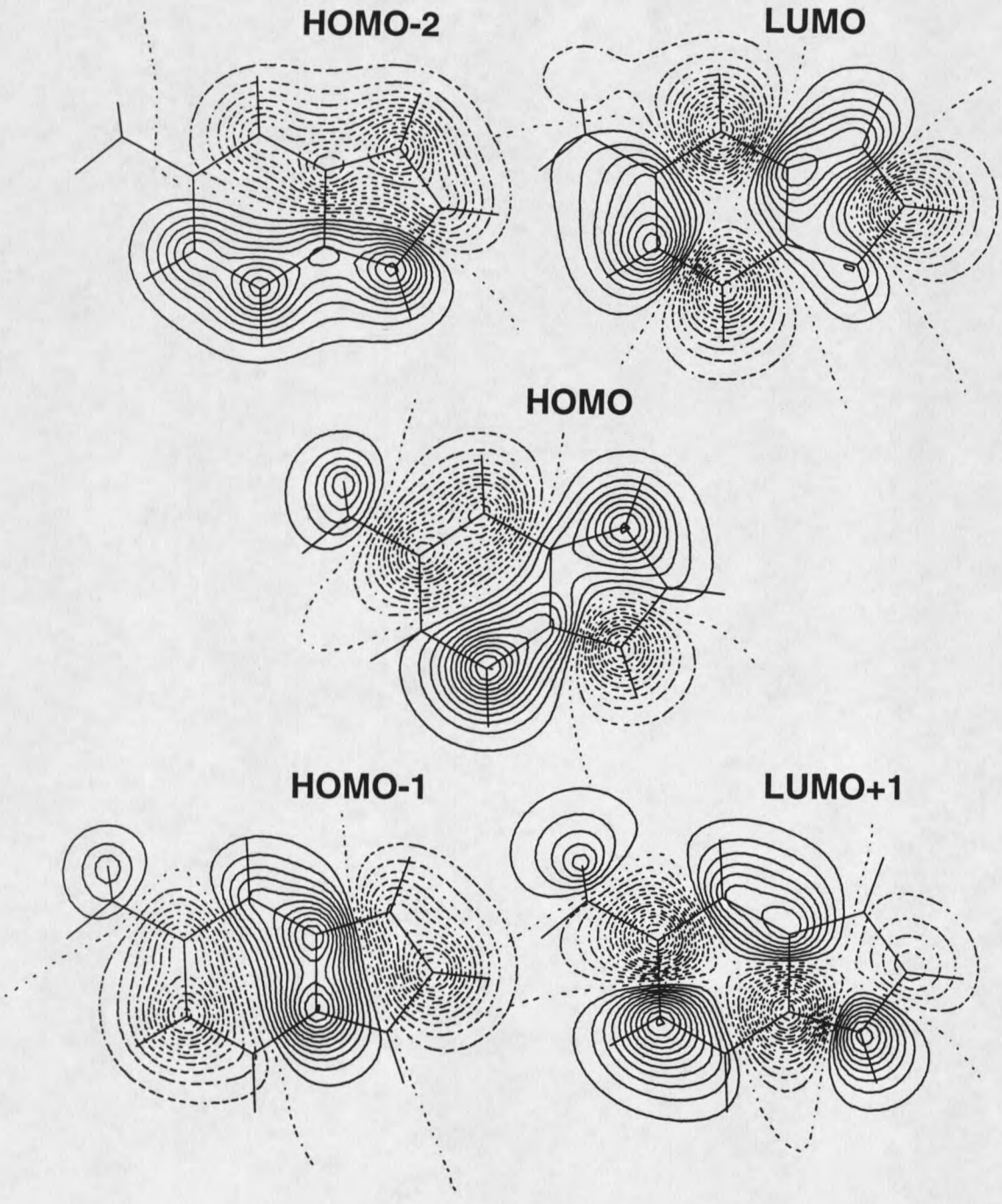

Figure 39. 5-Methyl indole HF/6-31G π molecular orbitals at 1.323 Bohr (0.7 Å) above the molecular plane, ^1L_b geometry. Contour width: 0.01 Bohr$^{-3/2}$. Contour range: -0.10 to 0.10 Bohr$^{-3/2}$.

Ground and Excited State Geometries

Table 56 lists the calculated equilibrium bond lengths and bond angles of 3-methyl indole in its ground, ^1L_a, and ^1L_b states, with the ground state geometry compared to the crystal structure. For each state, the carbon skeleton remains planar in the equilibrium geometry, and so the dihedral angles are omitted from the Table. The equilibrium geometry for each state puts one of the methyl hydrogens coplanar with the carbon skeleton, eclipsing H2, while the other two methyl hydrogens are situated above and below the molecular plane in the manner that retains the C_s symmetry. The insignificant deviations from planarity and methyl group local C_s symmetry in the calculated equilibrium geometry are attributable to the numerical imprecisions of the calculation.

At the HF/6-31G(d) level of theory, the effect of 3-methyl substitution is most pronounced in the N-C2 and C3-C9 bonds, which are predicted to increase in length by 0.0035 and 0.0054 Å. At the MP2/6-31G(d) level, the same modification causes only the C3-C9 bond length to increase, by 0.0169 Å, while all remaining ring-forming bonds are shorter than those of indole. In general, methyl substitution causes much larger changes at the correlated level of theory. There is a particularly large decrease in the C2-C3 bond length (by 0.0215 Å) and C8-C9 (by 0.0294 Å) at MP2/6-31G(d). Methyl substitution has meager effects on the benzene ring bonds at either HF/6-31G(d) or MP2/6-31G(d). Each of the MP2/6-31G(d) bond lengths deviate from the crystal structure by less than 0.8%, with the pyrrole bonds generally underestimated and the phenyl bonds generally overestimated.

The differences in equilibrium geometry between the ground state of 3-methyl

Table 56. 3-Methyl Indole ground and excited state bond lengths (Å) and bond angles (degrees)

	G					^1L_b	^1L_a
	3-21G	6-31G	6-31G*	MP2/6-31G*	EXP[a]	6-31G	6-31G
N1-C2	1.3850	1.3867	1.3760	1.3773	1.380	1.4027	1.3578
C2-C3	1.3484	1.3531	1.3483	1.3508	1.358	1.3638	1.4089
C3-C9	1.4472	1.4499	1.4473	1.4470	1.436	1.4360	1.4194
C4-C9	1.3933	1.3973	1.3982	1.3997	1.398	1.4030	1.4149
C4-C5	1.3750	1.3793	1.3757	1.3774	1.381	1.4170	1.4117
C5-C6	1.3997	1.4037	1.4035	1.4053	1.396	1.4173	1.3828
C6-C7	1.3750	1.3793	1.3755	1.3773	1.372	1.4112	1.4400
C7-C8	1.3893	1.3934	1.3941	1.3953	1.395	1.4047	1.3768
C8-C9	1.4009	1.4044	1.4008	1.4016	1.410	1.4566	1.4308
N1-C8	1.3740	1.3763	1.3685	1.3686	1.374	1.3616	1.3909
N1-H1	0.9876	0.9885	0.9920	0.9910		0.9897	0.9917
C2-H2	1.0663	1.0677	1.0715	1.0716		1.0662	1.0658
C3-C10	1.4944	1.4968	1.4995	1.4993		1.4960	1.4893
C4-H4	1.0725	1.0737	1.0761	1.0761		1.0714	1.0721
C5-H5	1.0719	1.0730	1.0754	1.0755		1.0723	1.0733
C6-H6	1.0721	1.0733	1.0757	1.0757		1.0715	1.0722
C7-H7	1.0723	1.0735	1.0760	1.0761		1.0714	1.0720
C8-C9-C3	107.26	107.28	107.17	107.18	106	106.87	107.26
C9-C3-C10	126.15	126.20	126.70	126.55		125.69	127.16
C9-C3-C2	106.38	106.32	105.96	105.94	106	107.40	107.46
C3-C2-H2	127.47	129.20	129.16	129.11		130.02	129.60
C3-C2-N1	110.18	110.17	110.60	110.58	111	109.21	108.03
C8-N1-H1	125.84	125.82	125.80	125.86		125.12	124.27
C8-C9-C4	119.26	119.26	119.11	119.21	123	119.04	118.86
C9-C4-H4	120.49	120.56	120.51	120.54		121.56	121.27
C9-C4-C5	119.10	119.07	119.15	119.09	116	118.05	118.08
C4-C5-H5	120.41	119.93	119.92	119.94		120.39	118.78
C4-C5-C6	120.79	120.80	120.78	120.77	122	122.55	122.06
C5-C6-H6	119.25	119.28	110.29	119.27		119.18	120.18
C5-C6-C7	121.24	121.26	121.30	121.32	121	121.12	120.92
C8-C7-H7	121.25	121.33	121.33	121.41		121.83	122.37

[a]Reference 91.

indole and the ^1L_a and ^1L_b excited states are presented vectorially in Figure 40. Like indole, the ^1L_a transition results in a large increase of the C2-C3 and C6-C7 bond lengths, while the ^1L_b transition is results in radial expansion of the benzene moiety. Appropriately, the excited state equilibrium geometries are not predicted to differ from the equilibrium geometry of the ground state in terms of rotation around the C3-C10 bond axis, which would appear in the Figure as out-of-plane amplitude centered on the methyl hydrogens. Furthermore, the methyl group is correctly predicted to not undergo asymmetric deformation upon excitation, a circumstance which would manifest itself through a $\leftrightarrow$ e transitions in the fluorescence spectra. The C3-C10 bond length is 0.007 Å shorter in the ^1L_a state than the ground or ^1L_b states, implying a greater delocalization of methyl group electron density.

A transition state is obtained when the methyl group is rotated from its energy minimum conformation by 60° so that H4 is eclipsed by the in-plane methyl hydrogen. The negative eigenvalue of the transition state corresponds to the methyl torsion mode of vibration. The transition state is 500 cm^{-1} less stable than the energy minimum at HF/6-31G, 556 cm^{-1} less stable at HF/6-31G(d) (as obtained elsewhere[92]), and 438 cm^{-1} less stable at MP2/6-31G(d). The latter result is in excellent agreement with the observed ground state rotation barrier of 454 cm^{-1}.[28] The diminished stability of the H4-eclipsed configuration is somewhat surprising considering the double bond character of the C2-C3 linkage. It may be attributed in part to the proximity of the in-plane methyl hydrogen to H4 (1.90 Å at MP2/6-31G(d), compared to a distance of 1.95 Å from H2 in the minimum energy conformation), and perhaps to a less favorable hyperconjugative interaction with the indole ring π electrons. The latter circumstance

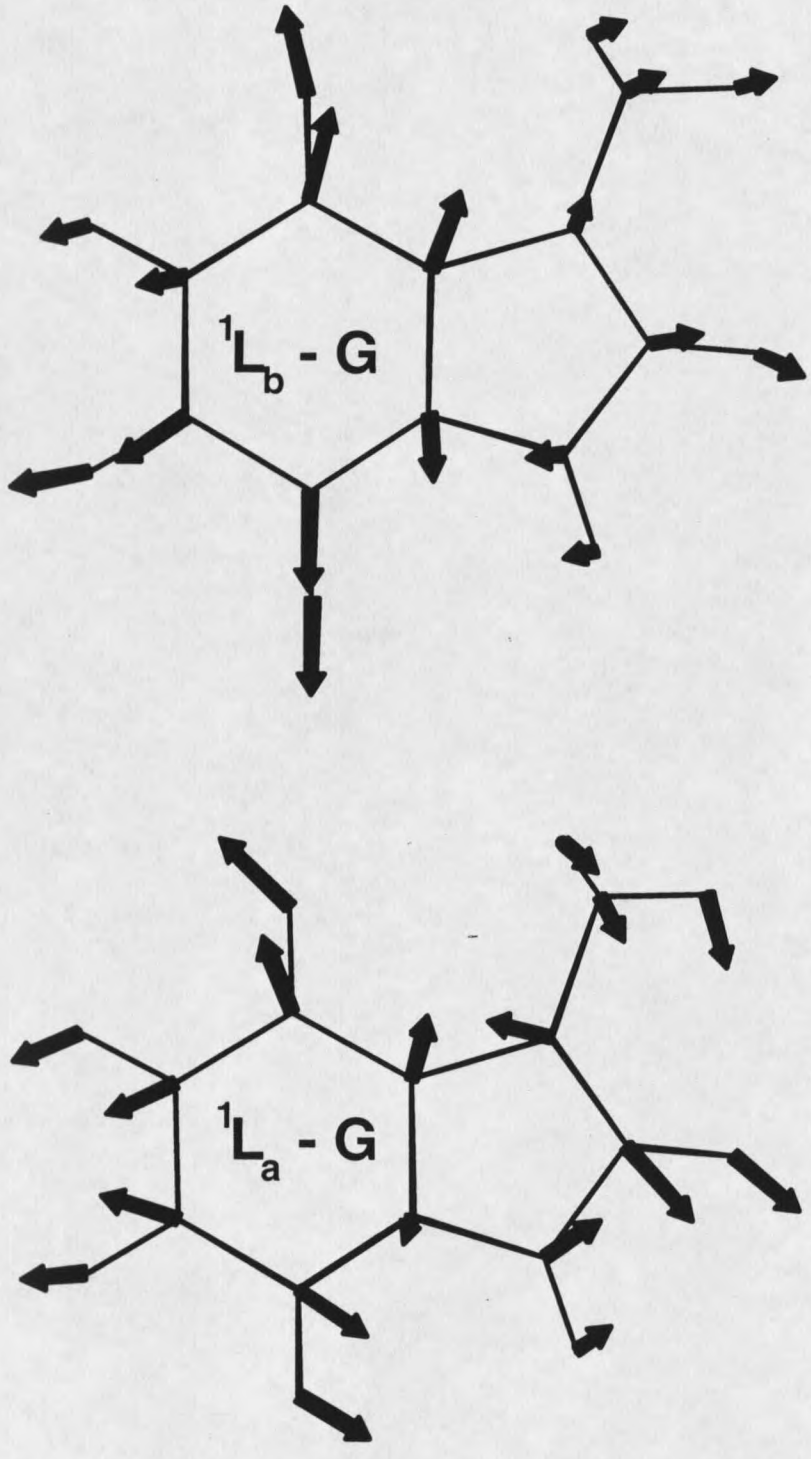

Figure 40. 3-Methyl indole ^1L_a - ground state and ^1L_b - ground state HF-CIS(11,11)/6-31G geometry differences (×20).

is suggested by a slightly longer C3- C10 bond in the transition state (1.5007 Å at MP2/6-31G(d), compared to 1.4956 Å in the ground state.)

The ^1L_a and ^1L_b H4-eclipsed conformations are also transition states. The ^1L_a (^1L_b) transition state is 147 cm^{-1} (411 cm^{-1}) less stable than the minimum at the CIS(11,11)/6-31G zero energy level. These results are also compatible with the estimated rotation barrier of 100 cm^{-1} in the ^1L_a state and the observed barrier of 308 cm^{-1} in the ^1L_b state.[28] At CIS/6-31G, the ^1L_a H4-eclipsed configuration is 38 cm^{-1} less stable than the minimum, which has the methyl group rotated 10° from the H2-eclipsed configuration. The H2-eclipsed configuration is a transition state with an imaginary frequency of only 5i cm^{-1} and corresponding to rotational motion around the exocyclic bond axis. However, the 'transition state' is only 0.15 cm^{-1} less stable than the 'minimum' at the CIS/6-31G zero energy level, a difference too small to be significant. It appears that internal motion by the methyl group is even less constrained in the ^1L_a state when it is below ^1L_b.

For 5-methyl indole, the in-plane methyl hydrogen eclipses H4 in the HF/6-31G energy minimum geometry, and a 60° rotation of the methyl group corresponds to a transition state 121 cm^{-1} higher in energy. A ground state rotation barrier of 133 cm^{-1} has been measured for this molecule.[29] Geometry optimizations at the MP2/6-31G(d) level also indicate that the H4-eclipsed configuration is more stable in the ground state, 148 cm^{-1} beneath the H6-eclipsed configuration. The preference for the former configuration is partly due to the separation between the in-plane methyl hydrogen and H4 (2.371 Å at MP2/6-31G(d), compared to a distance of 2.346 Å from H6 in the transition state), and a stronger hyperconjugation interaction as suggested by the C5-

C10 bond length (1.5080 Å, compared to 1.5098 Å in the transition state).

In the ^1L_b state, the H6-eclipsed configuration is the minimum, 101 cm^{-1} lower than the H4-eclipsed configuration, which is a transition state, at CIS(13,14)/6-31G and 245 cm^{-1} lower at CIS/6-31G. A 60° change in conformation is anticipated because of the lengthy progression observed in the methyl torsion mode. Measured ^1L_b rotation barriers of 81 and 85 cm^{-1} have been reported.[28,29] The methyl group is not predicted to deform in any sense upon excitation, which agrees with the strong similarity between ground and ^1L_b internal rotational constants. In the ^1L_a state, the H4-eclipsed configuration is also the minimum, 225 cm^{-1} beneath the H6-eclipsed, a transition state, at CIS(13,14)/6-31G, or 174 cm^{-1} lower at CIS/6-31G.

Methyl Rotor Potential Energy Curves

The height of 3-methyl indole's ground state rotation barrier is moderately sensitive to basis and method (Figure 41), as already demonstrated by the aforementioned transition state optimizations. (The present single point calculations yield barriers only 20 cm^{-1} greater than the transition state optimizations, so the effect of geometry relaxation is apparently not very important in this regard.) The widths of the rotation barriers were obtained by fitting the calculated data to the first three terms of the torsion potential cosine expansion, $V = V_3(1-\cos(3\theta))/2 + V_6(1-\cos(6\theta))/2 + V_9(1-\cos(9\theta))/2$. The barrier width is determined primarily by V_6. This gives V_6 = -7.1 cm^{-1} at HF/6-31G, -8.1 cm^{-1} at HF/6-31G(d), and -17.8 cm^{-1} at MP2/6-31G(d). Negative values of V_6 reflect a curve more narrow than a cosine wave and increasingly large negative values indicate an increasingly more narrow barrier. The V_9 term is 1.1 cm^{-1} at MP2/6-31G(d) and smaller at the HF level.

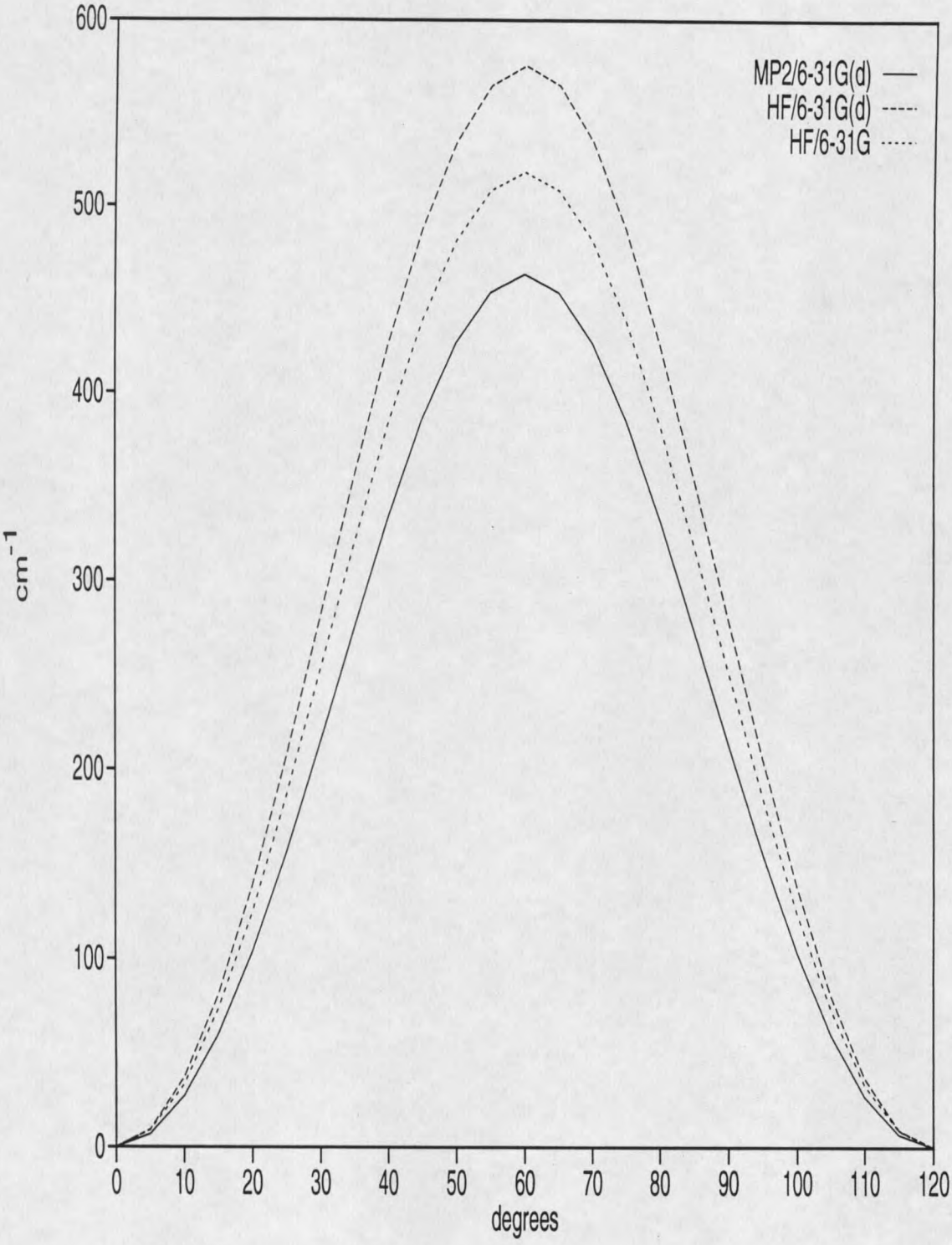

Figure 41. 3-Methyl indole ground state methyl torsion potential energy barrier.

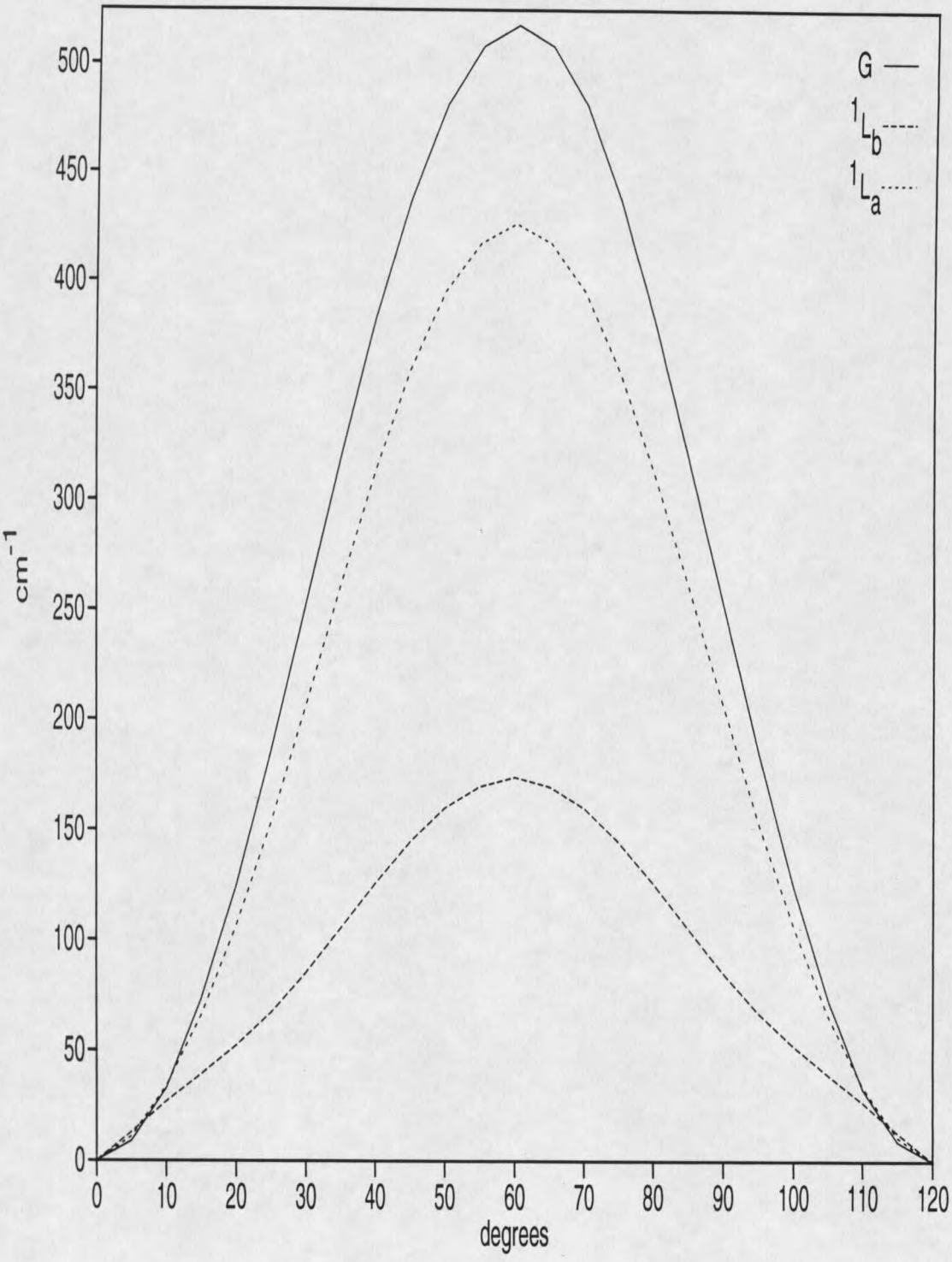

Figure 42. 3-Methyl indole HF/6-31G and CIS(11,11)/6-31G methyl torsion potential energy barriers.

The excited states, particularly ^1L_a, exhibit smaller calculated barriers to rotation, thereby accounting for the weak Franck-Condon activity in the methyl torsion mode.

Rotation around the C3-C10 axis has a small but significant effect on the separation between ^1L_a and the ground and ^1L_b states. At CIS(13,14)/6-31G, in the ground state and ^1L_b geometries, a 60° rotation lowers ^1L_a by about 300 cm^{-1} relative to the ground state and 240 cm^{-1} relative to ^1L_b. In the ^1L_a geometry, ^1L_a is lowered 437 cm^{-1} relative to the ground state and 357 cm^{-1} relative to ^1L_b. The order of ^1L_a and ^1L_b in the computed manifold is consequently inverted. The avoided crossing is apparent near 10° and 110° in the CIS(13,14)/6-31G potential energy curve, Figure 43, and shown explicitly in Figure 44. The adiabatic surfaces pass within a mere 10.5 cm^{-1} at $\theta = 11°$, implying small diabatic coupling. The avoided crossing is absent from the CIS(11,11)/6-31G curve because of a larger gap between the ^1L_a and ^1L_b surfaces at the ^1L_a geometry (700 cm^{-1}, 500 cm^{-1} greater than CIS(13,14)/6-31G).

The relative order of the closely spaced ^1L_a and ^1L_b states has a profound impact on the height of the ^1L_a torsion barrier, as Figure 43 shows. The width of the ^1L_a barrier is also affected. Curve fits give $V_6 = 0.03$ cm^{-1} at CIS(11,11)/6-31G, compared to -13.6 cm^{-1} and -12.2 cm^{-1} at CIS(13,14)/6-31G and CIS/6-31G. The higher order terms in the cosine expansion are needed to describe the CIS(11,11)/6-31G ^1L_a barrier shape, as $V_9 = 12.9$ cm^{-1} in this case. This is reflected in the absence of a tail near the curve's minima. Conversely, V_9 is 1.7 cm^{-1} at CIS/6-31G and 0.4 cm^{-1} at CIS/6-31G. For ^1L_b, the separation is too great and the effect is much smaller ($V_6 = -9.4$ cm^{-1} at CIS(13,14)/6-31G and -5.8 cm^{-1} at CIS(11,11)/6-31G compared to a measured[93] value of -10.9 cm^{-1}).

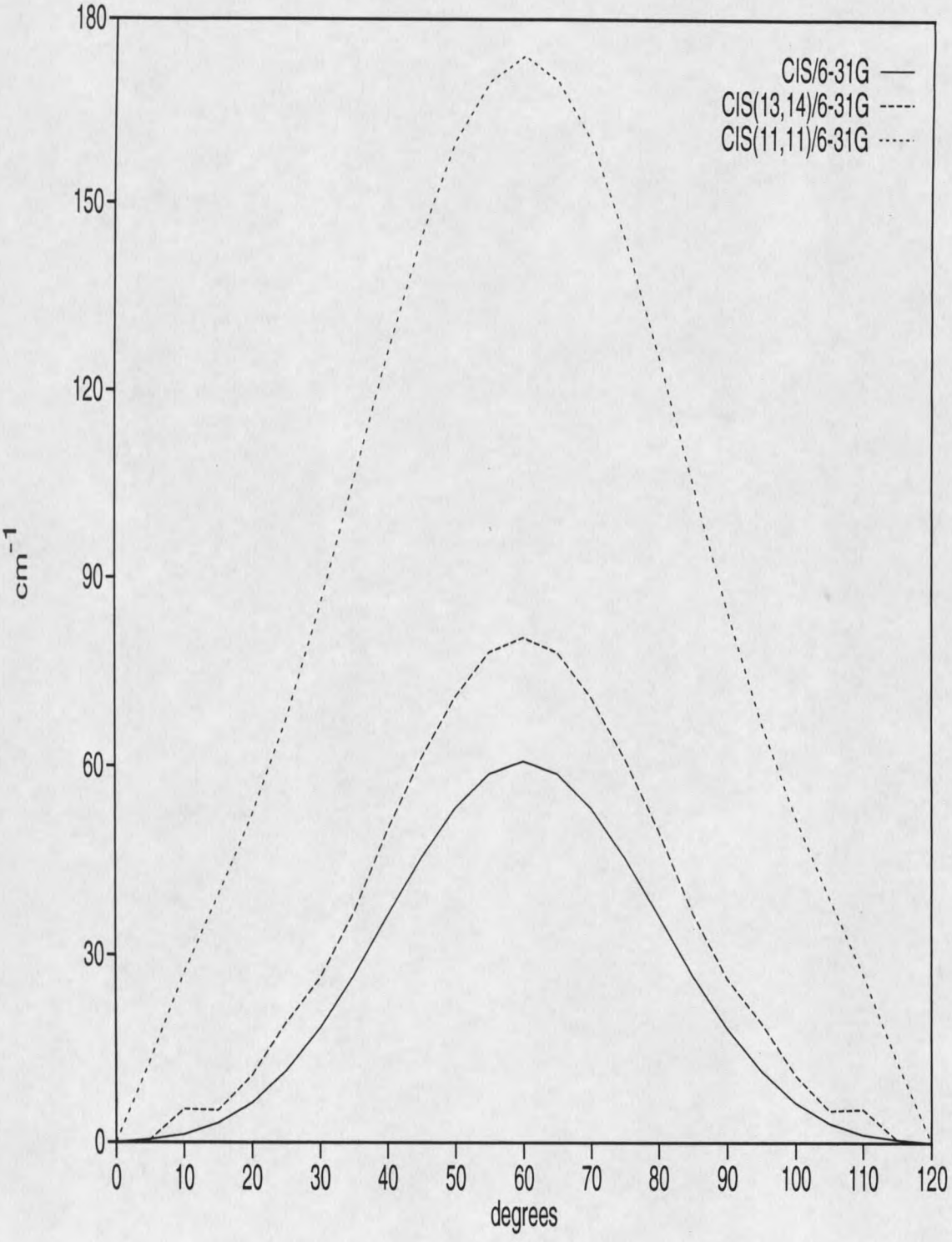

Figure 43. 3-Methyl indole ^1L_a methyl torsion potential energy barrier.

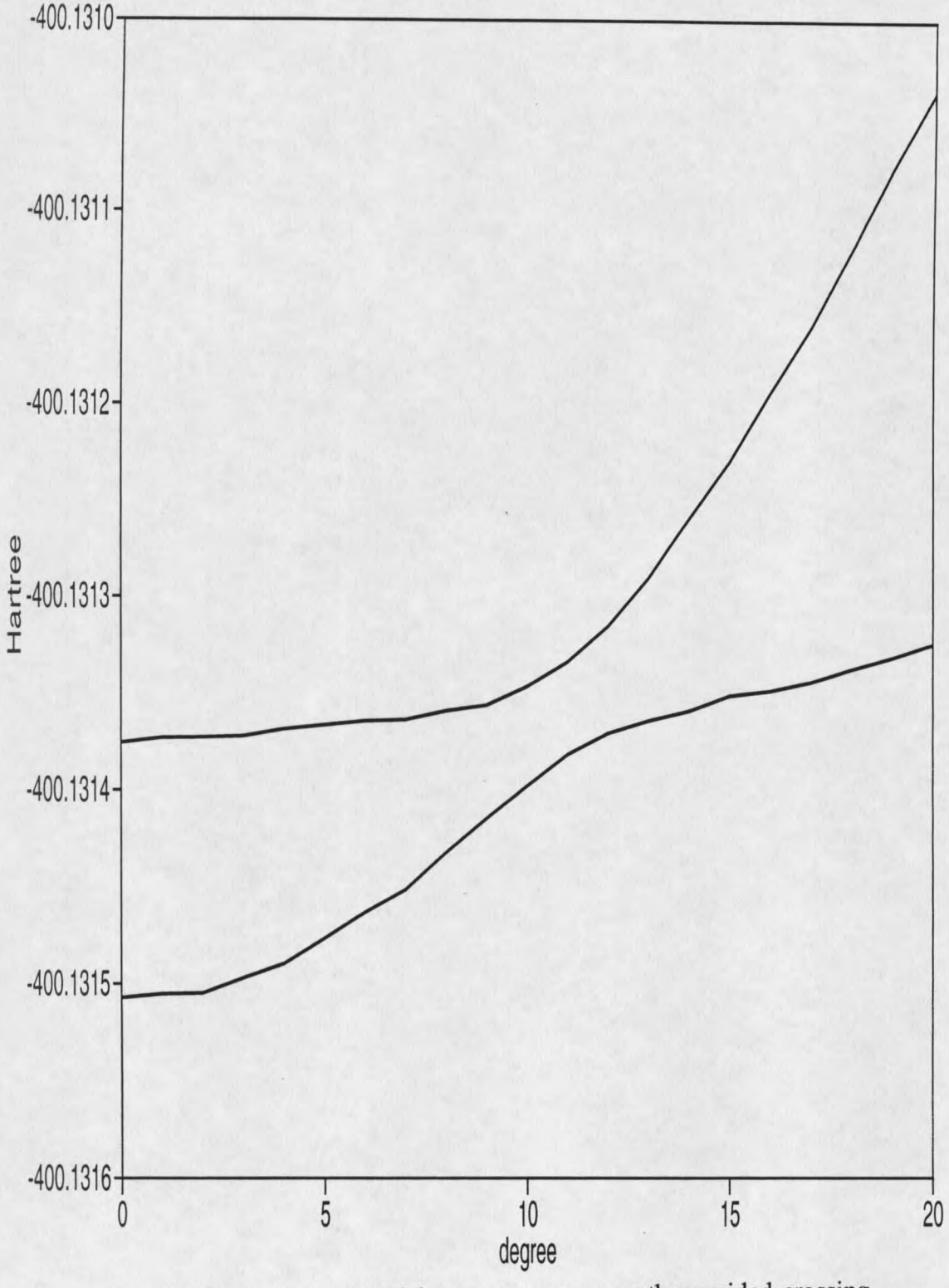

Figure 44. 3-Methyl indole potential energy curves near the avoided crossing.

For 5-methyl indole, V_6 = -0.6 cm^{-1} at HF/6-31G and -13.4 cm^{-1} at MP2/6-31G(d), indicating a slightly wider ground state barrier than that of 3-methyl indole. The computed barrier is compared to the empirical potential obtained from the measured expansion factors of V_3 = 132.7 cm^{-1} and V_6 = -8.1 cm^{-1} in Figure 43.[29] The barrier width decreases upon ^1L_b excitation both experimentally[29] and at CIS(13,14)-HF/6-31G or CIS-HF/6-31G. However, the measured ^1L_b barrier (V_6 = -21.4 cm^{-1} and -28.1 cm^{-1})[29,93] is much more narrow than what is predicted (V_6 = -12.4 cm^{-1} at CIS(13,14)/6-31G, -5.4 at CIS/6-31G). Excitation to the ^1L_a state also decreases the width of the rotation barrier (V_6 = -4.6 cm^{-1} at CIS(13,14)/6-31G and CIS/6-31). The V_9 term is negligible (< '0.5' cm^{-1}) in each state at each computational level.

In contrast to 3-methyl indole, the rotation barrier shows greater computational sensitivity in the ^1L_b state. This is demonstrated in Figure 46, where comparison is also made to the measured potential.[29,93] The much larger barrier at CIS/6-31G is partly due to neglect of geometry relaxation; the aforementioned transition state optimization gives a 150 cm^{-1} smaller barrier. The remaining difference might be due to changes in the computed manifold. At CIS/6-31G, the ^1L_b state lies 1,700 cm^{-1} below ^1L_a at the ^1L_b minimum, and a 60° rotation around C5-C10 destabilizes ^1L_a relative to ^1L_b by over 200 cm^{-1}. Thus, the stabilization imparted upon ^1L_b by intersurface repulsion is maximized at 0° and the CIS/6-31G barrier is exaggerated. With truncated CIS, the separation at the ^1L_b minimum is twice as great and ^1L_a is slightly stabilized relative to ^1L_b by the 60° rotation. In this case, the variation in intersurface repulsion between 0 and 60° is less pronounced and a more accurate barrier height is obtained.

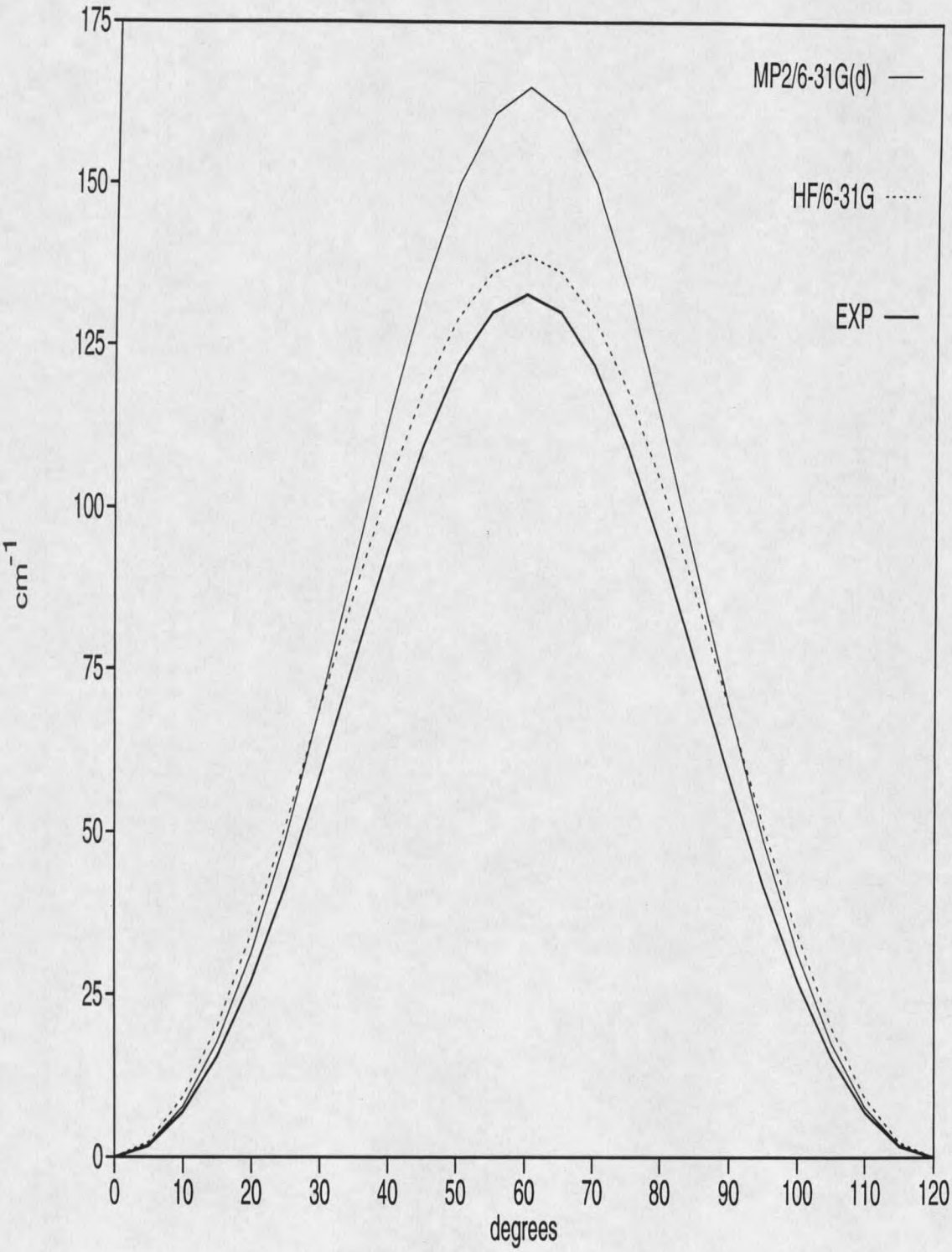

Figure 45. 5-Methyl indole ground state methyl torsion potential energy barrier.

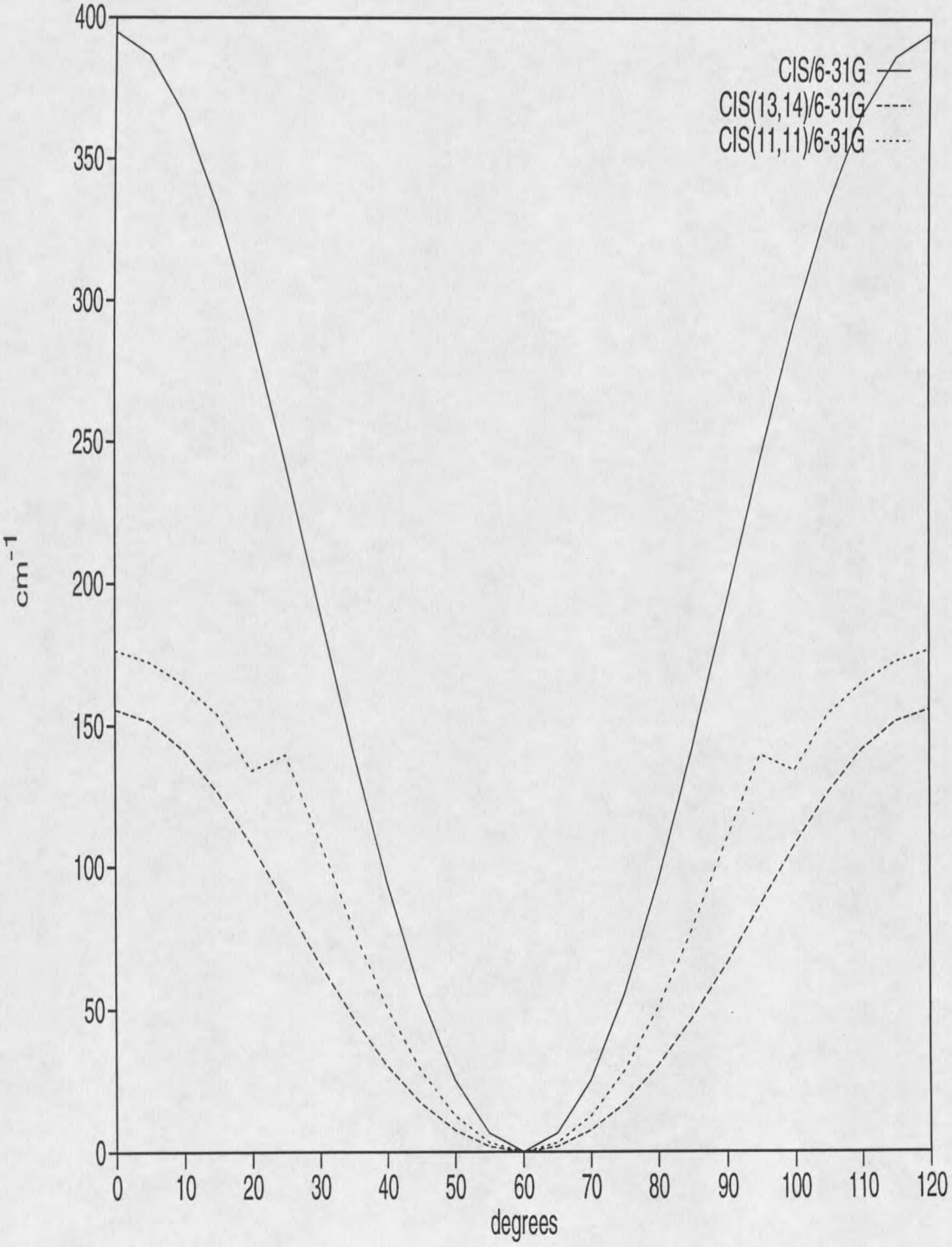

Figure 46. 5-Methyl indole ^1L_b methyl torsion potential energy barrier.

Ionization Potential

Table 57 demonstrates the insensitivity of the eigenvalue of 3-methyl indole's HOMO to a range of split valence basis sets. Figure 37 shows that the shape of this MO is very similar to indole's HOMO, but that it is distinctly antibonding to the methyl group. Consequently, the HOMO is raised in energy and, according to Koopmans' Theorem, the first ionization potential of 3-methyl indole is 1,095 cm^{-1} smaller than that of indole at HF/6-31++G(p,d) (Table 11). A measured decrease of 1,290 cm^{-1} would be expected from references 52 and 94. Physically, the stabilization of the cation results from an enhanced hyperconjugation interaction due to lost π density in the indole ring and a corresponding delocalization of positive charge on to the methyl group. The eigenvalues of the other π MOs are also consistent with the nodal patterns in Figure 37. For instance, the HF/6-31++G(p,d) HOMO-1 and HOMO-2 eigenvalues are increased in energy by 683 and 2346 cm^{-1} on going from indole and 3-methyl indole.

Table 57. 3-Methyl Indole first vertical ionization potential (eV)

3-21G	6-31G	6-31G(d)	6-31+G(d)	6-31++G(p,d)	EXP.[a]
7.52	7.54	7.48	7.66	7.66	7.63

[a]Reference 94.

Mulliken Populations

Tables 58 and 59 show the 3-methyl indole ground, ^1L_a, and ^1L_b Mulliken populations. In the ground state hyperconjugation is towards C2 (increased by 0.029 π e relative to indole at HF/6-31G), rather than towards C9 (increased by 0.009 π e). Similar results pertain to the CIS(13,14)/6-31G ^1L_b state. In the ^1L_a state methyl electrons shift mostly to C4 and C7, which are both increased by ~0.030 π e at

CIS(13,14)/6-31G (compared to CIS(11,11)/6-31G indole), while C2 (C9) is increased by 0.019 (0.014) π e.

Table 58. 3-methyl indole ground state Mulliken populations

	MP2/6-31G(d)			HF/6-31G(d)			HF/6-31G		
	σ	π	total	σ	π	total	σ	π	total
N1	6.072	1.630	7.702	6.128	1.715	7.842	6.260	1.732	7.992
H1	0.632	0.000	0.632	0.611	0.000	0.611	0.625	0.000	0.625
C2	4.921	1.096	6.017	4.921	1.047	5.969	4.848	1.045	5.893
H2	0.819	0.000	0.819	0.789	0.000	0.789	0.775	0.000	0.775
C3	4.899	1.067	5.966	4.939	1.075	6.014	4.934	1.074	6.008
C10	5.414	1.124	6.538	5.380	1.115	6.495	5.348	1.090	6.439
C9	4.967	1.035	6.002	5.008	1.051	6.058	5.125	1.054	6.179
C4	5.170	1.030	6.200	5.203	0.998	6.200	5.142	0.992	6.134
H4	0.833	0.000	0.833	0.799	0.000	0.799	0.795	0.000	0.795
C5	5.152	1.630	6.182	5.174	1.052	6.225	5.174	1.050	6.224
H5	0.838	0.000	0.838	0.809	0.000	0.809	0.811	0.000	0.811
C6	5.162	1.034	6.196	5.206	1.003	6.209	5.208	1.005	6.213
H6	0.837	0.000	0.837	0.806	0.000	0.806	0.806	0.000	0.806
C7	5.135	1.050	6.185	5.150	1.069	6.219	5.067	1.061	6.128
H7	0.833	0.000	0.833	0.802	0.000	0.802	0.796	0.000	0.796
C8	4.695	1.040	5.735	4.681	0.983	5.664	4.683	0.987	5.670
H10	0.825	0.000	0.825	0.828	0.000	0.828	0.834	0.000	0.834
H10	0.825	0.000	0.825	0.828	0.000	0.828	0.834	0.000	0.834
H10	0.833	0.000	0.833	0.833	0.000	0.828	0.842	0.000	0.842
N1-C2	0.421	0.120	0.541	0.543	0.079	0.622	0.334	0.045	0.631
C2-C3	0.498	0.372	0.870	0.845	0.483	1.328	0.789	0.475	1.264
C3-C9	0.396	0.192	0.588	0.852	0.155	1.007	0.725	0.138	0.863
C8-C9	0.516	0.224	0.740	0.888	0.297	1.185	0.802	0.288	1.090
C4-C9	0.568	0.206	0.774	0.832	0.245	1.077	0.737	0.236	0.973
C4-C5	0.560	0.311	0.871	0.774	0.353	1.127	0.724	0.339	1.063
C5-C6	0.644	0.230	0.874	0.800	0.258	1.058	0.755	0.248	1.003
C6-C7	0.578	0.305	0.883	0.785	0.348	1.133	0.732	0.334	1.066
C7-C8	0.556	0.227	0.783	0.824	0.260	1.084	0.738	0.251	0.989
N1-C8	0.311	0.135	0.446	0.500	0.105	0.605	0.231	0.069	0.300
C3-C10	0.605	0.003	0.608	0.664	0.008	0.672	0.531	-0.029	0.688

Table 59. 3-methyl indole CIS(13,14)/6-31G Mulliken populations

	^1L_a			^1L_b		
	σ	π	total	σ	π	total
N1	6.344	1.575	7.919	6.295	1.682	7.977
H1	0.603	0.000	0.603	0.618	0.000	0.618
C2	4.833	1.052	5.885	4.827	1.089	5.916
H2	0.753	0.000	0.753	0.772	0.000	0.772
C3	5.066	0.964	6.030	4.957	1.044	6.001
C10	5.348	1.110	6.458	5.348	1.094	6.442
C9	5.062	1.077	6.139	5.132	1.033	6.165
C4	5.082	1.098	6.179	5.112	1.049	6.162
H4	0.810	0.000	0.000	0.794	0.000	0.794
C5	5.175	1.024	6.199	5.214	0.992	6.206
H5	0.821	0.000	0.821	0.808	0.000	0.808
C6	5.167	1.068	6.236	5.195	1.027	6.221
H6	0.822	0.000	0.822	0.808	0.000	0.808
C7	5.055	1.135	6.190	5.040	1.110	6.150
H7	0.811	0.000	0.811	0.798	0.000	0.798
C8	4.662	1.025	5.687	4.686	0.976	5.662
H10	0.810	0.000	0.810	0.830	0.000	0.830
H10	0.810	0.000	0.810	0.830	0.000	0.830
H10	0.836	0.000	0.836	0.839	0.000	0.839
N1-C2	0.273	0.069	0.342	0.335	-0.019	0.316
C2-C3	0.751	0.221	0.972	0.797	0.395	1.192
C3-C9	0.705	0.221	0.926	0.724	0.170	0.894
C8-C9	0.822	0.137	0.959	0.797	0.072	0.869
C4-C9	0.756	0.083	0.839	0.736	0.134	0.870
C4-C5	0.758	0.170	0.928	0.723	0.137	0.860
C5-C6	0.764	0.307	1.071	0.742	0.161	0.903
C6-C7	0.750	0.020	0.770	0.739	0.112	0.851
C7-C8	0.747	0.248	0.995	0.738	0.150	0.888
N1-C8	0.176	0.035	0.211	0.194	0.044	0.282
C3-C10	0.530	-0.021	0.509	0.532	-0.030	0.502

Dipole Moments

Methyl substitution at the 3-position decreases indole's ground state dipole by ~ 0.10 D experimentally, at the Hartree-Fock level regardless of basis, and at MP2/6-31G(d) (Table 60). This is consistent with hyperconjugation directed primarily toward C2 rather than C9. Hyperconjugation apparently introduces more electron density into the pyrrole ring than induction removes, thus decreasing the ground state dipole. The stronger, phenyl-directed hyperconjugation interaction in the ^1L_a state increases the dipole by 0.5 D at CIS(11,11)/6-31G and by 0.2 D at CIS/6-31G. The former result seems more appropriate because 3-methyl indole exhibits red-shifted fluorescence emission in much lower concentrations of polar solvent than indole.[68] The CIS(11,11)/6-31G ^1L_b dipole is diminished by 0.2 D and the CIS/6-31G ^3L_a dipole is virtually unchanged relative to indole.

Methyl substitution at the 5 position decreases indole's ground state dipole by 0.15 D according to Table 60, suggesting that induction removes more electron density from the phenyl ring than is introduced via hyperconjugation. An even greater disparity between the strengths of these two effects is present in the ^1L_b state, where the dipole decreases by over 0.7 D at CIS/6-31G. The ^1L_a dipole is virtually unchanged by this modification, which is consistent with the comparative dependence on solvent concentration shown by 5-methyl indole's solvatochromism.

Judging by the dipoles of the transition states, the polarity of the methyl indoles is only marginally affected by CH_3 torsion, regardless of the basis set, computational method, or electronic state. A comparatively large (-0.15 D) change is noted for the ^1L_a dipole of 5-methyl indole at CIS/6-31G.

Table 60. 3- and 5-Methyl Indole ground and excited state dipole moments (Debye)

	method/basis//density	μ	θ
G	HF/3-21G//SCF	1.73	-38.6
	HF/6-31G//SCF	1.75	-38.8
	HF/6-31G(d)//SCF	1.91	-40.9
	HF/6-31+G(d)//SCF	1.94	-38.8
	HF/6-31++G(p,d)//SCF	1.93	-38.0
	MP2/6-31G(d)//MP2	2.10	-41.8
	EXP[a]	2.10	
	HF/6-31G//SCF[b]	1.78	-37.0
	HF/6-31G(d)//SCF[b]	1.94	-39.1
	MP2/6-31G(d)//MP2[b]	2.13	-40.5
^1L_a	CIS(11,11)/6-31G//CIS	4.11	-10.9
	CIS(13,14)/6-31G//CIS	4.10	-10.8
	CIS/6-31G//CIS	3.29	-17.0
	CIS/6-31G//CIS[b]	3.30	-17.0
^1L_b	CIS(11,11)/6-31G//CIS	1.86	-28.3
	CIS(13,14)/6-31G//CIS	1.88	-27.8
	CIS(11,11)/6-31G//CIS[b]	1.90	-26.0
^3L_a	CIS/6-31G(d)//CIS	1.43	-22.9
	CIS/6-31G(d)//CIS[c]	0.74	
		5-METHYL INDOLE	
G	HF/6-31G//SCF	1.71	-51.3
	MP2/6-31G(d)//MP2	2.01	-51.3
	HF/6-31G//SCF[b]	1.68	-48.4
	MP2/6-31G(d)//MP2[b]	1.97	-49.3
^1L_a	CIS(11,11)/6-31G//CIS	3.53	-22.7
	CIS(13,14)/6-31G//CIS	3.51	-22.9
	CIS/6-31G//CIS	2.93	-27.2
	CIS/6-31G//CIS//CIS[b]	2.77	-28.4
^1L_a	CIS(11,11)/6-31G//CIS	1.52	-43.4
	CIS(13,14)/6-31G//CIS	1.49	-44.4
	CIS/6-31G//CIS//CIS	1.57	-46.3
	CIS/6-31G//CIS//CIS[b]	1.50	-46.4

[a]Reference 95. [b]Transition state. [c]Non-planar configuration.

Normal Modes and Frequencies

The presence of a methyl group adds nine normal modes to indole: one methyl torsion, three C-H stretches, and five C-H bends (Figure 47). In order to facilitate the comparison to indole, the vibrational modes localized primarily on the methyl group are numbered as 51 through 43 in Table 61, in order of decreasing frequency. The remaining modes are enumerated as before, 42 - 30 for a″ (Figure 48) and 29 - 1 for a′ (Figure 49), in order of decreasing frequency. The C-H and N-H stretching modes are omitted from Figure 49. The calculated frequencies are tentatively compared to data from a variety of sources.

Modes without amplitude on C3 or H3 in indole correlate to a single vibration in 3-methyl indole and are very similar in frequency. Conversely, the modes with amplitude on C3 or H3 tend to be extensively mixed with other vibrations in 3-methyl indole. In a few instances, the internal vibrational motion of the methyl group is clearly split between a few modes, appearing as plus and minus combinations with a mode localized on the indole ring. This is very apparent at the Hartree-Fock level, but the MP2/6-31G(d) modes 25, 26 and 27 or 10 and 11 of Figure 47 or modes 38 and 39 of Figure 48 also faintly exhibit this pattern. In most cases, however, the mixing is too complicated to describe in a simple manner.

Indole's mode 29 has amplitude on C3 and H3 and yet correlates very strongly to 3-methyl indole's mode 29. This is because the amplitude on C3 and H3 is of a similar magnitude and of the same phase. The corresponding mode of 3-methyl indole is seen from Figure 49 to have large in-plane amplitude uniformly distributed between each methyl group atom. The amplitudes project from each atom in the same

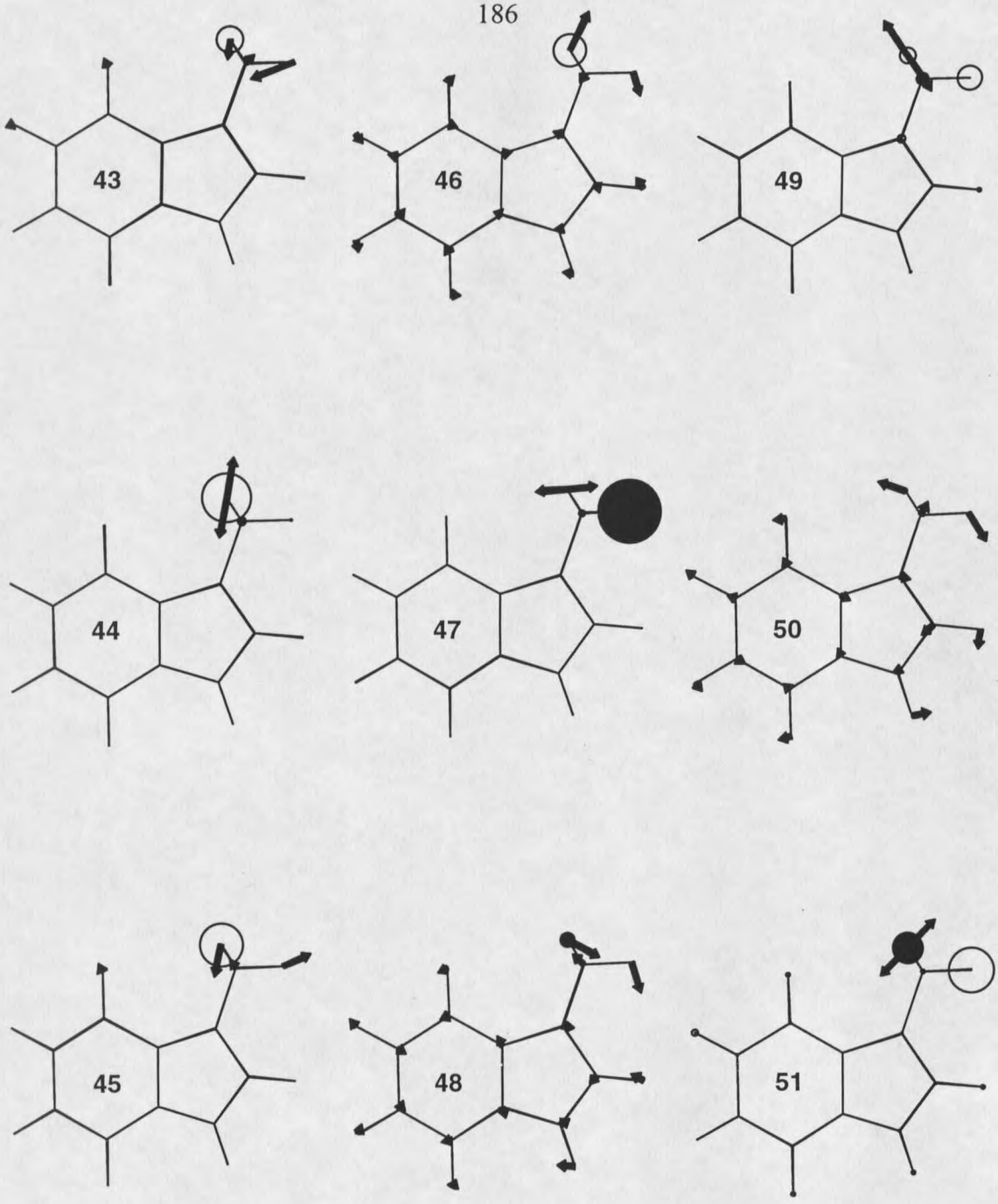

Figure 47. 3-methyl indole MP2/6-31G(d) methyl group normal modes of vibration

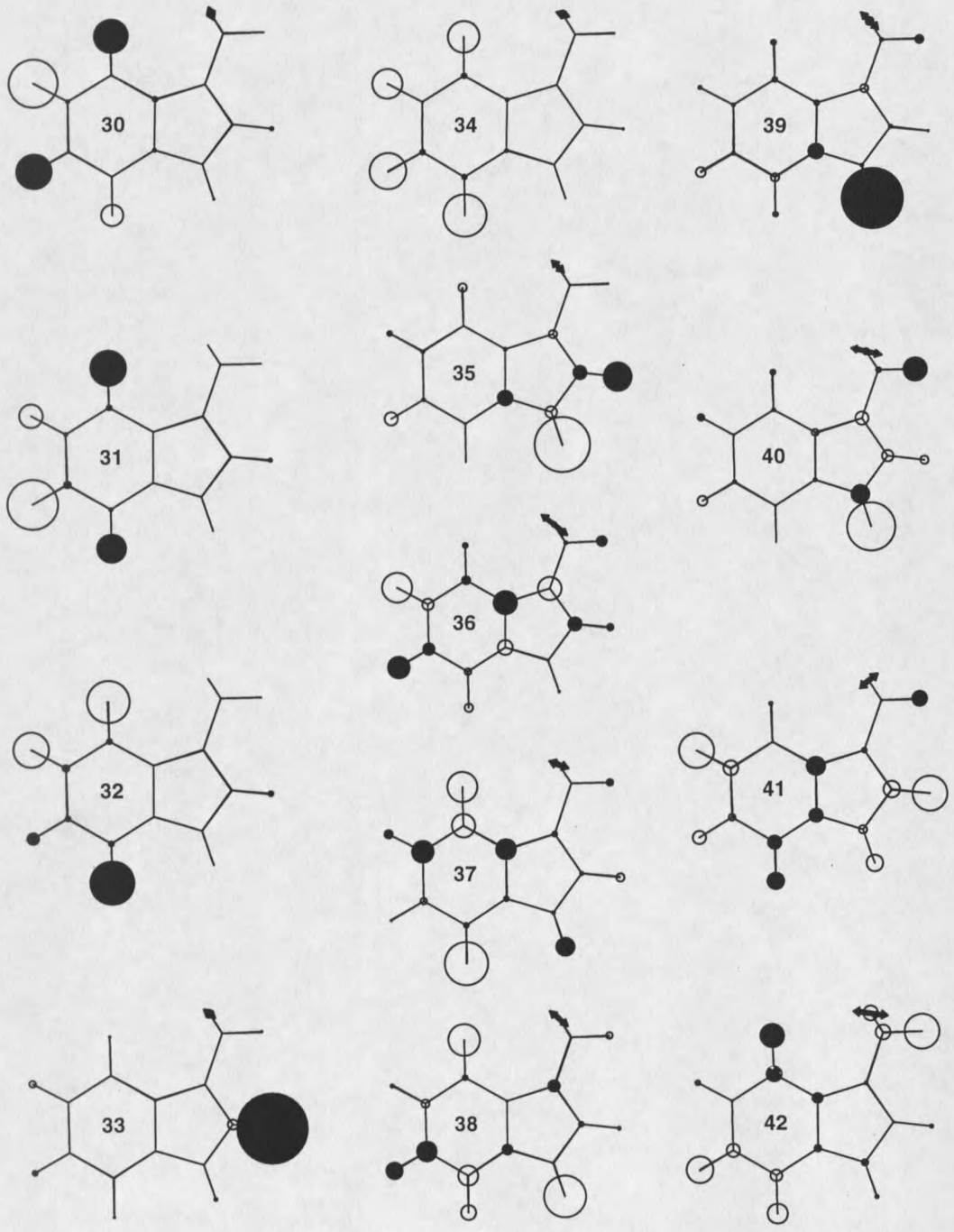

Figure 48. 3-methyl indole MP2/6-31G(d) a″ normal modes of vibration

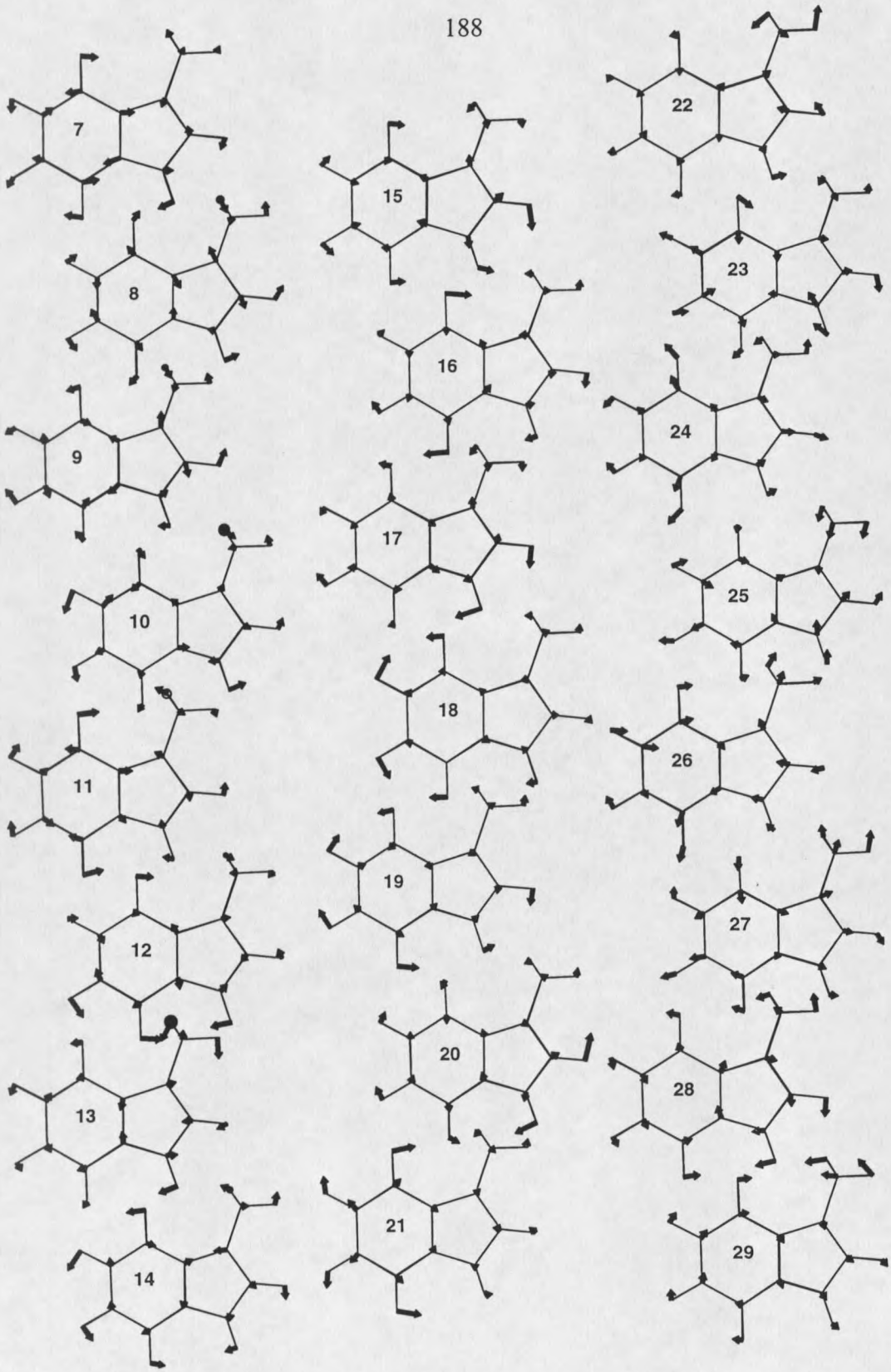

Figure 49. 3-methyl indole MP2/6-31G(d) a′ normal modes of vibration.

Table 61. 3-Methyl Indole ground and CIS(11,11) excited state frequencies (cm^{-1})

	G				^1L_a	^1L_b	
mode	HF/6-31G	HF/6-31G*	EXP	MP2/6-31G	6-31G	6-31G	EXP
51	150	160		121	226	185	
50	1107	1079		1019	1072	1150	
49	1202	1160	1085[a]	1087	1175	1220	
48	1588	1544	1380[a]	1473	1580	1585	
47	1642	1603	1435[a]	1542	1641	1649	
46	1656	1622		1565	1646	2066	
45	3177	3173	2860[b]	3091	3173	3177	
44	3228	3223		3166	3230	3233	
43	3256	3250		3185	3261	3261	
42	172	165		150	131	143	125[d]
41	251	243		218	212	204	
40	365	289		252	330	323	
39	487	381		332	365	364	
38	578	473		389	568	454	
37	655	631		394	606	615	
36	690	661		550	704	707	
35	870	827		590	729	724	
34	883	835		714	752	813	
33	970	927	805[b]	719	807	829	
32	1004	954		796	892	894	
31	1108	1065		838	904	988	
30	1158	1105		864	1099	1023	
29	245	239		222	246	242	409[e]
28	514	502		467	504	500	420
27	586	571		541	583	546	427
26	625	607		573	627	597	468
25	780	764		726	780	739	608
24	837	820		779	818	808	618
23	975	950		899	949	935	715
22	1123	1105		1053	1083	1055	738
21	1192	1169		1109	1159	1085	747
20	1206	1184	1090[b]	1137	1187	1175	818
19	1259	1232		1181	1240	1205	822
18	1289	1236		1209	1292	1299	864
17	1357	1338		1288	1348	1314	918
16	1401	1364		1293	1386	1384	
15	1429	1389		1358	1417	1429	
14	1439	1422		1402	1483	1479	
13	1502	1481		1463	1542	1534	
12	1593	1573		1493	1585	1574	
11	1632	1612		1538	1594	1622	
10	1671	1651		1557	1616	1673	
9	1757	1741	1550[c]	1635	1668	1747	
8	1790	1773	1578[c]	1651	1710	1776	
7	1823	1810	1614[c]	1701	2159	1805	
6	3348	3337	2860[a]	3212	3355	3370	
5	3358	3345	2925[a]	3217	3379	3381	
4	3371	3357	2970[a]	3229	3382	3394	
3	3385	3369	3055[a]	3241	3394	3405	
2	3447	3415	3080[a]	3286	3474	3462	
1	3948	3940	3420[b]	3678	3911	3934	

[a]Reference 96. [b]Reference 97. [c]Reference 98. [d]Reference 28. [e]Reference 89.

direction, so that the force constant is virtually unchanged from its value for indole. However, the methyl group gives the mode a smaller reduced mass, resulting in a 180 cm^{-1} decrease in frequency at MP2/6-31G(d). Similar observations pertain to 3-methyl indole's mode 42, which corresponds to indole's mode 41 but is 70 cm^{-1} lower at MP2/6-31G(d).

In the excited states, vibronic coupling has an enormous impact on the frequency of mode 29 in the ^1L_a state. At CIS/6-31G, with ^1L_a and ^1L_b inverted and greatly separated, mode 29 has an unremarkable frequency of 219 cm^{-1}. With the properly ordered and reasonably spaced CIS(11,11)/6-31G manifold, this mode is blue-shifted 1,940 cm^{-1}, to 2,159 cm^{-1}, and its IR intensity increases to 3,948 KM/mole. Finally, although going from CIS(11,11)/6-31G to CIS(13,14)/6-31G results in a 1,900 cm^{-1} increase in the adiabatic separation between ^1L_a and ^1L_b, the frequency of mode 29 also increases, to 6,074 cm^{-1}. This result explains the large increase in the adiabatic separation. Because of the pronounced vibronic activity, the ^1L_a zero-point energy is 2,194 cm^{-1} greater than ^1L_b at CIS(13,14)/6-31G, so the 0-0 gap increases even though the separation between the bottoms of the potential wells decreases to 1,579 cm^{-1}.

Fittingly, the force constant for this mode is 212.93 mDyne/Å at CIS(13,14)/6-31G, about 10 times larger than a typical C-C stretch, while the reduced mass, 9.80 amu, is unexceptional. The CIS(13,14)/6-31G IR intensity of mode 29 (Figure 50) is at least 100,000 KM/mole (i.e., larger than what the format of the output statement is set to print in Gaussian94.) This mode is extensively mixed, having 25% mode 29 character, 17% mode 25 character, 9% mode 24 character, and at least 1% character of 12 other modes at CIS(13,14)/6-31G. It also has the second largest projection onto the geometry difference between ^1L_a and ^1L_b.

The absence of large frequency shifts in the ^1L_b vibrational manifold suggests that this avoided crossing is closer to the ^1L_a minimum. This may be partially confirmed in a somewhat artificial manner by performing a frequency calculation on the ^1L_b state in the ^1L_a geometry. In this case, the potential energy surface along the

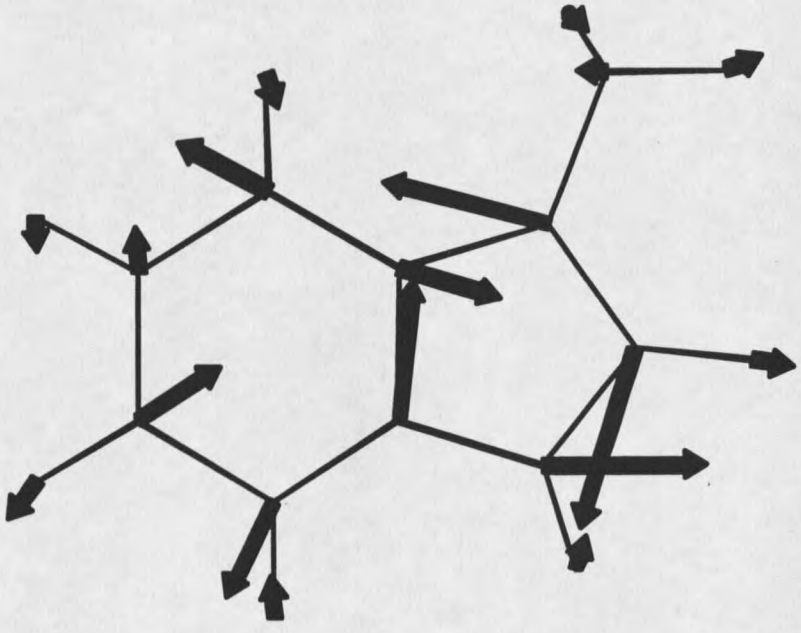

Figure 50. 3-methyl indole ^1L_a Hertzberg-Teller active mode at CIS(13,14)/6-31G.

vibronically active mode corresponds to a frequency of 5,938i cm^{-1}, meaning that it is very steep and of positive curvature. Motion along this normal coordinate is strongly repulsive in the lower ^1L_b state, which is consistent with a strong pseudo-Jahn-Teller effect.

3-Methyl Indole Emission

The CIS/6-31G and HF/6-31G geometries and the MP2/6-31G(d) normal modes and frequencies are used to calculate 3-methyl indole's ^1L_a emission spectrum in Figure 51. A total of 931 lines are present with an intensity at least 10^{-4} times that of the origin, summing to 0.98. The calculated stick spectra and broadened spectra bear little resemblance to the experimental data.[99]

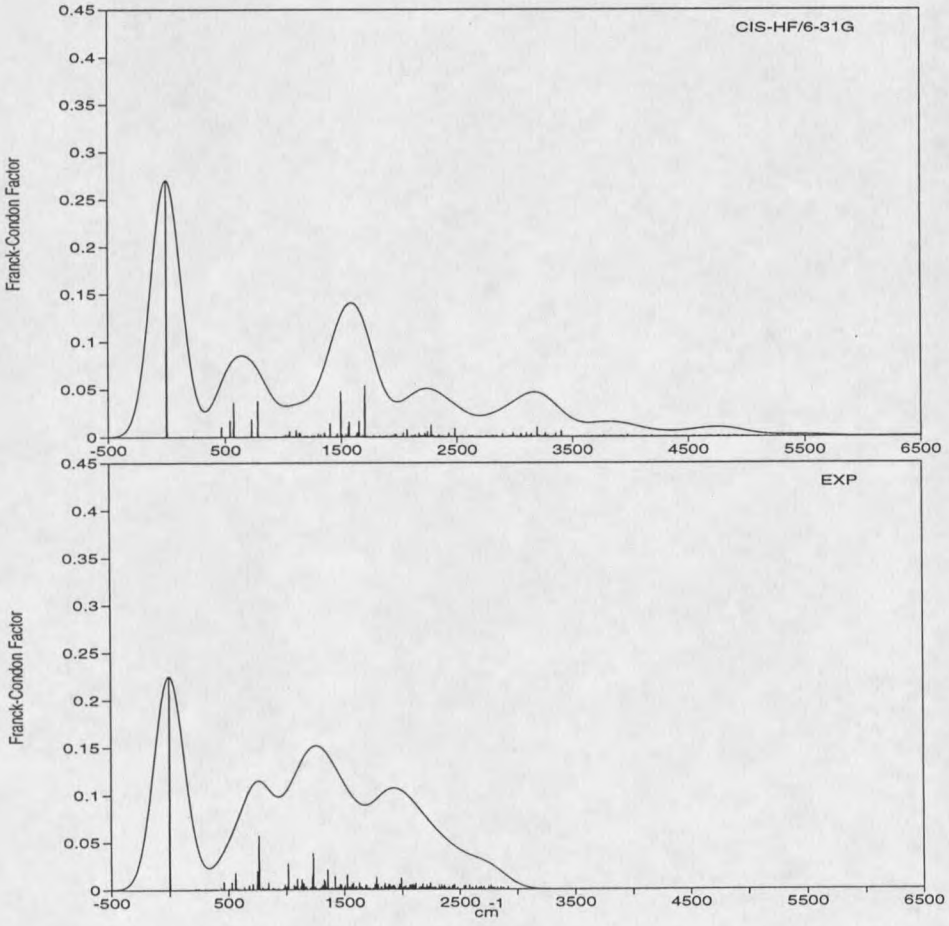

Figure 51. 3-methyl indole ^1L_a fluorescence emission spectra.

1:1 and 1:2 Water Complexes

The σ-complex formed between ground state 3-methyl indole and water (Figure 52) is very similar in geometry to that of indole and water. It has a 0.21 kcal/mol smaller binding energy at HF/6-31G (Table 62, without the BSSE correction) and similar intermolecular normal coordinates. The HF/6-31G frequency of the intermolecular stretch, 147 cm^{-1}, is surprisingly close to the observed value of 140 cm^{-1}.[20]

In further correlations with indole, (at least) two energy minimum conformations are found for 3-methyl indole's 1:2 complexes with water (Figure 52) at HF/6-31G. The HF/6-31++G(p,d) level of theory also leads to two minima differing primarily in regards to which of the lone pair electrons on the π-complexed water acts as the proton acceptor to the σ-complexed water. The 3-MIW2b complex apparently has a much deeper potential energy well than its indole analogue, as it was not necessary to relax the convergence criteria in order for the structure to be considered an energy minimum at either HF/6-31G or HF/6-31++G(p,d). This follows from the slightly greater π electron density above the pyrrole ring. Nonetheless, the 1:2 complex binding energies differ little from their indole analogues (Table 62).

According to HF/6-31G single point calculations, the methyl torsion barrier decreases by 5 cm^{-1}, to 513 cm^{-1}, upon σ-complex formation and by 24 cm^{-1} upon 1:2-complex (3MIW2a) formation. According to CIS optimizations, the methyl rotor of water-complexed 3-methyl indole remains unchanged in phase upon ^1L_a or ^1L_b excitation.

Calculations on the ^1L_b complexes of 3-methyl indole were performed with the truncated CIS wave function, and their interpretation is muddled by the size inconsistency error. The CIS(14,13)/6-31G (CIS(16,16)/6-31G) basis was used to account for the 3 occupied and 2 virtual MOs localized on the water moiety in the CI calculation. The reported σ-complex binding energies in Table 62 are relative to the CIS(11,11)/6-31G (CIS(13,14)/6-31G) uncomplexed molecule. A 227 cm^{-1} red shift of

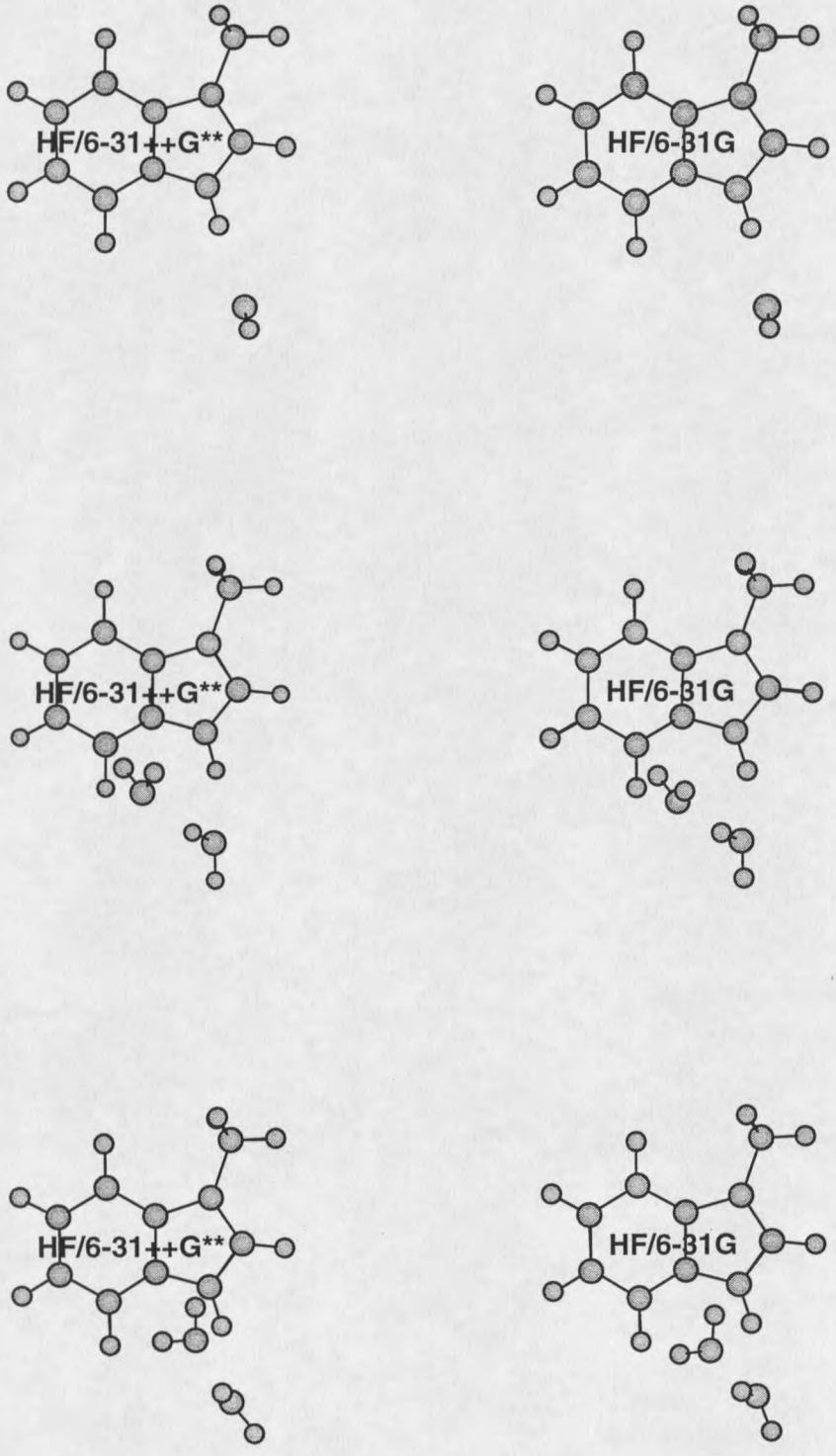

Figure 52. 3-Methyl indole:water HF/6-31++G(p,d) 1:1 and 1:2 complexes.

Table 62. 3-Methyl Indole:Water interaction energies (kcal/mol)

	σ-complex		1:2 a		1:2 b	
method/basis	$-\Delta E_{int}$	ΔZPE	$-\Delta E_{int}$	ΔZPE	$-\Delta E_{int}$	ΔZPE
G HF/6-31G	7.35	1.65	19.48	4.59	19.00	4.31
HF/6-31++G(p,d)	5.04		12.63		12.35	
^1L_b CIS(19,18)/6-31G			21.77	4.61		
CIS(16,16)/6-31G	7.93	1.58				
CIS(14,13)/6-31G	7.89	0.24				
^1L_a CIS/6-31G	8.92	1.83	23.71	5.28		
CIS(19,18)/6-31G			26.29	-1.69		
CIS(16,16)/6-31G	10.11	-5.70				
CIS(14,13)/6-31G	<0					

indole:water

	σ-complex		1:2 a		1:2 b	
method/basis	$-\Delta E_{int}$	ΔZPE	$-\Delta E_{int}$	ΔZPE	$-\Delta E_{int}$	ΔZPE
G HF/6-31G	7.59	1.68	19.76	4.63	19.25	4.25
^1L_b CIS/6-31G	8.25	1.86	21.89	5.12		
CIS(17,15)/6-31G			21.93	4.77		
CIS(14,13)/6-31G	8.16	1.57				
^1L_a CIS/6-31G	8.91	1.83	23.31	5.21		
CIS(17,15)/6-31G			26.06	3.54		
CIS(14,13)/6-31G	3.96	3.41				

the ^1L_b complex origin is predicted at CIS(16,16)-HF/6-31G, compared to the observed value of 235 cm^{-1}.[93] A less accurate result is obtained at CIS(14,13)/6-31G due to a small ΔZPE. The large difference in ΔZPE between CIS(14,13)/6-31G and CIS(16,16)/6-31G is due almost entirely to the change in 3-methyl indole's zero point

energy between CIS(11,11)/6-31G and CIS(13,14)/6-31G. This suggests that vibronic coupling is suppressed in the σ-complex, a result that seems justified in light of Figure 16, indole's HT active mode, which shows large amplitude bending motion on the N-H group. It also concurs with the contention that the greater red shift of the σ-complex origin obtained on going from indole to 3-methyl indole results from a stabilization of the excited state rather than a stronger interaction.[99]

In the ^1L_a state, the binding energies of the σ-complex and 3MIW2A increase by 1.57 kcal/mol and 4.23 kcal/mol in relation to the ground state, at CIS/6-31G, and thus differ little from the analogous indole clusters in this regard. However, the ^1L_a interaction energy is a very sensitive function of the CIS expansion length. The ^1L_a σ-complex is unbound at CIS(14,13)/6-31G but 2 kcal/mol more strongly bound than the ^1L_b σ-complex at CIS(16,16)/6-31G. The negative ^1L_a ΔZPEs suggest an even greater suppression of vibronic coupling with complexation. The ^1L_b σ-complex is 469 cm^{-1} below ^1L_a in the adiabatic sense at CIS(16,16)/6-31G, and the zero point energy is 347 cm^{-1} smaller in the ^1L_a complex. The two states are virtually degenerate in the CIS(19,18)/6-31G 1:2 complex, with virtually identical zero-point energies. Whether these are meaningful results or simply artifacts of a size-inconsistent method will have to remain uncertain for now.

Chapter 4

CONCLUSION

The basis and method dependencies of indole's computed properties have been examined in the ground and excited states. While a few of indole's properties, such as the ground state dipole and ionization potential, are converged and accurately described by an uncorrelated method and small basis, most properties show no signs of convergence even at HF/6-31++G(p,d) or CIS/6-31+G(p,d). In particular, larger basis sets do not lead to more accurate calculated vibronic spectra under the one particle approximation. A method that correlates electronic motion in the excited state is apparently needed for this purpose.

Some properties of ^3L_a indole are basis independant and well reproduced at the CIS level, due in part to correlation inherent to the spin-adapted triplet wave function. The weakness of the CIS ^3L_a dipole agrees with the sharpness of indole's phosphorescence. Theoretically, the low polarity results from a partial cancellation between the diagonal dipole moment matrix element of the dominant configuration in the ^3L_a wave function and off-diagonal elements involving minor configurations. Physically, the small dipole simply results from a retention of electron density at N and C2 relative to the ^1L_a state. A non-planar conformation of T_1 indole is stable but differs considerably from the ground state in geometry and is therefore

spectroscopically inaccessible due to poor Franck-Condon overlap.

Calculations with the truncated CIS wave function give qualitatively accurate lower excited manifolds of the indoles and provide ample evidence of vibronic coupling between the ^1L_a and ^1L_b states of indole and 3-methyl indole. In addition, surprisingly accurate methyl torsion potentials are obtained with this method.

Indole's ground electronic state σ-complex with water does not exhibit non-rigid behavior in the strictest sense of the term. That is, the minimum above the indole ring is not accessible to the water moiety, at least in the first 10 two-dimensional vibrational states. For the one-dimensional indole:water complex, vibrational wave functions with amplitude over the π cloud correspond to high energy van der Waals states ($\Delta E > 600$ cm^{-1}) and are strongly delocalized over the entire indole molecular. Nevertheless, the σ-complexed water molecule is predicted to show considerable floppy behavior, particularly in the direction parallel to indole's long axis. The calculations presented herein also indicate that the harmonic oscillator model is a good approximation only for the first three or four vibrational states.

The hypothesis of a much stronger interaction between electronically excited indole and one or two polar molecules is not supported by the theoretical evidence presented herein. The excited state CIS binding energies of the 1:1 complexes are only 1 kcal/mol greater than those of the Hartree-Fock ground state after BSSE and zero-point corrections are applied. For the σ-complex, the small increase in binding strength upon excitation is due to a more acidic nature, as evidenced by H1 Mulliken populations, and perhaps a stronger interaction with the phenyl ring. The 1:2 complex

binding energy increases by about 2 kcal/mol upon excitation, due in part to a stronger cooperative effect. Other calculated properties of the complexes, such as the dipoles, intermolecular stretching frequencies, or the hydrogen bond lengths, do not conform to the exciplex model either. Moreover, the strong similarities between the ^1L_a and ^1L_b 1:1 and 1:2 complex intermolecular geometries weakly suggest similar equilibrium solvent cages for these states in polar solvents. The results are consistent with a dipolar relaxation description of indole's solvatochrism.

The 1:1 and 1:2 3-methyl indole:water complexes differ little from their indole analogues in terms of structure and stability at either the Hartree-Fock or full CIS computational level. Calculations at the truncated CIS level suggest that complex formation has a considerable stabilizing effect on the excited states, particularly ^1L_a, by damping the zero point energy due to vibronic coupling.

REFERENCES

1. J. R. Platt, *J. Chem. Phys.*, 17, 484(1949).
2. B. J. Fender, D. M. Sammeth, P. R. Callis, *Chem. Phys. Let*, 239, 31(1995).
3. E. H. Strickland, J. Horwitz, C. Billups, *Biochemistry*, 9, 4914(1970).
4. L. S. Slater, P. R. Callis, *J. Phys. Chem.*, 99, 8572(1995).
5. L. Serrano-Andres, B. O. Roos, *J. Am. Chem. Soc.*, 118, 185(1996).
6. F. Wilkinson, A. Garmer, *J. Chem. Soc. Farad. Trans 2.*, 73, 222(1977).
7. P. - S. Song, W. E. Kurtin, *J. Am. Chem. Soc., 91*, 4892(1969).
8. D. K. Hahn, P.R. Callis, *J. Phys. Chem. A.*, 101,2686(1997).
9. J. T. Vivian , P. R. Callis, *Chem. Phys. Let.*, 229, 153(1994).
10. J. T. Vivian, L. S. Slater, P. R. Callis, *Chem. Phys. Let.*, 224, 53(1995).
11. G. Fischer, Vibronic Coupling, (Academic, New York, 1984).
12. S. V. Konev,Fluorescence and Phosphorescence of Proteins and Nucleic Acids, (Plenum Press, New York, 1967).
13. P. Suppan, *Photochem. Photobiol.*, 50, 293(1990).
14. D. W. Pierce, S. G. Boxer, *Biophys. J.*, 68, 1583(1995).
15. H. Lami, N. Glasser, *J. Chem. Phys.*, 84, 597(1986).
16. M. S. Walker, T. W. Bednar, R. Lumry, *J. Chem. Phys.*, 47, 1020(1967).
17. M. V. Hershberger, R. Lumry, R. Verrall, *Photochem. Photobiol.*, 33, 609(1981).
18. M.V. Hershberger, R. Lumry, *Photochem. Photobiol.*, 23, 391(1976).
19. P. L. Muiño, P. R. Callis, *Chem. Phys. Let.*, 100, 4093(1994).

20. M. J. Tubergen, D. H. Levy, *J. Phys. Chem.*, 95, 2175(1991).

21. T. M. Korter, J. Küpper, D. W. Pratt, *J. Phys. Chem.*, 102, 7211(1998).

22. J. R. Carney, T. S. Zwier, F. C. Hagemeister, *J. Chem. Phys.*, 108, 3379(1998).

23. K. W. Short, P. R. Callis, *J. Chem. Phys.*, 108, 10189(1998).

24. S. Suzuki, P. G. Green, R. E. Bumgarner, S. Dasgupta, W. A. Goddard, G. A. Blake, *Science*, 257, 942(1992).

25. J. Zuclich, J. U. Von Shütz, A. M. Maki, *J. Am. Chem. Soc.*, 96, 710(1974).

26. S. Papp, J. M. Vanderkooi, *Photochem. Photobiol.*, 49, 775(1989).

27. D. M. Sammeth, S. S. Siewert, L. H. Spangler, P. R. Callis, *Chem. Phys. Let.*, 193, 532(1992).

28. D. M. Sammeth, S. S. Siewert, L. H. Spangler, P. R. Callis, *J. Phys. Chem.*, 5771(1992).

29. G. A. Bickel, G. W. Leach, D. R. Demmer, J. W. Hager, S. C. Wallace, *J. Chem. Phys.*, 88, 1(1988).

30. B. J. Fender, Ph. D. Thesis, Montana State University,(1997).

31. M. J. Frisch, M. Head-Gordon, J. B. Foresman, G. W. Trucks, K. Raghavachari, H. B. Schlegel, M. Robb, J. S. Binkley, C. Gonzalez, D. J. Defrees, D. J. Fox, R. A. Whiteside, R. Seeger, C. F. Melius, J. Baker, L. R. Kahn, J. J. P. Stewart, E. M. Fluder, S. Topiol, J. A. Pople, "Gaussian94", Gaussian, Inc., Pttsburgh, PA 15213.

32. H. B. Schlegel, *J. Comp. Chem.*, 3, 214(1982).

33. M. W. Schmidt, K. K. Baldridge, J. A. Boatz, S. T. Elbert, M. S. Gordon, J. H. Jensen, S. Koseki, N. Matsunaga, K. A. Nguyen, S. J. Su, T. L. Windus, M. Dupuis, J. A. Montgomery, *J. Comp. Chem.*, 14, 1347(1993).

34. J. A. Pople, R. Krishnam, H. B. Schlegel, J. S. Binkley, *Int. J. Quant. Chem. Symp.*, 13, 225(1979).

35. J. T. Vivian, Master's Thesis, Montana State University,(1993).

36. E. V. Doktorov, I. A. Malkin, V. I. Man'ko, *J. Mol. Spect.*, 64, 359(1976).

37. S. F. Boys, F. Bernardi, *Mol. Phys.*, 19, 533(1970).

38. K. Kitaura, K. Morokuma, *Int. J. Quant. Chem.*, 10, 325(1976).

39. G. E. Kimball, G. H. Shortley, *Phys. Rev.*, 45, 815(1934).

40. J. W. Hager, D. R. Demmer, S. C. Wallace, *J. Phys. Chem.*, 91, 1375(1987).

41. P. R. Callis, *J. Chem. Phys.*, 95, 4230(1991).

42. E. T. Harrigan, N. Hiroti, *J. Am. Chem. Soc.*, 97, 6647(1975).

43. J. B. Foresman, M. Head-Gordon, J. A. Pople, M. J. Frisch, *J. Phys. Chem.*, 96, 135(1992).

44. Y. Yamamoto, J. Tanaka, *Bull. Chem. Soc. Jpn.*, 45, 1362(1972).

45. L. A. Phillips, D. H. Levy, *J. Chem. Phys.*, 85, 1327(1986).

46. B. Albinsson, B. Nórden, *J. Phys. Chem.*, 96, 6204(1992).

47. G. Berden, W. L. Meerts, G. Jalviste, *J. Chem. Phys.*, 103, 9596(1995).

48. R. Pariser, *J. Chem. Phys.*, 24, 250(1956).

49. S. Nagaoka, V. Nagashima, *J. Phys. Chem.*, 94, 4467(1990).

50. P. C. Mishra, K. Jug, *Theor. Chim. Acta*, 61, 559(1982).

51. A. Szabo, N. S. Ostlund, Modern Quantum Chemistry: Introduction to Advanced Electronic Structure Theory, (Macmillan, New York, 1982).

52. M. H. Palmer, S. M. F. Kennedy, *J. Chem. Soc., Perkins II*, 15, 1893(1974)

53. A. L. McClellan,Tables of Experimental Dipole Moments, (Freeman, London, 1963).

54. C. T. Chang, C. Y. Wu, A. R. Muirhead, J. R. Lombardi, *Photochem. Photobiol.*, 19, 347(1974).

55. M. Majoube, G. Vergoten, *J. Raman Spectrosc.*, 23, 431(1992).

56. K. Raghavachari, *J. Chem. Phys.*, 76, 3668(1982).

57. G. A. Bickel, D. R. Demmer, E. A. Outhouse, S. C. Wallace, *J. Chem. Phys.*, 91, 6013(1989).

58. T. Vondrák, S. - i. Sato, K. Kimura, *J. Phys. Chem. A*, 101, 2384(1997).

59. L. H. Slater, Master's Thesis, Montana State University,(1994).

60. Y. Nibu, H. Abe, N. Mikami, M. Ito, *J. Phys. Chem.*, 87, 3898(1983).

61. J. K. Burdett, *Chem. Phys. Let.*, 5, 10(1970).

62. P. R. Callis, *Int. J. Quant. Chem., Symposium 18*, 579(1984).

63. C. S. Parmenter, K. Y. Tang, W. R. Ware, *Chem. Phys.*, 17, 359(1976).

64. A. Hiraya, K. Shobatake, *J. Chem. Phys.*, 94, 7700(1991).

65. W. D. Gwinn, *Chem. Phys. Let.*, 106, 455(1984).

66. J. W Longworth, *Photochem. Photobiol.*, 7, 587(1968).

67. R. Bersohn, U. Even, J. Jortner, *J. Chem. Phys.*, 80, 1050(1984).

68. M. V. Hershberger, A. H. Maki, Lumry, W. C. Galley, *Biochem.*, 19, 2204(1980).

69. B. J. Fender, K. W. Short, D. K. Hahn, P. R. Callis, *Int. J. Quant. Chem.*, 72, 347(1999).

70. J. E. Braun, T. L. Grebner, H. J. Neusser, *J. Phys. Chem. A*, 102, 3273(1998).

71. S. J. Humphrey, D. W. Pratt, *J. Chem. Phys.*, 104, 8332(1996).

72. A. Kadari, A. Boucetta, B. Benali, G. Nouchi, *Spectrochimica Acta, Part A*, 49, 1153(1993).

73. D. R. Linde, CRC Handbook of Chemistry and Physics, (CRC Press, London, 1993).

74. R. C. Dunbar, *J. Phys. Chem. A*, 102, 8946(1998).

75. J. E. Braun, T. L. Grebner, H. J. Neusser, *J. Phys. Chem. A*, 102, 3273(1998).

76. P. M. Andrews, M. B. Berger, M. R. Topp, *J. Phys. Chem. A*, 101, 6222(1997).

77. A. C. Legon, D. J. Millen, *Chem. Soc. Rev.*, 21, 72(1992).

78. P. I. Nagy, G. J. Durant, *J. Am. Chem. Soc.*, 115, 2912(1993).

79. S. Scheiner, *Ann. Rev. Phys. Chem.*, 45, 23(1994) and references therein.

80. P. Hobza, R. Zahradnik, *Chem. Rev.*, 88, 871(1988).

81. D. A. Chignell, W. B. Gratzir, *J. Phys. Chem.*, 72, 2934(1968).

82. J. Hager, M. Ivanco, M. A. Smith, S. C. Wallace, *Chem. Phys.*, 105, 397(1986).

83. P. L. Muiño, P. R. Callis, *Proc. SPIE-Int. Soc. Opt. Eng.*, 2137, 278,(1994).

84. M. Schütz, T. Bürgi, S. Leutwyler, T. Fischer, *J. Chem. Phys.*, 98, 3763(1993).

85. M. Schmitt, H. Müller, V. Henrichs, M. Gerhards, W. Perl, Ch. Deusen, K. Kleinermanns, *J. Chem. Phys.*, 103, 584(1995)

86. K. W. Short, P. R. Callis, unpublished result.

87. G. Karlström, P. Linse, A. Wallqvist, B. Jönsson, *J. Am. Chem. Soc.*, 105, 3777(1983).

88. H. Popkie, H. Kistenmacher, E. Clementi, *J. Chem. Phys.*, 59, 1325(1973).

89. B. Albinsson, M. Kubista, B. Norden, *J. Phys. Chem.*, 93, 6649(1989).

90. E. H. Strickland, C. Billups, *Biopolymers*, 12, 1989(1973).

91. A. W. Hanson, *Acta Crystallogr.*, 17, 559(1964).

92. D. S. Maxwell, J. Tirado-Rives, W. L. Jorgensen, *J. Comp. Chem.*, 16, 984(1995).

93. D. M. Sammeth, Ph. D. Thesis, Montana State University,(1992).

94. H. Gusten, L. Klasnic, B. Ruščič, *Z. Naturforsch*, 31A, 1051(1976).

95. A. B. Hudson, *J. Comp. Chem.*, 6, 173(1985).

96. M. A. Shashidhar, K. Suryanarayana Rao, *Indian J. Phys.*, 52B, 162(1977).

97. The Aldrich Library FT - IR Spectra, (Aldrich, Milwaukee, 1989).

98. J. A. Sweeney, S. A. Asher, *J. Phys. Chem.*, 94, 4784(1990).

99. K. W. Short, P. R. Callis, unpublished result.

100. S. Arnold, M. Sulkes, *J. Phys. Chem.*, 96, 4768(1992).